

**STAR FORMING REGIONS AND THE IMF ALONG THE HUBBLE
SEQUENCE**

by
Fabio Bresolin

**A Dissertation Submitted to the Faculty of the
DEPARTMENT OF ASTRONOMY
In Partial Fulfillment of the Requirements
For the Degree of
DOCTOR OF PHILOSOPHY
In the Graduate College
THE UNIVERSITY OF ARIZONA**

1 9 9 7

INFORMATION TO USERS

This manuscript has been reproduced from the microfilm master. UMI films the text directly from the original or copy submitted. Thus, some thesis and dissertation copies are in typewriter face, while others may be from any type of computer printer.

The quality of this reproduction is dependent upon the quality of the copy submitted. Broken or indistinct print, colored or poor quality illustrations and photographs, print bleedthrough, substandard margins, and improper alignment can adversely affect reproduction.

In the unlikely event that the author did not send UMI a complete manuscript and there are missing pages, these will be noted. Also, if unauthorized copyright material had to be removed, a note will indicate the deletion.

Oversize materials (e.g., maps, drawings, charts) are reproduced by sectioning the original, beginning at the upper left-hand corner and continuing from left to right in equal sections with small overlaps. Each original is also photographed in one exposure and is included in reduced form at the back of the book.

Photographs included in the original manuscript have been reproduced xerographically in this copy. Higher quality 6" x 9" black and white photographic prints are available for any photographs or illustrations appearing in this copy for an additional charge. Contact UMI directly to order.

UMI

**A Bell & Howell Information Company
300 North Zeeb Road, Ann Arbor MI 48106-1346 USA
313/761-4700 800/521-0600**

**STAR FORMING REGIONS AND THE IMF ALONG THE HUBBLE
SEQUENCE**

by
Fabio Bresolin

**A Dissertation Submitted to the Faculty of the
DEPARTMENT OF ASTRONOMY
In Partial Fulfillment of the Requirements
For the Degree of
DOCTOR OF PHILOSOPHY
In the Graduate College
THE UNIVERSITY OF ARIZONA**

1 9 9 7

UMI Number: 9806801

UMI Microform 9806801
Copyright 1997, by UMI Company. All rights reserved.

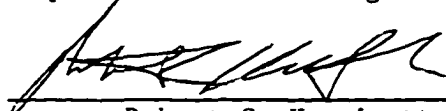
**This microform edition is protected against unauthorized
copying under Title 17, United States Code.**

UMI
300 North Zeeb Road
Ann Arbor, MI 48103

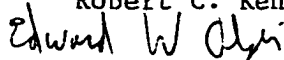
THE UNIVERSITY OF ARIZONA ©
GRADUATE COLLEGE

As members of the Final Examination Committee, we certify that we have
read the dissertation prepared by Fabio Bresolin
entitled Star forming regions and the IMF along the Hubble sequence

and recommend that it be accepted as fulfilling the dissertation
requirement for the Degree of Doctor of Philosophy



Robert C. Kennicutt



Edward W. Olszewski



Hans-Walter Rix

18 June 1997

Date

June 18 1997

Date

June 18, 1997

Date

Date

Date

Final approval and acceptance of this dissertation is contingent upon
the candidate's submission of the final copy of the dissertation to the
Graduate College.

I hereby certify that I have read this dissertation prepared under my
direction and recommend that it be accepted as fulfilling the dissertation
requirement.



Dissertation Director Robert C. Kennicutt

6/26/97

Date

STATEMENT BY AUTHOR

This dissertation has been submitted in partial fulfillment of requirements for an advanced degree at The University of Arizona and is deposited in the University Library to be made available to borrowers under rules of the Library.

Brief quotations from this dissertation are allowable without special permission, provided that accurate acknowledgment of source is made. Requests for permission for extended quotation from or reproduction of this manuscript in whole or in part may be granted by the head of the major department or the Dean of the Graduate College when in his or her judgment the proposed use of the material is in the interests of scholarship. In all other instances, however, permission must be obtained from the author.

SIGNED: 

ACKNOWLEDGMENTS

Several people helped, more or less consciously, to the happy ending of my graduate career. If this Ph.D. means anything, I also owe it to them. If it doesn't, I owe it to me.

My advisors and collaborators in Padova, Massimo Capaccioli and Giampaolo Piotto, taught me the basics of astronomical research, and something else. They helped me cross the ocean.

On my landing on the Western shores of Alabama, Connie and Jack Sulentic have been great hosts and friends, providing good wine and happy times in their *domus romana*. I wish them a great future as emperors. Carlos Rabaca has been an invaluable companion through many ups and downs. I also thank all the Faculty, particularly Ron Buta, in the Astronomy Department in Tuscaloosa.

At Steward Observatory my advisor Rob Kennicutt has provided lots of good sense and encouragement, and lots of data. I gained much from his insight and patience. I also thank the co-PIs of the HST Key Project on the Distance Scale, Jeremy Mould, Wendy Freedman and Rob Kennicutt, and all the other team members for the images and photometry used in a part of my work. For providing data and help, I thank in particular Laura Ferrarese, John Graham, Paul Harding, Lucas Macri, Randy Phelps, Daya Rawson, Shoko Sakai, Nancy Silbermann, Peter Stetson and Anne Turner. Without them one of the chapters of this thesis would have been delayed some decades. Claus Leitherer and the organizers of the meeting *From Stars to Galaxies* in Crete put together a good meeting and a great deal of useful material. Thanks to Don Garnett for advice on H II region modeling, and to Gary Ferland for making CLOUDY generally available. The US Government made my sustenance possible, and for protecting some beautiful spots in the Southwest it has my gratitude. I will miss the desert and the Grand Canyon. I just wish they hadn't flown all those helicopters over my house at night.

My parents, Angin and Gina, have always been very supportive, and made me feel at home when I travelled home. It goes without saying what I won't say. My wife Eliana (Mora) made all the rest possible, especially our pyrophoric son Sebastiano (Piro). We know about the rest, in peace.

As someone once said, "many, many thanks".

DEDICATION

A Mora, Sebastiano, e ...

TABLE OF CONTENTS

ABSTRACT	9
1 INTRODUCTION	11
1 Background	11
1.1 The IMF in extragalactic star forming regions	13
2 Organization of this work	20
2 PRESENT STUDY	23
APPENDIX A THE IONIZING STARS OF EXTRAGALACTIC H II REGIONS	28
1 Introduction	30
2 Observations and data reduction	32
2.1 MMT echellette spectra	33
2.2 Blue spectra	35
2.3 Analysis of spectra	37
3 Photoionization models	42
3.1 Input parameters	44
3.2 Model results	53
4 General results	85
4.1 Cluster ages (Figs. 18-26)	85
4.2 Ionization parameter (Figs. 13, 22, 31)	88
4.3 Sensitivity to different IMFs (Figs. 18-26)	88
4.4 The H β Equivalent Width (Figs. 12, 21, 30)	89
4.5 The He I λ 5876 line (Figs. 11, 20, 29)	92
4.6 The N/O abundance ratio (Figs. 14, 23, 32)	93
4.7 Additional remarks	95

5	Temperature of the ionizing stars	100
5.1	Diagnostic diagrams involving η'	102
5.2	T_* as a function of metallicity and Hubble type	102
6	Discussion: does the IMF change with metallicity ?	108
6.1	Tests for the upper IMF: what is next?	112
7	Tables with model results	113
APPENDIX B AN <i>HST</i> STUDY OF EXTRAGALACTIC OB ASSOCIATIONS . . .		133
1	Introduction	135
2	Data analysis	136
3	Association properties	156
4	The stellar luminosity function	158
4.1	Consequences for the upper IMF	160
5	Star cluster candidates	164
6	Conclusions	165
APPENDIX C AN <i>HST</i> STUDY OF OB ASSOCIATIONS AND STAR CLUSTERS IN M101		173
1	Introduction	176
2	Observations and data reduction	177
3	Massive stars	177
4	Identification of OB associations	178
5	Size distribution of the OB associations	180
6	Properties of the OB associations	180
6.1	The stellar luminosity function	180
6.2	Reddening	181
6.3	The color-magnitude and color-color diagrams	181
6.4	Estimating the age	182
7	On the upper mass limit of the IMF	183

8	Populous star clusters	184
9	Conclusions	185
APPENDIX D <i>UBVR</i> AND $H\alpha$ PHOTOMETRY OF H II REGIONS AND OB ASSOCIATIONS IN GALAXIES: A TEST FOR A VARIABLE IMF		
1	Introduction	191
2	Observations	191
3	Results	192
3.1	General results	192
3.2	Equivalent widths distribution vs Hubble type	193
3.3	Broadband luminosity functions	194
4	Discussion	194
REFERENCES		197

ABSTRACT

This thesis examines the properties of star forming regions in galaxies across the Hubble sequence. It focuses on the stellar populations of giant extragalactic H II regions and OB associations, addressing in particular the question of Initial Mass Function (IMF) variations with metallicity and/or galaxy morphology. This work is composed of three main sections:

(a) 3650–10,000 Å spectroscopy of nearly 100 H II regions in 20 spiral galaxies (Sa through Sm). Two indicators of the ionizing cluster effective temperature (T_*) are analyzed: the intensity of the He I $\lambda 5876$ line, and the ‘radiation softness’ parameter $\eta = (O^+/O^{++})/(S^+/S^{++})$. The interpretation of the data relies on CLOUDY photoionization models. A positive T_* gradient of 7000–8000 K is found between $2 Z_\odot$ and $0.2 Z_\odot$. The diagnostic diagrams and the T_* – metallicity relation are consistent with an upper mass limit of the IMF of $\sim 100 M_\odot$ and an age of ~ 1 Myr, irrespective of chemical abundance or Hubble type.

(b) An investigation of extragalactic OB associations, based on Hubble Space Telescope images. The size distribution of the associations (found with an automated search algorithm) is similar in all galaxies examined, with a mean size around 80 pc. An indication is found that the average number of bright blue stars depends on the parent galaxy Hubble type. The upper stellar V luminosity function is comparable among galaxies, with slope $d \log N/dM_V = 0.61 \pm 0.03$. A few star cluster candidates are identified.

(c) $UBVR$ and $H\alpha$ photometry of 266 H II regions in 10 spiral galaxies (Sa through Sd). The $H\alpha$ equivalent width is independent of Hubble type. The continuum and $H\alpha$ luminosity functions show similar trends, namely a steeper

slope and a smaller characteristic luminosity for early-type galaxies. These results lead to the conclusion that changes in the properties of H II regions and associations along the Hubble sequence are most likely due to variations in the number of stars per star forming region and in the number of regions per unit area, rather than the mass function.

CHAPTER 1

INTRODUCTION

1. Background

The evolution of galaxies is governed by the star formation process, and in fact the star formation rate and the history of star formation are among the defining traits of the galaxy morphological sequence (Searle *et al.* 1973, Larson & Tinsley 1978, Kennicutt 1983). In the most extreme cases single regions of violent star formation dominate the energetics and the chemical enrichment of the parent galaxies.

These galactic-scale starbursts (*e.g.* M82, Rieke *et al.* 1993, and NGC 1569, González-Delgado *et al.* 1997), together with nearby, scaled-down versions of such phenomena, including 30 Doradus in the LMC and NGC 604 in M33 (Walborn 1991, Hunter *et al.* 1996a), offer us a unique means to study the star formation mechanism and its effects on the surrounding environment. As a reference for the following discussion, in 30 Dor, the prototypical giant extragalactic H II region, ~ 1000 ionizing O stars provide 10^{52} ionizing photons s^{-1} , and roughly $10^6 M_{\odot}$ of ionized gas are contained in a region of 400 pc in diameter (Leitherer 1997).

Regions of recent or current star formation, and giant extragalactic H II regions in particular, are exceptional laboratories for the investigation of the stellar populations in galaxies. The study of resolved stars has provided detailed information on the massive stellar content of nearby galaxies, and has been successfully applied to the investigation of star formation and the Initial Mass Function (IMF) in the Magellanic Clouds (Parker & Garmany 1993, Hunter *et al.* 1995, Massey *et al.* 1995a). With HST the study of the brightest resolved stars, OB associations and star clusters has been extended beyond our immediate galactic neighborhood, to include a variety of environments (Hubble types, regions of different chemical composition and star forming rate, etc.), in the optical (O'Connell *et al.* 1994, Hunter & Thronson 1995, Bresolin *et al.* 1996) and the UV (Meurer *et al.* 1995). Even at relatively large distances (tens of Mpc), where only integrated measurements of stellar populations can be carried out, the signatures of the most massive stars can be detected directly (via the UV stellar wind spectral features) or indirectly (via the recombination lines of H II regions), allowing us to determine, or at least constrain, parameters such as the IMF, the age of the star forming events and the chemical composition of the interstellar gas.

Advancements in the development of the necessary theoretical tools, such as stellar atmospheres and stellar structure models, evolutionary synthesis and photoionization modeling techniques, largely contributed to the understanding of the massive stellar populations in galaxies (see the review by García-Vargas 1996). Relying upon these tools and based on different observational databases, several authors have attempted to unveil the associations and star clusters responsible for the ionization of extragalactic H II regions. The most recent works (*e.g.* García-Vargas *et al.* 1995, Stasińska & Leitherer 1996, García-Vargas *et al.* 1997, to cite just a few dealing with optical spectroscopy) are leading to a clearer picture

on the subject. In particular they suggest that a universal mass function is able to describe the star formation process in galaxies, in spite of diversities in galaxy type or chemical abundance, on the basis of a comparison of observational data with evolutionary models.

A power-law form of the IMF will be used throughout this thesis:

$\phi(m)dm \propto m^{-\alpha}dm$ is the number of stars formed between masses m and $m + dm$ per unit time, with lower and upper mass limits M_{low} and M_{up} . For a classical Salpeter (1955) IMF, $\alpha = 2.35$. This is equivalent to $\Gamma = -1.35$ in logarithmic mass notation: $\Gamma = d \log \xi(\log M)/d \log M$, where $\log \xi(\log M)$ is the number of stars formed per logarithmic mass interval per unit area per unit time. We will refer to the 'standard' or 'canonical' IMF as the one with $\alpha = 2.35$ and $M_{up} = 100 M_{\odot}$.

1.1. The IMF in extragalactic star forming regions

Since early work on extragalactic H II regions by Searle (1971), and later by Shields (1974) and Shields and Tinsley (1976), excitation gradients in spiral galaxies have been identified, and recognized as partly related to the increasing hardness of the ionizing radiation field with decreasing abundance. To explain this trend a variation of the upper mass limit for star formation with metallicity was proposed by Shields and Tinsley. This idea has since influenced the investigation of stellar populations. Several times in the past two decades there have been suggestions that the stellar content, particularly its mass function, might be different as the chemical abundance or the star formation rate are varied. Changes in both the slope (Terlevich & Melnick 1981) and the upper mass limit (Viallefond 1985, Vilchez and Pagel 1988) have been proposed. While such claims have been often weakened by the introduction of a new generation of investigative tools (HST, improved stellar models and atomic data), the issue is far from being settled.

Many studies on the IMF can be found in the literature, and the field is too vast to cover in a simple introduction like this one. A comprehensive review, summarizing the knowledge in the field up to the mid-1980's, is given by Scalo (1986). See also Pagel (1990) and Scalo (1990). In what follows I summarize some of the recent results on the upper IMF in extragalactic star forming regions, particularly in relation to resolved star studies and H II region spectroscopy, since these will be part of the work presented in the next chapters.

Resolved stars

The direct method of measuring the upper IMF by counting stars as a function of mass, though straightforward in principle, requires careful observations (both photometric and spectroscopic) to place stars in an H-R diagram. Visual magnitudes alone are inadequate, because of their insensitivity to differences in the effective temperature of O and B stars, which emit most of their energy in the UV. The need for spectral information to define the stellar types of massive stars has limited most investigations to our Galaxy and the Magellanic Clouds. Much of this work has been carried out over the past years by P. Massey and his collaborators (see Massey *et al.* 1995a,b). A summary of IMF determinations based on resolved stars is given by Hunter *et al.* (1997), which includes results on clusters and OB associations in the Galaxy, the Magellanic Clouds, M33 and M31. The IMF parameters show no significant variation, with slope α around the Salpeter value and upper mass limit around $100 M_{\odot}$, independent of metallicity, galaxy type or stellar concentration. This also applies to R136, the starburst cluster at the center of 30 Doradus in the Large Magellanic Cloud, for which Hunter *et al.* (1995) find $\alpha = -2.2 \pm 0.1$, despite a much higher stellar density and a larger number of

massive stars than normal OB associations.

A related issue, left relatively unexplored until recently, is the discrepancy between the total ionizing flux accounted for by the resolved stellar content in associations and the same quantity derived from nebular emission of the surrounding H II regions. For a few LMC OB associations the first has been found larger than the second, as measured by the integrated H α measurements of Kennicutt & Hodge (1986), by up to a factor of two (Massey *et al.* 1989. Garmany *et al.* 1994). In other cases good agreement is found instead (Parker *et al.* 1992). The re-examination of the data by Oey & Kennicutt (1997) supports the idea that a considerable fraction of the ionized nebulae might be density-bounded. They find that 0-62% of the ionizing radiation escapes the nebulae. Leakage of ionizing photons from the H II regions would explain the disagreement between the resolved stars and the nebular emission. We emphasize that the Oey and Kennicutt sample is heavily weighted to bubble-like H II regions, which might be more leaky than the average.

H II region spectroscopy

The study of nebulae ionized by massive stars is the most popular method for obtaining information about the stellar populations in extragalactic star forming regions. The interpretation of the signatures of the ionizing stars, in the form of optical and near-IR emission lines of spatially integrated spectra, requires careful comparisons with photoionization models, and as such it depends on the accuracy of atomic databases, stellar evolutionary models and stellar atmosphere models. Advancements in any of these fields has led to a better understanding of distant stellar populations.

I will only briefly summarize the most recent results on the IMF of the ionizing clusters of extragalactic H II regions. Several good reviews on extragalactic nebulae exist (Shields 1990, Kennicutt 1991, Stasińska 1996, García-Vargas 1996). One of the key steps in understanding the IMF of extragalactic H II regions has been the availability, since the mid-1980's, of a new generation of stellar evolution models, providing theoretical tracks for different metallicities, in addition to different stellar masses. McGaugh (1991) showed how the softening of the radiation field with increasing abundance predicted by the Maeder (1990) models could naturally explain the dependence of the effective temperature of the ionizing clusters of H II regions on metallicity (Vílchez and Pagel 1988), or the parallel gradient in the nebular electron temperature (Campbell 1988). This effects, known since the work of Shields & Tinsley (1976), had provided one of the main observational indications for a metallicity-dependent upper IMF (*e.g.* Viallefond 1985, Vílchez and Pagel 1988).

The high H α luminosity of giant extragalactic H II regions ($10^{38} - 10^{41}$ erg s $^{-1}$) implies ionization by a star cluster, rather than a single star. Improvement on McGaugh's zero-age models came with the inclusion of the time evolution of these clusters (evolutionary synthesis). This newer generation of models includes the works of García-Vargas & Díaz (1994), Cerviño & Mas-Hesse (1994), García-Vargas *et al.* (1995) and Stasińska & Leitherer (1996). Older evolutionary models were computed also by Melnick *et al.* (1985), and Olofsson (1989). The most important effect predicted by these models, and which mostly differentiate them from single-star models, is the drastic change in the shape of the ionizing continuum that occurs after the most massive stars evolve into the WR phase, around 3 Myr (1 Myr = 10^6 years) after the initial burst of star formation. These WR stars, with their high effective temperature and luminosity, dominate the total output

of ionizing photons from the clusters, as the stellar evolution models for massive stars show (Maeder & Conti 1994, Maeder 1996). Different authors use different prescriptions for their evolutionary models, which include either Padova or Geneva stellar tracks and different stellar atmospheres to describe the ionizing continuum of massive stars; a photoionization code (CLOUDY, PHOTO. etc) is used to compute nebular models. Despite differences in the models, in the observational data and in the diagnostics used to extract information, most of these recent works reach similar conclusions concerning the upper IMF. Cerviño and Mas-Hesse (1994) derived a T_{eff} gradient with metallicity for a sample of low-abundance emission-line galaxies (H II galaxies) which they explain, at least partly, without a metallicity dependence of the IMF. This is confirmed, using a larger H II galaxy sample, by Stasińska & Leitherer (1996), who conclude that the standard starburst model, with an instantaneous burst of star formation, and IMF with Salpeter slope and $M_{up} = 100 M_{\odot}$, is able to reproduce the observed emission-line properties in the $\sim 0.025 Z_{\odot}$ – $\sim 0.25 Z_{\odot}$ metallicity range. An upper mass cutoff of $50 M_{\odot}$ is instead excluded, based on the observed H β equivalent width distribution. For H II regions at higher metallicity (approximately larger than solar) García-Vargas *et al.* (1995) found consistency between the observational data and their models using a standard IMF, regardless of chemical composition. In conclusion, the dependence of T_{eff} on stellar mass and metallicity from stellar evolution models, combined with abundance effects on the stellar atmospheres (blanketing) seem sufficient to explain the observed trend of ionizing cluster effective temperature with metallicity, without the need to invoke an additional IMF variation. The results are also consistent with resolved star investigations in the nearest galaxies.

UV lines

Spectral features typical of massive stars are found in the UV, in the form of strong resonance lines, which originate predominantly in the stellar wind of O stars (Kudritzki & Hummer 1990). The broad C IV $\lambda 1550$ and Si IV $\lambda 1400$ lines in particular can be used to investigate the massive stellar content of starbursts (Leitherer & Lamers 1991). The equivalent width of these lines, $W(\text{Si IV})$ and $W(\text{C IV})$, are correlated with spectral type (or mass), and make the $W(\text{Si IV})/W(\text{C IV})$ ratio sensitive to the slope of the upper IMF (Sekiguchi & Anderson 1987, Mas-Hesse & Kunth 1991). Application of this technique to IUE spectra of starburst galaxies by Sekiguchi & Anderson (1987) gave a slope $\alpha = 2.23 \pm 0.45$, consistent with the Salpeter value. The IUE data also allowed Robert *et al.* (1993) to constrain, on the basis of the velocity shifts due to winds and the profiles of the UV lines, the upper mass limit of the IMF to $M_{\text{up}} > 30 M_{\odot}$ for starburst galaxies with nearly solar metallicity. With their spectral synthesis analysis of spatially integrated IUE spectra Vacca *et al.* (1995) concluded that $M_{\text{up}} \geq 50 M_{\odot}$ in the starburst region 30 Dor, in agreement with resolved star studies (*e.g.* Parker & Garmany 1993).

The blueshifted absorption and P Cygni profiles can provide important information on the upper IMF (Leitherer *et al.* 1995). With the higher spectral resolution of HST compared to IUE, the analysis of the line profiles has been carried out in starbursts. In NGC 4214 Leitherer *et al.* (1996) derive $\alpha = 2.35 - 3$, $M_{\text{up}} = 60 - 80 M_{\odot}$, and similar conclusions are found for NGC 1741 (Conti *et al.* 1996). Even if these investigations are usually limited to rather low (below solar) abundances, they support the concept of a universal IMF, and their conclusions agree with the other methods to constrain the IMF parameters.

A universal IMF?

I have so far summarized the conclusions of several studies, and shown that there is a general agreement as to the shape ($\alpha = 2.35 \pm 0.5$) and upper mass limit ($M_{up} = 60 - 100$) of the IMF. To not leave the impression that everything is settled, and that discordant results do not exist, I will give here a few examples which clash, more or less strongly, with the view of a universal mass function.

Several investigations have suggested that the IMF in starburst galaxies is peculiar with respect to the solar neighborhood (see a summary in Scalo 1990). Rieke *et al.* (1980, 1993) found indications for an IMF biased toward high-mass stars in the prototypical starburst M82. 'Top heavy' IMFs have been proposed by Kennicutt *et al.* (1987) and Sekiguchi & Anderson (1987). Flat slopes ($\alpha = 1 - 2$) were more recently found from a comparison of the WR/O ratios in young starbursts with evolutionary models (Meynet 1995, Contini *et al.* 1995), even though Schaerer (1996) showed how the data available can be reconciled with a Salpeter IMF. Variations in the upper mass limit have also been proposed by Doyon *et al.* (1992) on the basis of the He I 2.06μ /Br γ ratio. They find that for a large fraction of galaxies in their sample the upper mass limit $M_{up} \simeq 30 M_{\odot}$. However the reliability of the He I 2.06μ recombination line as a T_{eff} indicator has been questioned (Shields 1993).

In conclusion, while the majority of the most recent investigations in 'normal' H II regions and OB associations point toward a universal IMF, we cannot exclude variations of the IMF parameters in regions of enhanced star formation activity. Besides, most of these results depend on stellar evolution and stellar atmosphere models, which still contain uncertainties. For example, modern atmosphere models are still inadequate in reproducing the extreme UV spectra of the B giants ϵ CMa

and β CMa (Cassinelli *et al.* 1995, 1996).

2. Organization of this work

This thesis is a study of star formation in galaxies, examined from different perspectives, but with a single, unifying goal: to investigate if, and how, the stellar content of the star forming regions depends on global properties and the galactic environment, such as the morphological type or the metallicity. Among the pending issues is the Hubble type sensitivity and metallicity sensitivity of the upper IMF. As an attempt to clarify the picture, Appendix A presents a study of nearly 100 H II regions, distributed in 20 spiral galaxies (Sa through Sm). Medium-resolution spectra from 3650 Å to 10,000 Å allowed me the analysis of different indicators of the effective temperature, T_* , of the ionizing stars: the equivalent width of H β , the He I λ 5876 emission line intensity, and the 'radiation softness' parameter $\eta = (O^+/O^{++})/(S^+/S^{++})$ of Vílchez and Pagel (1988). No previous large H II region sample had such a large wavelength coverage, including the near-IR, so that the T_* behavior could be extensively investigated by means of η . To impose constraints on the IMF variations, photoionization models have been calculated with CLOUDY (Ferland 1996), adopting as the ionizing source both Kurucz (1992) atmospheres and clusters synthesized with different slopes and upper mass cutoffs of the IMF. From a comparison between the theoretical models and the observations I draw some conclusions about the IMF changes with metallicity and morphological type. A functional form of the T_* – metallicity relation is derived, dependent upon the adopted stellar atmosphere models. The observations for this work were obtained by my thesis advisor, R. C. Kennicutt, during a period of several years, and I have reduced the data under his supervision. The modeling and the interpretation have

benefited from discussions with him and from the M101 work (in preparation) by D. Garnett and R. Kennicutt.

Beyond the Magellanic Clouds little is known about the properties of extragalactic OB associations, which contain tens or hundreds of massive stars, and represent tracers of recent or ongoing star formation, being often associated with ionized gas clouds. It is still poorly known if the galaxy type determines properties like the size distribution of the associations (is there a universal scale for the clustering of stars in galaxies?), or the number of stars in each star forming event. Moreover, the upper end of the luminosity function of resolved populations, which provides a characterization of the massive stellar content (albeit with some limitations) has not yet been investigated extensively beyond the Local Group. The study of extragalactic OB associations has been made difficult, and somewhat biased, by subjective procedures and lack of spatial resolution (Hodge 1986). These problems can be alleviated with HST imaging, and with the application of ‘objective’ search algorithms to the spatial distribution of the brightest blue stars in resolved galaxies (Wilson 1992). In Appendix B and Appendix C I apply such a method to a sample of seven galaxies, observed by HST as part of the Key Project on the Distance Scale, to which the author is collaborating. The size distribution of the resulting associations is analyzed, and the luminosity function for the brightest stars is compared among galaxies. A search for compact star clusters yields a few ‘blue’ globular cluster candidates, similar in photometric properties to the blue clusters in the LMC and SMC. This work, apart from the data acquisition, is entirely my own. P. Stetson provided the crowded-field photometry software.

Unresolved extragalactic OB associations and H II regions are the subject of Appendix D. Here we present *UBVR* and H α photometry of 266 H II regions in 10

spiral galaxies, distributed over a wide range of Hubble types (Sa through Scd). observed with the Steward 2.3m telescope. The main motivation of this work is to investigate the origin of the trend in star formation activity along the Hubble sequence. Variations in the upper IMF have been invoked among the possible causes (van den Bergh 1976), since a smaller upper mass limit would produce the generally fainter H II regions observed in early-type spirals, when compared with late-type galaxies. To test this idea, we investigate the Hubble type dependence of the H II region H α equivalent width, which is sensitive to the presence of massive, ionizing stars. Moreover, the continuum and the H α luminosity functions are analyzed, in order to provide information on both the stellar associations (the principal sources of the continuum flux) and the gas ionized by them. The observations, data reduction and most of the interpretation are my own. My advisor R. Kennicutt provided some new ideas about the interpretation.

CHAPTER 2

PRESENT STUDY

The methods, results, and conclusions of this study are presented in the papers appended to this dissertation. The following is a summary of the most important findings in these papers.

In this study I have tried to constrain the changes of the IMF with metallicity and Hubble type. For this purpose I have used different techniques: extragalactic H II region spectroscopy (Appendix A), HST imaging of resolved populations (Appendix B and Appendix C), and ground-based photometry of unresolved H II regions and associations (Appendix D). The galaxies examined span the morphological sequence from Sa to Sm, while the metallicity of the H II regions ranges from $\sim 0.2 Z_{\odot}$ to $\geq 2 Z_{\odot}$. This work of course does not provide the ultimate solution to the question of IMF variations, given the difficulty (or virtual impossibility) with the adopted techniques and observations to detect differences in IMFs having, for example, M_{up} in the range 60-100 M_{\odot} . The diagnostics used in this work do not provide much information on the slope of the mass function, either. The result on the luminosity function (Appendix B), though excluding large

variations in the IMF slope among galaxies, cannot provide good constraints on the absolute value of α . Advancements have been made, however, with respect to previous works, regarding the following points:

- the IMF in normal extragalactic H II regions has been investigated in a larger metallicity range: similar studies have been so far usually limited to samples of metal-poor H II galaxies or metal-rich spirals;
- two different T_e indicators have been analyzed, and in particular the softness parameter η , which has been measured for the largest number of extragalactic H II regions so far;
- photometry of a large number (almost 300) of H II regions has been measured, which has been rarely attempted in other studies;
- the study of resolved stars and OB associations outside the Local Group has just begun, and in Chapter 3 I have analyzed the largest sample of galaxies so far for which an automated association search has been carried out in a completely consistent way;

There is still space for improvement, and at the end of Appendix A I have indicated a few ways to extend our knowledge on the upper IMF.

The main results of this thesis are here briefly summarized:

1. Two T_e indicators (η and He I $\lambda 5876$) allowed me to establish a change in the effective temperature of the ionizing clusters of H II regions with metallicity. While the absolute values of T_e depend on the adopted (Kurucz 1992) stellar atmospheres, the relative trend is less sensitive to the choice of atmospheres.

The indicators give similar results, and indicate a 7.000 - 8.000 K drop in T_e from $\sim 0.2 Z_\odot$ to $\sim 2 Z_\odot$.

2. To check if this temperature gradient implies a metallicity-dependent IMF, the observational data have been compared to the Geneva stellar models. The good agreement with the 1 Myr tracks (the typical age suggested by the set of diagnostic diagrams of Appendix A) implies that no abundance effect on the IMF is required. A single upper mass limit of the order of 100 M_\odot across the whole metallicity range examined (0.2 to 2 Z_\odot) is consistent with the data. Relatively modest changes in the slope (*e.g.* from $\alpha = 2.35$ to $\alpha = 3.3$) or in the upper mass limit from 60 M_\odot to 100 M_\odot cannot be detected with the observations and modeling techniques used in this work.
3. The results on the upper V luminosity function in OB associations in seven spiral galaxies resolved into individual stars by HST exclude large variations in the upper IMF among galaxies. The average slope is $s = d \log N / dM_V = 0.61 \pm 0.03$. The relative insensitivity of broad-band photometry to stellar spectral types, the difficulty of isolating evolved (supergiant) from main sequence stars, combined with typical crowded-field photometry problems (incompleteness, superposition of stars, binaries, etc.) makes it difficult to constrain the IMF parameters. The luminosity function has been measured for $M_V < -5$, and is likely to be affected by the presence of evolved stars.
4. The invariance of the IMF with respect to abundance changes is accompanied by the invariance with respect to galaxy morphological type. I have shown (Appendix A and Appendix D) that the H II region equivalent width (EW) of the Balmer lines ($H\alpha$ and $H\beta$) is distributed in similar ways for both

early-type (Sa-Sb) and late-type (Sbc and later) spiral galaxies. Since the equivalent width is a measure of the ratio of massive ($M > 10 M_{\odot}$), ionizing stars to the total number of stars in a star forming region, we would expect lower EW values where the IMF is truncated at lower masses. Since this effect is not observed as a function of Hubble type, we can exclude large variations of the upper IMF between, for example, Sb and Sc galaxies as a possible explanation for their differing star formation properties. The narrow-band ($H\alpha$) and continuum (V) $H II$ region/association luminosity functions show similar behavior: increasing slope and higher typical luminosity in later Hubble types. The conclusion of these findings is that the most likely cause of the star formation differences along the Hubble sequence is in the clustering properties of massive stars, rather than the mass function.

5. With the availability of high-resolution HST images of spirals, and the application of an automated method for the search of OB associations, I have produced more evidence that the size distribution of the associations is comparable among galaxies, with apparently no dependence on galaxy type. The mean size is 80 pc, which would correspond to the size of the elementary cells of star formation in galaxies. While this and similar automated procedures are an improvement over past methods, there is still a certain degree of subjectivity involved.
6. I find direct evidence (from star counting) that OB associations in Sb galaxies contain, on average, a smaller number of bright stars (around 30–40% less) than those in Sc galaxies. The sample is small, but the effect is in the direction expected if early-type galaxies produce lower-luminosity star forming regions because of a smaller number of stars formed, and not

because of an IMF deficient in high-mass stars. in agreement with the result of Appendix D previously discussed.

7. Finally, I have identified a number of blue star clusters from a visual search of the HST images. Their photometric properties are comparable to those of the blue clusters identified in M33 and the Magellanic Clouds, making at least some of them populous cluster candidates. Not much more can be said about them with V and I photometry alone. U or B photometry would help to discriminate clusters from background galaxies, and to better constrain the stellar populations.

APPENDIX A

THE IONIZING STARS OF EXTRAGALACTIC H II REGIONS

To be submitted for publication in *The Astrophysical Journal*.

The Ionizing Stars of Extragalactic H II Regions

F. Bresolin

Steward Observatory, University of Arizona, Tucson, AZ 85721

email: fabio@as.arizona.edu

1. Introduction

Giant extragalactic H II regions, ionized by the massive stars of their young embedded clusters, provide powerful tools for measuring the chemical composition of the interstellar medium and for understanding the massive stellar populations in external galaxies (see reviews by Shields 1990, Kennicutt 1991, Stasińska 1996). Evidence for abundance gradients across the disks of spiral galaxies was presented by Searle (1971), following pioneering work by Aller (1942) on the radial trends of emission-line ratios. The excitation of H II regions, measured by the ratios $[\text{OIII}]/\text{H}\beta$ and $[\text{OIII}]/[\text{OII}]$, was found to increase with galactocentric distance, and interpreted as an effect of the shift from infrared fine-structure transitions to optical $[\text{OIII}]$ emission as the principal cooling mechanism at the lower metallicities typical of larger radii. Later work confirmed the existence of composition gradients by direct observation of the $[\text{OIII}] \lambda 4363$ line at low abundances (*e.g.* Smith 1975). To explain the observed gradients in excitation and in the equivalent width of the $\text{H}\beta$ emission ($\text{EW}(\text{H}\beta)$) an additional gradient of the color temperature of the ionizing field, T_* , was proposed (Shields 1974, Shields & Tinsley 1976, Shields & Searle 1978), with the ionizing radiation becoming harder with increasing radius. The work of Shields & Tinsley (1976) suggested a metallicity-dependent upper mass limit for star formation, $M_u \propto Z^{-1/2}$. It also pointed out that a change in the temperature of the hottest stars is to be expected, even in the absence of a metallicity effect on M_u , because of opacity effects that would lower the effective temperatures of metal-rich stars.

Subsequent efforts were concentrated on this general picture, with the calculation of extensive grids of single-star photoionization models. While Evans & Dopita (1985) argued that the available data on the trends in the emission-line

ratios was consistent with a single ionizing temperature ($\simeq 41,500$ K) and a varying nebular geometry through changes in the ionization parameter. Most authors confirmed the increase of T_* with decreasing abundance (Stasińska 1980, Campbell *et al.* 1986, Vílchez & Pagel 1988), together with a possible increase in the ionization parameter (Campbell 1988). Several mechanisms have been postulated to explain this trend: a metallicity effect on either the upper mass limit of the Initial Mass Function (IMF, Shields & Tinsley 1976), or its slope (Terlevich 1985); increased stellar line blanketing (Balick & Sneden 1976) or internal dust absorption (Sarazin 1976) with metallicity. The softening of the stellar ionizing spectra with increasing abundance predicted by more recent stellar evolutionary models made the introduction of these effects unnecessary for H II region models (McGaugh 1991, Garnett & Kennicutt 1997). Moreover, the introduction of cluster photoionization models, in which the single star with given T_* is substituted by an evolving stellar cluster synthesized with a given IMF as the ionizing source, has produced results consistent with a so-called *universal* IMF (García-Vargas *et al.* 1995, Stasińska & Leitherer 1996).

There is still much interest in the functional dependence of the effective temperature of the ionizing star cluster in a giant H II region on metallicity, even though the absolute scale remains model dependent. T_* is generally estimated by (1) a method requiring the measurement of [OIII] $\lambda 4363$ (Stasińska 1980), and therefore restricted to high-excitation, low-metallicity objects, or (2) via the 'radiation softness' parameter $\eta = (O^+/O^{++})/(S^+/S^{++})$ introduced by Vílchez and Pagel (1988), following previous work by Shields & Searle (1978) and by Mathis (1982, 1985). This method is based on the observation of strong lines, but requires the measurement of [SIII] $\lambda\lambda 9069, 9532$, which are strongly affected by atmospheric water vapor absorption. Despite observational difficulties, and the uncertainties in

the adopted stellar atmospheres and the atomic data for sulfur. η remains a rather good indicator of T_* , at least in relative if not absolute terms (Garnett 1989).

The η method has been generally applied to studies of a few H II regions in individual galaxies, by combining it with the empirical abundance indicator $R_{23} = ([\text{OII}] + [\text{OIII}])/\text{H}\beta$ (Pagel *et al.* 1979) to simultaneously constrain the metallicity, the effective temperature and the ionization parameter (Díaz *et al.* 1987, Vílchez *et al.* 1988, Díaz *et al.* 1991). Recently Garnett & Kennicutt (1997) studied the metallicity dependence of T_* for 41 H II regions in M101, using nebular photoionization models to fit η and R_{23} . We extend here their work by analyzing 3650–10,000 Å spectrophotometry of 95 H II regions in 20 spiral galaxies, with two main goals: to quantify the relationship between T_* and the gaseous abundance, and to constrain IMF variations with metallicity. The dependence of the physical properties of the giant star forming regions on Hubble type is also investigated. To this end photoionization models including as ionizing source either an evolving star cluster or a single stellar atmosphere are computed, to study the effect of different IMFs, and to estimate the dependence of the radiation field on abundance.

2. Observations and data reduction

The galaxy sample (Table 1) spans the Hubble sequence from type Sa to type Sm, and should therefore provide good indication of trends of star forming region properties with morphological type (and metallicity). Nearly all of the H II region observations are new to this work, and were obtained by R. C. Kennicutt during several runs in the 1988-1992 period; the few exceptions are indicated in Table 1. The main observational material (redwards of H β) consists of MMT echellette spectra; the 'blue' spectra (which include the [OII] λ 3727 line) were obtained both

at the MMT and at the Steward Observatory 90-inch telescope.

2.1. MMT echellette spectra

The Red Channel Spectrograph at the MMT was used in cross-dispersed mode to obtain spectral coverage from 4700 Å to 10,000 Å. This allowed the inclusion of all the main spectral features from H β to [SIII] $\lambda\lambda$ 9069, 9532. In this observing mode a 2'' \times 20'' slit was cross-dispersed into five orders on a TI 800 \times 800 CCD (0''.625 pixel⁻¹ after binning), providing extended wavelength coverage combined with intermediate resolution. Exposure times ranged from 5 to 40 minutes.

Data reduction included a few procedures particular to the echellette observations (see also Skillman & Kennicutt 1993 and Kennicutt & Garnett 1996). Standard stars frames taken at low airmass were used to trace the aperture for each of the five orders and to remove the curvature introduced by the cross-disperser. Wavelength and flux calibrations were accomplished with HeNeAr lamp frames and observations of standard stars from Oke & Gunn (1983) and Massey *et al.* (1988), respectively. The calibrations were checked for internal consistency using lines in the overlap regions between adjacent orders. The residuals from the standard star fits indicate a typical ± 0.05 mag accuracy or better in all orders except the reddest one ($\lambda > 8000$ Å). Here the water absorption features in the near-IR introduce a larger uncertainty in the flux calibration. The extinction was then modeled as a function of wavelength by tracing the absorption features observed in the standard star spectra. This procedure satisfactorily removes most of the unwanted telluric features around the [SIII] $\lambda\lambda$ 9069, 9532 lines, as indicated by the mean observed $\lambda 9532/\lambda 9069$ ratio = 2.47 ± 0.05 (the theoretical value is 2.44).

One-dimensional spectra were extracted with variable apertures, typically 8

Table 1. The galaxy sample

Galaxy		Type ^a	$M_{B_T}^{0,i}$ ^a	v_0 ^a (km s ⁻¹)	Source of ^b Blue Spectra
NGC 224	(M31)	SbI-II	-21.61	-10	90"
NGC 598	(M33)	Sc(s)II-III	-19.07	69	90"
NGC 5194	(M51)	Sbc(s)I-II	-20.72	541	90"
NGC 3031	(M81)	Sb(r)I-II	-20.75	124	MMT
NGC 628	(M74)	Sc(s)I	-20.87	861	MRS
NGC 1569		SmIV	-15.34	144	90"
NGC 2403		Sc(s)III	-19.47	299	90", MRS
NGC 2841		Sb	-20.65	714	MMT
NGC 3310		Sbc(r)	-19.94	1073	90"
NGC 3351	(M95)	SBb(r)II	-19.78	641	MMT
NGC 3368	(M96)	Sab(s)II	-20.53	758	MMT
NGC 3521		Sbc(s)II	-20.50	627	ZKH
NGC 3623	(M65)	Sa(s)II	-20.60	675	MMT
NGC 4258	(M106)	Sb(s)II	-21.17	520	MMT
NGC 4736	(M94)	RSab(s)	-19.93	345	MMT
NGC 4861		SBmIII	-17.76	836	90"
NGC 5236	(M83)	SBc(s)II	-20.24	275	Dufour+
NGC 5701		(PR)SBa	-19.62	1424	MMT
NGC 6384		Sb(r)I.2	-21.40	1735	MMT
NGC 7331		Sb(rs)I-II	-21.72	1114	MMT

^aFrom Sandage & Tammann 1987; corrected to $H_0 = 75 \text{ km s}^{-1} \text{ Mpc}^{-1}$

^b90": B&C + Steward Observatory 90-inch telescope; MMT: Red Channel + MMT; MRS: McCall *et al.* 1985; ZKH: Zaritsky *et al.* 1994; Dufour+: Dufour *et al.* 1980

arcseconds, but depending on the seeing and the size of the objects, centered on the peak of the $H\alpha$ emission line.

2.2. Blue spectra

Coverage of the 3650–5100 Å spectral range was obtained with two different instruments and setups. The majority of our targets in early-type galaxies were observed with the Red Channel CCD spectrograph on the MMT and a slit size of $2'' \times 180''$. These observations have been described in detail by Oey & Kennicutt (1993) in their project on abundances in early-type galaxies. However new one-dimensional extractions were made, to match the extractions of the red echellette spectra.

Additional objects (marked 90" in Table 1) were observed with the B&C spectrograph on the Steward Observatory 90-inch telescope (600 groove mm^{-1} grating blazed at 3568 Å, 9 Å resolution), with a $4''.5 \times 180''$ slit. Standard reduction procedures for these long-slit data were followed. The $H\pi$ regions in three galaxies (M31, M33 and NGC 2403) were observed in the red also with the 90-inch telescope (300 groove mm^{-1} grating blazed at 6690 Å, 20 Å resolution), thus providing an additional check on the corresponding MMT echellette spectra.

Examples of combined red+blue spectra covering the whole spectral range for two of our targets are given in Figure 1. These were chosen to show the large variation in the excitation, measured by the ratio of $[\text{OIII}] \lambda\lambda 4959, 5007$ to $H\beta$, present in our data.

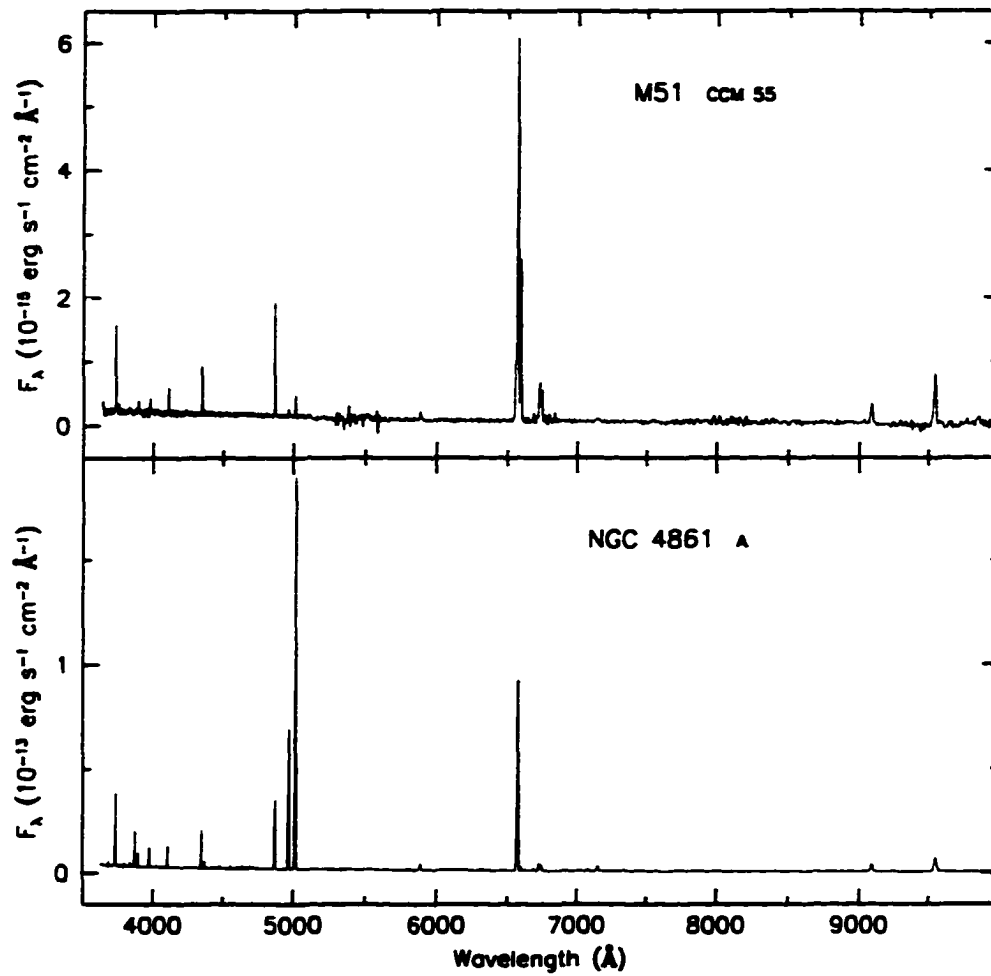


Figure 1 Examples of combined red+blue spectra: (*top*) a low excitation H II region in M51; (*bottom*) the brightest H II region in NGC 4861, a high excitation object.

2.3. Analysis of spectra

The emission line fluxes for the atomic transitions of interest were measured with the IRAF task SPLOT, by integrating over the line profiles. We assumed a stellar underlying continuum Balmer absorption equivalent width of 2 Å, the mean value found by McCall *et al.* (1985) in their H II region sample, and calculated the reddening with the $H\alpha/H\beta$ and $H\beta/H\gamma$ ratios. Table 2.2 lists the measured fluxes, corrected for reddening, for the most important emission lines, as well as offsets in arcseconds from the galaxy nucleus, and the $EW(H\beta)$. The latter is an average of the values obtained from the two echellette orders containing the $H\beta$ line and the blue spectra. As in Kennicutt & Garnett (1996), who analyzed H II region spectra in M101 taken with the same setup as the observations discussed in this work, the quoted errors were calculated by adding in quadrature the contributions from the statistical noise, the calibration ($\sim \pm 3\%$), the flat fielding ($\sim \pm 1\%$), the relative scaling of the echellette orders ($\sim \pm 4\%$) and the uncertainty in the reddening corrections. A 20% uncertainty was assigned to the combined [SIII] $\lambda\lambda 9069, 9532$ flux.

We performed a few tests, in order to check the quality of the data. In Figure 2a the [SIII] $\lambda 9532$ /[SIII] $\lambda 9069$ ratio is plotted against the empirical abundance indicator R_{23} . The observed values are consistent with the theoretical one. The density-sensitive [SII] $\lambda 6716$ /[SII] $\lambda 6731$ ratios (Figure 2b) fall near or below the low-density limit ($= 1.42$), with an average value of 1.37 ± 0.02 , therefore justifying the assumption of low-density ($10\text{--}100 \text{ cm}^{-3}$, Osterbrock 1989) made for the model nebulae (*cf.* Section 3). In Figure 3 our data (filled circles) for two excitation sequences, [OII]/ $H\beta$ vs [OIII]/ $H\beta$ and [OIII]/ $H\beta$ vs [NII]/ $H\alpha$, are compared to the data of McCall *et al.* (1985, open circles), consisting of emission

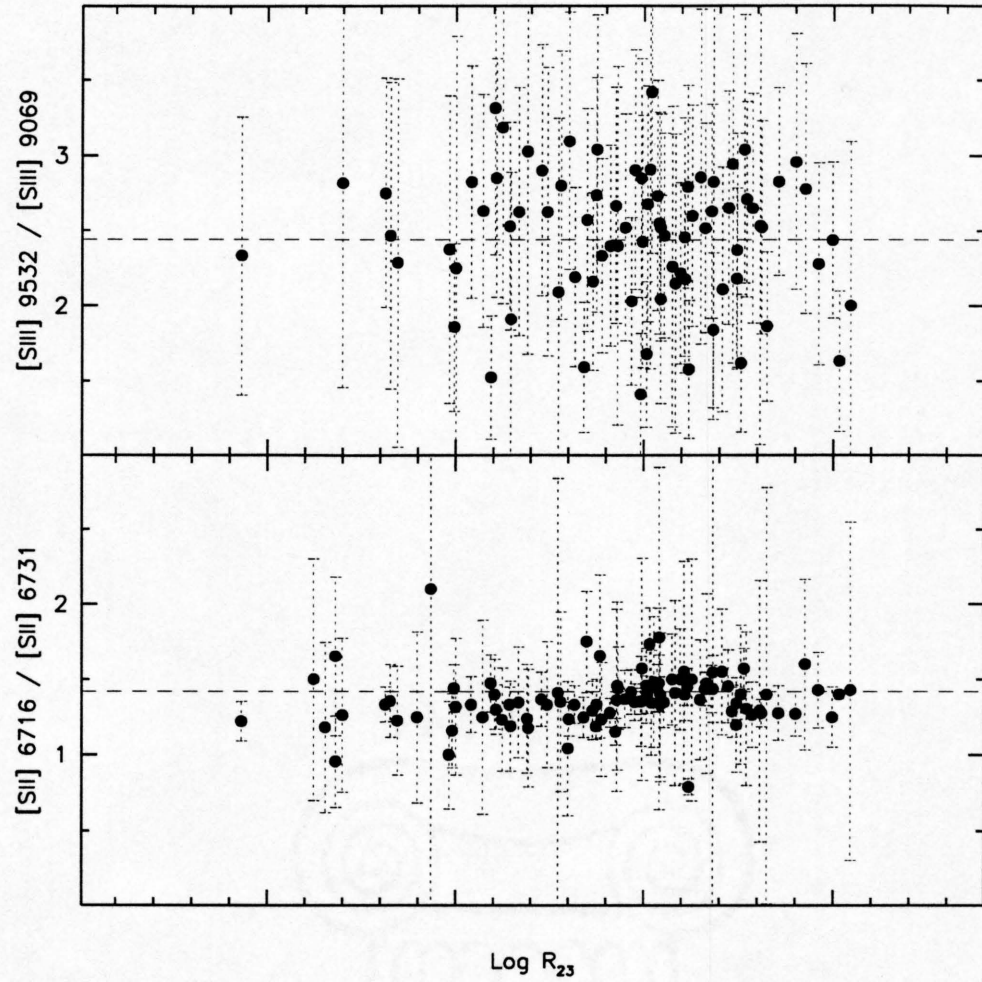


Figure 2 Observed line ratios for the sulfur lines compared to the theoretical values: (a) The $[\text{SIII}] \ \lambda 9532 / [\text{SIII}] \ \lambda 9069$ ratio plotted against the empirical abundance indicator $R_{23} = ([\text{OII}] + [\text{OIII}]) / \text{H}\beta$. The theoretical value is indicated by the dashed line. (b) The $[\text{SII}] \ \lambda 6716 / [\text{SII}] \ \lambda 6731$ ratio plotted against R_{23} . The low-density limit is indicated by the dashed line.

TABLE 2.2. Reddening-corrected line fluxes.

No.	Offset ^a		[OII]	[OIII]	HeI	[NII]	[SII]	[SIII]	EW(H β)	Name ^b
	α	δ	3727	4959+5007	5876	6548+6583	6716+6731	9069+9532		
M31										
1	-157	-3244	209 \pm 11	347 \pm 14	11 \pm 1	22 \pm 1	11 \pm 1	35 \pm 5	128	P7
2	-840	-1498	160 \pm 8	40 \pm 2	13 \pm 3	127 \pm 5	47 \pm 2	86 \pm 14	38	P258
3	-1165	-717	184 \pm 14	39 \pm 11	10 \pm 5	88 \pm 8	66 \pm 6	50 \pm 8	375	P286
4	-838	-663	206 \pm 11	30 \pm 1	12 \pm 1	174 \pm 7	81 \pm 3	71 \pm 11	135	P309
5	561	-377	223 \pm 11	87 \pm 3	16 \pm 3	137 \pm 6	66 \pm 2	70 \pm 10	243	P420
6	867	1972	330 \pm 18	86 \pm 4	35 \pm 2	89 \pm 4	43 \pm 1	49 \pm 7	103	P729
M33										
1	-824	-24	156 \pm 8	641 \pm 26	13 \pm 1	21 \pm 1	25 \pm 1	95 \pm 15	111	NGC588
2	553	420	224 \pm 11	235 \pm 9	13 \pm 1	32 \pm 2	39 \pm 1	95 \pm 15	337	NGC604
3	-220	113	237 \pm 12	169 \pm 7	15 \pm 1	55 \pm 2	24 \pm 1	124 \pm 19	244	NGC595
M51										
1	34	12	38 \pm 10	7 \pm 8	0 \pm 3	74 \pm 6	24 \pm 6	0 \pm 0	15	CCM 37A
2	15	30	0 \pm 10	0 \pm 10	0 \pm 5	70 \pm 8	21 \pm 9	0 \pm 0	5	CCM 6A
3	3	57	27 \pm 3	0 \pm 1	9 \pm 1	105 \pm 4	40 \pm 2	20 \pm 4	72	CCM 107
4	70	138	106 \pm 6	18 \pm 3	10 \pm 2	162 \pm 6	47 \pm 3	53 \pm 7	37	CCM 10
5	-83	-108	70 \pm 6	0 \pm 4	0 \pm 2	121 \pm 7	49 \pm 7	46 \pm 9	13	CCM 71
6	-88	-82	57 \pm 3	8 \pm 1	9 \pm 1	150 \pm 6	49 \pm 2	60 \pm 9	61	CCM 72
7	90	-135	88 \pm 5	22 \pm 3	9 \pm 1	153 \pm 6	42 \pm 3	65 \pm 10	116	CCM 55
8	104	-116	104 \pm 6	24 \pm 3	10 \pm 2	162 \pm 6	46 \pm 3	77 \pm 12	82	CCM 53
9	-66	50	83 \pm 17	35 \pm 21	9 \pm 8	172 \pm 13	45 \pm 11	98 \pm 12	23	CCM 84
10	-60	119	157 \pm 16	42 \pm 13	0 \pm 6	144 \pm 13	47 \pm 10	0 \pm 0	15	CCM 91
11	-134	-188	167 \pm 10	70 \pm 5	10 \pm 3	161 \pm 8	70 \pm 4	97 \pm 16	90	CCM 71A
12	-59	-125	91 \pm 9	7 \pm 7	0 \pm 3	168 \pm 8	54 \pm 6	0 \pm 0	17	CCM 68
13	-23	-122	48 \pm 7	0 \pm 4	0 \pm 2	120 \pm 7	45 \pm 7	0 \pm 0	19	CCM 64
M81										
1	107	-291	249 \pm 27	101 \pm 14	13 \pm 6	115 \pm 9	36 \pm 7	81 \pm 13	53	HK268, GS1
2	40	-250	262 \pm 38	121 \pm 16	13 \pm 7	111 \pm 9	41 \pm 8	63 \pm 13	40	HK343-50, GS2
3	-290	89	339 \pm 27	252 \pm 19	13 \pm 5	93 \pm 8	30 \pm 6	115 \pm 17	285	HK767, GS4
4	-273	-19	340 \pm 27	106 \pm 14	12 \pm 7	135 \pm 11	71 \pm 10	81 \pm 14	80	HK741-4, GS7
5	-196	292	222 \pm 22	89 \pm 13	13 \pm 6	159 \pm 10	80 \pm 8	77 \pm 12	168	HK652, GS9
6	-92	300	191 \pm 22	159 \pm 17	13 \pm 7	122 \pm 10	49 \pm 8	67 \pm 11	87	HK500-9, GS11
7	-47	260	334 \pm 39	71 \pm 26	12 \pm 9	126 \pm 12	51 \pm 11	83 \pm 13	62	HK453, GS12
8	146	7	139 \pm 33	48 \pm 31	12 \pm 16	141 \pm 21	41 \pm 20	68 \pm 16	295	HK230, GS13
9	237	-845	209 \pm 36	902 \pm 73	14 \pm 10	48 \pm 13	34 \pm 13	54 \pm 12	150	Münch1
10	-142	526	156 \pm 31	415 \pm 23	15 \pm 5	76 \pm 6	36 \pm 6	76 \pm 11	369	Münch18
NGC 628										
1	49	52	196 \pm 16	48 \pm 10	14 \pm 5	128 \pm 8	38 \pm 6	90 \pm 14	91	H292
2	-74	-22	152 \pm 15	23 \pm 13	10 \pm 7	114 \pm 10	56 \pm 8	58 \pm 9	89	H451
3	-60	-107	245 \pm 18	37 \pm 6	11 \pm 3	129 \pm 7	64 \pm 4	81 \pm 13	108	H572
4	42	-116	255 \pm 22	58 \pm 18	12 \pm 10	104 \pm 13	54 \pm 12	72 \pm 12	51	H598
5	-42	-154	235 \pm 15	189 \pm 14	14 \pm 6	53 \pm 8	30 \pm 8	90 \pm 14	84	H627
6	-186	86	418 \pm 23	111 \pm 8	12 \pm 3	81 \pm 5	54 \pm 4	84 \pm 13	232	H154-155
7	-89	192	325 \pm 17	157 \pm 8	12 \pm 2	72 \pm 4	39 \pm 3	71 \pm 10	173	H13

TABLE 2.2. (continued)

No.	Offset ^a		[OII]	[OIII]	HeI	[NII]	[SII]	[SIII]	EW(H β)	Name ^b
	α	δ	3727	4959+5007	5876	6548+6583	6716+6731	9069+9532		
NGC 1569										
1	-7	3	116 \pm 6	922 \pm 37	20 \pm 1	6 \pm 0	12 \pm 0	50 \pm 7	94	HK45
2	25	-12	100 \pm 6	895 \pm 36	19 \pm 1	10 \pm 1	18 \pm 1	55 \pm 5	263	HK23
NGC 2403										
1	-96	35	300 \pm 15	257 \pm 10	20 \pm 2	80 \pm 4	75 \pm 3	118 \pm 19	174	
2	-45	55	210 \pm 11	148 \pm 6	14 \pm 1	74 \pm 4	47 \pm 3	111 \pm 17	36	
3	-186	45	241 \pm 12	236 \pm 9	14 \pm 1	44 \pm 2	39 \pm 2	98 \pm 15	160	
4	10	32	228 \pm 12	184 \pm 7	14 \pm 1	51 \pm 2	49 \pm 2	110 \pm 16	63	
5	-133	-146	258 \pm 13	460 \pm 19	13 \pm 2	30 \pm 2	41 \pm 3	111 \pm 16	125	
6	63	-49	234 \pm 20	35 \pm 19	9 \pm 11	116 \pm 16	86 \pm 16	68 \pm 13	84	
7	165	136	207 \pm 12	461 \pm 24	12 \pm 4	12 \pm 6	12 \pm 6	63 \pm 9	229	
8	45	69	365 \pm 41	117 \pm 37	14 \pm 20	50 \pm 24	28 \pm 24	68 \pm 18	142	
9	-194	137	406 \pm 25	235 \pm 57	10 \pm 10	24 \pm 13	39 \pm 13	53 \pm 11	111	
NGC 2841										
1	29	-116	134 \pm 14	22 \pm 13	16 \pm 7	154 \pm 11	61 \pm 10	0 \pm 0	45	HK27
2	-42	86	64 \pm 13	15 \pm 11	0 \pm 5	113 \pm 9	36 \pm 8	0 \pm 0	23	HK51
3	-42	77	43 \pm 7	5 \pm 7	0 \pm 3	127 \pm 10	61 \pm 9	0 \pm 0	37	HK52
4	0	71	87 \pm 7	9 \pm 4	0 \pm 2	145 \pm 9	40 \pm 7	54 \pm 10	82	HK62
NGC 3310										
1	-9	-6	267 \pm 14	380 \pm 16	12 \pm 1	53 \pm 2	41 \pm 1	74 \pm 12	251	HK53
2	6	1	408 \pm 21	204 \pm 9	9 \pm 2	47 \pm 4	34 \pm 3	73 \pm 12	68	HK35
3	1	5	269 \pm 14	314 \pm 13	13 \pm 1	61 \pm 3	36 \pm 1	97 \pm 16	82	HK85
NGC 3351										
1	14	67	32 \pm 4	10 \pm 4	0 \pm 2	77 \pm 6	30 \pm 8	0 \pm 0	14	HK45
2	-58	-135	104 \pm 6	23 \pm 3	9 \pm 2	160 \pm 7	36 \pm 3	82 \pm 14	102	HK80
3	-88	-26	56 \pm 4	11 \pm 3	9 \pm 2	118 \pm 5	33 \pm 3	52 \pm 10	132	HK101
4	-105	-86	137 \pm 7	32 \pm 2	11 \pm 2	179 \pm 7	45 \pm 3	78 \pm 13	96	HK109
5	29	-192	228 \pm 13	93 \pm 8	9 \pm 4	142 \pm 8	59 \pm 5	75 \pm 11	124	
NGC 3368										
1	54	-24	81 \pm 5	18 \pm 3	6 \pm 3	151 \pm 8	83 \pm 4	100 \pm 13	40	
2	-52	25	131 \pm 8	24 \pm 4	0 \pm 1	149 \pm 9	56 \pm 8	141 \pm 25	125	
NGC 3521										
1	13	97	189 \pm 21	110 \pm 44	14 \pm 1	109 \pm 4	47 \pm 2	82 \pm 13	117	
2	-6	80	119 \pm 15	20 \pm 10	14 \pm 1	150 \pm 6	49 \pm 2	60 \pm 9	66	
3	-48	47	220 \pm 21	37 \pm 12	13 \pm 1	123 \pm 5	57 \pm 2	51 \pm 8	73	
NGC 3623										
1	-3	-86	123 \pm 6	17 \pm 5	10 \pm 3	109 \pm 6	46 \pm 6	32 \pm 7	15	

TABLE 2.2. (continued)

No.	Offset ^a		[OII]	[OIII]	HeI	[NII]	[SII]	[SIII]	EW(H β)	Name ^b
	α	δ	3727	4959+5007	5876	6548+6583	6716+6731	9069+9532		
NGC 4258										
1	-318	183	364 \pm 19	100 \pm 6	0 \pm 1	97 \pm 9	47 \pm 9	0 \pm 0	61	
2	-152	-37	333 \pm 17	209 \pm 9	11 \pm 3	91 \pm 6	87 \pm 6	71 \pm 17	26	
3	-32	141	236 \pm 12	92 \pm 4	0 \pm 1	126 \pm 7	82 \pm 6	86 \pm 16	37	
4	-25	130	219 \pm 11	128 \pm 5	10 \pm 2	104 \pm 4	47 \pm 3	103 \pm 16	148	
5	-19	121	248 \pm 13	95 \pm 4	18 \pm 2	118 \pm 5	66 \pm 4	112 \pm 17	104	
NGC 4736										
1	37	9	206 \pm 11	117 \pm 5	12 \pm 1	134 \pm 5	48 \pm 2	103 \pm 16	178	HK8
2	37	3	199 \pm 10	67 \pm 3	13 \pm 2	175 \pm 7	56 \pm 2	121 \pm 19	65	HK9
3	-29	14	174 \pm 9	45 \pm 4	9 \pm 2	155 \pm 7	54 \pm 3	57 \pm 8	139	HK45
4	-38	9	173 \pm 9	34 \pm 2	9 \pm 1	174 \pm 7	63 \pm 3	67 \pm 10	62	HK52
5	-39	20	203 \pm 10	90 \pm 4	12 \pm 1	156 \pm 6	29 \pm 1	97 \pm 14	198	HK53
NGC 4861										
1	0	0	115 \pm 6	799 \pm 33	11 \pm 1	5 \pm 1	17 \pm 1	59 \pm 9	154	
2	6	6	192 \pm 10	653 \pm 27	12 \pm 2	9 \pm 3	26 \pm 4	68 \pm 11	130	
NGC 5236										
1	53	58	46 \pm 12	4 \pm 13	8 \pm 7	117 \pm 11	43 \pm 8	42 \pm 7	21	D2
2	-103	11	95 \pm 16	5 \pm 13	8 \pm 7	126 \pm 10	51 \pm 8	26 \pm 7	31	D3
3	-224	-27	145 \pm 18	45 \pm 13	13 \pm 7	135 \pm 10	40 \pm 8	76 \pm 12	80	D5
4	-262	36	126 \pm 16	21 \pm 13	12 \pm 6	153 \pm 10	54 \pm 7	58 \pm 9	84	D6
NGC 5701										
1	-7	-87	209 \pm 11	186 \pm 9	15 \pm 2	117 \pm 5	45 \pm 5	103 \pm 15	153	
2	79	-60	216 \pm 12	115 \pm 6	12 \pm 4	137 \pm 10	61 \pm 8	84 \pm 16	190	
NGC 6384										
1	-2	-83	181 \pm 11	50 \pm 5	0 \pm 2	148 \pm 8	78 \pm 6	98 \pm 14	80	
2	51	37	81 \pm 10	5 \pm 7	0 \pm 4	120 \pm 27	31 \pm 13	0 \pm 0	80	
3	53	45	115 \pm 10	18 \pm 8	0 \pm 4	145 \pm 12	110 \pm 6	67 \pm 11	63	
4	-32	76	266 \pm 16	71 \pm 8	17 \pm 5	122 \pm 8	72 \pm 10	0 \pm 0	49	
5	-41	70	256 \pm 15	92 \pm 8	0 \pm 3	95 \pm 16	50 \pm 14	0 \pm 0	63	
6	130	110	285 \pm 17	225 \pm 12	10 \pm 4	72 \pm 8	102 \pm 13	84 \pm 14	54	
NGC 7331										
1	-26	-62	225 \pm 21	43 \pm 13	0 \pm 5	129 \pm 12	52 \pm 10	0 \pm 0	64	HK95
2	-31	-27	232 \pm 16	38 \pm 8	0 \pm 3	149 \pm 9	105 \pm 9	0 \pm 0	28	HK98
3	-32	16	200 \pm 21	42 \pm 17	0 \pm 5	143 \pm 10	69 \pm 11	0 \pm 0	13	HK101
4	27	80	250 \pm 16	126 \pm 11	0 \pm 3	130 \pm 8	75 \pm 7	62 \pm 12	34	HK40

Notes to Table 2.2.

Fluxes given in units of $H\beta = 100$ ^aPositive in E and N directions^bMeaning of catalog names: HK: Hodge & Kennicutt 1983; H: Hodge 1976; P: Pellet *et al.* 1978;CCM: Carranza *et al.* 1969; GS: Garnett & Shields 1987; D: Dufour *et al.* 1980

lines for 99 H II regions in 20 galaxies (six are in common with our sample), but limited to $\lambda < 7500 \text{ \AA}$. The sequences for the two datasets closely follow each other.

3. Photoionization models

In order to interpret the emission-line data for our H II regions, a set of nebular models were calculated with CLOUDY (Ferland 1996), version 90.01. Given the spectral energy distribution (SED) of the ionizing source (both a single star and a stellar cluster were considered), the ionizing photon luminosity, the chemical composition and the geometry of the gas, the code solves for the ionization and thermal equilibrium of the nebula. A relevant aspect of the version of the code used for these calculations is the inclusion of Opacity Project data. For our models the important change (approaching a factor of two) with respect to previous versions of the code regards the O^+ photoionization cross section, which no longer shows a jump at the $2s - 2p$ edge. A further change in the OII - OIII balance is caused by new collision strengths for some OIII lines. To assess the effect of the new atomic data on the final results, a set of single-star photoionization models (described in the next Section) were calculated with an older version of CLOUDY (*v.* 84.12), and compared with the results of *v.* 90.01. The newer version predicts an average decrease of the [OII] line intensity of approximately 20%, mostly counterbalanced by an increase in the [OIII] emission. The effect on the empirical abundance indicator is an average $\Delta(\log R_{23}) = \log R_{23}(v. 84) - \log R_{23}(v. 90) \simeq 0.028$ ($\log R_{23} = -0.3$ to 1.1), decreasing from $\Delta(\log R_{23}) \simeq 0.07$ at $\log R_{23} = 0$ to $\Delta(\log R_{23}) \simeq -0.01$ at $\log R_{23} = 1$. This translates into an approximate 0.025 dex increase in the (O/H) abundance scale, based on the calibration given by Zaritsky *et al.* (1994).

In the following the input parameters of the models will be described, and the

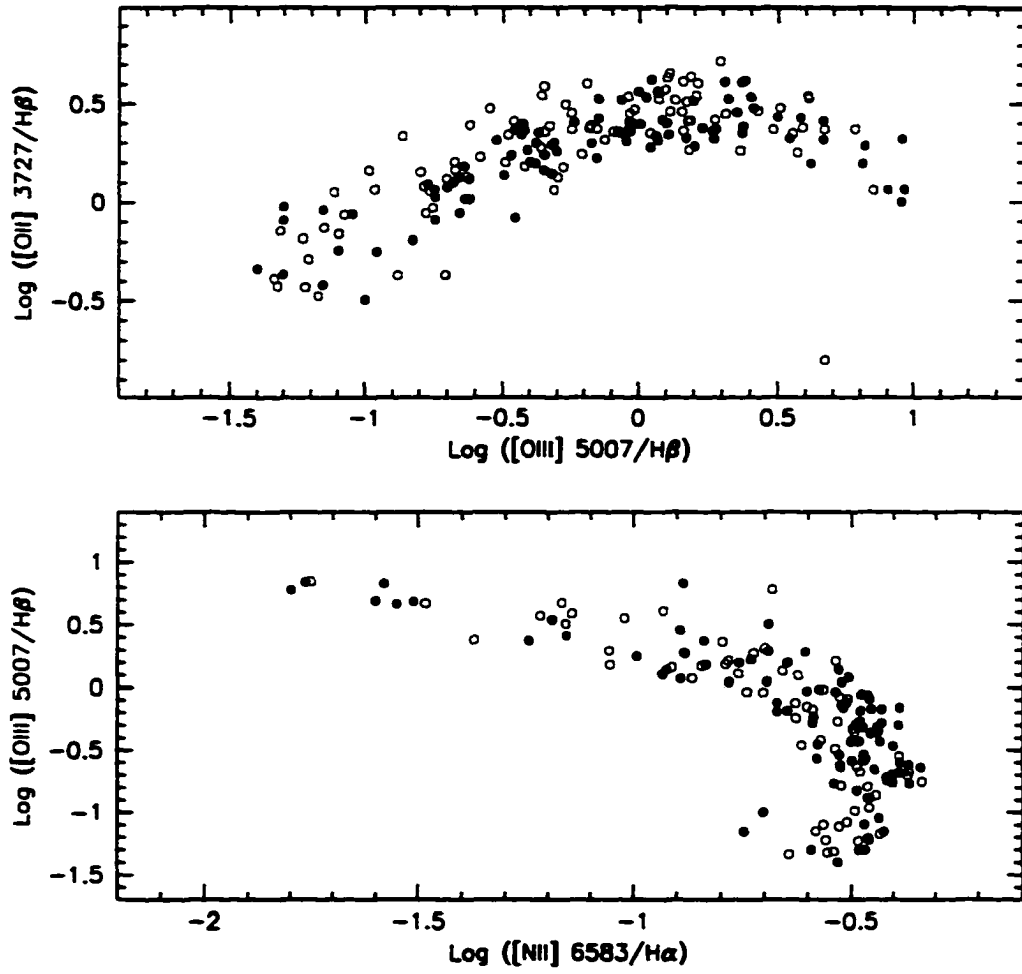


Figure 3 Excitation sequences in terms of (a) $[\text{OII}]/\text{H}\beta$ vs $[\text{OIII}]/\text{H}\beta$ and (b) $[\text{OIII}]/\text{H}\beta$ vs $[\text{NII}]/\text{H}\alpha$. Filled circles indicate observations from this work, open circles are data from McCall *et al.* (1985).

model results will be shown in terms of diagnostic diagrams. Tables containing the predicted intensities for the most important emission lines will also be presented.

3.1. Input parameters

Spectral energy distributions

As mentioned above, to better interpret the data two different SEDs were considered as the ionizing source:

Single star - The line-blanketed LTE Kurucz (1992) stellar atmospheres, which include the effects of bound-free opacity from heavy elements, were adopted for consistency with the cluster models. The $\log g = 5$ models were chosen to match the nebular metal abundance (Figure 4). Nebular models were calculated at $Z = 0.1 Z_{\odot}$, $0.25 Z_{\odot}$, Z_{\odot} and $2 Z_{\odot}$, and for $T_{\text{eff}} = 37,500$ K, $40,000$ K, $45,000$ K, $50,000$ K and $60,000$ K.

The choice of the available stellar atmospheres (*e.g.* Hummer & Mihalas 1970, Mihalas 1972 and Kurucz 1979) produces well-known differences when computing H II region photoionization models (Skillman 1989, Evans 1991). Non-LTE, line blanketed atmosphere models which include the effects of stellar winds are now becoming available (Kunze *et al.* 1992, Schaerer & de Koter 1997). The predicted modifications, especially on the He II continuum above 54 eV, with respect to older models have important consequences for the ionization structure of H II regions (Stasińska & Schaerer 1997). In spite of the complexity of this field, our choice of the Kurucz models is justified by our goal, which is to construct a sequence of effective temperature vs metallicity, rather than define an absolute scale (in this regard, see the discussions in Skillman 1989 and Garnett 1989).

Star cluster - Following the work by McGaugh (1991), who considered as the

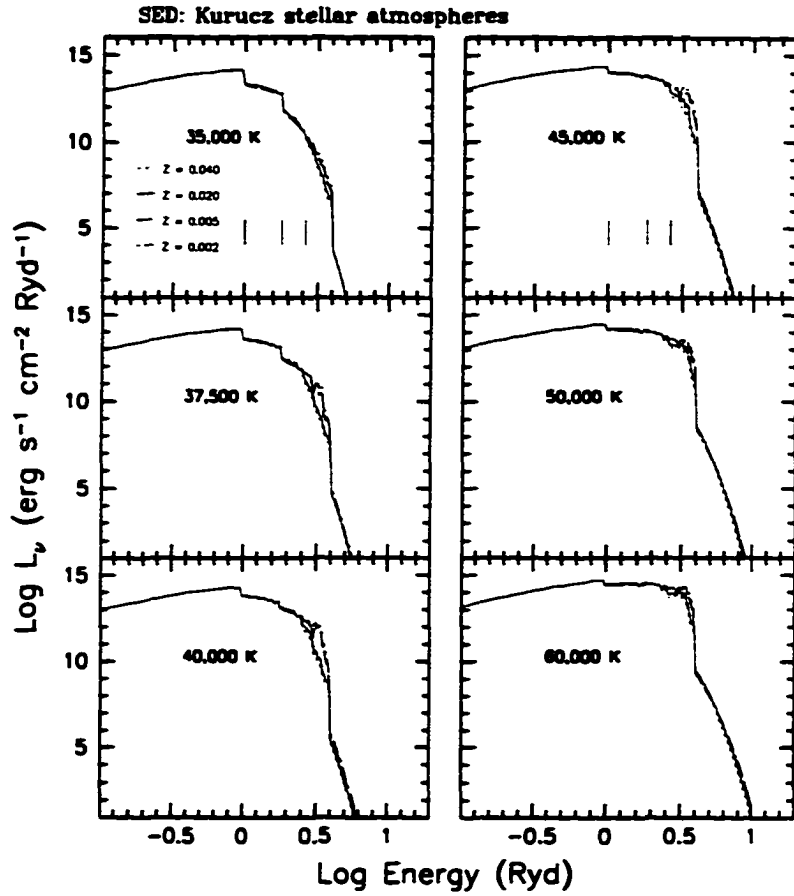


Figure 4 SEDs for the Kurucz stellar atmospheres. The energies corresponding to the ionization potential of Hydrogen (1 Ryd), Helium (1.8 Ryd) and Oxygen (2.6 Ryd) are indicated by the vertical marks.

ionizing photon source for the model nebulae a zero-age cluster synthesized with a nearly-Salpeter IMF and stellar evolutionary tracks by Maeder (1990). different authors have calculated cluster SEDs with different IMFs and the newer stellar models from the Geneva or Padova groups, taking into account the temporal evolution of the clusters (García-Vargas & Díaz 1994, Cerviño & Mas-Hesse 1994, García-Vargas *et al.* 1995, Leitherer & Heckman 1995). These evolutionary population synthesis models showed the importance of later stages of massive star evolution (Wolf-Rayet phase) in the emission-line spectra after 3-4 Myr from the initial burst of star formation.

For our nebular models we adopted the SEDs calculated by Leitherer & Heckman (1995), as presented in Leitherer *et al.* (1996a) (available either via CD-ROM or anonymous ftp). These SEDs (Figures 5, 6 and 7) were calculated for four different metallicities ($0.1 Z_{\odot}$, $0.25 Z_{\odot}$, Z_{\odot} and $2 Z_{\odot}$) and three IMFs ($\alpha = 2.35$ and $M_{up} = 100 M_{\odot}$, $\alpha = 2.35$ and $M_{up} = 30 M_{\odot}$, $\alpha = 3.35$ and $M_{up} = 100 M_{\odot}$, where the IMF is given by $dN/dm \propto m^{-\alpha}$ between $M_{low} = 1 M_{\odot}$ and M_{up}), at 1 Myr intervals from 1 to 25 Myr. The stellar models of Maeder (1990) and Maeder & Meynet (1988) were used for the synthesis, together with Kurucz's (1992) atmospheres for the non-WR phases, and the non-LTE models of Schmutz *et al.* (1992), which include the effects of an expanding atmosphere, for WRs. Both the instantaneous burst and the continuous star formation results were used in our photoionization models. The latter were calculated for ages 1 to 6 Myr, since at older ages most clusters will lack the necessary ionizing luminosity to produce an H II region (García-Vargas & Díaz 1994). For more details on the cluster SEDs, the reader is referred to the original paper.

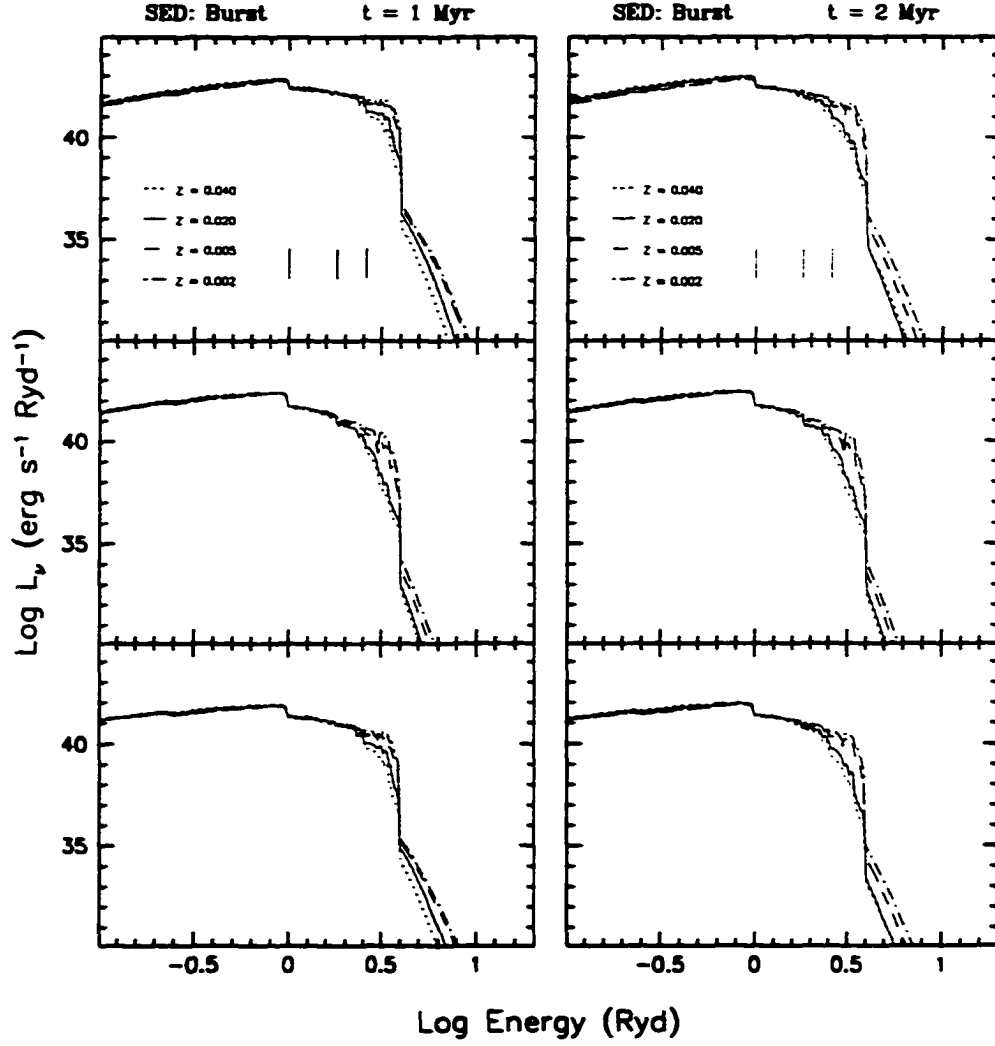


Figure 5 Cluster SEDs for ages of 1 (left) and 2 (right) Myr after the initial burst, and for the Salpeter (top), $M_{up} = 30 M_{\odot}$ (middle), and $\alpha = 3.30$ (bottom) IMFs. The energies corresponding to the ionization potential of Hydrogen (1 Ryd), Helium (1.8 Ryd) and Oxygen (2.6 Ryd) are indicated by the vertical marks.

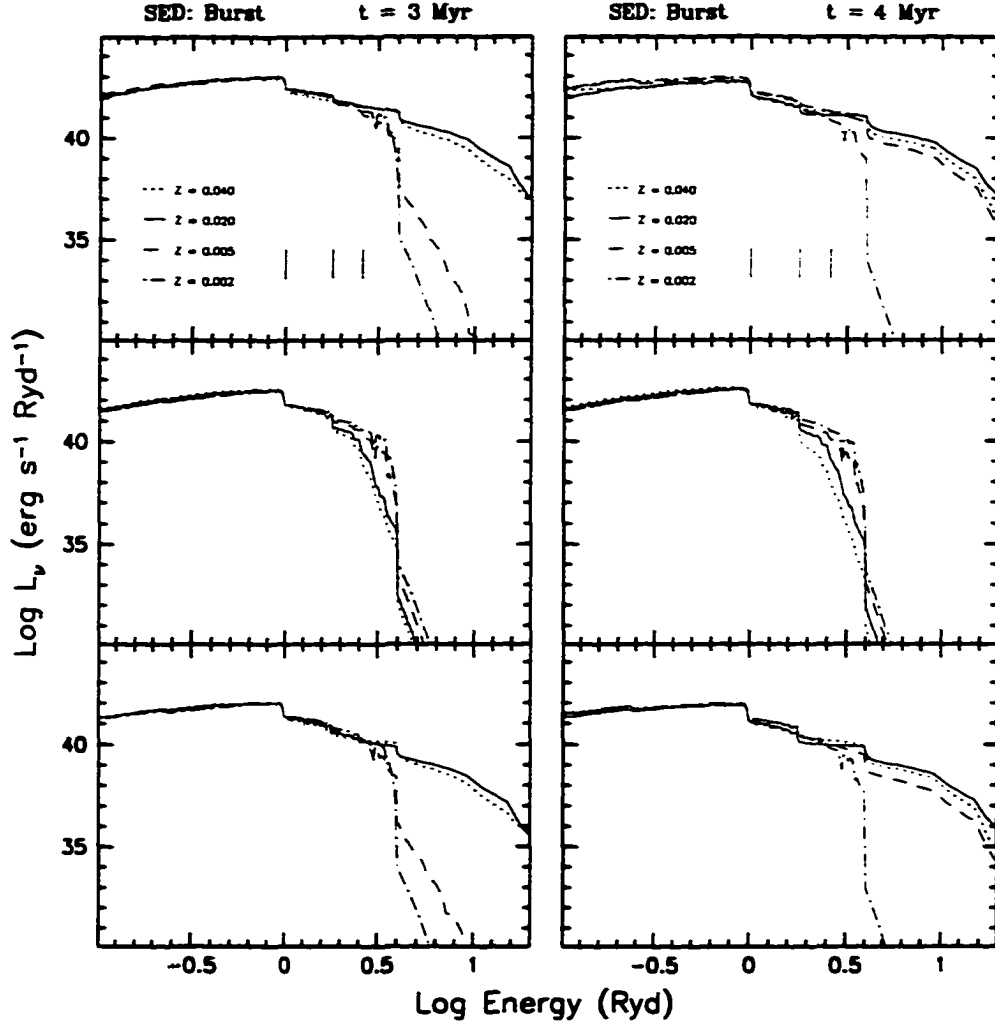


Figure 6 Cluster SEDs for ages of 3 (left) and 4 (right) Myr after the initial burst, and for the Salpeter (top), $M_{up} = 30 M_{\odot}$ (middle), and $\alpha = 3.30$ (bottom) IMFs. The energies corresponding to the ionization potential of Hydrogen (1 Ryd), Helium (1.8 Ryd) and Oxygen (2.6 Ryd) are indicated by the vertical marks.

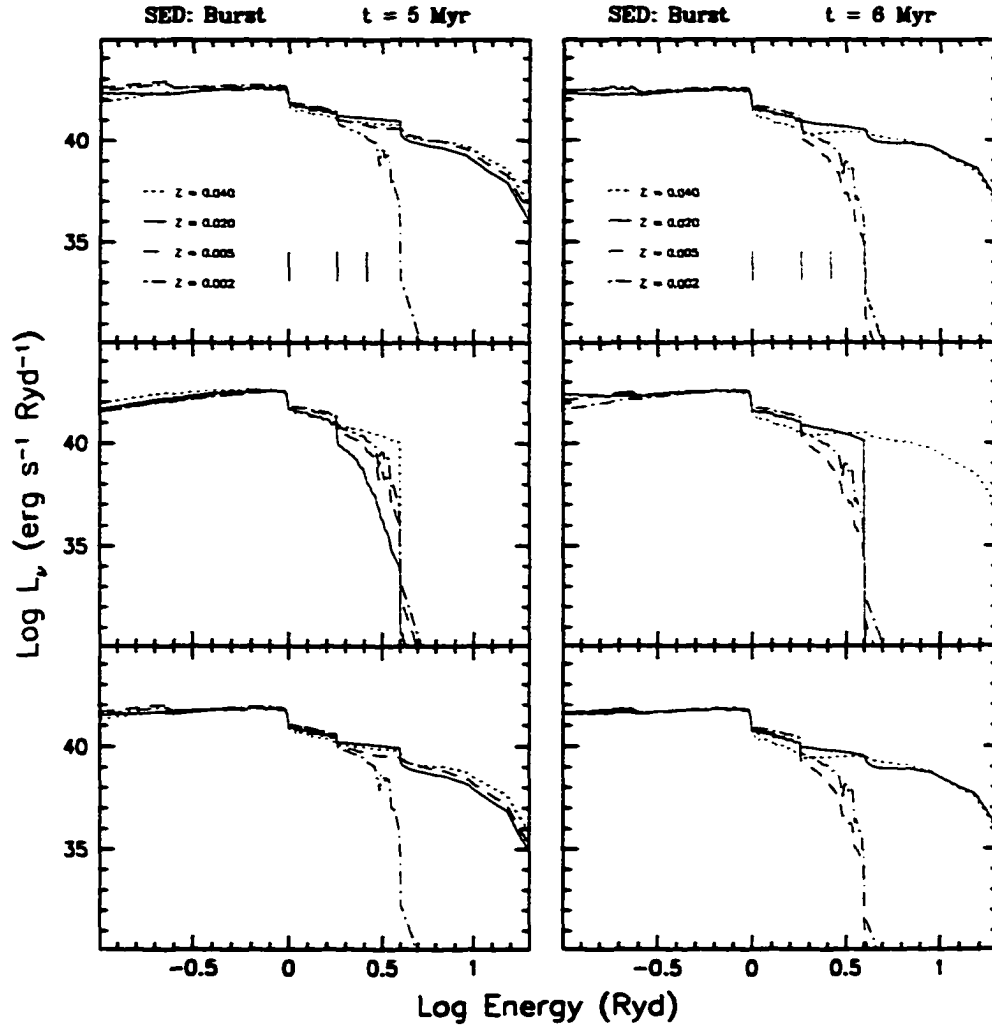


Figure 7 Cluster SEDs for ages of 5 (left) and 6 (right) Myr after the initial burst, and for the Salpeter (top), $M_{up} = 30 M_\odot$ (middle), and $\alpha = 3.30$ (bottom) IMFs. The energies corresponding to the ionization potential of Hydrogen (1 Ryd), Helium (1.8 Ryd) and Oxygen (2.6 Ryd) are indicated by the vertical marks.

Nebular gas parameters

The abundance of the gas is consistent with the metallicity of the ionizing stars. The solar elemental abundances are adopted as defined in Grevesse & Anders (1989). To take depletion of refractory elements onto dust grains into account the elements Mg, Al, Ca, Fe, Ni and Na were depleted by a factor of 10, and Si by a factor of 2 (Garnett *et al.* 1995), relative to the solar abundance (consistent with Garnett & Kennicutt 1997). The He abundance was scaled according to $Y = Y_p + \Delta Y / \Delta Z Z$, where $Y = 4y / (1 + 4y)$, $y = \text{He}/\text{H}$ by number, and Z is the metallicity ($Z_\odot = 0.02$). We have adopted $Y_p = 0.23$ (Pagel *et al.* 1992), and $\Delta Y / \Delta Z = 2.5$, but this value is uncertain. Table 3 summarizes the adopted solar composition, with the above-mentioned depletions taken into account. A few models were also calculated for a N/O ratio dependent on metallicity (larger N/O at higher abundances).

The adopted geometry was spherical, with a constant gas density $n = 50 \text{ cm}^{-3}$, and with a filling factor ϵ adjusted so as to obtain models with three different ionization parameters, $\log U = -2, -3$ and -4 . The dimensionless ionization parameter U is defined as

$$U = \frac{Q_{H^0}}{4\pi R_s^2 n c},$$

where Q_{H^0} is the number of hydrogen-ionizing photons ($E > 13.6 \text{ eV}$) emitted per second, R_s is the Strömgren radius, n is the hydrogen density and c is the speed of light. U depends on the electron temperature, T_e , through the Strömgren radius dependence on the case B recombination coefficient $\alpha_B(T)$:

$$R_s = \left(\frac{3}{4\pi} \frac{Q_{H^0}}{\alpha_B n^2 \epsilon} \right)^{1/3},$$

Table 3. Adopted solar abundances

Element	log abundance ^a
He.....	-1.00
C.....	-3.44
N.....	-3.95
O.....	-3.07
Ne.....	-3.91
Mg.....	-5.42
Al.....	-6.53
Si.....	-4.75
S.....	-4.79
Ar.....	-5.44
Ca.....	-6.64
Fe.....	-5.33
Ni.....	-6.75
Na.....	-6.67

^arelative to HTable 4. Q_{He^0}/Q_{H^0} from model stellar atmospheres

T_{eff} (K)	$2 Z_{\odot}$	Z_{\odot}	$0.25 Z_{\odot}$	$0.1 Z_{\odot}$
60,000	0.35	0.38	0.45	0.48
50,000	0.26	0.28	0.32	0.34
45,000	0.20	0.22	0.25	0.26
40,000	0.10	0.10	0.10	0.11
35,000	0.01	0.01	0.01	0.01

with $\alpha_B(T) \propto T_e^{-1}$, so that we can rewrite

$$U = A(Q_{H^0} n \epsilon^2)^{1/3}.$$

with $A \propto T_e^{-2/3}$. We had therefore to iterate a few times, from an initial guess for the filling factor, to obtain the desired $\log U$. A few models were calculated for $n = 10 \text{ cm}^{-3}$ and $n = 150 \text{ cm}^{-3}$, to estimate gas density effects, which are quite strong at higher metallicities (Díaz *et al.* 1991).

We fixed the total number of ionizing photons to $Q_{H^0} = 10^{51} \text{ s}^{-1}$, the equivalent of ~ 90 O7 V stars (Vacca 1994), which, assuming a standard IMF, corresponds to an initial cluster mass of $\gtrsim 2 \times 10^4 M_\odot$ (including stars in the 1–100 M_\odot range). The exact value is of no practical importance, since it acts as a scaling factor, and models with a given ionizing spectrum shape and differing Q_{H^0} , n and ϵ , but with the same U are homologous, producing the same emission-line relative strengths (as long as the density is below the critical limit for collisional de-excitation) and the same nebular ionization structure. The initial cluster mass considered here is large enough that our models remain unaffected by the stochastic effects described by García-Vargas & Díaz (1994) and Cerviño & Mas-Hesse (1994). We also emphasize that CLOUDY computes nebular models in which a compact ionizing source lies at the center of a spherically symmetric gas distribution. We don't expect significant changes in the case of a more extended ionizing source (*e.g.* a loose OB association) as long as it remains unresolved by the spectrograph slit, since the emission-line properties are controlled by a quantity integrated over the volume of the nebula (the ionization parameter). From our data we do not see any measurable effect related to the fact that for the nearest galaxies the slit aperture is sampling a region much smaller than the Strömgren radius. The integration along the line of sight through the nebula is likely to be responsible for this.

All of our models are ionization-bounded, with the calculation stopped at a gas temperature of 100 K (the optical opacity of the gas is negligible even at a much higher temperature), and include a 30 km s^{-1} turbulent velocity term. This additional velocity field increases the line widths (already broadened by thermal motions), affecting the energy budget of the H II regions. A cooling of the nebulae results through infrared fine-structure lines, which can become optically thin as a result of the line broadening. The effects of dust have not been taken into account, except for the depletion of refractory elements.

3.2. Model results

A useful quantity that can be readily estimated from the stellar atmosphere SEDs is the ratio of He⁰ ionizing photons ($\lambda \leq 504 \text{ \AA}$) to H ionizing photons ($\lambda \leq 912 \text{ \AA}$), $Q_{\text{He}^0}/Q_{\text{H}^0}$, for each metallicity and T_{eff} . For a particular atmosphere model, this ratio describes the hardness of the radiation field, and has been used (Mas-Hesse & Kunth 1991, García-Vargas & Díaz 1994) to define an equivalent ionizing temperature, T_{eq} , as the T_{eff} of a star whose SED produces a given $Q_{\text{He}^0}/Q_{\text{H}^0}$. A calibration of this ratio for the Kurucz (1992) $\log g = 5$ atmospheres is given in Table 4. Clearly the radiation field becomes harder as T_{eff} increases and at lower metallicities.

The $Q_{\text{He}^0}/Q_{\text{H}^0}$ ratios for the cluster models are shown in Table 5. As pointed out by García-Vargas *et al.* (1995), the evolution of T_{eq} is non-monotonic at higher metallicities, due to the hardening of the radiation after the WR phase sets in. This effect disrupts the T_{eq} – metallicity relationship which is clearly present for ages smaller than about 3 Myr. The effects is stronger with increasing metallicities, because of the larger number of WR stars produced.

Table 5. Q_{He^p}/Q_{He^0} from cluster models

age (Myr)	2 Z_{\odot}	Z_{\odot}	0.25 Z_{\odot}	0.1 Z_{\odot}
$M_{up} = 100$ $\alpha = 2.35$				
1.....	0.19	0.22	0.30	0.35
2.....	0.11	0.15	0.24	0.29
3.....	0.27	0.22	0.13	0.16
4.....	0.29	0.21	0.18	0.10
5.....	0.29	0.31	0.14	0.05
6.....	0.24	0.25	0.01	0.03
$M_{up} = 30$ $\alpha = 2.35$				
1.....	0.07	0.08	0.12	0.15
2.....	0.05	0.07	0.11	0.14
3.....	0.03	0.05	0.09	0.13
4.....	0.01	0.03	0.06	0.11
5.....	0.18	0.01	0.03	0.06
6.....	0.24	0.20	0.01	0.03
$M_{up} = 100$ $\alpha = 3.30$				
1.....	0.17	0.19	0.26	0.30
2.....	0.10	0.13	0.21	0.26
3.....	0.18	0.15	0.12	0.16
4.....	0.23	0.15	0.13	0.10
5.....	0.25	0.25	0.10	0.05
6.....	0.20	0.21	0.01	0.03

A direct comparison of our model results with those of other authors is made difficult by the use of different input parameters and photoionization codes. However, a small set of solar composition models, with $n = 10 \text{ cm}^{-3}$, was compared with the models by Stasińska & Leitherer (1996). The latter were calculated with the code PHOTO (Stasińska 1990) and the same cluster SEDs used in the present work, for different cluster masses. Due to the evolution of the massive stars, the total ionizing luminosity (and hence the ionization parameter) is a function of cluster age, while in our models we have kept it constant, in order to set the ionization parameter to the desired values. The Stasińska & Leitherer models for cluster masses $M_* = 10^3$ and $10^6 M_\odot$ and ages between 1 and 6 Myr ($M_{up} = 100 M_\odot$) have a ionization parameter in the range -1.6 to -2.9 , and can therefore be compared to our $\log U = -2$ and -3 models. Figure 8 shows the comparison regarding $[\text{OIII}] \lambda 5007$ vs $\text{H}\beta$ and $[\text{OII}] \lambda 3727$ vs $\text{H}\beta$. There is a good agreement, considered the differences in ionization parameter between the two sets of models, and the different photoionization codes used.

Our models are here presented in the form of tables and figures, and will be discussed in the following sections. The tables are appended at the end of this Chapter (Section 7).

Plots with the model results

A set of figures follows, comparing the cluster models with the observations. The same model sequences are shown for the single-star models (Figures 9–17), the cluster models with burst star formation mode (Figures 18–26) and the cluster models with continuous star formation mode (Figures 27–35). In the case of the cluster models the plots show the results from 1 to 6 Myr for the three IMFs

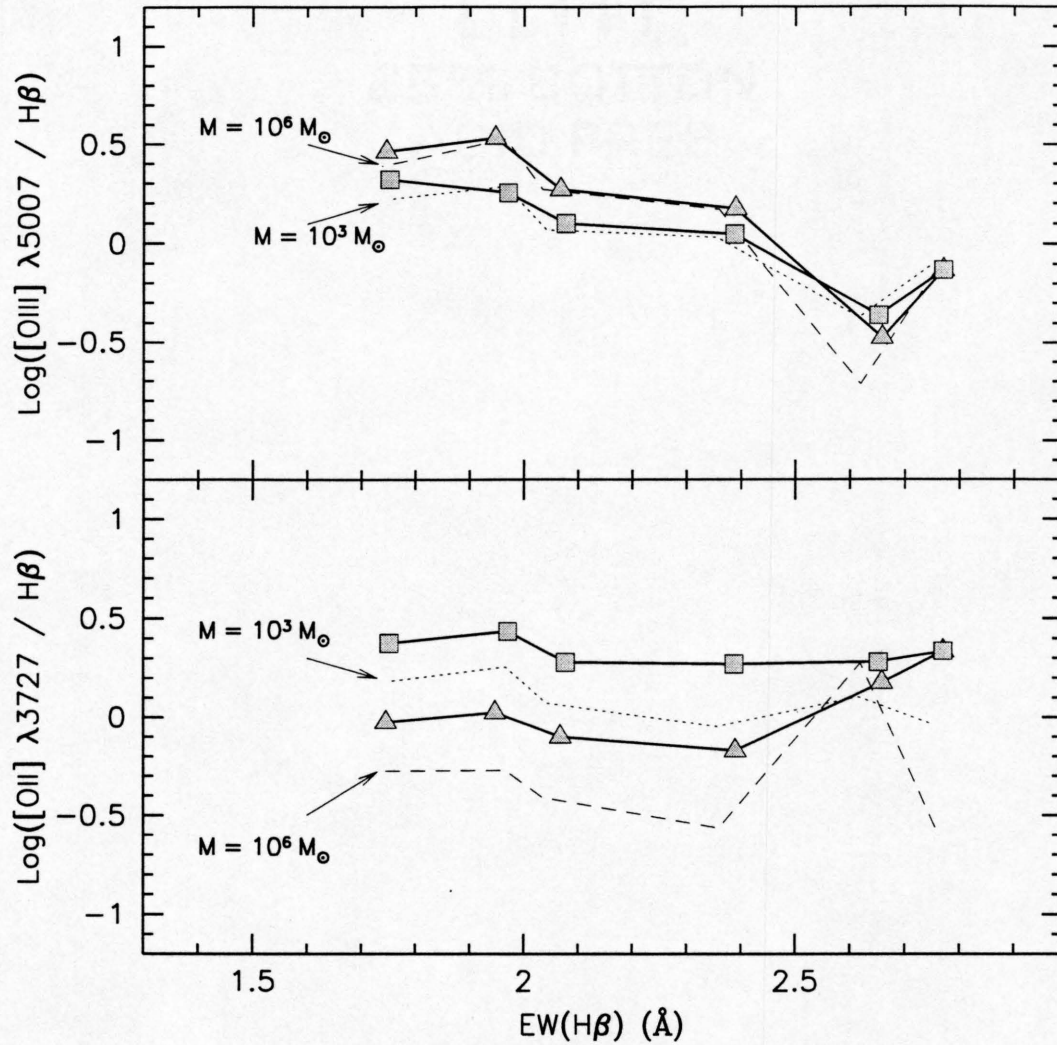


Figure 8 Comparison with the models of Stasińska & Leitherer (1996). These are shown for an ionizing cluster mass $M = 10^3$ and $M = 10^6 M_\odot$, with dotted and dashed lines, respectively. Our models for $\log U = -2$ and $\log U = -3$ (calculated for $n = 10 \text{ cm}^{-3}$) are shown by the continuous lines with triangle and square symbols, respectively. All models are for solar composition. (*Top*) $[OIII] \lambda 5007$ vs $EW(H\beta)$. (*Bottom*) $[OII] \lambda 3727$ vs $EW(H\beta)$.

considered: $M_{up} = 100 M_{\odot}$, $\alpha = 2.35$ (Salpeter). $M_{up} = 30 M_{\odot}$, $\alpha = 2.35$.
and $M_{up} = 100 M_{\odot}$, $\alpha = 3.30$. Different symbols are used for the 3 ionization
parameters ($\log U = -2, -3, -4$), as explained in the captions.

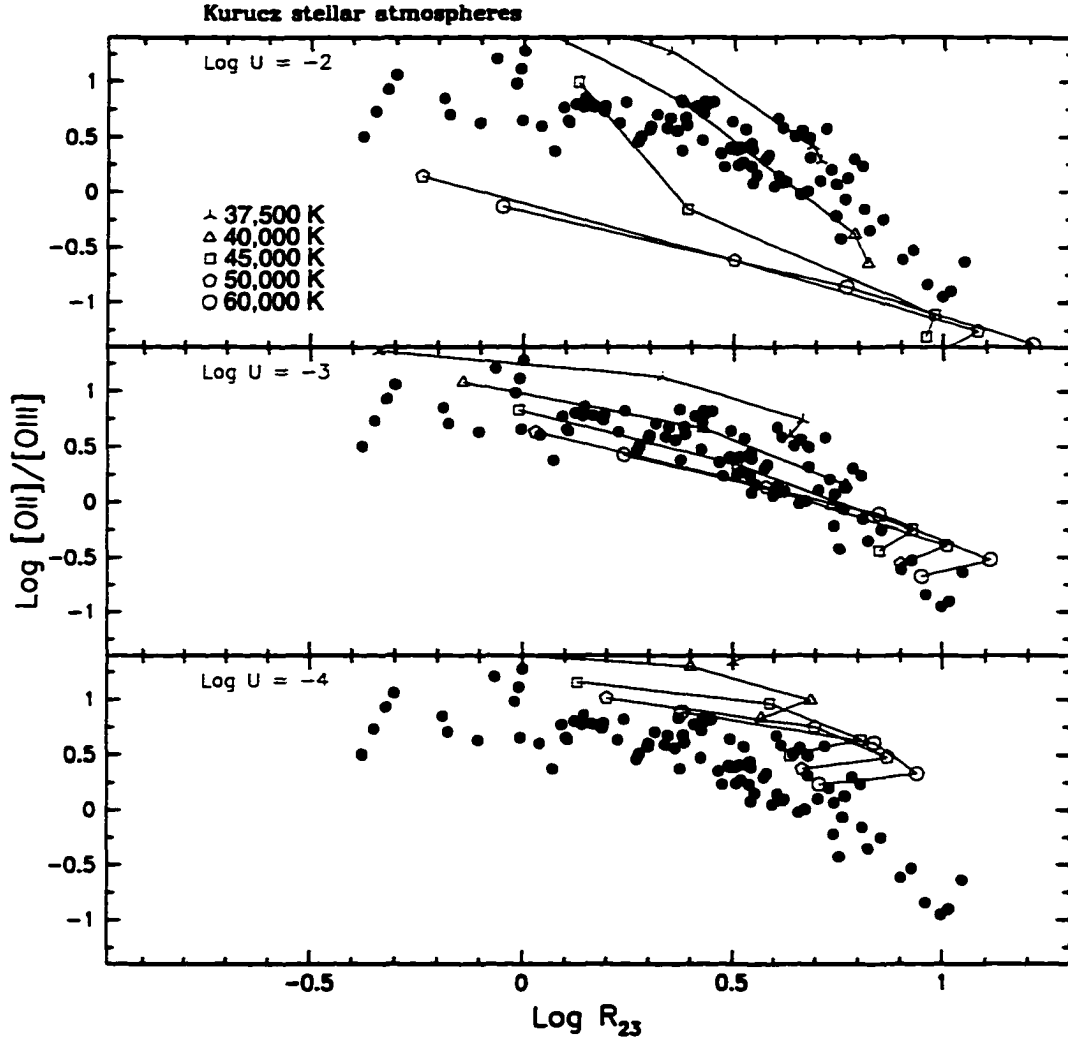


Figure 9 Single-star model results for $[\text{OII}]/[\text{OIII}]$ vs $\log R_{23}$, for $\log U = -2$ (top), $\log U = -3$ (middle) and $\log U = -4$ (bottom). The lines connect points at the 4 metallicities considered ($0.1 Z_{\odot}$, $0.25 Z_{\odot}$, Z_{\odot} and $2 Z_{\odot}$). The stellar T_{eff} is coded as follows: 37,500 K: three-pointed star; 40,000 K: triangle; 45,000 K: square; 50,000 K: pentagon; 60,000 K: circle. The dots are the observed values.

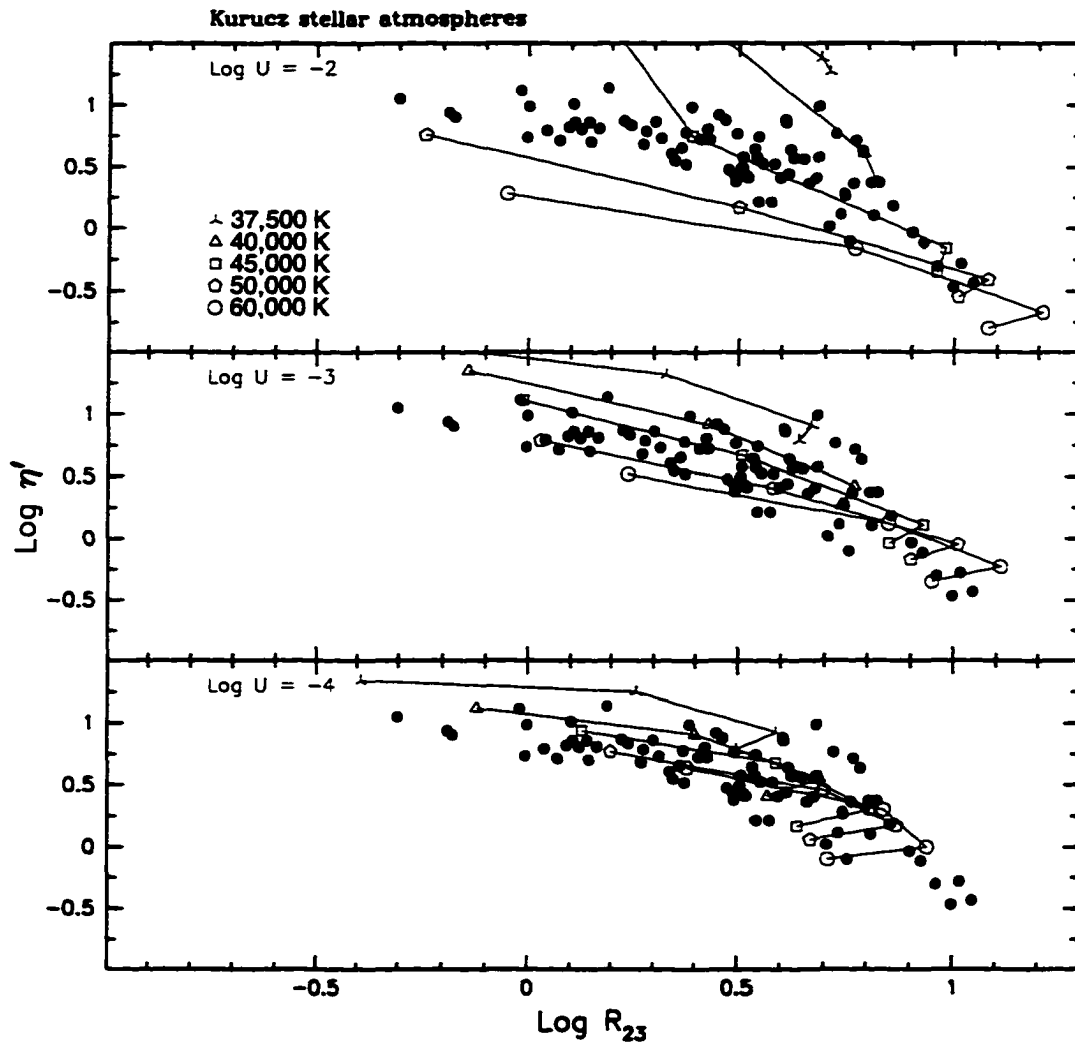


Figure 10 Single-star model results for η' vs $\text{Log } R_{23}$. See Figure 9 for explanations.

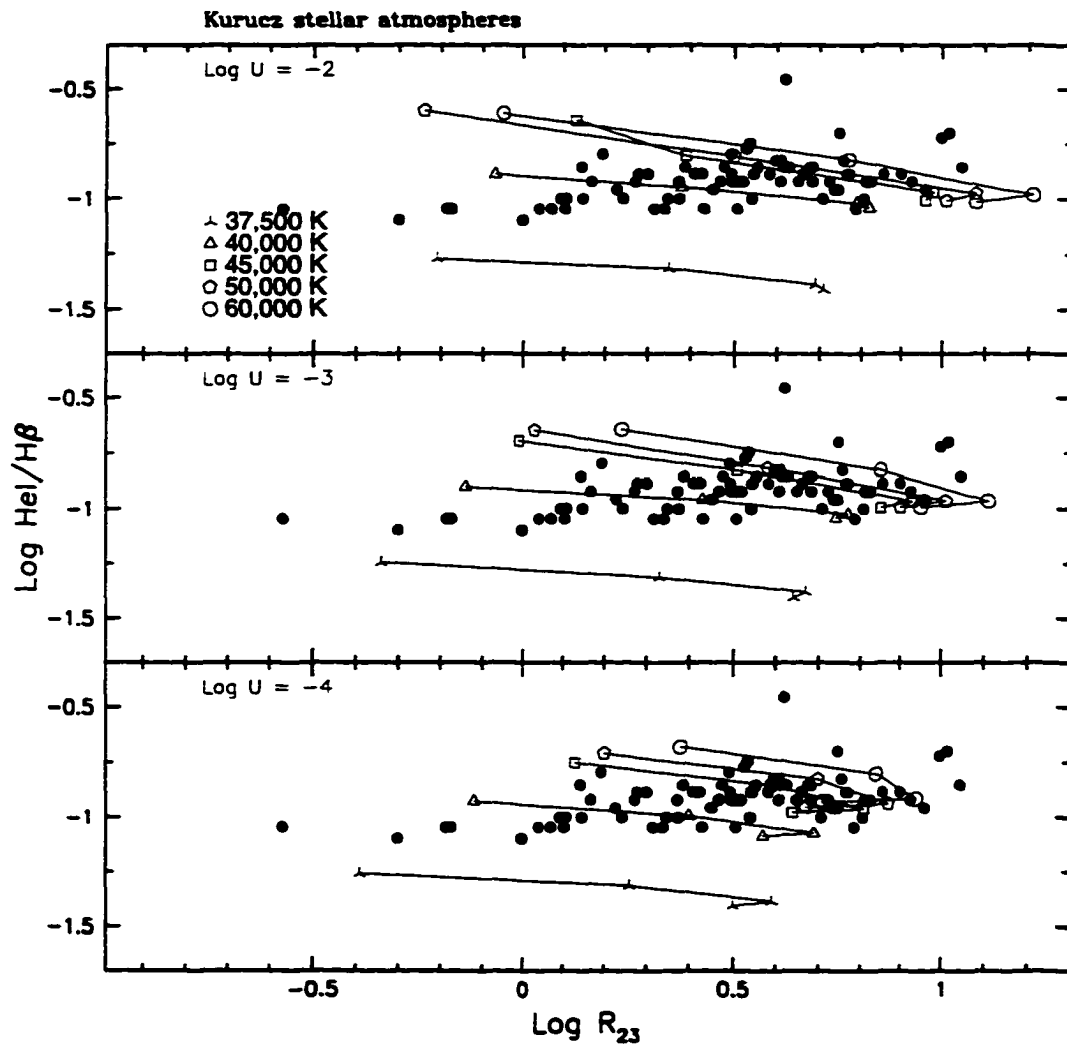


Figure 11 Single-star model results for He I $\lambda 5876/H\beta$ vs Log R_{23} . See Figure 9 for explanations.

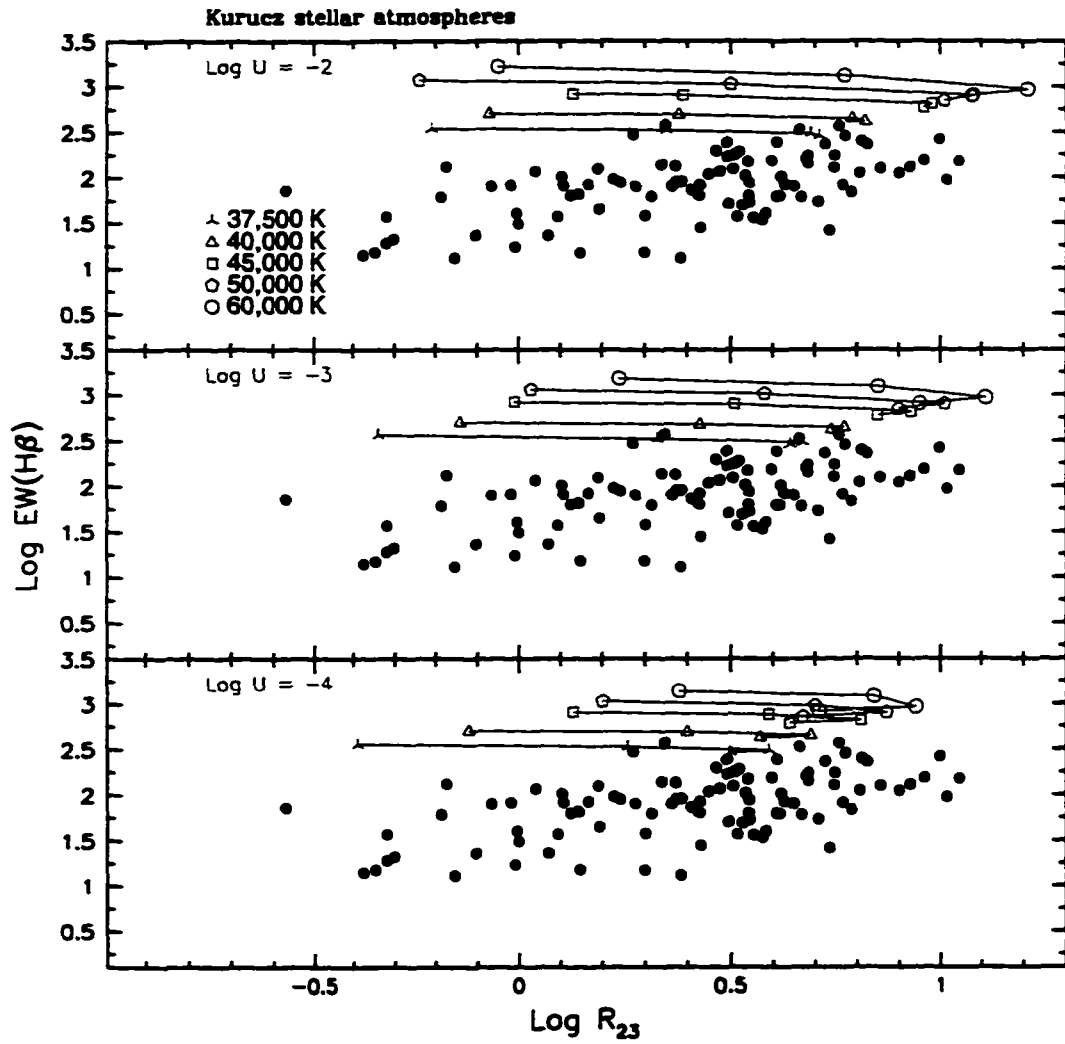


Figure 12 Single-star model results for $\text{EW}(\text{H}\beta)$ vs $\text{Log } R_{23}$. See Figure 9 for explanations.

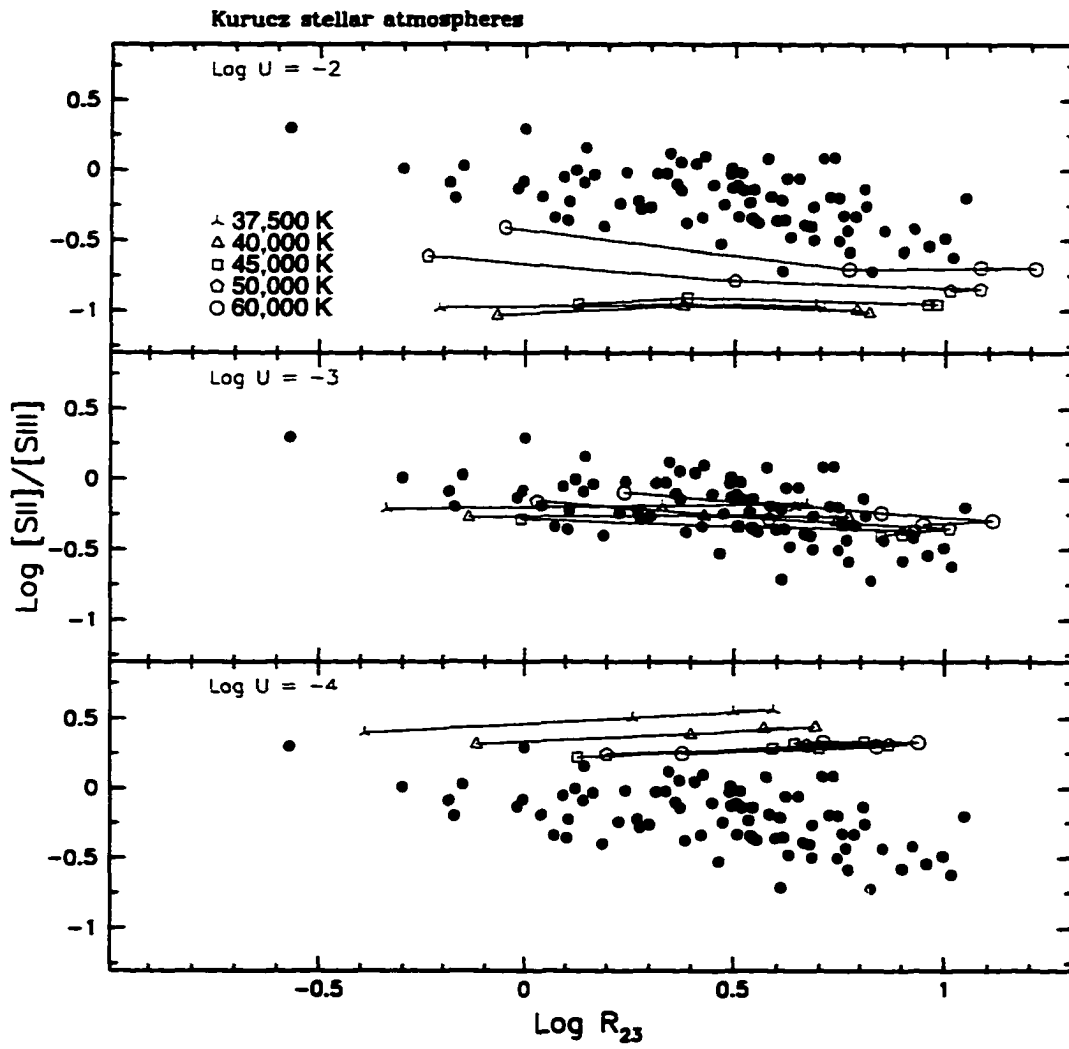


Figure 13 Single-star model results for $[\text{SII}]/[\text{SIII}]$ vs $\text{Log } R_{23}$. See Figure 9 for explanations.

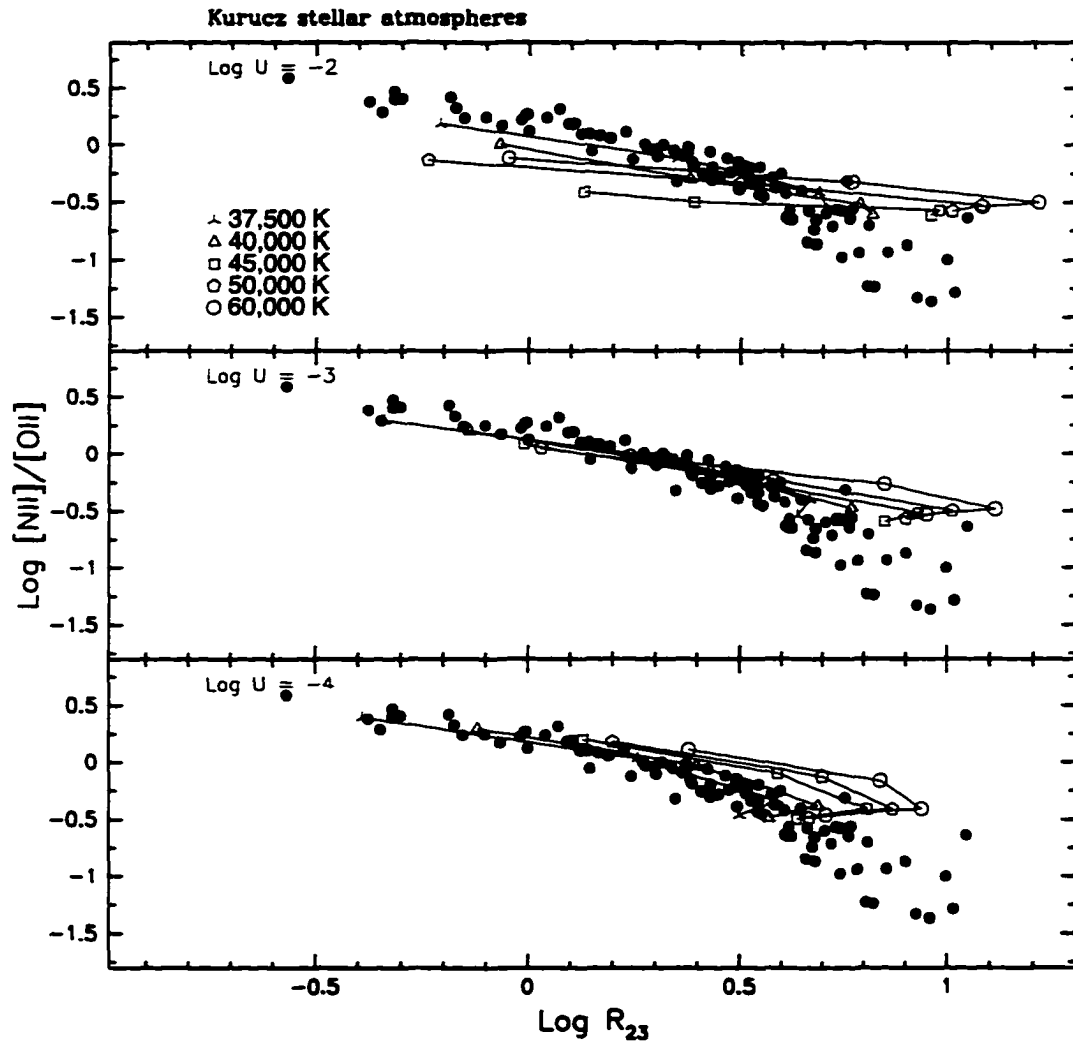


Figure 14 Single-star model results for $[\text{NII}]/[\text{OII}]$ vs $\text{Log } R_{23}$. See Figure 9 for explanations.

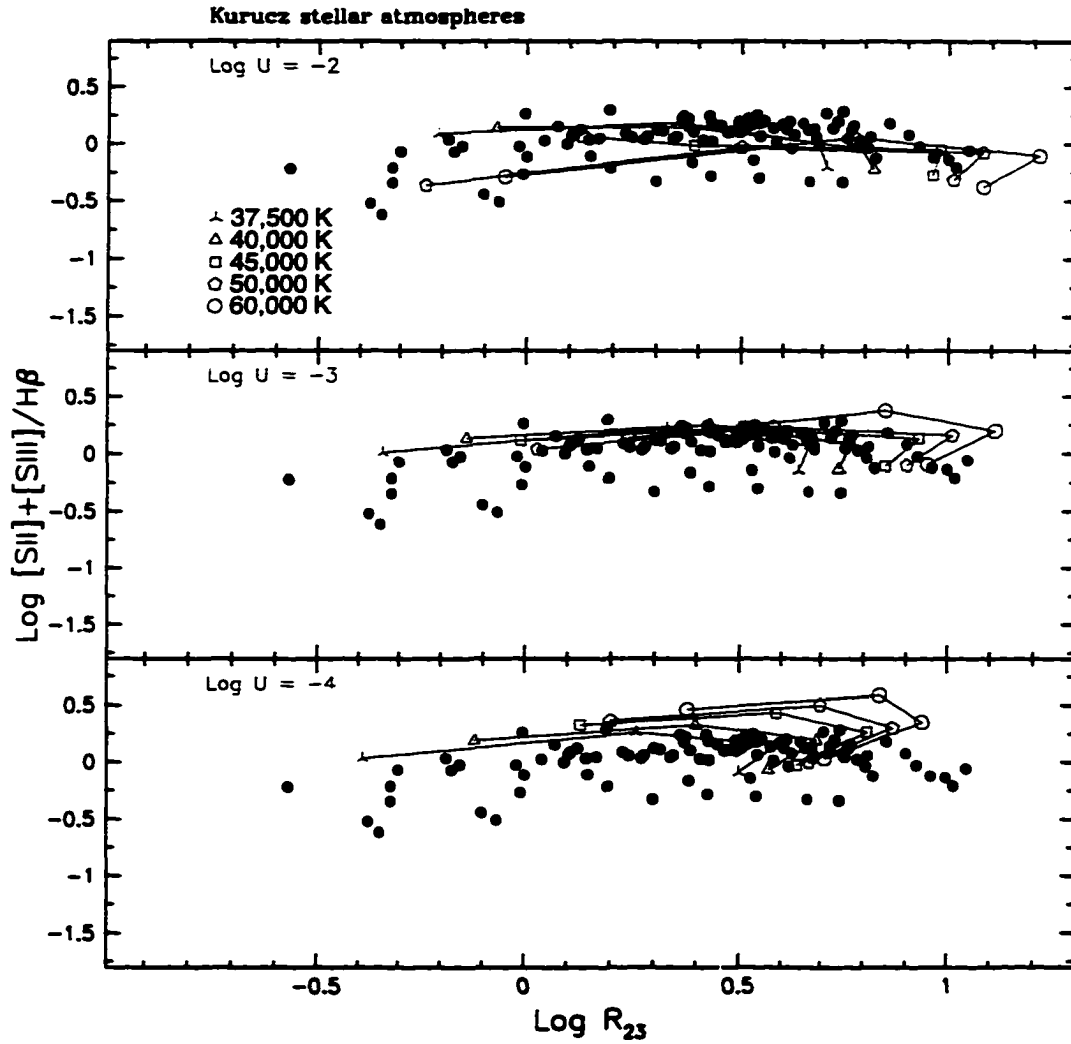


Figure 15 Single-star model results for $([SII] + [SIII]) / H\beta$ vs Log R_{23} . See Figure 9 for explanations.

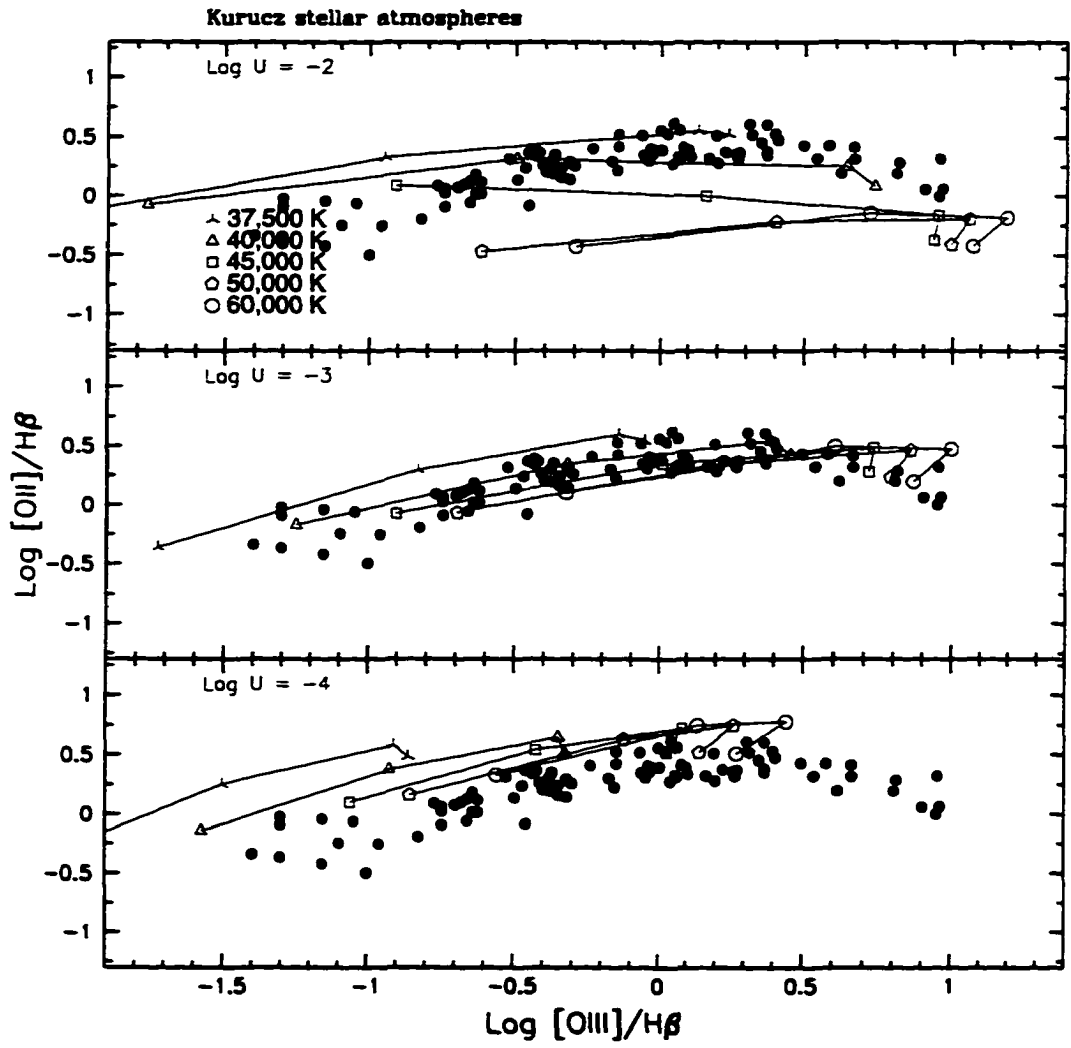


Figure 16 Single-star model results for $[\text{OII}]/\text{H}\beta$ vs $[\text{OIII}]/\text{H}\beta$. See Figure 9 for explanations.

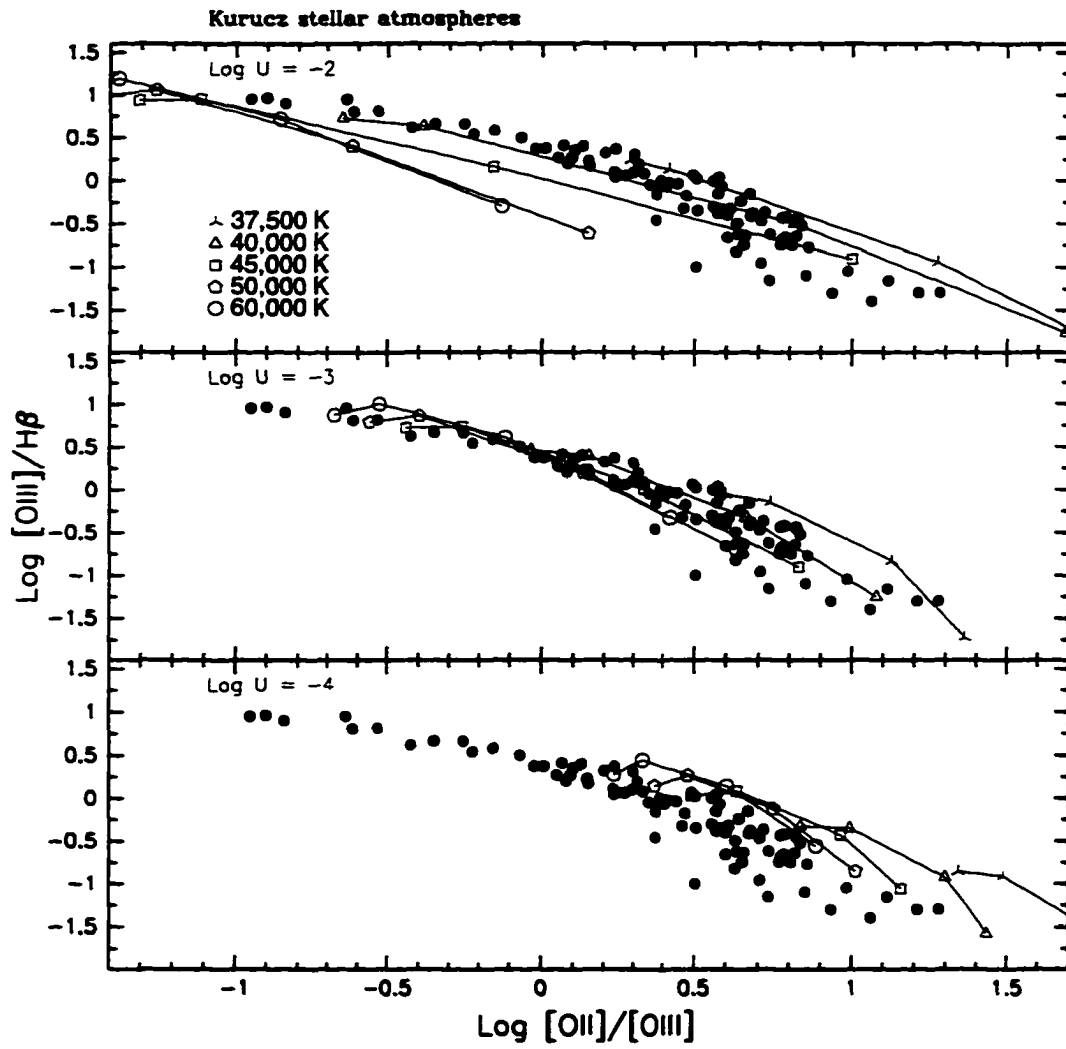


Figure 17 Single-star model results for $[\text{OIII}]/\text{H}\beta$ vs $[\text{OII}]/[\text{OIII}]$. See Figure 9 for explanations.

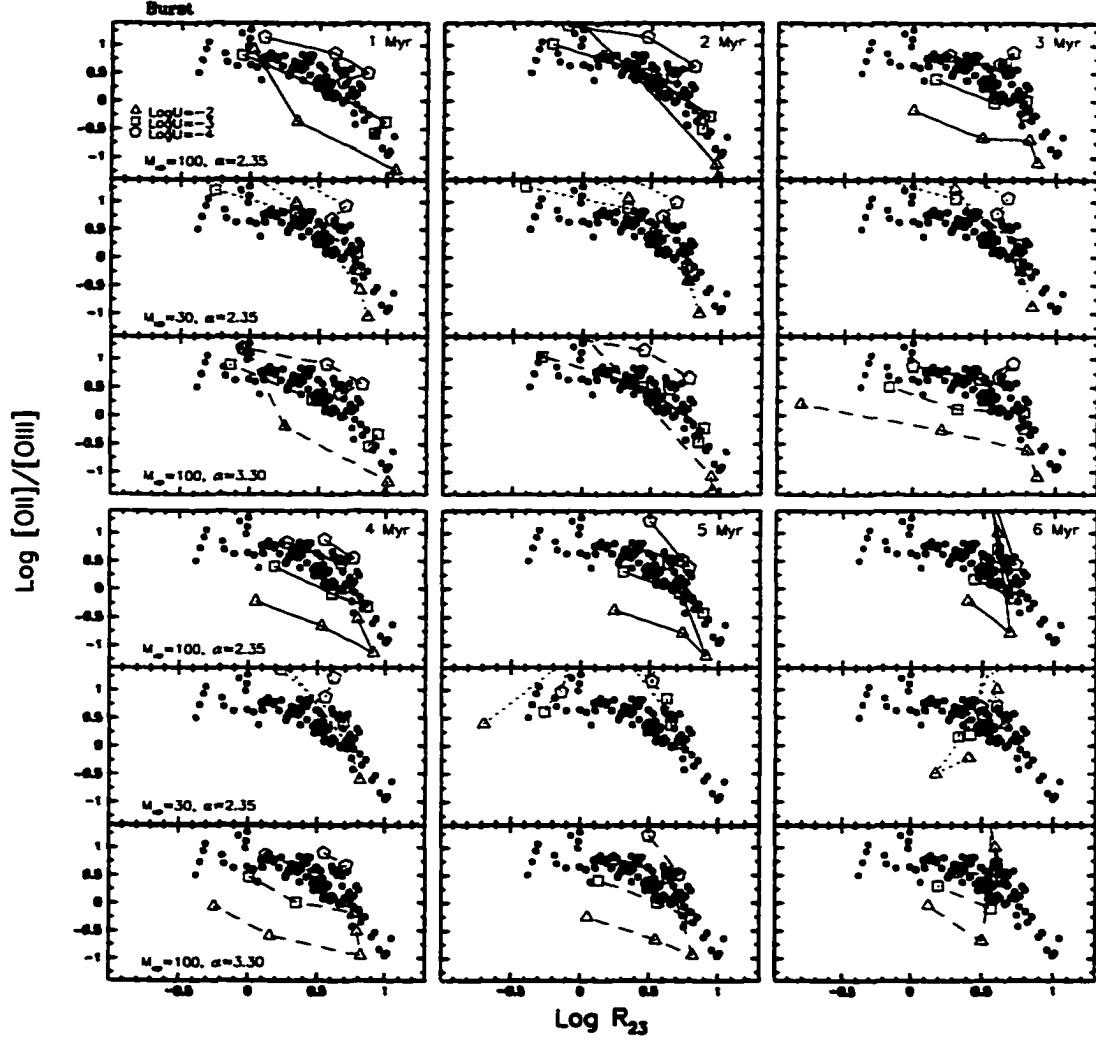


Figure 18 Cluster model results for $[\text{OII}]/[\text{OIII}]$ vs $\text{Log } R_{23}$ (burst SF). In this and in the following plots the three top panels (left to right) refer to ages 1 to 3 Myr, the three lower panels (left to right) refer to ages 4 to 6 Myr. Each of these panels gives results for the Salpeter (top), $M_{up} = 30 M_{\odot}$ (middle), and $\alpha = 3.30$ (bottom) IMFs. The lines connect points at the 4 metallicities considered ($0.1 Z_{\odot}$, $0.25 Z_{\odot}$, Z_{\odot} and $2 Z_{\odot}$). The ionization parameter is coded by the following symbols: triangle ($\log U = -2$), square ($\log U = -3$) and pentagon ($\log U = -4$). The dots are the observed values.

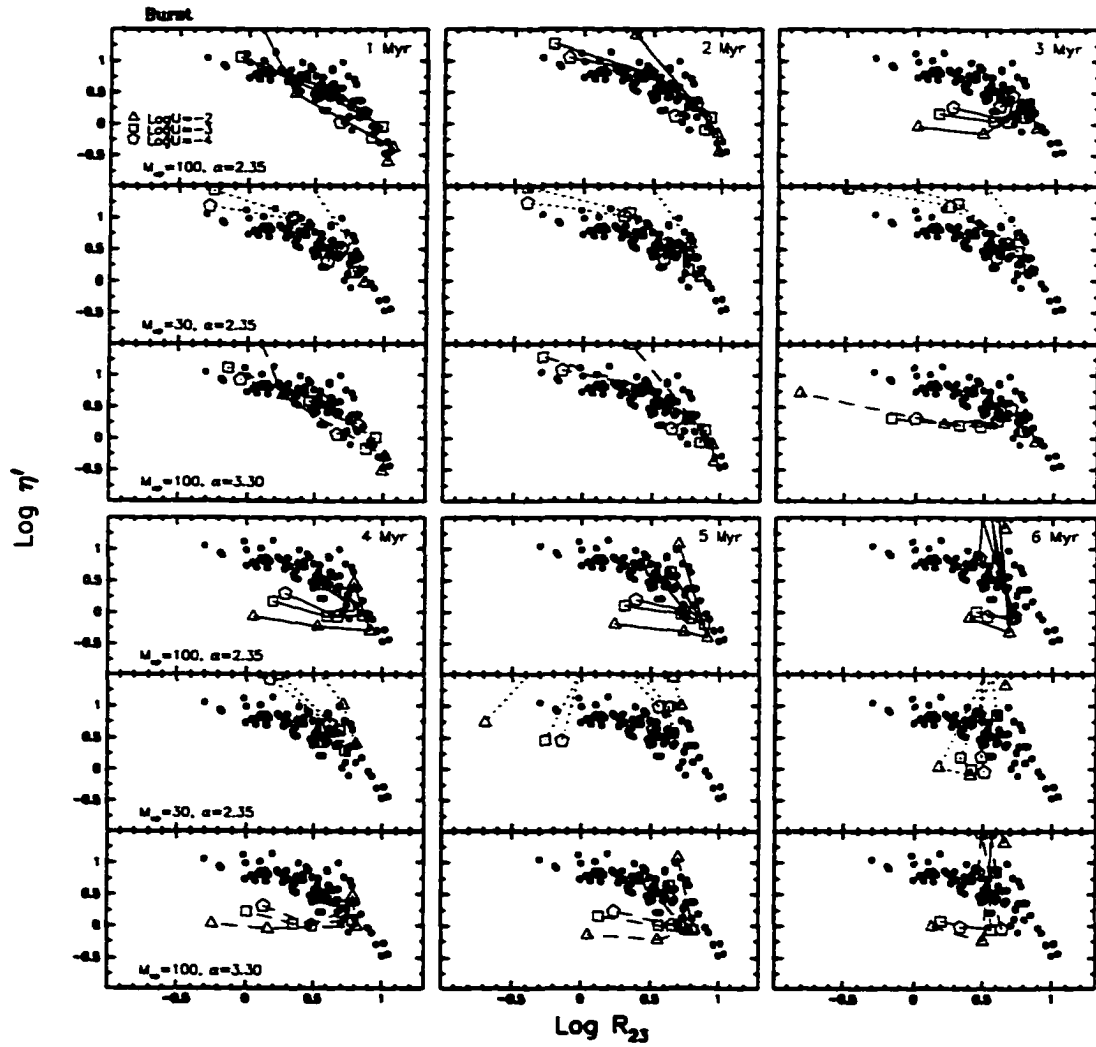


Figure 19 Cluster model results for η' vs $\text{Log } R_{23}$ (burst SF). See Figure 18 for explanations.

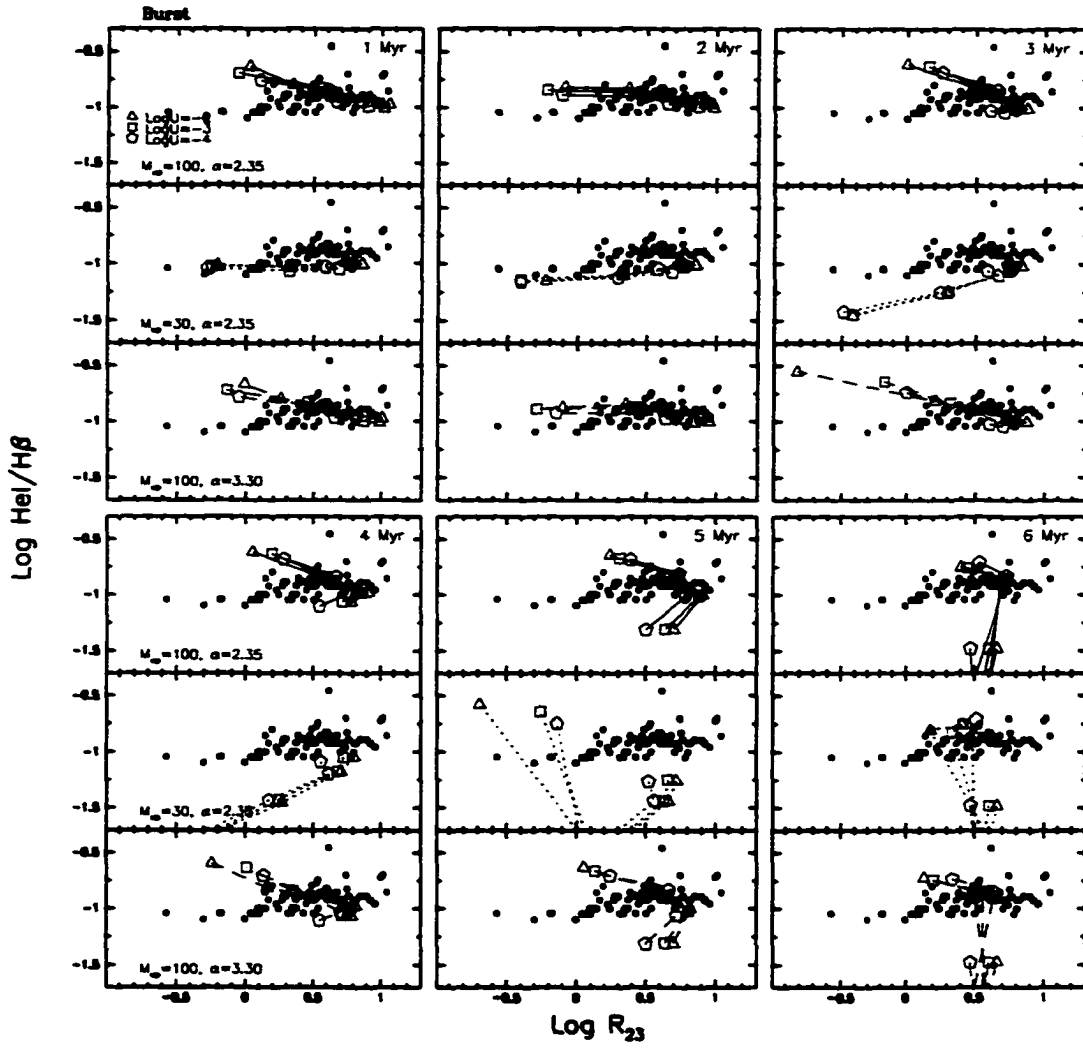


Figure 20 Cluster model results for He I $\lambda 5876/\text{H}\beta$ vs $\text{Log } R_{23}$ (burst SF). See Figure 18 for explanations.

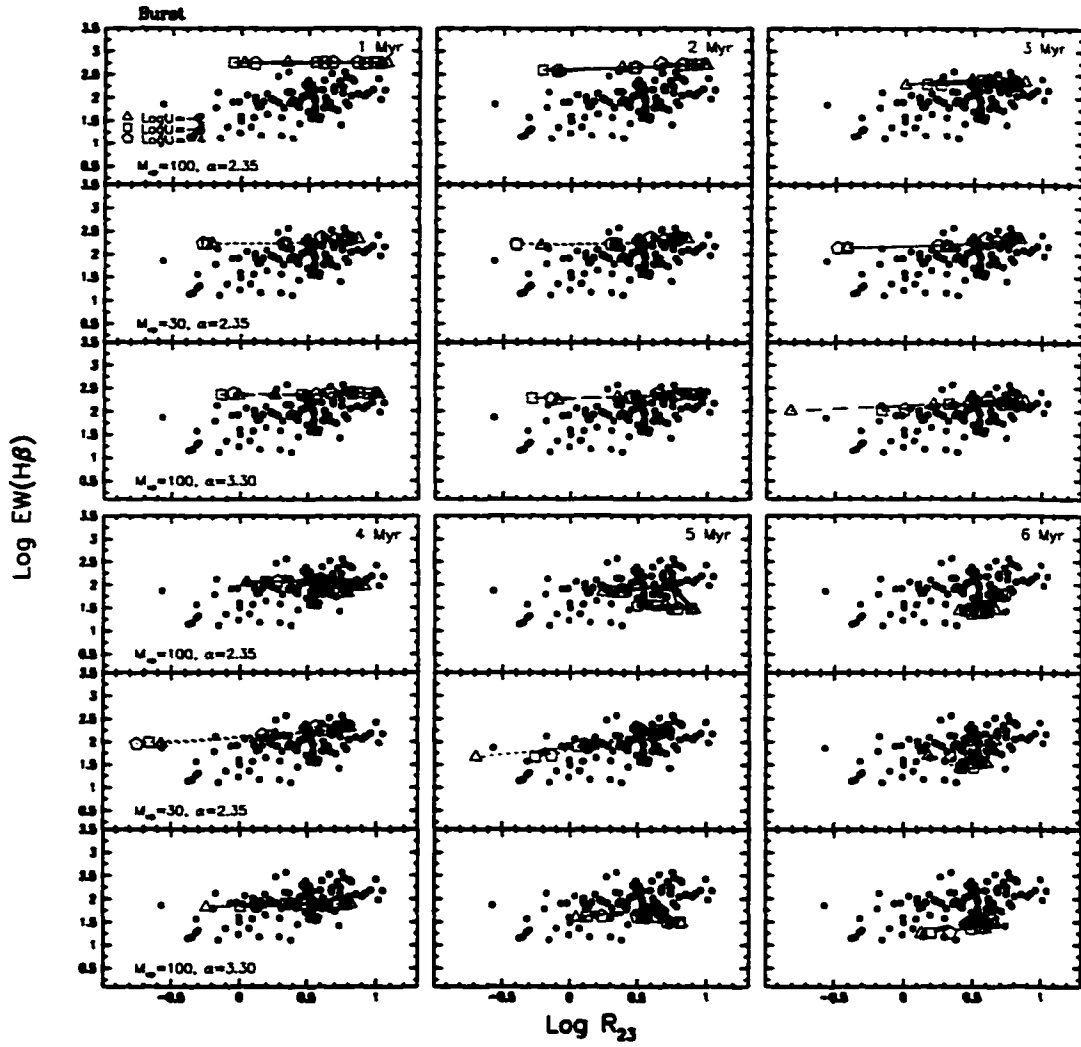


Figure 21 Cluster model results for $\text{EW(H}\beta\text{)}$ vs $\text{Log } R_{23}$ (burst SF). See Figure 18 for explanations.

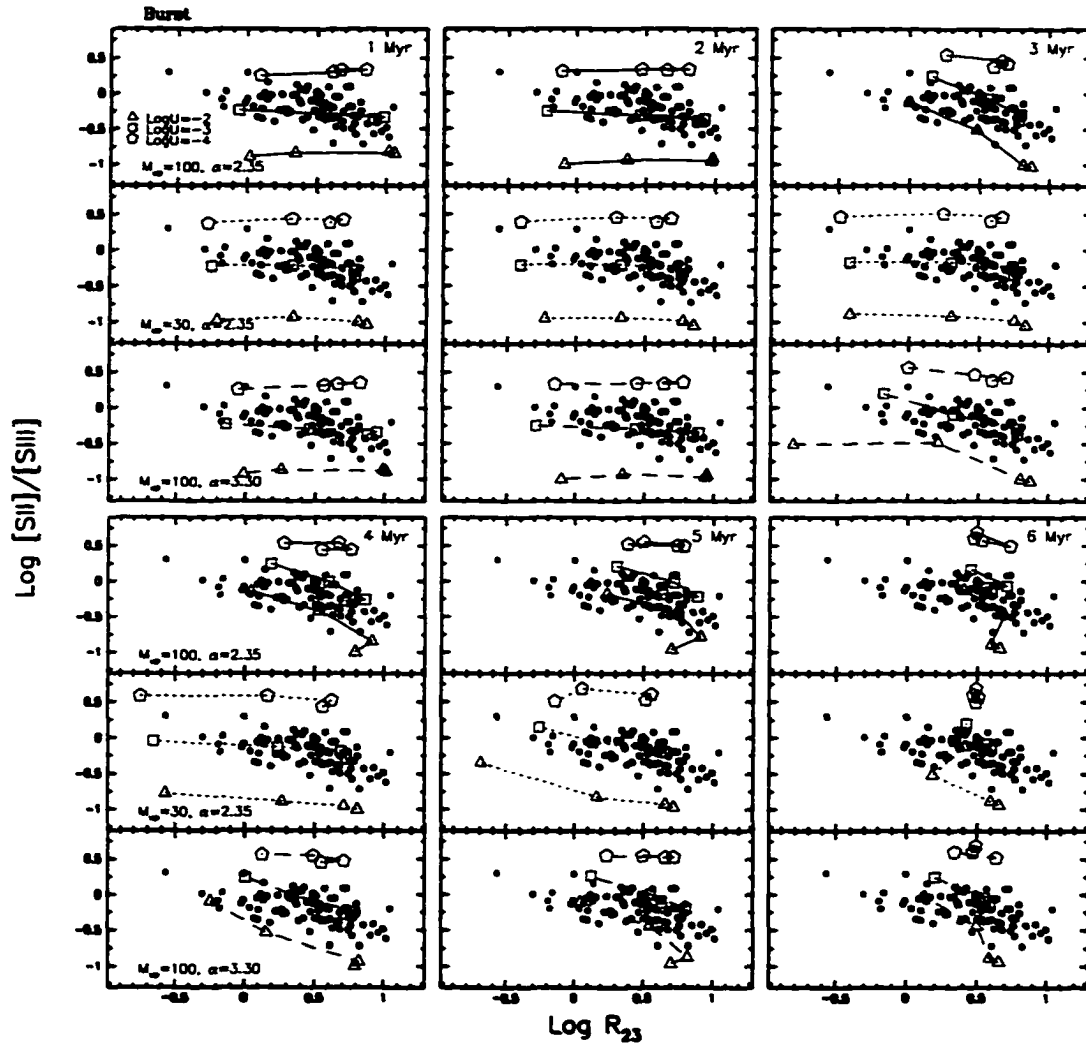


Figure 22 Cluster model results for $[\text{SII}]/[\text{SIII}]$ vs $\text{Log } R_{23}$ (burst SF). See Figure 18 for explanations.

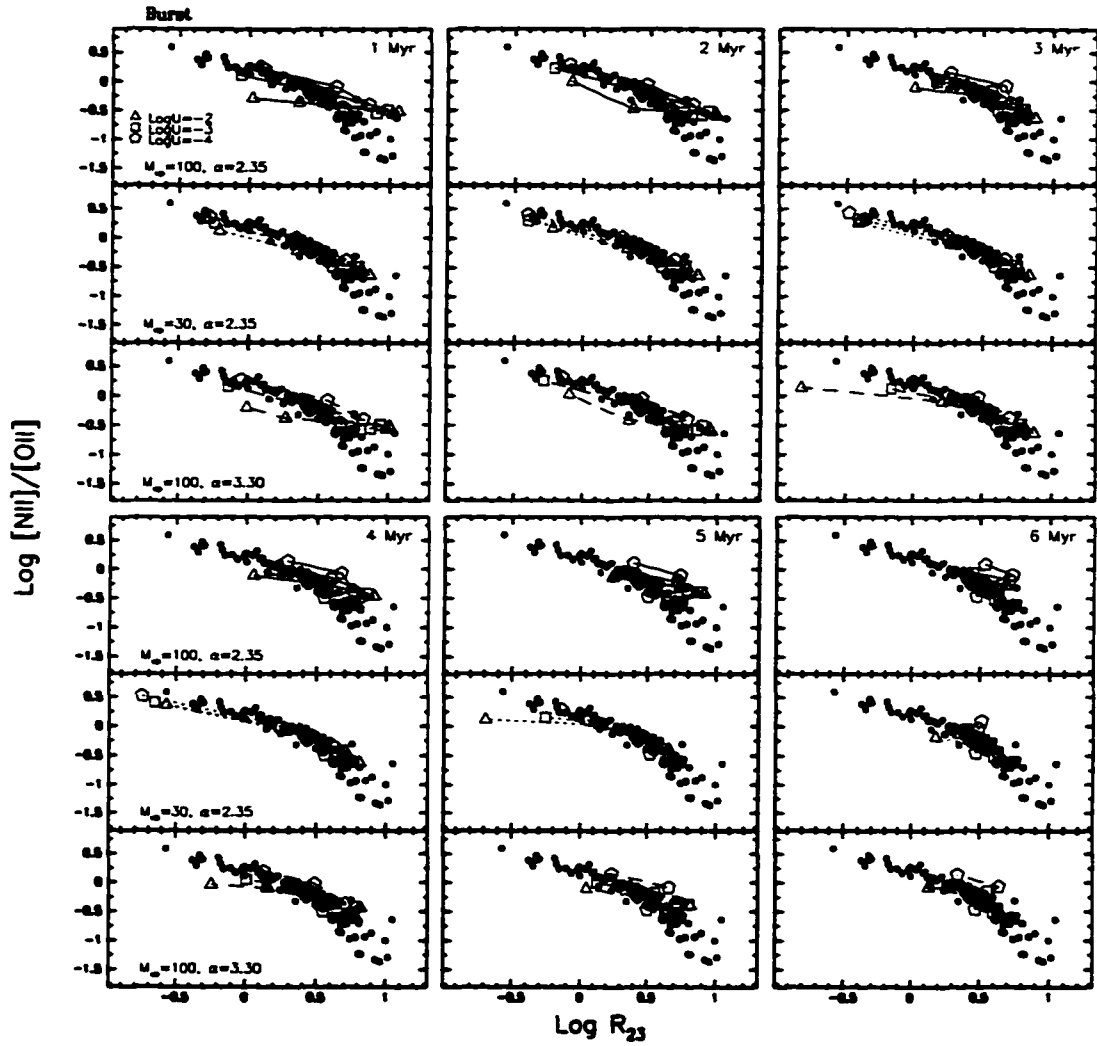


Figure 23 Cluster model results for $[\text{NII}]/[\text{OII}]$ vs $\text{Log } R_{23}$ (burst SF). See Figure 18 for explanations.

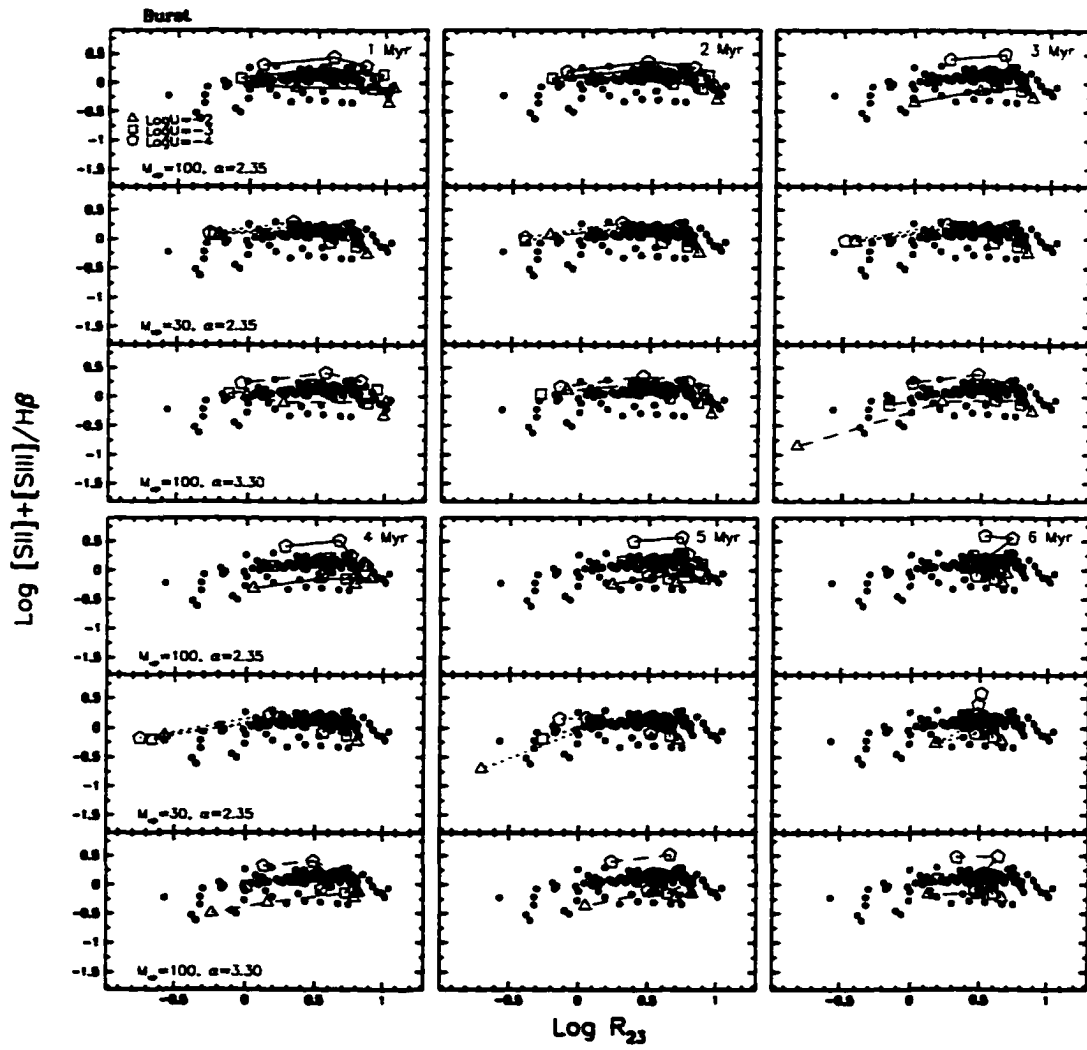


Figure 24 Cluster model results for $([\text{SII}]+[\text{SIII}])/\text{H}\beta$ vs $\text{Log } R_{23}$ (burst SF). See Figure 18 for explanations.

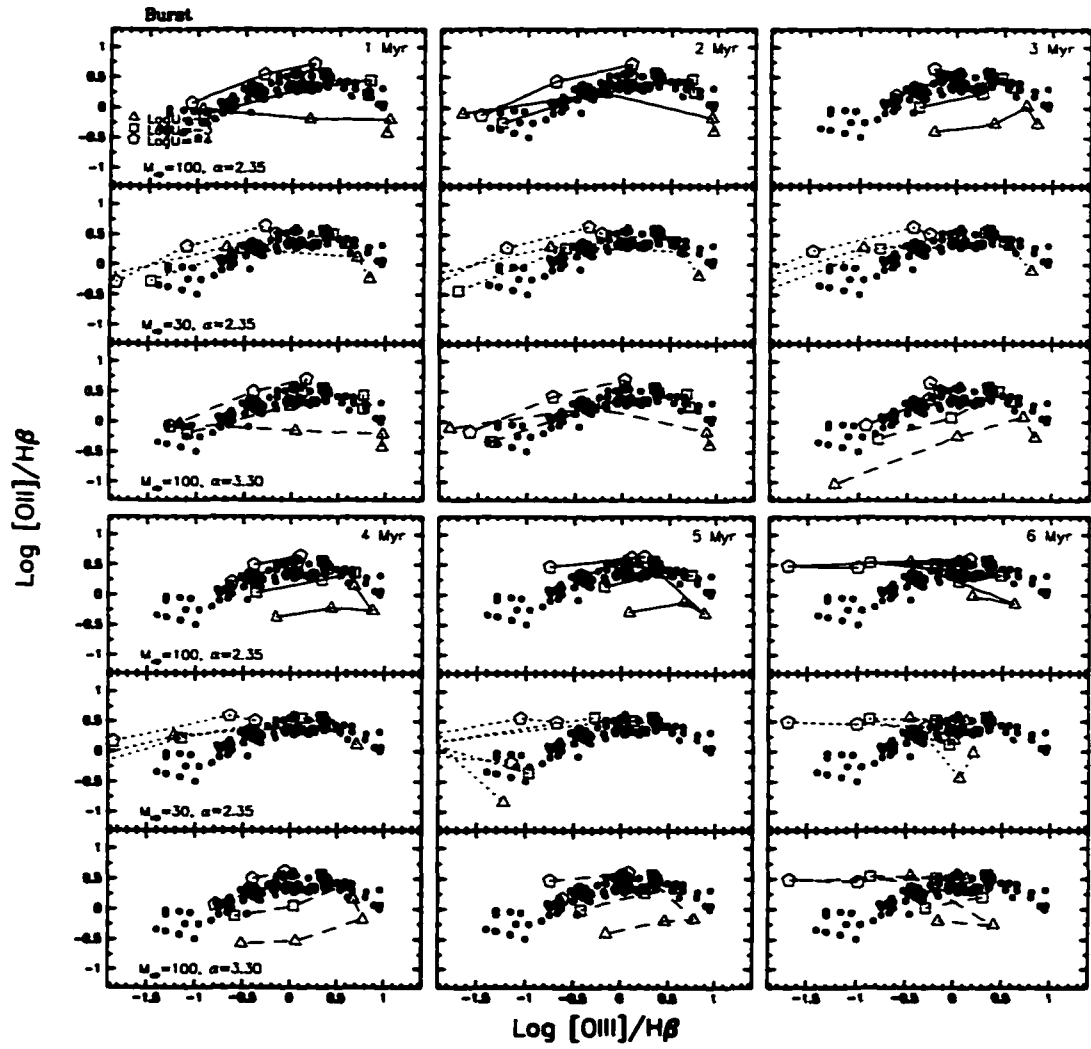


Figure 25 Cluster model results for $[\text{OII}]/\text{H}\beta$ vs $[\text{OIII}]/\text{H}\beta$ (burst SF). See Figure 18 for explanations.

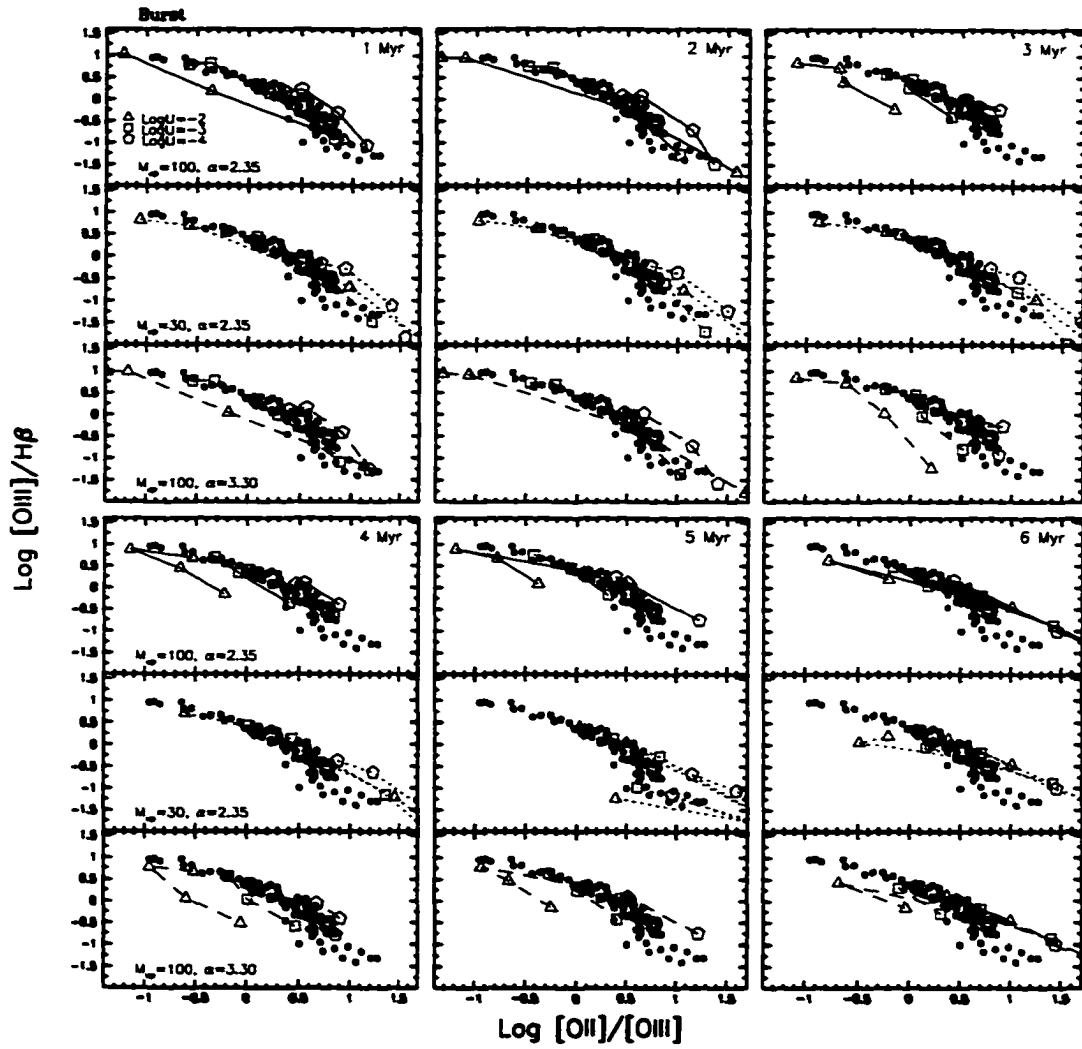


Figure 26 Cluster model results for $\text{[OIII]}/\text{H}\beta$ vs $\text{[OII]}/\text{[OIII]}$ (burst SF). See Figure 18 for explanations.

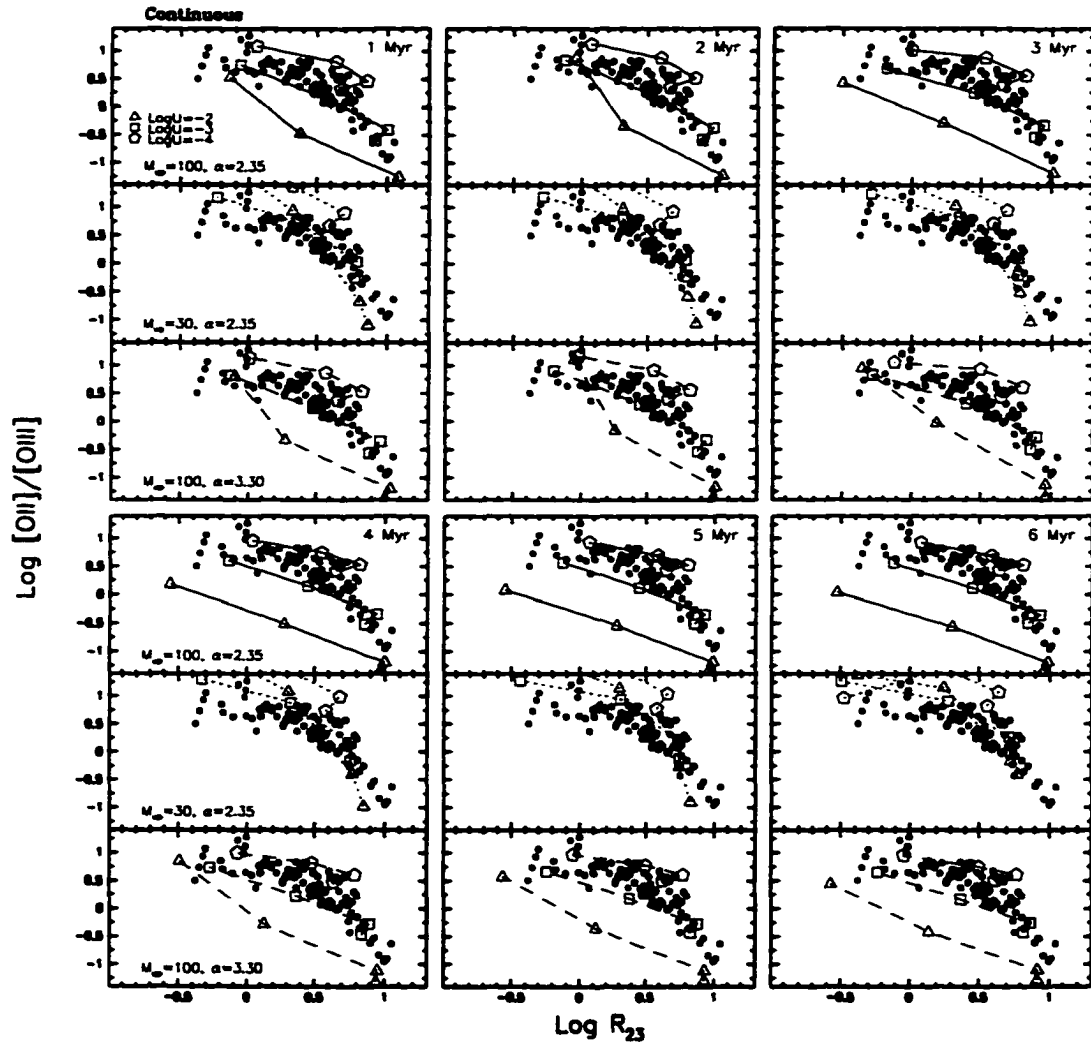


Figure 27 Cluster model results for $[\text{OII}]/[\text{OIII}]$ vs $\text{Log } R_{23}$ (continuous SF). See Figure 18 for explanations.

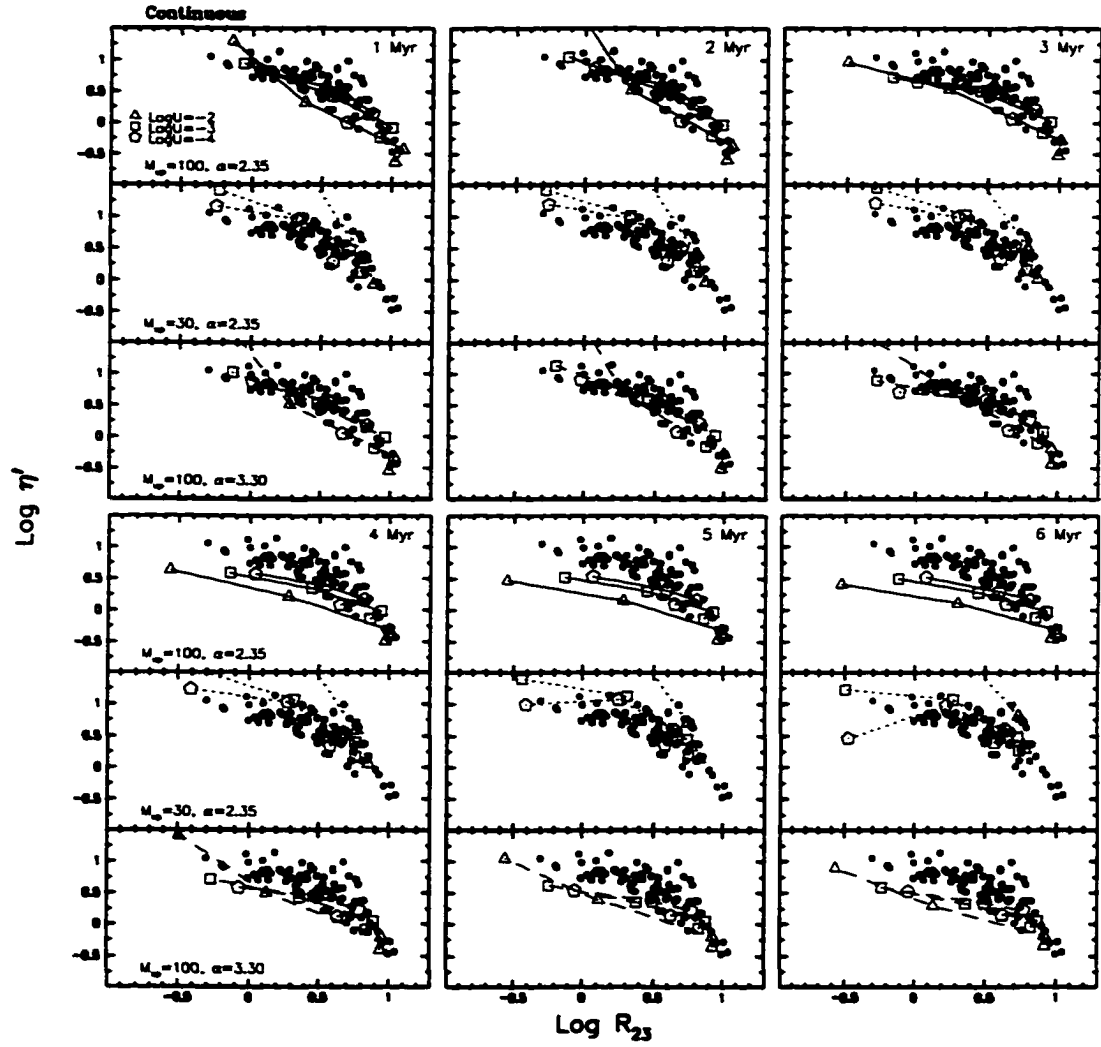


Figure 28 Cluster model results for η' vs $\text{Log } R_{23}$ (continuous SF). See Figure 18 for explanations.

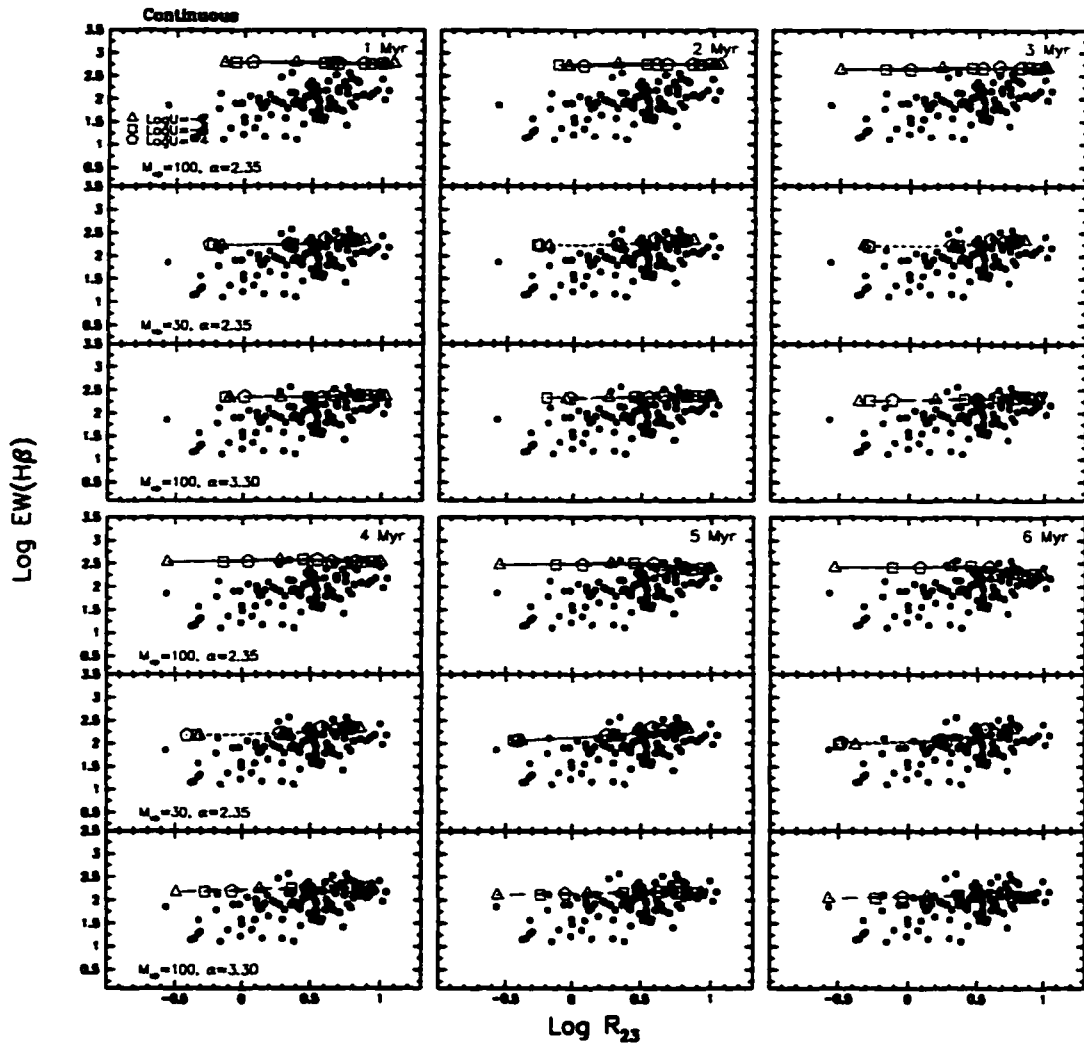


Figure 30 Cluster model results for $\text{EW(H}\beta\text{)}$ vs $\text{Log } R_{23}$ (continuous SF). See Figure 18 for explanations.

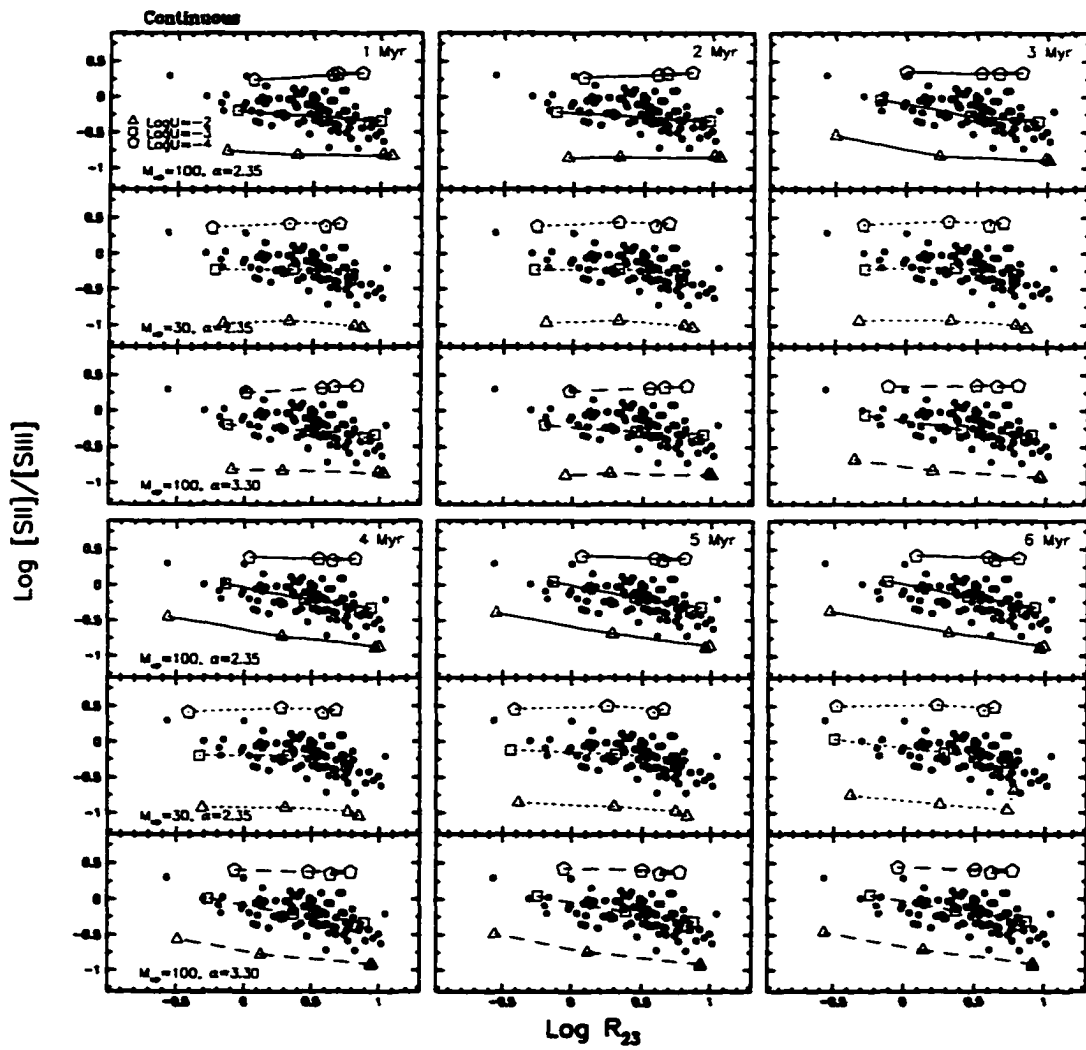


Figure 31 Cluster model results for $[\text{SII}]/[\text{SIII}]$ vs $\text{Log } R_{23}$ (continuous SF). See Figure 18 for explanations.

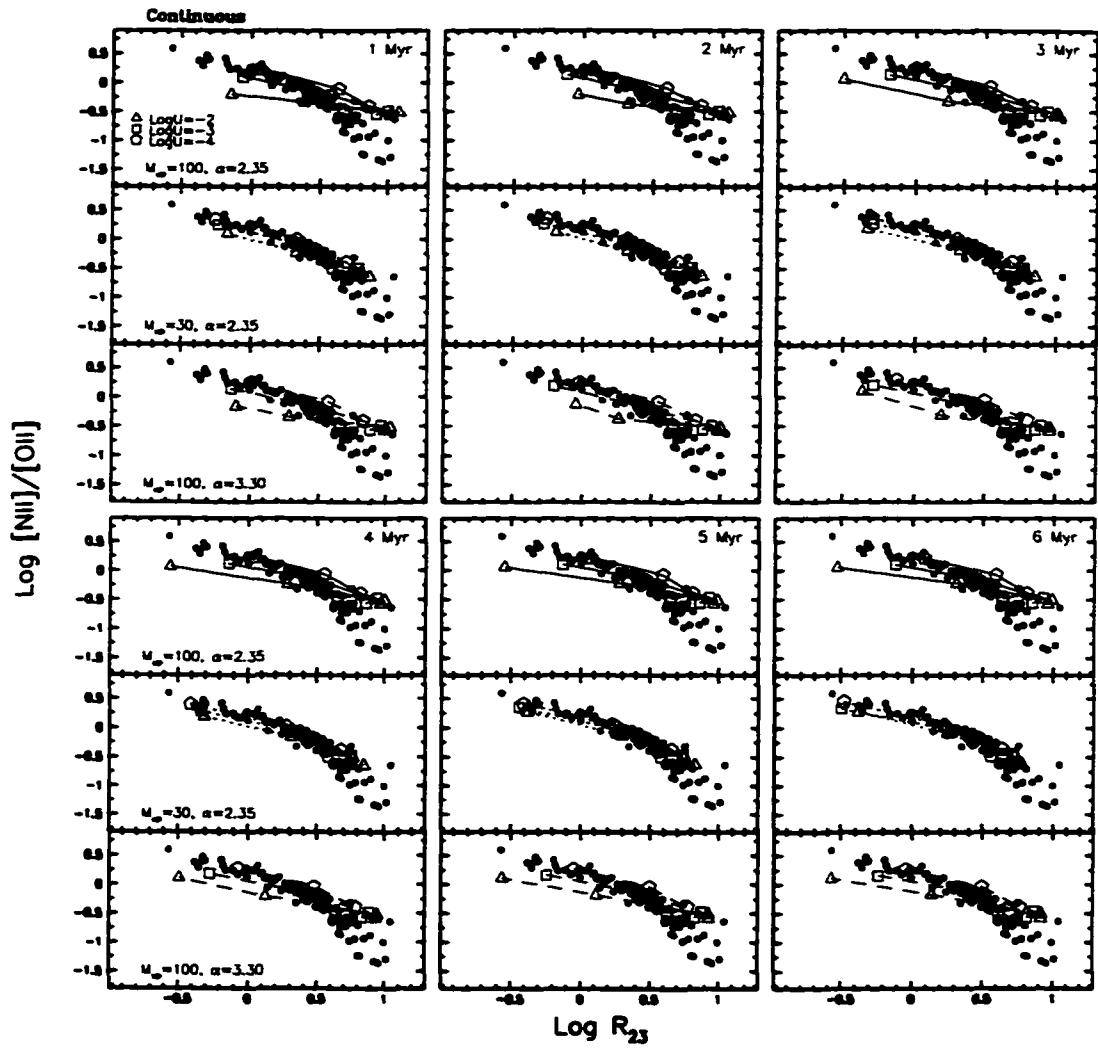


Figure 32 Cluster model results for $[\text{NII}]/[\text{OII}]$ vs $\text{Log } R_{23}$ (continuous SF). See Figure 18 for explanations.

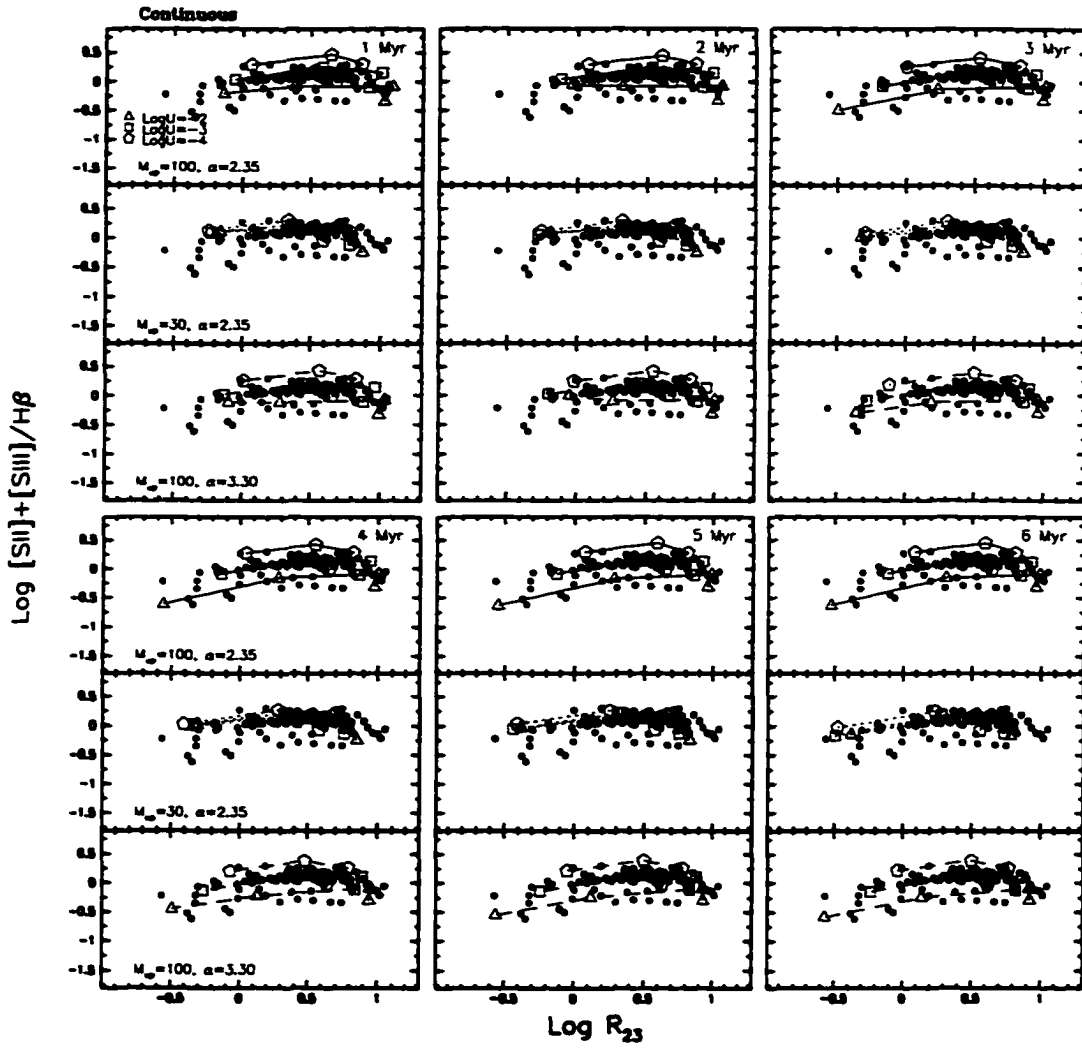


Figure 33 Cluster model results for $([SII] + [SIII])/H\beta$ vs $\text{Log } R_{23}$ (continuous SF). See Figure 18 for explanations.

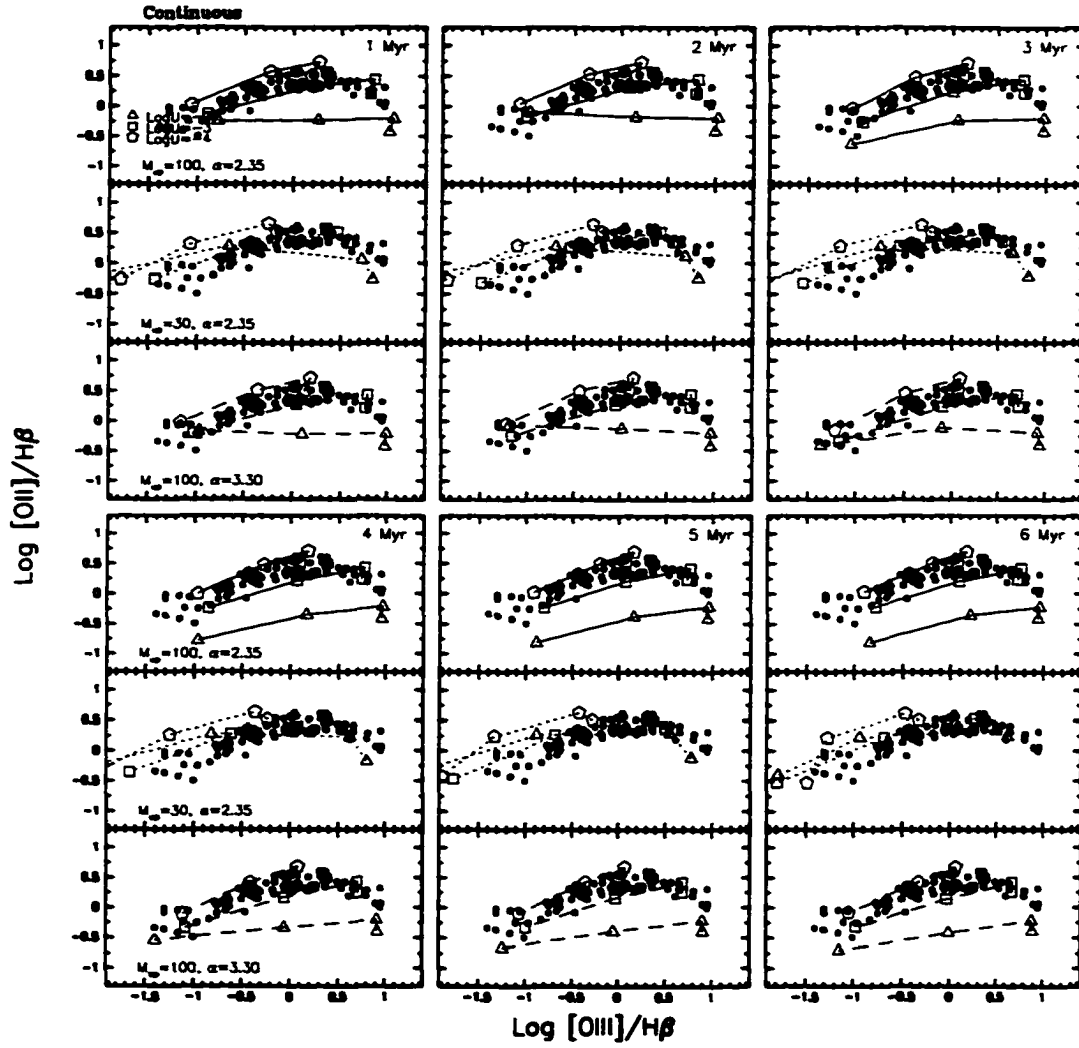


Figure 34 Cluster model results for $[\text{OII}]/\text{H}\beta$ vs $[\text{OIII}]/\text{H}\beta$ (continuous SF). See Figure 18 for explanations.

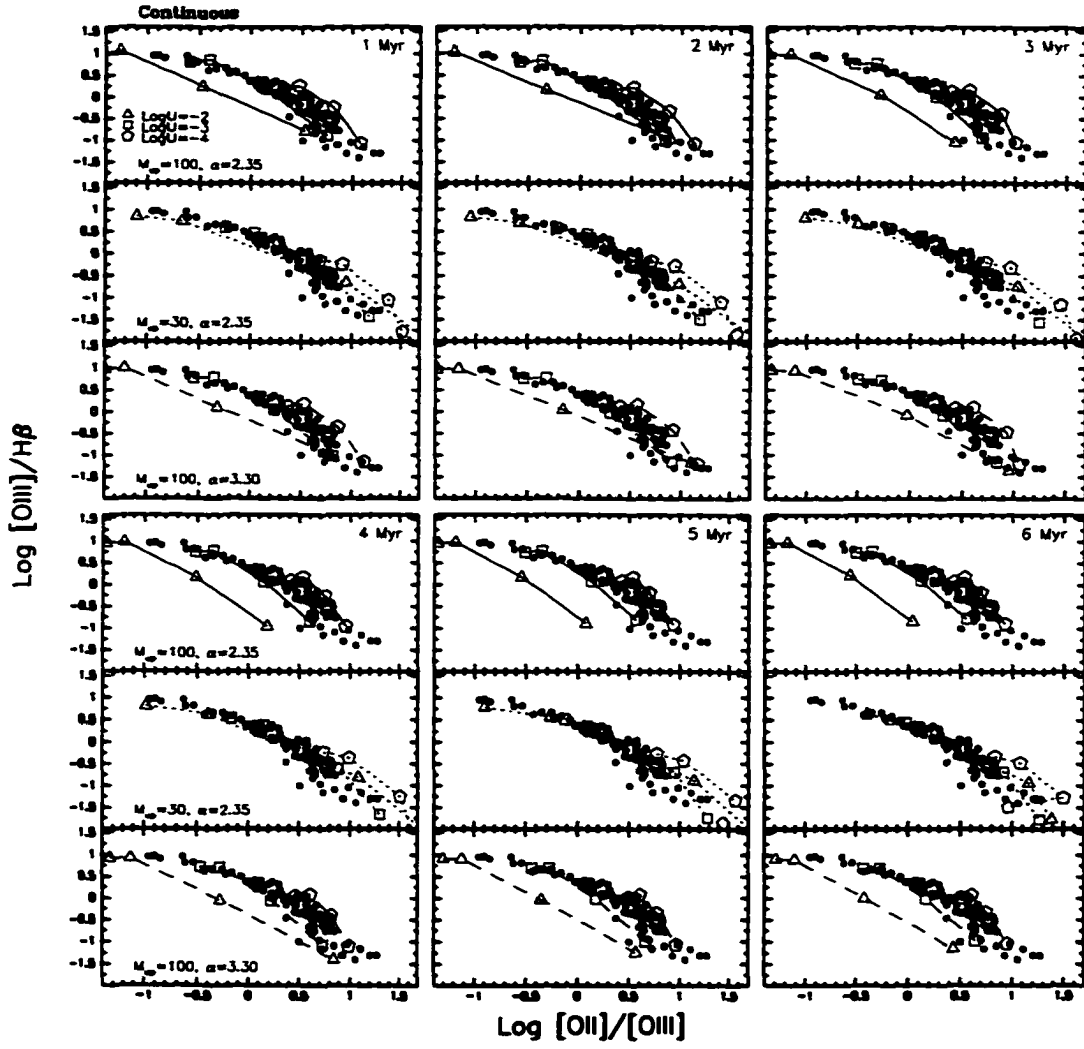


Figure 35 Cluster model results for $[\text{OIII}]/\text{H}\beta$ vs $[\text{OII}]/[\text{OIII}]$ (continuous SF). See Figure 18 for explanations.

4. General results

In this section we will discuss a few results from the models presented in Sect. 3.2. The analysis of T_* will follow in section 5. Both sections have benefited from the procedures and results of the M101 work by Garnett & Kennicutt (1997).

4.1. Cluster ages (Figs. 18-26)

A perusal of the diagnostic diagrams corresponding to the cluster models with burst star formation mode (Figures 18-26) shows that the models are in general consistent with the data only for young ages ($t < 3$ Myr). The theoretical predictions diverge considerably from the observations at later times. This does not exclude that a few older H II regions are present in our sample, but the bulk of the H II region sequences shown are best reproduced by the 1 and 2 Myr models. As a consequence of this age limit the T_{eq} -metallicity relation discussed previously would in general hold, since most of our objects would not be old enough to have evolved their most massive stars into hotter WR stars. In turn, the observation of a relation between T_* and metallicity (Section 5) is probably an indication that a limit on the age must exist, or that the WR phase is not as important as predicted by the evolutionary models.

In order to check if this result is peculiar of the adopted cluster models, we examined the CLOUDY photoionization models of García-Vargas *et al.* (1995), who used different stellar models (the Padova sets of Bressan *et al.* 1993 and Fagotto *et al.* 1994a,b) and stellar atmospheres for the hot stars (Clegg & Middlemass 1987) than the ones adopted by Leitherer & Heckman (1995). As an example the evolution of η vs $\text{Log } R_{23}$ from 1 to 5.4 Myr (the largest age considered in their models) is shown in Figure 36. These models too are consistent with the data only

for a limited cluster age interval, from ~ 3 to 4.5 Myr. These values are higher than the best-fit age range (1–3 Myr) found in our models. It is well-known that the adoption of different stellar evolutionary tracks is responsible for relatively large differences in the emission-line spectra of model nebulae (Stasińska & Leitherer 1996). WR stars are also treated differently between the Geneva and Padova models; moreover the stellar atmospheres for WR stars differ in the evolutionary models of Leitherer & Heckman (1995) and García-Vargas *et al.* (1995), as mentioned above. As our simple comparison demonstrates, the results we are going to discuss are somewhat sensitive to the input physics and to the details of the modeling.

An interesting result of our photoionization calculations is that the continuous star formation cluster models (Figures 27-35) often provide as good a fit to the observations as the burst models. While in the literature photoionization calculations based on burst models are preferentially found, this suggests that continuous models should also be considered as valid solutions. Star formation extending over time (an age spread of a few Myr), as in the case of individual star clusters formed in subsequent bursts, but close enough to remain unresolved by the spectrograph slit, or 'extended bursts' lasting a few Myr, are scenarios that deserve further investigation. This is the case of 30 Dor, whose central ionizing cluster has an age of ~ 3 Myr; there is however evidence for previous episodes of star formation, as indicated by the presence of supergiants (Walborn 1991). These components of different age are spatially resolved, but they would not be if 30 Dor were at a much larger distance. Recent work (García-Vargas *et al.* 1997, González-Delgado *et al.* 1997) indicates the coexistence of young (~ 3 Myr) and old (~ 8 Myr) components in individual starbursts, supporting the idea of an age spread, and suggesting star formation in multiple, subsequent bursts as a likely mechanism in giant H II regions.

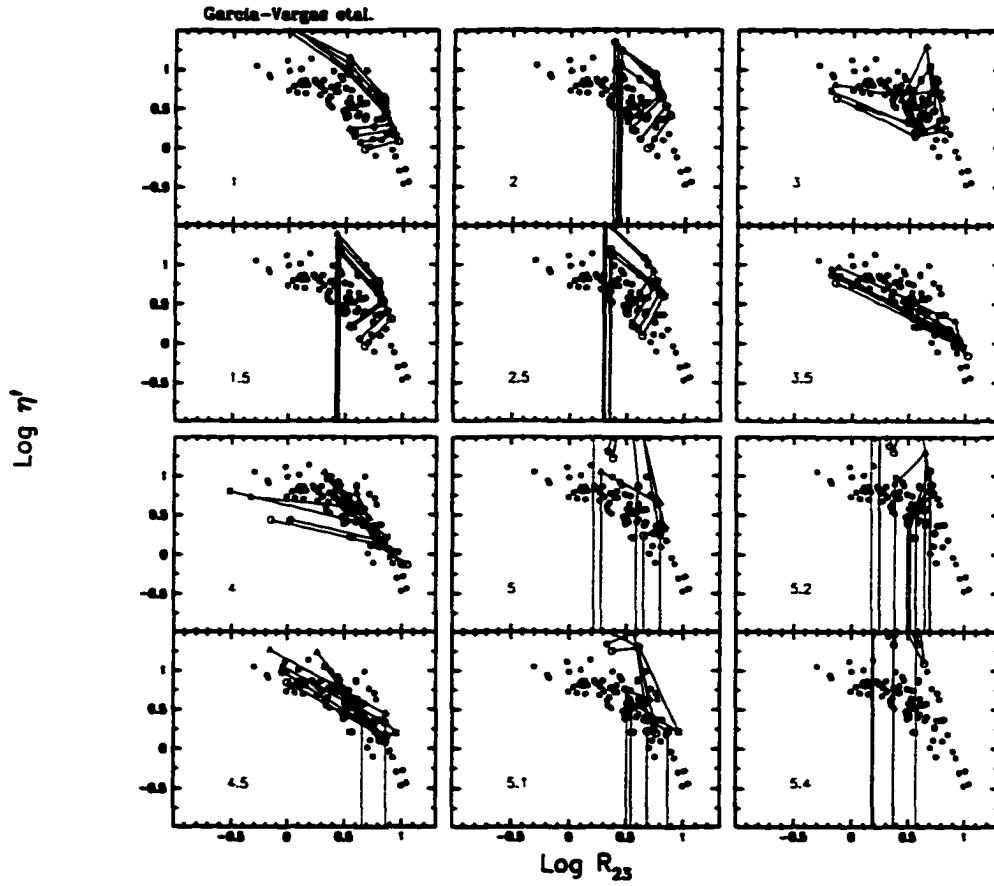


Figure 36 η' vs Log R_{23} plots from the models of García-Vargas *et al.* (1995). Each plot is labeled with the corresponding model cluster age (from 1 to 5.4 Myr). The lines connect models with the same cluster mass ($0.12 \times 10^5 M_{\odot}$: triangles; $0.2 \times 10^5 M_{\odot}$: squares; $0.4 \times 10^5 M_{\odot}$: pentagons; $0.6 \times 10^5 M_{\odot}$: circles) and different metallicity ($0.05 Z_{\odot}$, $0.2 Z_{\odot}$, $0.4 Z_{\odot}$, Z_{\odot} , $2.5 Z_{\odot}$). Vertical lines are plotted when one of the emission lines entering η' reaches zero intensity.

4.2. Ionization parameter (Figs. 13, 22, 31)

The plots presented in Section 3.2 show that the ionization parameters adopted for the models bracket our data, which are clustered around $\log U = -3$. This is particularly clear in Figures 13, 22 and 31, since $[\text{SII}]/[\text{SIII}]$ is a good measure of U . Díaz *et al.* (1991) gave a calibration of U in terms of this ratio, which has been refined by Garnett & Kennicutt (1997) to include the small metallicity dependence. Given the model sensitivity of the sulfur line ratio, however, we will not derive a new calibration here.

The comparison of the models with the observations indicates that a higher ionization parameter is required at low metallicities. This decrease of U as the metallicity increases confirms the result of previous investigations on H II galaxies (Campbell 1988, Stasińska & Leitherer 1996).

4.3. Sensitivity to different IMFs (Figs. 18-26)

One of the main reasons to run this set of photoionization models is to check the effect of different IMFs on the theoretical emission-line ratios, in the hope to define constraints on the IMF variations with metallicity. However, different combinations of cluster age, ionization parameter and IMF can reproduce the distribution of observed points in the diagrams involving $[\text{OII}]$, $[\text{OIII}]$, $[\text{SII}]$, $[\text{SIII}]$ and $[\text{NII}]$. The behavior of He I $\lambda 5876$ and $\text{EW}(\text{H}\beta)$ will be examined separately.

The two IMFs with slope $\alpha = 2.35$ and $\alpha = 3.30$ but having the same upper mass limit ($= 100 M_{\odot}$) are virtually indistinguishable in our diagrams: nebular spectra are insensitive to the slope of the mass function. For $M_{up} = 30 M_{\odot}$ the predictions are somewhat different, but the scatter of the actual data make it difficult to say which IMF better represent the data. Things are complicated by

the effects of density at high metallicity: changing the density of our models to $n = 10 \text{ cm}^{-3}$ (a value often used by other authors, see García-Vargas *et al.* 1995 and Stasińska & Leitherer 1996) can have a noticeable effect on the predicted line ratios.

To test Shields & Tinsley's (1976) idea that the upper mass limit of the IMF is lower at higher metallicity, we need to look at the model results for higher-than-solar metallicities. At lower abundances some of the diagnostics ($[\text{OII}]/[\text{OIII}]$ vs R_{23} , η' vs R_{23} , $[\text{OII}]$ vs $[\text{OIII}]$) rule out the low mass cutoff. At higher metallicities the canonical Salpeter IMF fits the data somewhat better than the low cut-off IMF for $[\text{OII}]/[\text{OIII}]$ and η' , but it is difficult to reach a conclusion on the basis of these considerations. We conclude that our qualitative comparisons suggest a better agreement of the data with the canonical IMF.

4.4. The $\text{H}\beta$ Equivalent Width (Figs. 12, 21, 30)

Dependence on Hubble type - Bresolin & Kennicutt (1997, see Appendix D) studied the distribution of the $\text{H}\alpha$ equivalent width ($\text{EW}(\text{H}\alpha)$) of H II regions in 10 galaxies of different Hubble type to test the idea that different upper mass limits of the IMF could be responsible for the changes in star forming region properties as a function of morphological type. The photometrically-determined $\text{EW}(\text{H}\alpha)$ values showed no dependence on Hubble type.

The distribution of the equivalent width of $\text{H}\alpha$ and $\text{H}\beta$ for our H II region sample is shown in Figure 37. This plot confirms the result just mentioned: the EW distribution is not a function of Hubble type. Since the equivalent width of the Balmer emission lines is a measure of the ratio of the number of hot, massive stars (producing the emission line flux through ionization of the nebula) to the total

number of stars (producing the continuum), our result points toward the invariance of the IMF across the morphological sequence. Bresolin & Kennicutt showed, from the invariance of $EW(H\alpha)$, that changes in the upper mass limit, if present, are limited to $M > 50 M_{\odot}$.

Dependence on metallicity - The data show a weak dependence of $EW(H\beta)$ on metallicity, with a large scatter, likely due to an age spread in the $H II$ region sample. A similar behavior was already measured by Searle (1971) on a small sample of $H II$ regions in M101. This result was interpreted by Shields & Tinsley (1976) as evidence for a gradient in the temperature of the hottest exciting stars, which in turn led them to hypothesize an abundance-dependent upper mass limit for star formation.

The photoionization models do not reproduce the observed sequence of $EW(H\beta)$ vs R_{23} . It is a well-known fact that the observed $EW(H\beta)$ values of extragalactic $H II$ regions are much lower than the theoretical predictions. The usual interpretation is that an underlying population of stars older than the ones responsible for the ionization of the nebulae is contributing to the stellar continuum, thus diluting the ionizing radiation and reducing the equivalent width (McCall *et al.* 1985). Díaz *et al.* (1991) proposed the coexistence of stellar clusters of different ages within giant $H II$ regions, as suggested by spatially resolved observations (Skillman 1985, Díaz *et al.* 1987). Internal extinction due to dust which would affect the nebular lines, but not the continuum, has been proposed as an alternate solution (Mayya & Prabhu 1996, García-Vargas *et al.* 1997). The dependence of $EW(H\beta)$ on both cluster age and upper IMF, combined with the problem just described, make it difficult to derive a T_{eff} - Z relationship from $EW(H\beta)$. We will therefore not attempt to use the observed $EW(H\beta)$ gradient to measure a T_{\star} gradient.

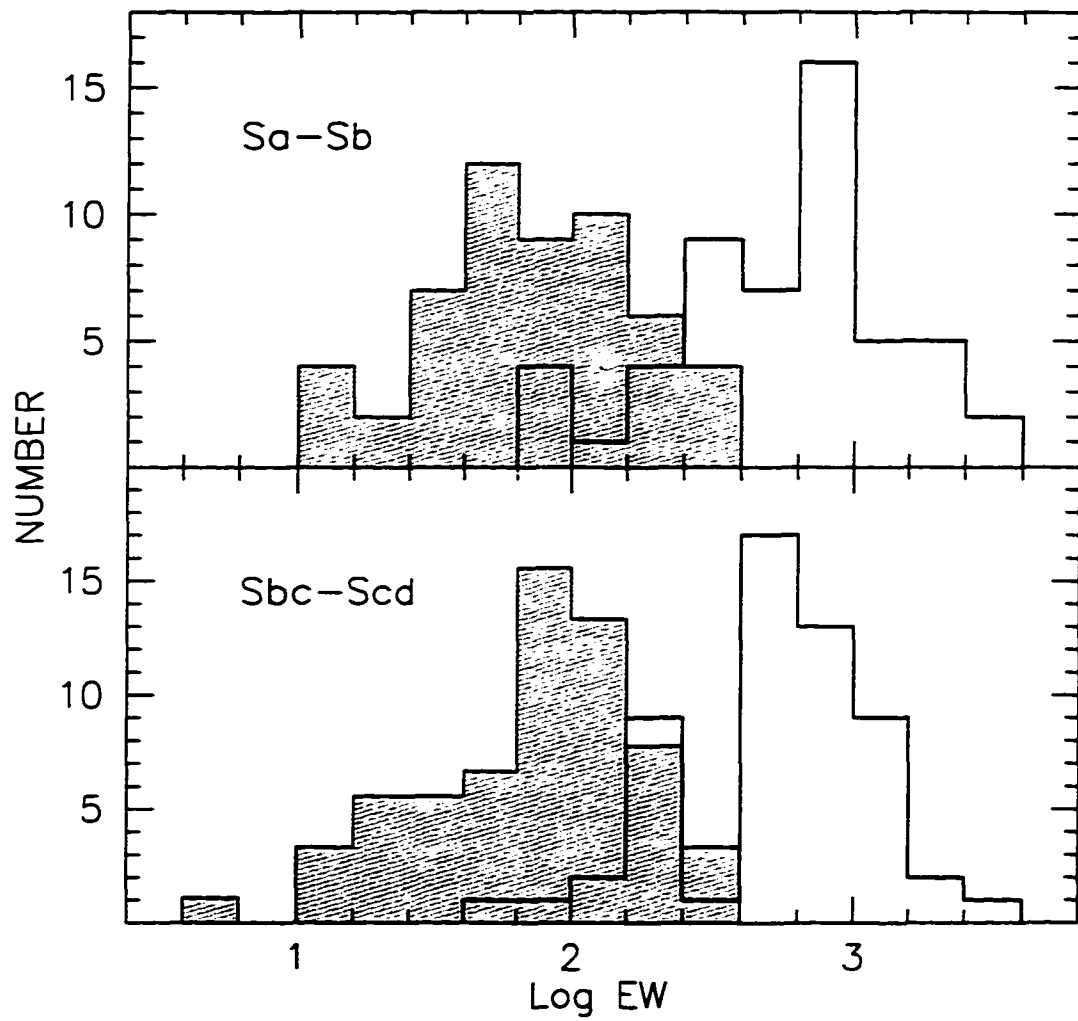


Figure 37 Distribution of the $H\alpha$ (heavy continuous line) and the $H\beta$ (shaded region) equivalent widths as a function of Hubble type: Sa-Sb (*top*) and Sbc-Scd (*bottom*).

4.5. The He I $\lambda 5876$ line (Figs. 11, 20, 29)

According to the cluster models, the results for He I $\lambda 5876$ line are at variance with respect to the other diagnostics introduced so far. In the case of the canonical IMF the predicted intensity at high abundance is higher than observed, and the IMF truncated at $30 M_{\odot}$ seems to best reproduce the data. A similar result was obtained by McCall *et al.* (1985), who suggested an increase of the helium abundance for high metallicity stars, so as to decrease the flux at the helium ionization edge, therefore leading to a smaller He⁺ zone in the H II regions. Such He abundance increase is included in the stellar evolutionary models (*e.g.* Schaller *et al.* 1992), which were calculated for $Y_{\odot} \simeq 0.30$ and $\Delta Y/\Delta Z \simeq 3$. We wish to explore other possibilities first. We note that the discrepancy is present for the high-metallicity H II regions, which have the weakest He I $\lambda 5876$ emission. Often this was the weakest feature measured in our spectra, and for several of the low-excitation objects it could not be detected. There are also a couple of effects that could artificially lower the measured intensity of this line. The Na I night-sky emission and the interstellar absorption ($\lambda = 5890 \text{ \AA}$) increase the uncertainty in the measurements, especially for the weakest objects. While the first effect is probably well corrected for, the absorption feature would tend, in some cases, to lower the observed emission line intensity. Secondly the data need to be corrected for the contribution of the underlying stellar continuum. Following McCall *et al.* (1985) we have considered a $EW = 0.5 \text{ \AA}$ correction when presenting our data and models (Figures 20, 29). Figure 38 shows how the agreement between the models and the data improves when considering a higher ($EW = 2 \text{ \AA}$) correction. Lowering the density of the models to 10 cm^{-3} or considering a fixed solar He/H nebular abundance ratio produces only a slight improvement. In conclusion, given the uncertainties related to the high-abundance objects observations, we do not

consider the above-mentioned discrepancy as a difficulty for our final conclusions on the IMF. In fact the small gradient in the He I $\lambda 5876$ line intensity vs R_{23} (Figure 11) is consistent with the temperature gradient expected from the stellar models.

4.6. The N/O abundance ratio (Figs. 14, 23, 32)

The [NII]/[OII] model sequences (Figures 14, 23 and 32) are not reproducing the observations at low abundances. The actual data show weaker [NII] lines relative to [OII] when compared to the theoretical values. Theory and observations could be reconciled by considering a metallicity-dependent N/O ratio. Evidence for such an effect in spirals has already been shown by several authors (*e.g.* McCall *et al.* 1985, Fierro *et al.* 1986, Díaz *et al.* 1991, Garnett & Kennicutt 1997), but there is no general agreement on the functional relation between N/O and O/H, if it exists at all (different spirals having different N/O gradients, Henry & Howard 1995). In low-abundance irregular galaxies the N/O ratio is found to be independent of O/H (Garnett 1990), supporting the idea of a primary origin for nitrogen at low metallicity: nitrogen is produced out of C and O synthesized during the evolution of stars. An abundance-sensitive N/O ratio would imply the presence of a secondary component, that is N produced by C and O already present in stars at their birth. The situation is less clear for S/O, for which the existence of a O/H dependence is uncertain (for example, see contradicting results in Díaz *et al.* 1991 and Garnett 1989). To represent a secondary component superposed on a primary component for N in spiral galaxies, a few models were calculated assuming the following relations (Garnett & Kennicutt 1997):

$$\begin{aligned} \log N/O &= -1.5 + (\log O/H + 3.7) & (\log O/H > -3.7) \\ \log N/O &= -1.5 & (\log O/H < -3.7) \end{aligned}$$

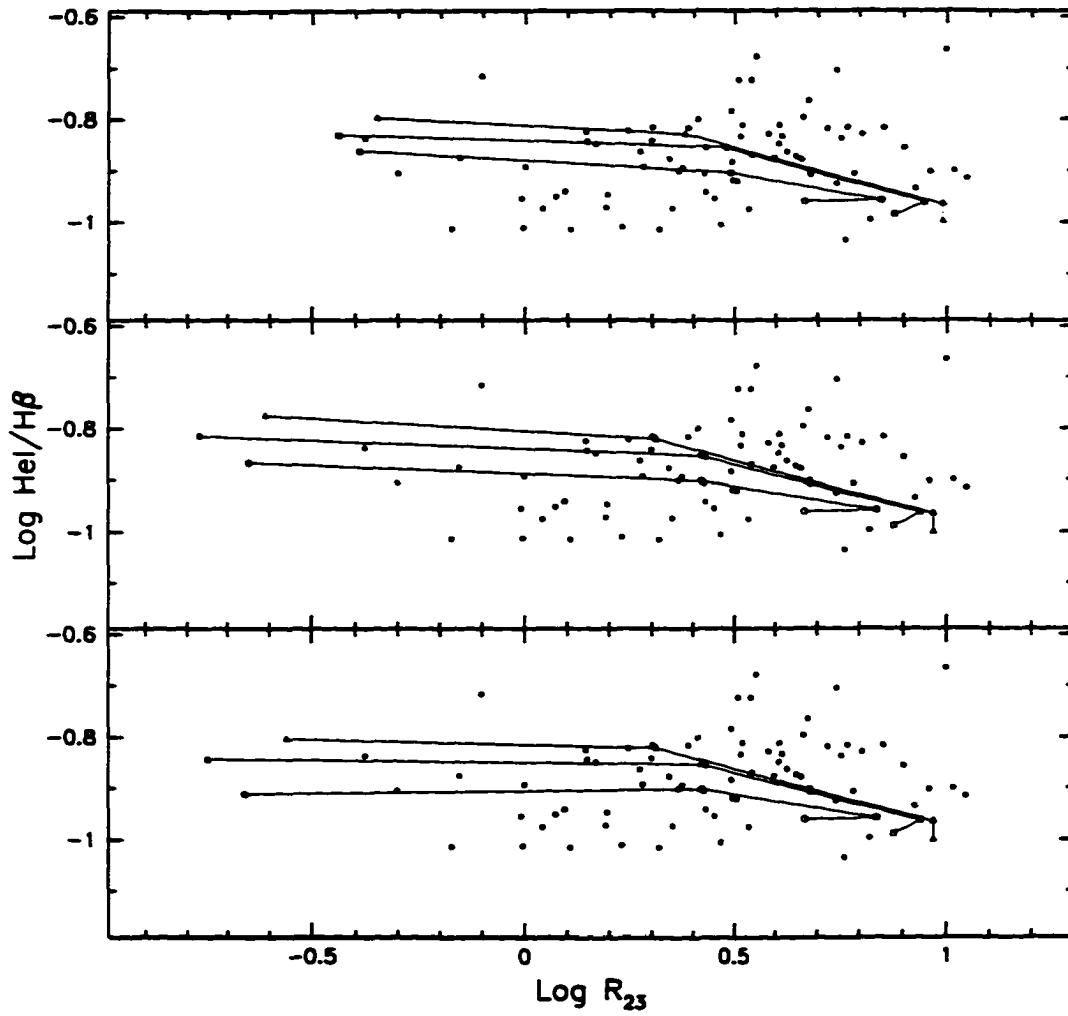


Figure 38 Effects of model parameter changes on He I $\lambda 5876$ vs $\text{Log } R_{23}$. The data have been corrected for a 2 \AA equivalent width absorption from the stellar clusters. A variable N/O ratio (see Section 4.6) has been adopted. *Top*: $N = 50 \text{ cm}^{-3}$; *middle*: $N = 10 \text{ cm}^{-3}$; *bottom*: solar He/H for the $2 Z_{\odot}$ models.

The results (Figures 39 and 40) are in much better agreement with the observations, lending more credibility to the presence of a secondary component for nitrogen in spiral galaxies, with a rather steep gradient. The models can now reproduce the steepening of the $[\text{NII}]/[\text{OII}]$ vs R_{23} relation that occurs in the data at $\text{Log } R_{23} > 0.5$. From the single-star models the increased scatter at large R_{23} can be attributed to the different T_{eff} of the ionizing clusters. The main secondary effect of the abundance-dependent N/O ratio is a shift of the $2 Z_{\odot}$ models to lower R_{23} values, due to the increased cooling of the nebulae caused by the larger abundance fraction of nitrogen. Models with a fixed, solar N/O ratio would therefore overestimate the metallicity for high-abundance objects (see discussion in Garnett & Kennicutt 1997). Excluding this change at high metallicity, the remaining diagnostic diagrams are only slightly affected by the different N/O ratio, and, except for $\eta/$ vs R_{23} (Figures 41, 42), will not be shown.

An important point to make about the $[\text{NII}]/[\text{OII}]$ sequence is that it refers to 20 spiral galaxies of different Hubble type. The tightness of the sequence is telling us that the relation between N/O and O/H is similar for all these galaxies, whatever the exact functional form might be. While for a few individual galaxies (*e.g.* M33, see Vilchez *et al.* 1988, or M81, see Garnett & Shields 1987) a N/O gradient seems not to be required, a 'universal' abundance-dependent N/O ratio seems to be necessary to explain the bulk of our observations.

4.7. Additional remarks

We have included the $[\text{OIII}]/\text{H}\beta$ vs $[\text{OII}]/[\text{OIII}]$ diagnostic diagram because it was the only one presented by García-Vargas *et al.* (1995) to conclude that no IMF change with abundance is required to reproduce the observations. A look at Figure 26 shows that the canonical IMF and the low cut-off mass IMF produce

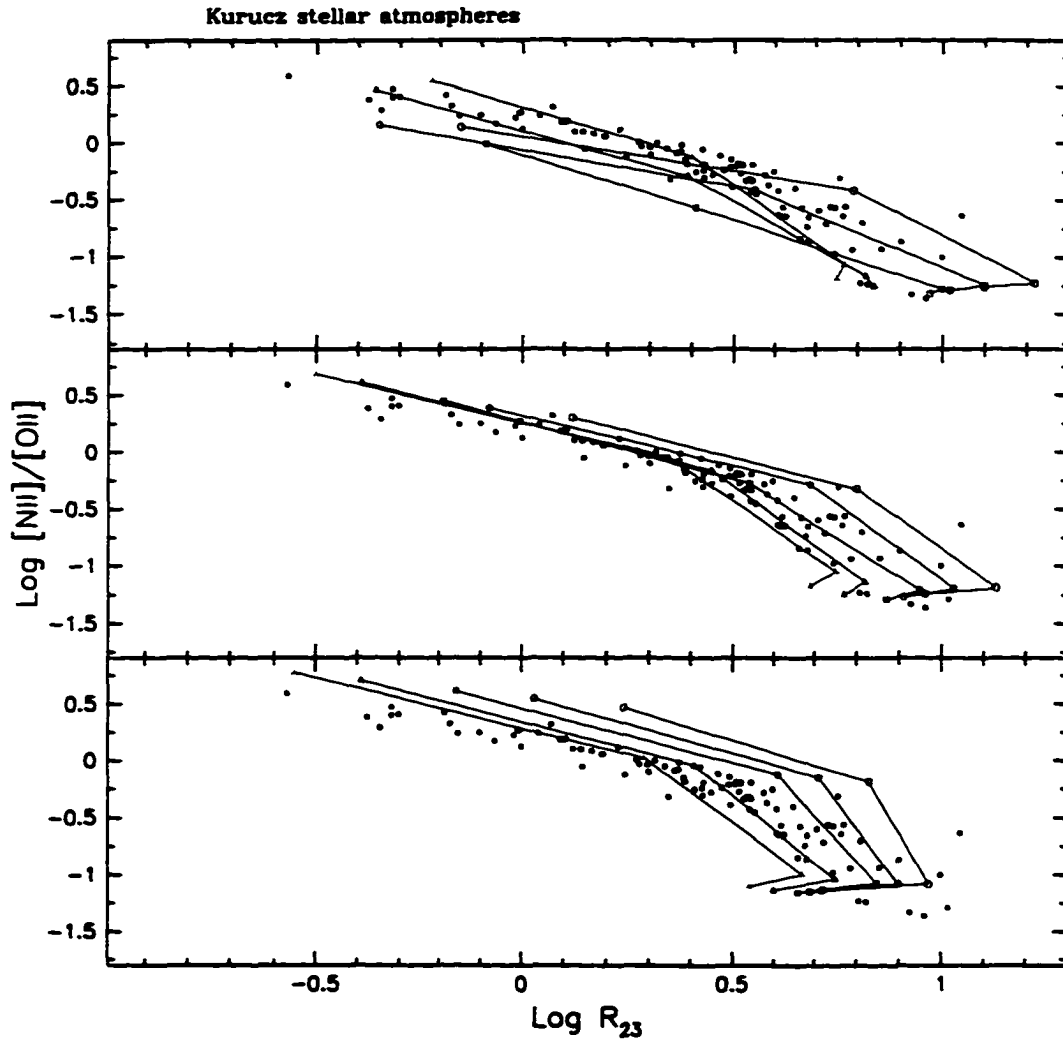


Figure 39 Effects of an abundance-dependent N/O ratio on the single-star models for $[\text{NII}]/[\text{OII}]$ vs $\text{Log } R_{23}$. See Figure 9 for explanations on the symbols used.

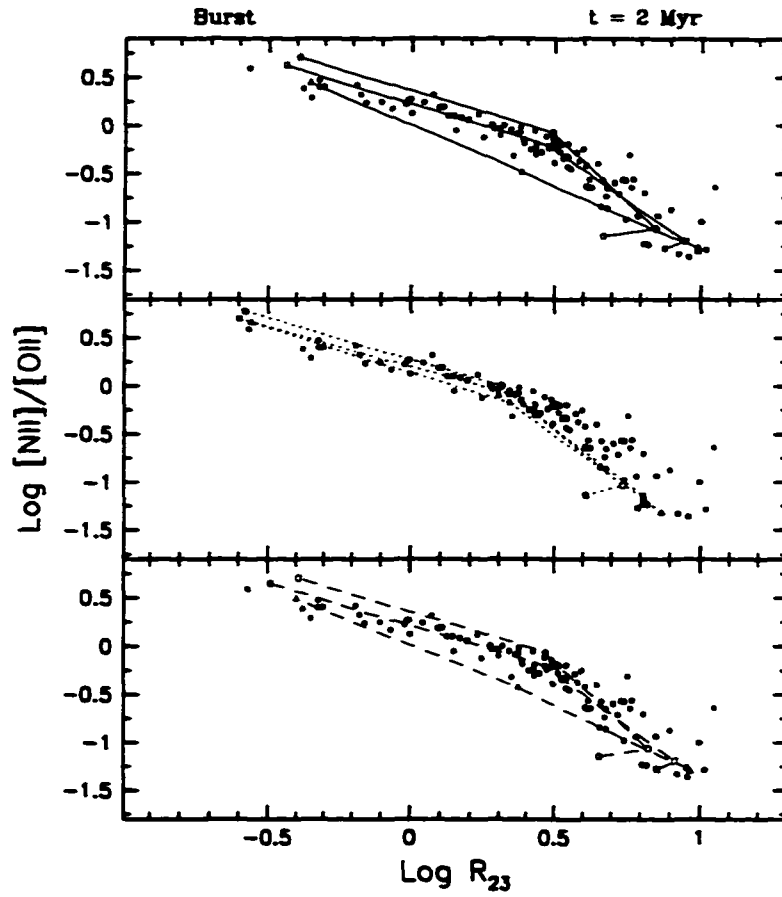


Figure 40 Effects of an abundance-dependent N/O ratio on the 2 Myr cluster models for $[\text{NII}]/[\text{OII}]$ vs $\text{Log } R_{23}$ (burst SF). See Figure 18 for explanations on the symbols used.

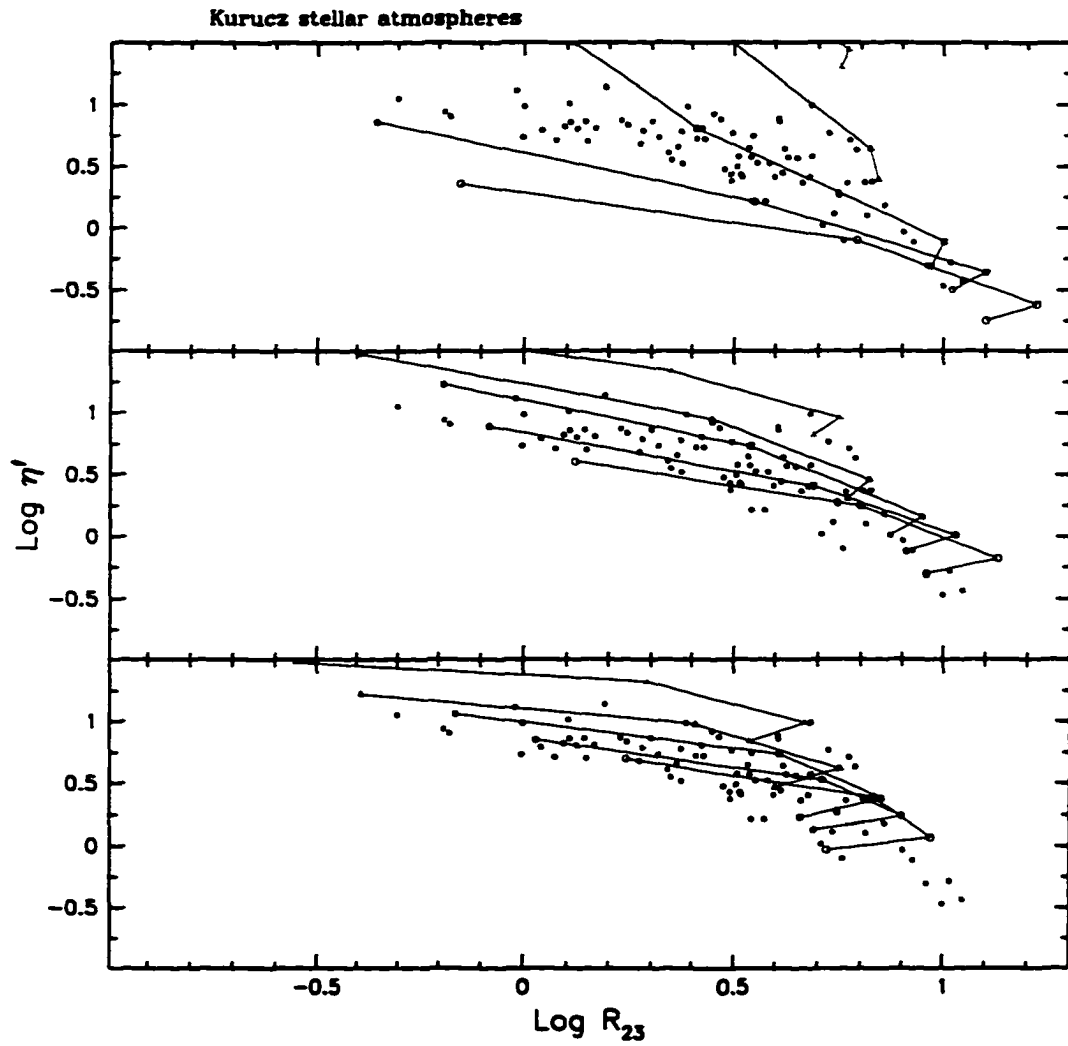


Figure 41 Effects of an abundance-dependent N/O ratio on the single-star models for η' vs Log R_{23} . See Figure 9 for explanations on the symbols used.

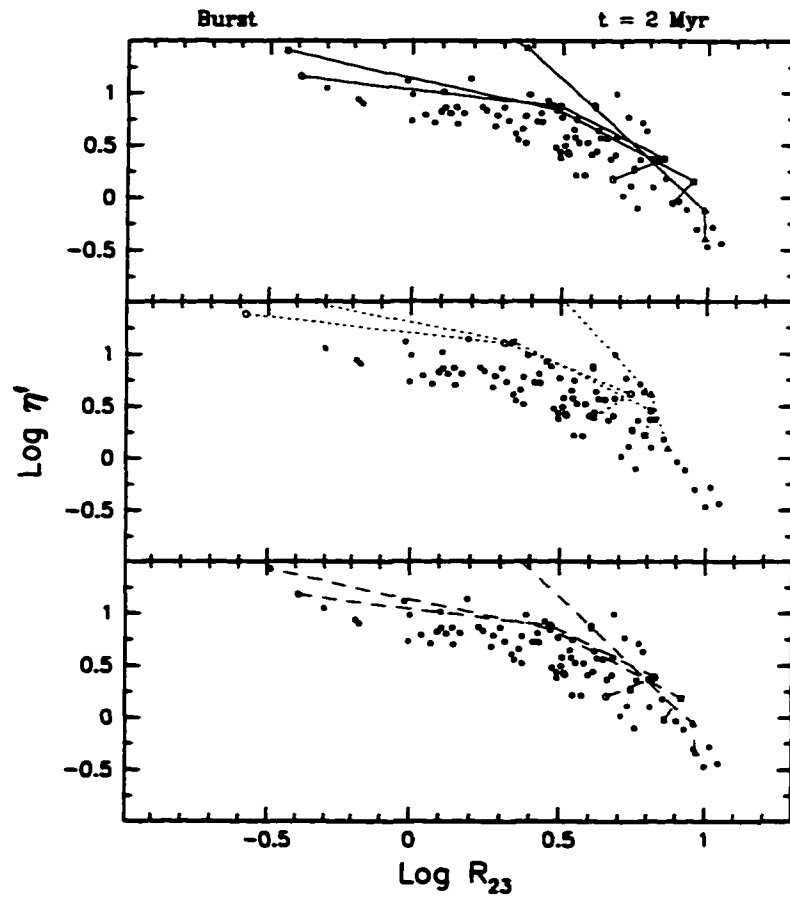


Figure 42 Effects of an abundance-dependent N/O ratio on the 2 Myr cluster models for η' vs $\text{Log } R_{23}$ (burst SF). See Figure 18 for explanations on the symbols used.

rather similar results at young ages (1 and 2 Myr). It is true that the canonical IMF is able to better reproduce both the high- and low-metallicity ends of the sequence (the low cut-off mass IMF models miss the low-excitation, high abundance objects). The same holds for the other diagnostics involving [OII] and [OIII] lines. We feel however that the use of this or similar diagrams alone is not sufficient to draw final conclusions on variations of the IMF.

5. Temperature of the ionizing stars

There is general agreement about the existence of T_{eff} gradients in spiral galaxies. Over the years there has been a debate over the cause of this gradient, whether it is a reflection of a change in the upper IMF or simply an effect of stellar evolution at different metallicities. In this Section we will use the simultaneous measurement of η' and R_{23} for a large number of H II regions to investigate this astrophysical problem.

The large body of [SIII] $\lambda 9069,9532$ observations presented here has been made possible by the general availability in the late 1980's of large-format CCDs and their high sensitivity at near-IR wavelengths. Shields & Searle (1978) were the first to point out the importance of the [SIII] lines to constrain the ionization structure of H II regions in the absence of temperature-sensitive lines, since sulfur is an effective coolant through its near-IR forbidden lines and its fine-structure lines at 19 and 33 μm . Mathis (1982, 1985) introduced a method to constrain the relative effective temperature scale, based on the $S^+/S^{++} - O^+/O$ diagram. The use of ratios of ionic stages of the same element makes this method almost independent of nebular abundance. Absolute values of T_e are much more difficult to obtain, due to the dependence on the adopted model atmospheres. Besides,

there is a 'saturation' effect for very hot stars, so that the method becomes less useful at high temperatures.

The 'radiation softness' parameter η was introduced by Vílchez & Pagel (1988) as a modification of Mathis' procedure, and is defined as

$$\eta = \frac{O^+/O^{++}}{S^+/S^{++}}.$$

It is almost independent of ionization parameter, reddening, electron density and temperature, and is linear with the observable quantity

$$\eta' = \frac{[OII] \lambda\lambda 3726, 3729 / [OIII] \lambda\lambda 4959, 5007}{[SII] \lambda\lambda 6717, 6731 / [SIII] \lambda\lambda 9069, 9532}$$

which is only weakly sensitive to nebular temperature, but shows a dependence on abundance and ionization parameter.

As a measure of the hardness of the radiation field, this parameter provides us with an indicator of the T_{eff} of the exciting stars of H II regions. The large difference in the ionization potentials of O^+ (35.1 eV) and S^+ (23.2 eV) is responsible for the sensitivity of η to the spectral energy distribution of the ionizing radiation. Spatially resolved observations of the Orion Nebula, NGC 604 in M33 and 30 Doradus in the LMC confirm the reliability of this method (Vílchez & Pagel 1988, Mathis & Rosa 1991), even though Ali *et al.* (1991) questioned it on the basis of possible effects of dielectronic recombination on the sulfur lines (the relative coefficient has not been computed yet).

Applications of the η method to study the physical properties of extragalactic H II regions include the works of Díaz *et al.* (1987), Vílchez & Pagel (1988), who derived a relationship between T_e and abundance, Díaz *et al.* (1991) for high-metallicity H II regions, and Garnett & Kennicutt (1997) for a large sample of objects in M101. Our dataset allows us the determination of η' values for a

large number of H II regions in a variety of spiral galaxies. In the following we can therefore examine the data in terms of variations of T_e with abundance and Hubble type.

5.1. Diagnostic diagrams involving η'

The data show a clear trend of η' as a function of R_{23} , which is related to the abundance sensitivity of the softness parameter (Figure 10). The single-star models also indicate an increase of T_e as the metallicity decreases. According to the cluster models, this is consistent with the expectations from the Salpeter, $M_{up} = 100 M_\odot$ IMF (Figures 19, 28), for ages of 1 and 2 Myr (both burst and continuous star formation modes). The points at low abundance (high R_{23}) correspond to a ionization parameter $\log U \simeq -2$. The bend of η' at larger metallicities is well reproduced with a decrease in $\log U$ ($\simeq -4$ at $2 Z_\odot$). The models corresponding to an upper mass limit of $30 M_\odot$ fail to match the data, both at high and low R_{23} values. Finally, the effects of an abundance-dependent N/O ratio are a lowering of the R_{23} values for the $2 Z_\odot$ models, and a slight increase of η' (Figure 41)

5.2. T_e as a function of metallicity and Hubble type

Caveat: The analysis that follows is to be considered preliminary, and at the time of writing work is still in progress to better define the metallicity dependence of T_e . The results of this section are very sensitive to the model surface fits adopted, and should be regarded with caution.

To derive a relationship between η' and T_e we rely on the single-star models that include the varying N/O abundance ratio (Figure 41). η' shows a dependence on metallicity (R_{23}), temperature and ionization parameter. As we will find later, the U dependence is small (but not negligible) when compared with the sensitivity

to the other two parameters, and this allows us to express $\eta' = \eta'(T_*, Z)$, where Z is the metallicity. Given that the ionization parameter for the H II regions is centered on the $\log U = -3$ value, a planar fit to the η' vs R_{23} models at fixed U ($\log U = -3$) was performed, without attempting a higher order fit, giving the sensitivity to the models adopted and the corresponding uncertainties. This is sufficient for our purpose to determine the relative T_* scale as a function of metallicity. We obtained:

$$T_* = 56.91 - 0.65 R_{23} - 13.33 \log \eta'$$

with T_* in units of 10^3 K. Fitting $\log R_{23}$ instead of R_{23} gives:

$$T_* = 63.86 - 13.10 \log R_{23} - 18.30 \log \eta'$$

which produces similar results for the calculated temperatures. Similarly for the $U - \eta'$ relation:

$$T_* = 48.52 - 1.15 \log U - 7.90 \log \eta'.$$

These results show a considerable sensitivity of T_{eff} to $\log R_{23}$, comparable to the sensitivity to $\log \eta'$. The $\log U$ dependence, while considerably smaller, can be neglected only to first order.

The limitations of this approach must be kept in mind. The planar fit simplifies, by definition, the intricacies of the models in the $R_{23} - \eta'$ plane, and consequently some information is lost. A look at Figure 10, for example, shows that especially at low abundances the planar fit might not be a good representation of the models. An estimate of the systematic effects introduced can be obtained by looking at the iso-thermal lines resulting from the planar fit. These lines are shown in Figure 43. The H II region sample has been divided according to the parent galaxy morphological type: early-type (Sa-Sb, open circles) and late-type (Sbc and

later, solid dots). There are additional limitations to this technique due to the effects of the ionization parameter on the nebular models. The results are also dependent on our choice of stellar atmospheres, and on the photoionization code.

To express η' as a function of abundance the indicator R_{23} needs to be converted to a metallicity scale. Since there are different calibrations of this parameter we have adopted the result of Zaritsky *et al.* (1994), who averaged the calibrations of Edmunds & Pagel (1984), McCall *et al.* (1985) and Dopita & Evans (1986). They provide a polynomial fit, repeated here for convenience:

$$12 + \log(\text{O}/\text{H}) = 9.265 - 0.33x - 0.202x^2 - 0.207x^3 - 0.333x^4 \quad (x = \log R_{23}).$$

Figure 44 suggests that there is a similar H II region T_e distribution, albeit with a large scatter, for spiral galaxies across the Hubble sequence. The T_e gradient with metallicity is also very clear. We have compared this gradient with the theoretical predictions for stellar models at different metallicities in Figure 45. The models of the Geneva group were used for the comparison (Schaller *et al.* 1992, Schaerer *et al.* 1993a, Schaerer *et al.* 1993b, Charbonnel *et al.* 1993). The predictions for the Zero Age Main Sequence (ZAMS, dotted line) and for an age of 1 Myr (continuous line) are shown for the 120 M_\odot , 85 M_\odot , 60 M_\odot , 40 M_\odot and 25 M_\odot models. Our H II region data have been binned and averaged to better show the T_e trend. There is a generally good agreement between the predictions and the observations. Given the uncertainties and the model-sensitivity of our η' - T_e calibration, and the intrinsic scatter of the H II region data, we can consider our result a rather good fit to the theoretical predictions. We note that if the IMF is truncated at 30-40 M_\odot for abundances above solar we should observe a much steeper T_e gradient, according to the present stellar evolutionary models.

The He I $\lambda 5876 - R_{23}$ gradient – As an additional test we have performed a planar

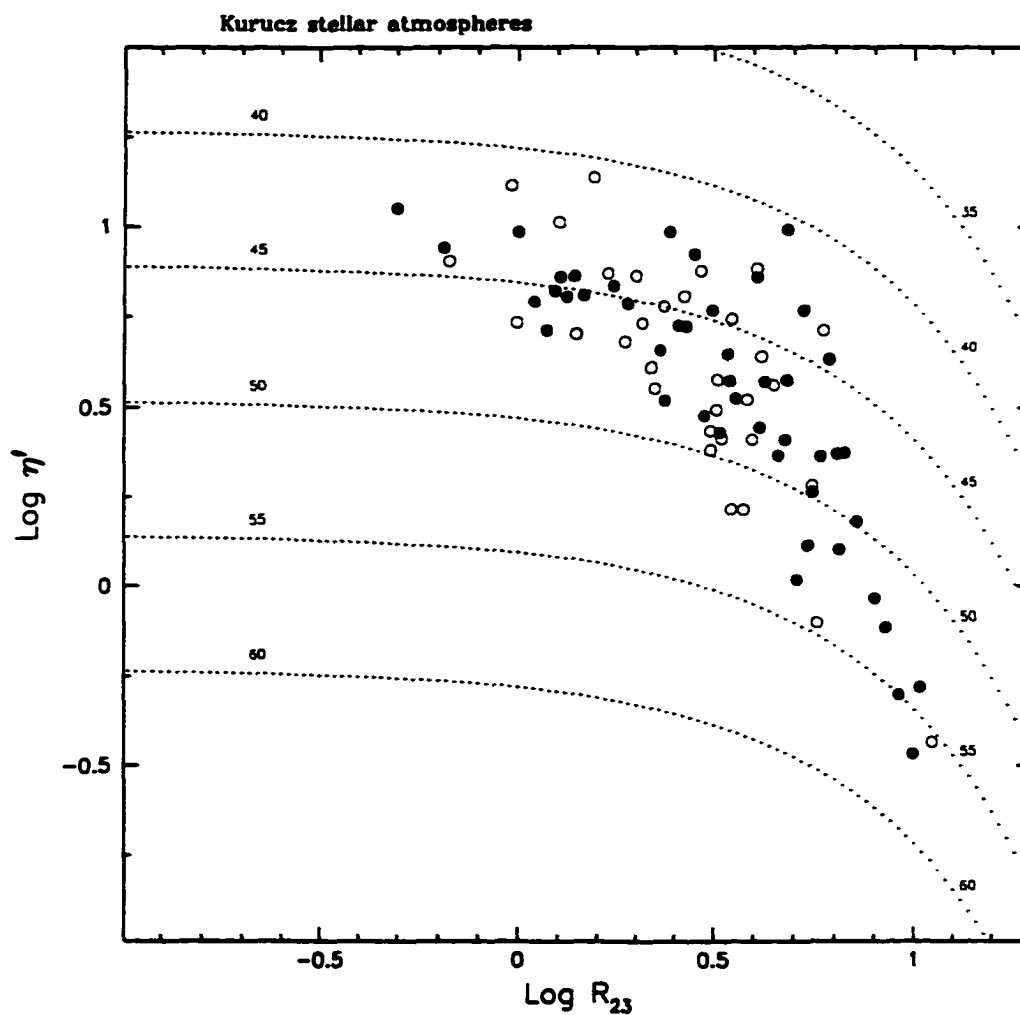


Figure 43 Lines of equal T_e according to the planar fit. Temperatures are given in units of 10^3 K. Open circles are used for H II regions in galaxy types Sa-Sb, solid dots for types Sbc and later.

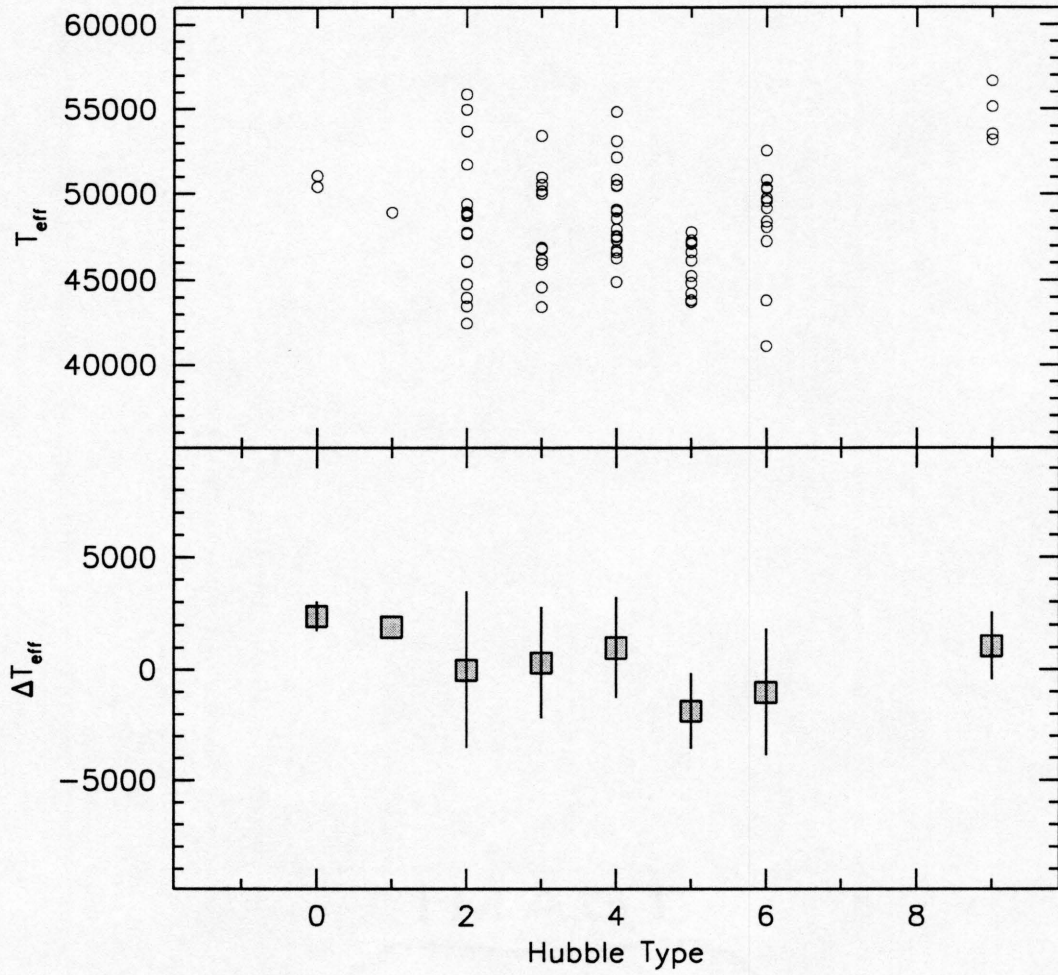


Figure 44 (*Top*) H II region T_{eff} as a function of the numerical Hubble type of the parent galaxy. (*Bottom*) The H II region T_{eff} vs Hubble type after a first-order correction for the trend with metallicity, using the average points of Fig. 45 to define the T_{eff} -Z trend.

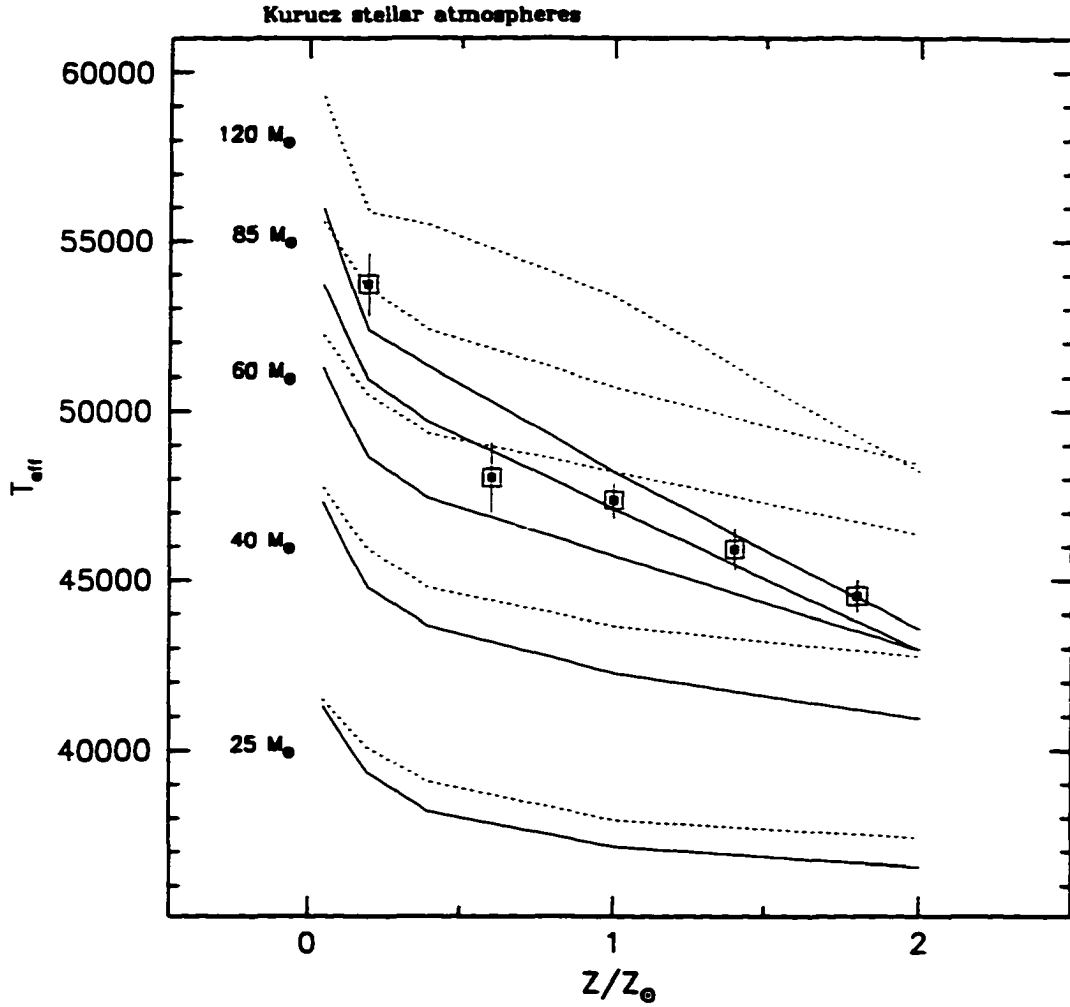


Figure 45 Comparison of the H II region Z - T_{eff} distribution derived from the $R_{23} - \log \eta'$ planar fit with the theoretical predictions for different stellar masses. The data have been binned in metallicity and averaged (squares). Stellar models are shown for the ZAMS (dotted lines) and for an age of 1 Myr (continuous lines). Open circles are used for H II regions in galaxy types Sa-Sb, solid dots for types Sbc and later. The error bars refer to the dispersion of the data.

fit to the model results for the He I $\lambda 5876$ gradient as a function of R_{23} . The resulting temperature distribution is shown against the metallicity in Figure 46. The temperature gradient is consistent with the trend found from η . A cooling of about 8,000 K is found between $\sim 0.2 Z_{\odot}$ and $\sim 2 Z_{\odot}$.

6. Discussion: does the IMF change with metallicity ?

The investigation on the possible variations of the IMF in star forming regions has often been stimulated by the Shields and Tinsley (1976) suggestion of a dependence of the upper mass limit on metallicity, $M_{up} \propto Z^{-a/2}$, with $a \simeq 1$. This followed from theoretical considerations by Kahn (1974), who argued that the increase of the interstellar grain opacity with Z would, as an effect of the consequent increase in radiation pressure, prevent further accretion onto a new star, and set an upper limit to the luminosity-to-mass ratio. Shields and Tinsley's theoretical $EW(H\beta)$ vs T_u (temperature of the hottest stars present) relation was, with the measured gradient of $EW(H\beta)$ in M101, only marginally consistent with a dependence of M_{up} on Z . Adopting a Salpeter slope ($\Gamma = -1.3$) for the IMF, instead of the steeper value used by Shields and Tinsley ($\Gamma \simeq -3$), would make the inferred T_u gradient inconsistent with a significant dependence of M_{up} on metallicity (Scalo 1986).

Direct counts of massive stars in resolved star clusters and OB associations in our Galaxy, the Magellanic Clouds and a few other Local Group galaxies do not show a variation of the IMF with the galactic environment or the metallicity (Massey *et al.* 1995a,b, Hunter *et al.* 1997). For more distant star forming regions, studies of the nebular recombination lines (*e.g.* García-Vargas *et al.* 1995, Stasińska & Leitherer 1996) and of the UV resonance lines (Robert *et al.* 1993) also point to a 'universality' of the IMF. In the previous sections we have compared several

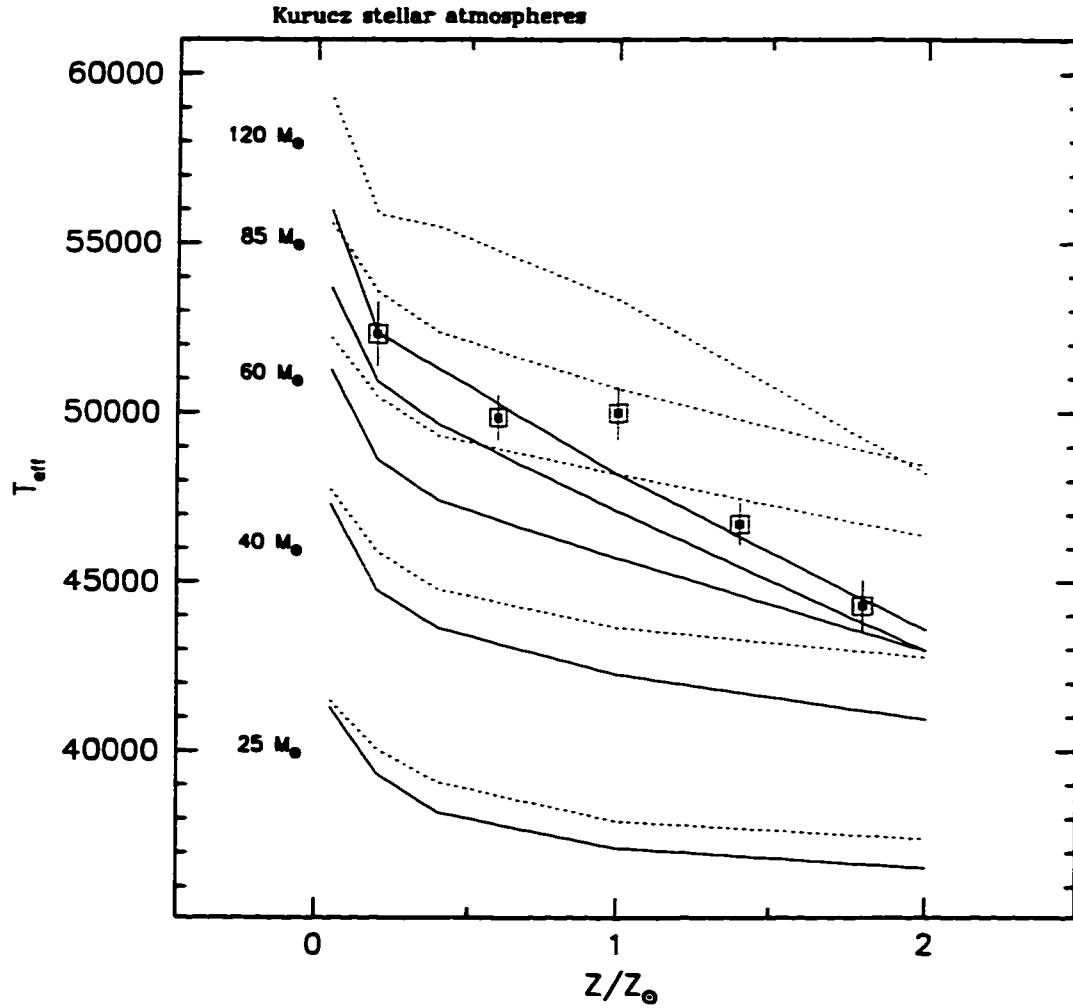


Figure 46 Comparison of the H II region Z - T_{eff} distribution derived from the $\log R_{23}$ - $\log \text{He I } \lambda 5876$ planar fit with the theoretical predictions for different stellar masses. The data have been binned in metallicity and averaged (squares). Stellar models are shown for the ZAMS (dotted lines) and for an age of 1 Myr (continuous lines). The error bars refer to the dispersion of the data.

emission-line diagnostics for a large H II region sample to theoretical photoionization predictions, and have accumulated evidence for an invariance of the IMF with metallicity. We will conclude with some comments on our results, also in order to summarize them.

The photoionization models with star clusters as ionizing sources often are, for the reasons explained in Section 4.3, difficult to interpret. However, taking into consideration the whole set of line diagnostics that we present, there is an indication that the canonical, Salpeter IMF is preferred over the low- M_{up} mass function. The former generally gives a better fit not only at small abundances (where the presence of high-mass stars provides the necessary high ionization parameter), but also at high metallicities, indicating that the upper mass limit is not sensibly decreasing over a large metallicity range. As mentioned earlier, no conclusion can be reached about the slope of the IMF. Our results are of course not only affected by the details of the nebular models (gas physical properties, the photoionization code and the atomic parameters used in it), but also by the shape of the ionizing continuum (determined by the stellar evolutionary tracks and the model atmospheres). Uncertainties in any of these will propagate to the final results. The adoption of different stellar tracks, for example, can produce non-negligible effects on the computed emission-line intensities (García-Vargas 1996, Stasińska & Leitherer 1996). The effects on the ionization structure of H II regions of the more recent atmosphere models, including departures from LTE and stellar winds, should also be investigated in detail.

The single-star models, though lacking the more complete approach of the cluster models, are also less complex and easier to interpret. We have derived a calibration of the softness parameter η' in terms of T_e and R_{23} , based on our

choice of stellar atmospheres. We derive a T_* gradient of $\sim 7000 - 8000$ K over the $0.2 - 2 Z_\odot$ metallicity range (the precise value of the high-abundance end is however uncertain, due to well-known difficulties in modeling R_{23} at such metallicities, see Oey & Kennicutt 1993). This is confirmed by the radial trend of the He I $\lambda 5876$ emission line intensity, and is consistent with the trend predicted by the 1 Myr Geneva stellar tracks. Metallicity effects on stellar evolution and atmosphere blanketing naturally produce a T_* gradient with a fixed IMF. If $M_{up} \propto Z^{-1/2}$, we find that the T_* gradient should be at least twice, $\simeq 15,000$ K, over the same metallicity range. Therefore, not only our observations are consistent with the canonical IMF, but they also rule out that the upper mass limit strongly depends on metallicity, in the way proposed by Shields & Tinsley. A milder dependence is not excluded, given the uncertainties in the stellar and nebular models, and in the procedure used to derive T_* . The lowest M_{up} value which is still consistent with the data at $Z = 2 Z_\odot$ is $\sim 60 M_\odot$ (with $M_{up} \simeq 100 M_\odot$ at low metallicities). The stellar tracks at older ages become steeper with metallicity, so they would not be appropriate for the comparison.

Finally, the H II region properties that we have examined, in particular T_* and the Balmer line equivalent widths, do not show a dependence on the morphological class of the parent galaxies. As we have seen, the ionizing stars of giant H II regions in Sa galaxies are as hot as those in Sc's and later type, once we account for the difference in metallicity. This result, together with the lack of a dependence of the equivalent widths on Hubble type, points to a similarity of the upper IMF in these vastly different stellar systems. Other physical causes must be responsible for the different properties of their star forming regions, namely the difference in luminosity and spatial density per unit galactic mass, across the Hubble sequence. As also suggested by Bresolin & Kennicutt (1997), some mechanism is producing

on average smaller ionizing clusters, and in smaller number, in early-type galaxies than in late-type galaxies.

6.1. Tests for the upper IMF: what is next?

The analysis of nearby planetary nebulae and small H II regions ionized by a single star, in the Galaxy and the Magellanic Clouds, would be important to test photoionization models similar to those presented here. A simplification in the interpretation would result from the ionization being provided by a single star rather than a star cluster. The observation of extragalactic H II regions in the far-IR, including the [OIII] 52.88 μm and [SIII] 19.33 μm lines, would also help in the determination of T_{eff} (Rubin *et al.* 1994), but the inferences for the IMF would still be model-dependent, since the nebular lines are produced by a complex interaction between the ionizing flux from the massive stars and the surrounding medium.

A direct signature of the massive stars in star forming regions is provided by the resonance UV lines Si IV $\lambda 1400$ and C IV $\lambda 1550$, which can put constraints on the upper IMF, in particular its slope α (Sekiguchi & Anderson 1987, Mas-Hesse & Kunth 1991). The sensitivity of these stellar-wind lines to the mass function derives from the wind momentum – luminosity relationship valid for individual stars (Kudritzki *et al.* 1996), combined with the mass – luminosity relation. Recent HST results on the required line-profile analysis show how the method can constrain the upper IMF (Leitherer *et al.* 1996b).

The only direct method to measure the upper IMF in star forming regions, counting individual stars, remains unfortunately limited to nearby galaxies. Even the investigation of the IMF in a handful of H II regions and OB associations beyond

the Magellanic Clouds (Hunter *et al.* 1996a,b) awaits confirmation by spectroscopic observations, since the IMF cannot be reliably determined from photometry alone. The painstaking job of classifying stars and measuring their brightness, in order to place them in an H-R diagram, can be carried out with current instrumentation only in a small number of galaxies. While this might be sufficient to investigate the influence of metallicity or location within a galaxy on the star formation process, more indirect methods such as the ones mentioned above are still required to study the IMF in a variety of galactic environments, and to better understand the starburst phenomenon and the massive stellar content of galaxies.

7. Tables with model results

We present here the tables containing the detailed results for the photoionization calculations discussed in Section 2.3: Tables 2.6 (a–c) for the single-star models, Tables 2.7 (a–i) for the stellar cluster models with burst star formation mode, and Tables 2.8 (a–i) for the stellar cluster models with continuous star formation mode. We report the predicted intensities (relative to $H\beta = 100$) of the most important emission-lines: [OII] $\lambda 3727$, [OIII] $\lambda 4959+5007$, He I $\lambda 5876$, [NII] $\lambda 6548+6584$, [SII] $\lambda 6716+6731$ and [SIII] $\lambda 9069+9532$ in columns 2 through 7. We also give $\log R_{23}$ (column 8), $\log \eta$ (column 9), and the equivalent width of $H\beta$, $EW(H\beta)$ (column 10). The latter was calculated considering both the stellar and the nebular continua. The first column in each table is the T_{eff} of the corresponding stellar atmosphere for the single-star models (Tables 2.6), and the age in Myr for the cluster models (Tables 2.7 and 2.8). The models are subdivided into the 4 metallicities studied: $0.1 Z_{\odot}$, $0.25 Z_{\odot}$, Z_{\odot} and $2 Z_{\odot}$. The caption in each table specifies the ionization parameter ($\log U$), and the parameters of the IMF in the

case of the cluster models (M_{up} and the slope α).

TABLE 2.6A									
SINGLE STAR MODELS			KURUCZ ATMOSPHERES					$\log I' = -2$	
T_E	[OII]	[OIII]	HeI	[NII]	[SII]	[SIII]	$\log R_{22}$	$\log \eta$	EW(H β)
0.1 Z_{\odot}									
37500	336	174	4	94	6	57	0.71	1.27	287
40000	121	541	9	30	5	54	0.82	0.37	409
45000	43	860	10	10	5	47	0.96	-0.35	590
50000	39	991	10	10	6	42	1.01	-0.55	698
60000	38	1178	10	11	7	35	1.08	-0.80	803
0.25 Z_{\odot}									
37500	358	137	4	137	10	90	0.69	1.38	303
40000	179	435	10	55	8	84	0.79	0.61	441
45000	69	894	11	19	9	80	0.98	-0.16	650
50000	64	1147	11	19	10	73	1.08	-0.41	797
60000	66	1556	10	21	13	65	1.21	-0.67	937
Z_{\odot}									
37500	213	11	5	163	15	138	0.35	2.23	333
40000	208	32	11	106	14	127	0.38	1.77	492
45000	101	144	16	32	11	86	0.39	0.75	800
50000	61	254	16	29	13	80	0.50	0.17	1062
60000	72	522	15	34	19	95	0.77	-0.16	1320
2 Z_{\odot}									
37500	62	1	5	95	12	111	-0.21	2.93	346
40000	84	2	13	86	12	126	-0.07	2.72	503
45000	123	12	23	47	12	104	0.13	1.95	826
50000	34	24	25	25	9	35	-0.24	0.76	1181
60000	38	51	25	29	14	37	-0.05	0.28	1671

TABLE 2.6B									
SINGLE STAR MODELS				KURUCZ ATMOSPHERES			$\log I' = -3$		
T_{eff}	[OII]	[OIII]	HeI	[NII]	[SII]	[SIII]	$\log R_{23}$	$\log \eta$	EW(II λ)
0.1 Z_{\odot}									
37500	352	89	4	103	28	44	0.64	0.79	291
40000	266	286	9	69	25	49	0.74	0.27	417
45000	189	522	10	48	22	56	0.85	-0.04	603
50000	170	618	10	46	23	56	0.90	-0.17	712
60000	156	740	10	46	26	54	0.95	-0.35	811
0.25 Z_{\odot}									
37500	395	72	4	157	48	71	0.67	0.91	305
40000	348	245	9	116	43	80	0.77	0.42	443
45000	302	543	11	92	41	94	0.93	0.11	657
50000	290	723	11	92	45	99	1.01	-0.05	804
60000	297	997	11	97	53	105	1.11	-0.23	936
Z_{\odot}									
37500	198	15	5	178	65	101	0.33	1.32	332
40000	220	48	11	158	64	114	0.43	0.92	481
45000	222	103	15	132	64	117	0.51	0.67	802
50000	221	163	15	132	69	113	0.58	0.41	1043
60000	309	403	15	168	87	150	0.85	0.12	1248
2 Z_{\odot}									
37500	44	2	6	86	39	64	-0.34	1.58	360
40000	68	6	13	107	47	89	-0.14	1.35	506
45000	84	13	20	102	45	86	-0.01	1.11	840
50000	86	20	23	96	45	85	0.03	0.79	1151
60000	126	47	23	110	61	75	0.24	0.52	1545

TABLE 2.6c									
SINGLE STAR MODELS					KURUCZ ATMOSPHERES			$\log I' = -4$	
T_{eff}	[OII]	[OIII]	HeI	[NII]	[SII]	[SIII]	$\log R_{13}$	$\log \eta$	EW(H β)
0.1 Z_{\odot}									
37500	305	14	4	105	64	18	0.50	0.79	204
40000	325	47	8	106	63	23	0.57	0.41	426
45000	333	107	11	107	64	31	0.64	0.17	616
50000	331	140	11	109	67	33	0.67	0.06	726
60000	323	188	12	111	74	34	0.71	-0.10	825
0.25 Z_{\odot}									
37500	381	12	4	175	113	31	0.59	0.93	306
40000	444	45	8	185	115	42	0.69	0.55	449
45000	528	122	11	205	126	59	0.81	0.30	658
50000	557	184	12	217	135	65	0.87	0.17	802
60000	600	280	12	234	154	72	0.94	0.00	930
Z_{\odot}									
37500	180	3	5	193	140	44	0.28	1.25	336
40000	238	12	10	222	152	62	0.40	0.91	489
45000	348	38	14	279	179	92	0.59	0.68	764
50000	426	75	15	321	210	107	0.70	0.46	961
60000	556	138	16	384	257	128	0.84	0.30	1200
2 Z_{\odot}									
37500	40	1	6	99	77	31	-0.39	1.34	358
40000	73	3	12	143	104	51	-0.12	1.12	605
45000	126	9	18	199	133	80	0.13	0.94	812
50000	145	14	20	217	148	84	0.20	0.77	1076
60000	214	28	21	275	187	105	0.38	0.64	1390

TABLE 2.7a
CLUSTER BURST MODELS $M_{up} = 100 M_{\odot}$, $\alpha = 2.35$ $\log I' = -2$

Age	[OII]	[OIII]	HeI	[NII]	[SII]	[SIII]	$\log R_{23}$	$\log \eta$	EW(H β)
0.1 Z_{\odot}									
1	38	1001	10	10	6	40	1.02	-0.60	554
2	40	905	10	10	5	45	0.98	-0.44	516
3	55	689	10	13	5	51	0.87	-0.07	230
4	142	480	9	35	5	54	0.79	0.47	66
5	286	218	5	79	6	55	0.70	1.08	35
6	326	134	3	93	6	54	0.66	1.33	28
0.25 Z_{\odot}									
1	63	1078	11	19	10	73	1.06	-0.38	571
2	67	876	11	18	9	78	0.97	-0.16	514
3	108	538	11	31	8	78	0.81	0.31	180
4	54	758	11	19	9	64	0.91	-0.30	93
5	49	762	10	10	10	59	0.91	-0.41	29
6	360	35	2	161	11	64	0.60	1.90	24
Z_{\odot}									
1	66	152	16	28	10	73	0.34	0.48	613
2	174	59	15	59	12	105	0.37	1.41	456
3	54	247	15	31	17	56	0.48	-0.15	250
4	61	276	15	34	20	52	0.53	-0.23	122
5	78	469	15	39	23	67	0.74	-0.32	98
6	70	423	14	37	22	64	0.69	-0.32	58
2 Z_{\odot}									
1	94	11	23	48	11	86	0.02	1.82	505
2	80	2	15	79	12	116	-0.09	2.58	384
3	40	59	24	32	19	26	0.00	-0.04	194
4	43	70	24	33	20	28	0.05	-0.07	113
5	51	121	23	38	23	35	0.24	-0.20	69
6	97	156	18	73	44	58	0.40	-0.09	27

TABLE 2.7b
CLUSTER BURST MODELS $M_{up} = 100 M_{\odot}$, $\alpha = 2.35$ $\log I' = -3$

Age	[OII]	[OIII]	HeI	[NII]	[SII]	[SIII]	$\log R_{23}$	$\log \eta$	EW(H β)
0.1 Z_{\odot}									
1	163	631	10	46	24	55	0.90	-0.22	567
2	179	557	10	47	23	56	0.87	-0.10	530
3	219	388	10	55	22	52	0.78	0.12	237
4	271	253	9	70	25	47	0.72	0.31	68
5	324	115	5	93	28	42	0.64	0.63	36
6	336	65	3	101	28	40	0.60	0.87	29
0.25 Z_{\odot}									
1	284	677	11	91	44	97	0.98	-0.04	581
2	295	533	11	91	41	93	0.92	0.10	523
3	310	301	10	104	41	80	0.79	0.31	184
4	236	487	11	89	44	80	0.86	-0.05	96
5	216	560	10	89	47	78	0.89	-0.20	30
6	350	13	2	156	48	59	0.56	1.50	24
Z_{\odot}									
1	219	139	15	135	59	117	0.55	0.49	583
2	218	70	14	141	58	110	0.46	0.80	451
3	175	185	15	123	73	86	0.56	0.05	262
4	180	218	14	127	82	84	0.60	-0.07	121
5	245	279	15	151	94	98	0.72	-0.03	98
6	210	305	14	138	86	100	0.71	-0.10	61
2 Z_{\odot}									
1	77	12	20	98	44	77	-0.00	1.06	579
2	55	5	14	94	43	77	-0.22	1.27	394
3	103	41	23	103	71	41	0.16	0.16	197
4	111	43	23	109	75	43	0.19	0.17	116
5	139	67	21	128	88	54	0.31	0.10	70
6	168	111	17	147	105	72	0.45	0.01	27

TABLE 2.7c									
CLUSTER BURST MODELS									
$M_{up} = 100 M_{\odot}$, $\alpha = 2.35$									
$\log I' = -4$									
Age	[OII]	[OIII]	HeI	[NII]	[SII]	[SIII]	$\log R_{23}$	$\log \eta$	EW(H β)
0.1 Z_{\odot}									
1	325	146	11	109	69	32	0.67	0.02	577
2	330	120	11	107	66	31	0.65	0.12	541
3	326	70	9	105	63	26	0.60	0.29	243
4	317	41	8	104	62	22	0.55	0.45	69
5	298	18	5	102	63	18	0.50	0.67	36
6	286	10	3	100	63	16	0.47	0.86	20
0.25 Z_{\odot}									
1	541	170	11	213	134	62	0.85	0.17	583
2	519	121	11	204	125	58	0.81	0.20	525
3	444	59	9	185	116	44	0.70	0.45	187
4	448	126	10	191	130	47	0.76	0.11	98
5	435	176	10	191	142	45	0.79	-0.10	31
6	308	2	2	154	106	22	0.49	1.50	24
Z_{\odot}									
1	357	49	14	285	188	94	0.61	0.50	582
2	274	20	12	240	160	74	0.47	0.81	464
3	355	105	14	295	236	81	0.66	0.06	244
4	349	119	14	295	255	74	0.67	-0.07	121
5	421	128	15	331	277	87	0.74	0.02	98
6	395	145	15	317	268	86	0.73	-0.06	60
2 Z_{\odot}									
1	119	9	17	193	132	74	0.10	0.89	502
2	74	3	13	146	106	52	-0.11	1.05	388
3	158	24	21	222	198	56	0.26	0.27	198
4	165	24	21	229	203	59	0.28	0.30	118
5	207	39	21	268	241	72	0.39	0.20	71
6	262	80	19	319	310	83	0.53	-0.00	27

TABLE 2.7d									
CLUSTER BURST MODELS									
$M_{up} = 30 M_{\odot}$, $\alpha = 2.35$									
$\log I' = -2$									
Age	[OII]	[OIII]	HeI	[NII]	[SII]	[SIII]	$\log R_{23}$	$\log \eta$	EW(H β)
0.1 Z_{\odot}									
1	58	669	10	13	5	51	0.86	-0.02	220
2	66	637	10	15	5	52	0.85	0.06	215
3	78	603	10	18	5	53	0.83	0.16	214
4	127	512	9	30	5	54	0.81	0.40	208
5	273	257	6	74	6	55	0.72	1.00	180
6	327	135	3	94	6	54	0.66	1.33	108
0.25 Z_{\odot}									
1	132	497	10	37	8	81	0.80	0.43	202
2	168	425	10	51	8	81	0.77	0.58	197
3	203	359	9	65	9	82	0.75	0.73	191
4	273	235	7	98	9	85	0.71	1.02	176
5	345	108	4	136	10	87	0.66	1.44	146
6	361	35	2	152	11	84	0.60	1.90	34
Z_{\odot}									
1	193	20	9	119	15	125	0.33	1.01	173
2	198	17	8	131	15	129	0.33	1.00	165
3	190	11	6	143	16	129	0.30	2.16	157
4	180	6	4	153	16	126	0.27	2.36	142
5	147	1	1	153	17	112	0.17	2.91	82
6	37	114	16	24	13	41	0.18	0.03	49
2 Z_{\odot}									
1	61	1	10	81	12	109	-0.21	2.79	171
2	58	1	7	86	12	106	-0.23	2.87	150
3	38	0	4	69	10	80	-0.42	2.87	139
4	27	0	1	62	11	64	-0.57	3.46	90
5	15	0	26	19	6	14	-0.69	0.74	46
6	97	158	18	73	45	59	0.41	-0.09	27

TABLE 2.7e									
CLUSTER BURST MODELS									
$M_{\text{up}} = 30 M_{\odot}$, $n = 2.35$									
$\log I = -3$									
Age	[OII]	[OIII]	HeI	[NII]	[SII]	[SIII]	$\log R_{12}$	$\log \eta$	EW(H β)
0.1 Z_{\odot}									
1	224	372	10	57	22	51	0.78	0.14	227
2	236	343	10	59	23	51	0.76	0.18	222
3	246	319	10	62	23	50	0.75	0.22	220
4	270	266	9	68	25	48	0.73	0.30	211
5	322	137	6	90	28	44	0.66	0.57	182
6	336	65	3	101	28	40	0.60	0.86	110
0.25 Z_{\odot}									
1	328	272	10	107	41	80	0.78	0.37	205
2	338	236	10	113	43	78	0.76	0.41	199
3	347	201	9	119	44	76	0.74	0.47	193
4	360	134	7	134	46	71	0.69	0.62	177
5	373	54	4	153	48	66	0.63	0.98	148
6	351	13	2	156	49	59	0.56	1.50	35
Z_{\odot}									
1	183	29	9	150	61	101	0.33	1.01	177
2	167	25	8	157	63	100	0.33	1.08	166
3	165	16	6	165	65	96	0.30	1.23	154
4	167	7	4	165	65	87	0.24	1.49	142
5	136	1	1	156	63	72	0.14	2.18	82
6	131	89	15	100	60	63	0.34	0.10	49
2 Z_{\odot}									
1	54	3	9	97	45	75	-0.25	1.43	171
2	37	2	7	74	36	58	-0.41	1.48	169
3	37	1	4	79	37	55	-0.42	1.70	138
4	22	0	1	56	30	34	-0.66	2.30	95
5	44	11	23	62	38	27	-0.26	0.46	40
6	164	101	18	144	102	63	0.42	0.00	27

TABLE 2.7f									
CLUSTER BURST MODELS									
$M_{\text{up}} = 30 M_{\odot}$, $n = 2.35$									
$\log I = -4$									
Age	[OII]	[OIII]	HeI	[NII]	[SII]	[SIII]	$\log R_{12}$	$\log \eta$	EW(H β)
0.1 Z_{\odot}									
1	325	66	9	105	62	26	0.59	0.31	231
2	324	60	9	104	62	25	0.58	0.34	227
3	323	53	9	104	62	24	0.58	0.37	225
4	321	42	8	104	62	23	0.56	0.44	215
5	307	21	5	104	63	19	0.52	0.63	185
6	286	10	3	101	63	16	0.47	0.86	111
0.25 Z_{\odot}									
1	443	51	9	184	115	43	0.69	0.51	209
2	432	44	9	182	114	41	0.68	0.55	202
3	420	36	8	179	113	38	0.66	0.60	196
4	393	23	6	174	112	34	0.62	0.71	180
5	353	9	4	166	111	27	0.56	0.99	149
6	309	2	2	155	107	22	0.49	1.50	35
Z_{\odot}									
1	201	8	9	202	143	52	0.32	0.97	174
2	188	6	8	195	140	48	0.29	1.03	167
3	169	3	6	184	136	41	0.24	1.18	157
4	148	1	4	172	131	34	0.17	1.43	141
5	115	0	1	149	119	24	0.06	2.12	82
6	257	52	14	235	187	60	0.40	0.20	49
2 Z_{\odot}									
1	51	1	9	116	89	38	-0.28	1.18	172
2	38	1	7	96	76	30	-0.41	1.24	163
3	32	0	4	86	70	24	-0.49	1.49	136
4	18	0	1	59	53	14	-0.75	2.16	90
5	66	7	18	126	109	33	-0.14	0.45	50
6	251	74	20	309	301	81	0.51	-0.04	28

TABLE 2.7a									
CLUSTER BURST MODELS									
$M_{up} = 100 M_{\odot}, n = 3.30$									
$\log U = -2$									
Age	[OII]	[OIII]	HeI	[NII]	[SII]	[SIII]	$\log R_{33}$	$\log \eta$	EW(H β)
0.1 Z_{\odot}									
1	38	928	10	10	6	42	0.99	-0.52	237
2	41	856	10	10	6	46	0.95	-0.38	234
3	55	685	10	13	6	51	0.87	-0.06	168
4	145	474	9	36	6	64	0.79	0.48	73
5	285	218	5	79	6	55	0.70	1.08	40
6	323	136	3	92	6	54	0.66	1.32	29
0.25 Z_{\odot}									
1	63	949	11	19	10	74	1.01	-0.29	228
2	68	800	11	19	8	78	0.94	-0.10	223
3	122	511	10	35	8	79	0.80	0.38	140
4	68	598	11	24	8	67	0.82	-0.01	77
5	60	596	10	28	8	63	0.82	-0.00	30
6	356	36	2	150	11	83	0.59	1.68	23
Z_{\odot}									
1	72	111	16	30	10	70	0.26	0.68	224
2	174	49	14	67	12	106	0.35	1.48	200
3	68	105	15	47	20	61	0.21	0.23	141
4	30	115	15	24	11	38	0.10	-0.05	76
5	64	292	15	35	20	56	0.55	-0.22	58
6	54	261	14	31	18	50	0.50	-0.24	37
2 Z_{\odot}									
1	92	7	22	59	11	94	-0.01	2.05	216
2	78	2	13	84	12	119	-0.10	2.68	178
3	9	6	28	13	3	11	-0.82	0.72	102
4	27	31	25	24	14	18	-0.24	0.03	66
5	40	71	23	32	19	24	0.05	-0.15	40
6	64	70	19	53	33	35	0.13	-0.01	18

TABLE 2.7b									
CLUSTER BURST MODELS									
$M_{up} = 100 M_{\odot}, n = 3.30$									
$\log U = -3$									
Age	[OII]	[OIII]	HeI	[NII]	[SII]	[SIII]	$\log R_{33}$	$\log \eta$	EW(H β)
0.1 Z_{\odot}									
1	167	582	10	46	23	55	0.87	-0.17	245
2	182	524	10	48	22	55	0.85	-0.07	242
3	220	385	10	55	22	52	0.78	0.12	174
4	273	249	9	71	25	47	0.72	0.32	75
5	323	115	5	93	28	42	0.64	0.63	41
6	333	66	3	100	28	40	0.60	0.86	30
0.25 Z_{\odot}									
1	279	590	11	90	42	93	0.94	0.01	235
2	293	481	11	92	40	90	0.89	0.13	229
3	319	283	10	106	41	80	0.78	0.34	143
4	249	370	10	96	42	75	0.79	0.68	70
5	220	422	10	96	45	72	0.81	-0.07	31
6	348	14	2	155	48	59	0.56	1.49	23
Z_{\odot}									
1	191	98	15	125	53	105	0.46	0.59	227
2	209	64	13	141	58	113	0.44	0.80	199
3	119	91	15	100	54	67	0.32	0.21	144
4	113	110	14	97	60	62	0.35	0.03	78
5	185	179	15	126	80	78	0.56	0.01	50
6	159	200	14	115	72	79	0.56	-0.06	38
2 Z_{\odot}									
1	64	8	10	93	43	72	-0.14	1.12	225
2	47	4	13	85	40	71	-0.29	1.29	189
3	52	16	23	68	45	28	-0.17	0.32	103
4	76	26	23	86	60	34	0.01	0.22	68
5	98	38	22	100	71	39	0.13	0.15	42
6	106	52	18	106	80	45	0.20	0.07	18

TABLE 2.7 CLUSTER BUNST MODELS $M_{up} = 100 M_{\odot}$, $\alpha = 3.30$ $\log t' = -4$									
Age	[OII]	[OIII]	HeI	[NII]	[SII]	[SIII]	$\log R_{23}$	$\log \eta$	EW(H β)
0.1 Z_{\odot}									
1	324	130	11	107	67	31	0.66	0.06	250
2	328	110	11	106	65	30	0.64	0.15	247
3	325	69	9	105	63	26	0.60	0.29	177
4	317	40	8	104	62	22	0.55	0.45	77
5	298	18	5	102	63	18	0.50	0.67	41
6	284	10	3	100	63	16	0.47	0.84	30
0.25 Z_{\odot}									
1	519	143	11	206	130	58	0.82	0.21	238
2	502	106	11	199	124	54	0.78	0.32	231
3	442	54	9	184	115	43	0.70	0.48	140
4	421	89	9	182	121	41	0.71	0.21	81
5	406	122	9	181	130	39	0.72	0.00	32
6	306	2	2	154	106	22	0.49	1.48	23
Z_{\odot}									
1	321	39	14	267	176	85	0.56	0.60	222
2	264	19	12	235	157	71	0.45	0.81	200
3	243	54	13	229	177	61	0.47	0.19	145
4	244	68	13	232	194	55	0.49	0.01	79
5	356	103	15	296	250	75	0.66	0.01	57
6	325	108	14	278	237	72	0.64	-0.04	37
2 Z_{\odot}									
1	84	5	17	157	110	61	-0.05	0.93	234
2	68	3	12	138	102	47	-0.15	1.08	181
3	88	12	18	153	135	37	0.00	0.31	110
4	119	16	20	164	164	46	0.13	0.31	71
5	150	25	20	215	198	55	0.24	0.23	42
6	172	46	19	238	237	60	0.34	-0.02	19

TABLE 2.8A CLUSTER CONTINUOUS MODELS $M_{up} = 100 M_{\odot}$, $\alpha = 2.35$ $\log t' = -2$									
Age	[OII]	[OIII]	HeI	[NII]	[SII]	[SIII]	$\log R_{23}$	$\log \eta$	EW(H β)
0.1 Z_{\odot}									
1	38	1021	10	10	6	39	1.02	-0.63	559
2	38	990	10	10	6	40	1.01	-0.59	547
3	38	935	10	10	6	42	0.99	-0.52	496
4	39	901	10	10	6	43	0.97	-0.49	327
5	39	878	10	10	6	43	0.96	-0.47	223
6	39	867	10	10	5	43	0.96	-0.45	177
0.25 Z_{\odot}									
1	63	1139	11	19	11	71	1.08	-0.43	583
2	63	1059	11	19	10	73	1.05	-0.37	564
3	63	949	11	19	10	74	1.01	-0.28	474
4	61	949	11	18	10	71	1.00	-0.32	338
5	61	925	11	19	10	70	0.99	-0.32	246
6	60	917	11	19	10	70	0.99	-0.32	190
Z_{\odot}									
1	59	178	16	27	11	72	0.38	0.33	635
2	66	142	16	28	10	72	0.32	0.52	590
3	58	113	16	28	9	63	0.23	0.54	485
4	45	146	16	26	11	58	0.28	0.21	379
5	42	148	16	25	11	56	0.28	0.15	323
6	44	162	16	26	12	57	0.31	0.11	272
2 Z_{\odot}									
1	50	17	25	36	9	53	-0.14	1.29	616
2	60	10	23	50	11	76	-0.04	1.74	531
3	23	9	26	27	7	25	-0.50	0.97	434
4	17	11	20	19	6	18	-0.56	0.63	343
5	15	13	26	17	7	16	-0.55	0.47	291
6	16	14	26	18	7	16	-0.53	0.41	256

TABLE 2.8a									
CLUSTER CONTINUOUS MODELS									
$M_{\text{up}} = 100 M_{\odot}$, $\alpha = 2.35$									
$\log I' = -3$									
Age	[OII]	[OIII]	HeI	[NII]	[SII]	[SIII]	$\log R_{23}$	$\log \eta$	EW(H β)
0.1 Z_{\odot}									
1	161	644	10	46	24	55	0.91	-0.24	572
2	164	624	10	46	23	55	0.90	-0.21	561
3	169	585	10	46	23	55	0.88	-0.16	510
4	171	561	10	47	23	54	0.86	-0.14	338
5	171	547	10	47	23	54	0.86	-0.13	231
6	172	539	10	47	23	54	0.85	-0.12	183
0.25 Z_{\odot}									
1	281	722	11	91	45	98	1.00	-0.08	593
2	283	666	11	91	44	96	0.98	-0.03	573
3	281	591	11	91	43	93	0.94	0.02	483
4	271	597	11	90	43	91	0.94	-0.02	347
5	266	588	11	90	43	90	0.93	-0.03	253
6	264	583	11	89	43	90	0.93	-0.03	195
Z_{\odot}									
1	222	158	15	136	61	117	0.58	0.43	600
2	210	126	15	132	57	113	0.53	0.52	570
3	178	101	15	121	54	99	0.45	0.51	479
4	164	117	15	116	57	90	0.45	0.34	383
5	160	120	15	115	58	87	0.45	0.30	326
6	161	124	15	115	60	87	0.45	0.28	278
2 Z_{\odot}									
1	74	13	21	93	42	66	-0.06	0.95	624
2	68	10	20	91	42	68	-0.12	1.05	547
3	55	11	22	76	39	43	-0.18	0.73	438
4	57	14	23	75	41	40	-0.14	0.58	347
5	59	16	23	75	43	38	-0.13	0.52	296
6	60	17	23	76	44	39	-0.12	0.50	260

TABLE 2.8c									
CLUSTER CONTINUOUS MODELS									
$M_{\text{up}} = 100 M_{\odot}$, $\alpha = 2.35$									
$\log I' = -4$									
Age	[OII]	[OIII]	HeI	[NII]	[SII]	[SIII]	$\log R_{23}$	$\log \eta$	EW(H β)
0.1 Z_{\odot}									
1	324	153	11	109	69	33	0.68	0.00	583
2	325	145	11	108	68	32	0.67	0.03	571
3	326	131	11	107	67	31	0.66	0.07	519
4	324	125	11	107	67	31	0.65	0.08	344
5	322	120	11	106	66	30	0.65	0.09	236
6	322	118	11	106	66	30	0.64	0.09	187
0.25 Z_{\odot}									
1	548	185	12	215	138	64	0.86	0.14	595
2	530	165	11	212	134	62	0.85	0.18	574
3	521	143	11	206	130	59	0.82	0.22	486
4	511	150	11	205	132	58	0.82	0.17	350
5	504	148	11	204	132	56	0.81	0.16	256
6	501	147	11	203	132	56	0.81	0.16	190
Z_{\odot}									
1	376	58	14	296	195	97	0.64	0.51	598
2	347	46	14	281	184	91	0.60	0.57	563
3	302	40	14	258	173	81	0.53	0.55	476
4	302	54	14	260	183	80	0.55	0.39	382
5	324	65	14	273	195	82	0.59	0.32	313
6	322	65	14	273	197	81	0.59	0.30	260
2 Z_{\odot}									
1	106	9	18	180	124	71	0.06	0.84	633
2	110	8	17	184	128	70	0.07	0.87	530
3	92	9	18	164	123	55	0.00	0.60	448
4	100	11	19	170	132	54	0.04	0.57	355
5	106	12	19	176	138	55	0.07	0.53	302
6	107	13	19	177	140	55	0.08	0.52	265

TABLE 2.8D									
CLUSTER CONTINUOUS MODELS									
$M_{up} = 30 M_{\odot}$, $\alpha = 2.35$									
$\log U = -2$									
Age	[OII]	[OIII]	HeI	[NII]	[SII]	[SIII]	$\log R_{12}$	$\log \eta$	EW(H β)
0.1 Z_{\odot}									
1	55	684	10	13	5	51	0.87	-0.06	223
2	58	668	10	13	5	51	0.86	-0.02	220
3	62	653	10	14	5	52	0.85	0.02	219
4	66	635	10	15	5	52	0.85	0.06	215
5	77	605	10	18	5	53	0.83	0.14	211
6	174	431	9	41	12	56	0.78	0.29	204
0.25 Z_{\odot}									
1	113	532	11	31	8	80	0.81	0.34	205
2	131	496	10	37	8	81	0.80	0.42	203
3	147	462	10	43	8	81	0.78	0.50	198
4	169	420	10	52	8	81	0.77	0.59	196
5	198	363	9	64	9	82	0.75	0.71	188
6	221	317	8	75	9	82	0.73	0.81	182
Z_{\odot}									
1	101	22	10	114	14	123	0.33	1.88	176
2	191	20	9	119	14	124	0.32	1.91	174
3	193	18	9	125	15	126	0.32	1.97	169
4	188	15	8	130	15	126	0.31	2.01	165
5	185	13	7	135	15	125	0.30	2.06	162
6	167	12	6	136	15	116	0.25	2.04	118
2 Z_{\odot}									
1	68	1	10	86	12	114	-0.16	2.75	171
2	64	1	9	85	12	111	-0.19	2.78	166
3	46	1	8	70	11	92	-0.33	2.72	167
4	49	1	7	76	11	95	-0.31	2.76	148
5	41	1	7	77	11	81	-0.38	2.07	114
6	40	2	15	74	11	61	-0.38	2.13	92

TABLE 2.8E									
CLUSTER CONTINUOUS MODELS									
$M_{up} = 30 M_{\odot}$, $\alpha = 2.35$									
$\log U = -3$									
Age	[OII]	[OIII]	HeI	[NII]	[SII]	[SIII]	$\log R_{12}$	$\log \eta$	EW(H β)
0.1 Z_{\odot}									
1	220	385	10	55	22	52	0.78	0.12	230
2	224	371	10	57	22	51	0.78	0.14	227
3	229	359	10	58	23	51	0.77	0.16	226
4	236	342	10	59	23	51	0.76	0.18	223
5	244	321	10	62	23	50	0.75	0.21	218
6	264	276	9	68	25	49	0.73	0.27	205
0.25 Z_{\odot}									
1	321	293	10	104	41	81	0.79	0.34	209
2	326	274	10	107	41	80	0.78	0.36	206
3	331	256	10	110	42	79	0.77	0.39	201
4	336	235	9	113	43	77	0.76	0.41	198
5	340	207	9	118	44	75	0.74	0.45	191
6	340	183	8	122	45	73	0.72	0.48	184
Z_{\odot}									
1	195	35	10	154	63	104	0.36	0.97	174
2	182	29	9	150	61	100	0.32	1.01	177
3	194	29	8	159	64	102	0.35	1.03	166
4	191	25	7	161	65	100	0.33	1.07	161
5	183	21	7	161	64	96	0.31	1.12	149
6	169	21	6	157	63	91	0.28	1.07	116
2 Z_{\odot}									
1	55	4	10	98	45	77	-0.23	1.41	172
2	49	3	9	91	42	71	-0.28	1.42	169
3	48	3	8	91	42	69	-0.29	1.46	161
4	44	2	7	86	41	64	-0.33	1.50	149
5	34	2	7	76	38	59	-0.44	1.40	117
6	30	2	12	64	35	33	-0.50	1.23	95

TABLE 2.8f
CLUSTER CONTINUOUS MODELS $M_{up} = 30 M_{\odot}$, $\alpha = 2.35$ $\log I' = -4$

Age	[OII]	[OIII]	HeI	[NII]	[SII]	[SIII]	$\log R_{13}$	$\log \eta$	EW(H β)
0.1 Z_{\odot}									
1	325	68	9	105	63	26	0.59	0.29	235
2	325	65	9	105	63	26	0.59	0.31	232
3	324	62	9	105	62	25	0.59	0.33	231
4	324	59	9	105	62	25	0.58	0.34	227
5	322	54	9	104	62	24	0.58	0.36	223
6	320	47	8	104	62	23	0.56	0.40	208
0.25 Z_{\odot}									
1	449	56	9	186	115	44	0.70	0.48	213
2	443	52	9	184	115	43	0.69	0.50	210
3	438	48	9	183	114	42	0.69	0.53	204
4	430	44	8	181	114	41	0.68	0.55	201
5	419	38	8	179	113	39	0.66	0.58	193
6	407	34	7	176	112	37	0.64	0.60	186
Z_{\odot}									
1	205	9	9	204	143	54	0.33	0.95	177
2	200	8	9	201	142	52	0.32	0.97	174
3	193	7	8	197	140	50	0.30	1.00	170
4	184	6	7	192	139	46	0.28	1.03	165
5	174	5	7	187	137	43	0.25	1.07	152
6	166	5	6	182	135	41	0.23	0.98	119
2 Z_{\odot}									
1	55	2	10	121	92	40	-0.25	1.16	174
2	54	1	9	120	92	38	-0.26	1.19	167
3	49	1	8	114	88	35	-0.30	1.22	159
4	38	1	7	96	76	29	-0.41	1.23	151
5	38	1	6	98	79	28	-0.41	0.99	115
6	30	3	11	84	72	23	-0.48	0.46	105

TABLE 2.8g
CLUSTER CONTINUOUS MODELS $M_{up} = 100 M_{\odot}$, $\alpha = 3.30$ $\log I' = -2$

Age	[OII]	[OIII]	HeI	[NII]	[SII]	[SIII]	$\log R_{13}$	$\log \eta$	EW(H β)
0.1 Z_{\odot}									
1	38	947	10	10	6	41	0.99	-0.55	234
2	38	921	10	10	6	42	0.98	-0.51	234
3	39	878	10	10	5	44	0.96	-0.44	228
4	40	839	10	10	5	45	0.94	-0.40	189
5	40	809	10	10	5	45	0.93	-0.36	146
6	41	789	10	11	5	45	0.92	-0.34	117
0.25 Z_{\odot}									
1	62	999	11	19	10	72	1.03	-0.34	228
2	63	937	11	19	9	74	1.00	-0.28	228
3	64	849	11	19	9	75	0.96	-0.20	213
4	62	824	11	19	9	73	0.95	-0.21	182
5	61	796	11	19	9	72	0.93	-0.20	142
6	61	773	11	19	9	71	0.92	-0.19	113
Z_{\odot}									
1	61	128	16	28	10	67	0.28	0.51	223
2	75	107	16	31	10	70	0.26	0.71	219
3	76	80	16	37	10	66	0.19	0.81	202
4	46	88	16	29	9	62	0.13	0.50	175
5	41	91	16	27	9	48	0.12	0.39	147
6	38	99	16	26	9	47	0.14	0.30	125
2 Z_{\odot}									
1	68	11	24	47	10	66	-0.10	1.61	217
2	83	6	21	63	11	88	-0.05	2.00	205
3	39	4	23	50	9	41	-0.36	1.63	182
4	28	4	25	37	8	28	-0.40	1.41	140
5	22	6	25	28	7	21	-0.50	1.05	128
6	20	7	26	25	7	19	-0.57	0.90	110

TABLE 2.8ii									
CLUSTER CONTINUOUS MODELS									
$M_{\text{up}} = 100 M_{\odot}$, $\alpha = 3.30$									
$\log t = -3$									
Age	[OII]	[OIII]	HeI	[NII]	[SII]	[SIII]	$\log R_{22}$	$\log \eta$	EW(H β)
0.1 Z_{\odot}									
1	165	595	10	46	23	55	0.88	-0.19	242
2	168	577	10	46	23	55	0.87	-0.16	242
3	175	544	10	47	23	54	0.86	-0.11	236
4	177	517	10	48	23	54	0.84	-0.09	196
5	181	494	10	49	23	53	0.83	-0.07	152
6	182	481	10	49	23	53	0.82	-0.05	121
0.25 Z_{\odot}									
1	275	828	11	90	43	94	0.96	-0.02	234
2	279	584	11	90	42	93	0.94	0.02	234
3	280	521	11	91	41	90	0.90	0.07	218
4	271	509	11	90	41	88	0.89	0.05	187
5	266	495	11	90	41	86	0.88	0.05	146
6	264	481	11	91	42	85	0.87	0.05	116
Z_{\odot}									
1	193	111	15	126	55	105	0.48	0.52	223
2	187	92	15	124	53	104	0.45	0.60	224
3	170	81	15	122	53	97	0.40	0.59	203
4	148	88	15	113	53	85	0.37	0.43	176
5	144	96	15	112	55	82	0.38	0.35	146
6	139	95	15	109	55	79	0.37	0.33	126
2 Z_{\odot}									
1	64	10	20	89	41	64	-0.13	1.02	227
2	56	7	19	87	41	65	-0.20	1.12	217
3	46	7	20	74	38	43	-0.28	0.89	187
4	45	8	21	69	37	36	-0.27	0.72	152
5	47	10	22	68	38	34	-0.24	0.62	131
6	48	11	22	68	38	33	-0.23	0.59	112

TABLE 2.8i									
CLUSTER CONTINUOUS MODELS									
$M_{\text{up}} = 100 M_{\odot}$, $\alpha = 3.30$									
$\log t = -4$									
Age	[OII]	[OIII]	HeI	[NII]	[SII]	[SIII]	$\log R_{22}$	$\log \eta$	EW(H β)
0.1 Z_{\odot}									
1	323	136	11	107	68	31	0.66	0.04	247
2	324	129	11	107	67	31	0.66	0.07	247
3	325	118	11	106	66	30	0.65	0.10	240
4	323	110	10	106	65	30	0.64	0.12	200
5	322	102	10	105	65	29	0.63	0.14	155
6	320	99	10	105	65	28	0.62	0.15	124
0.25 Z_{\odot}									
1	524	155	11	208	132	60	0.83	0.18	237
2	518	141	11	205	120	68	0.82	0.22	237
3	502	123	11	200	126	55	0.80	0.26	222
4	489	121	11	198	120	53	0.79	0.23	189
5	480	119	11	196	126	52	0.78	0.22	148
6	473	117	10	195	125	51	0.77	0.22	118
Z_{\odot}									
1	331	45	14	272	181	87	0.57	0.55	221
2	315	38	13	263	174	83	0.55	0.60	218
3	284	33	13	249	168	76	0.50	0.59	201
4	263	40	13	239	168	71	0.48	0.45	180
5	269	45	13	243	175	70	0.50	0.37	148
6	266	48	13	241	175	69	0.50	0.34	128
2 Z_{\odot}									
1	95	7	17	168	118	65	0.01	0.87	232
2	90	6	16	163	115	61	-0.02	0.90	214
3	70	6	16	139	105	48	-0.12	0.71	198
4	78	8	17	147	115	46	-0.07	0.60	158
5	80	9	17	149	119	45	-0.05	0.54	138
6	82	9	18	150	121	44	-0.04	0.52	118

REFERENCES

- Ali, B., Blum, R. D., Bumgardner, T. E., Cranmer, S. R., Ferland, G. J., Haefner, R. I., & Tiede, G. P. 1991, *PASP*, 103, 1182
- Aller, L. H. 1942, *ApJ*, 95, 52
- Balick, B., & Sneden, C. 1976, *ApJ*, 208, 336
- Bressan, A., Fagotto, F., Bertelli, G., & Chiosi, C. 1993, *A&AS*, 100, 647
- Bresolin, F., & Kennicutt, R. C. 1997, *AJ*, 113, 975
- Campbell, A. 1988, *ApJ*, 335, 644
- Campbell, A., Terlevich, R., & Melnick, J. 1986, *MNRAS*, 223, 811
- Carranza, G., Crillon, R., & Monnet, G. 1969, *A&A*, 1, 479
- Cerviño, M., & Mas-Hesse, J. M. 1994, *A&A*, 284, 749
- Charbonnel, C., Meynet, G., Maeder, A., Schaller, G., & Schaerer, D. 1993, *A&AS*, 101, 415
- Clegg, R. E. S., & Middlemass, D. 1987, *MNRAS*, 228, 759
- Díaz, A. I., Terlevich, E., Pagel, B. E. J., Vílchez, J. M., & Edmunds, M. G. 1987, *MNRAS*, 226, 19
- Díaz, A. I., Terlevich, E., Vílchez, J. M., Pagel, B. E. J., & Edmunds, M. G. 1991, *MNRAS*, 253, 245
- Dopita, M. A., & Evans, I. N. 1986, *ApJ*, 307, 431
- Dufour, R. J., Talbot, R. J., Jensen, E. B., & Shields, G. A. 1980, *ApJ*, 236, 119
- Edmunds, M. G., & Pagel, B. E. J. 1984, *MNRAS*, 211, 507
- Evans, I. N. 1991, *ApJS*, 76, 985
- Evans, I. N., & Dopita, M. A. 1985, *ApJS*, 58, 125

- Fagotto, F., Bressan, A., Bertelli, G., & Chiosi, C. 1994a. A&AS. 104. 365
- Fagotto, F., Bressan, A., Bertelli, G., & Chiosi, C. 1994b. A&AS. 105. 29
- Ferland, G. J. 1996, HAZY: A Brief Introduction to CLOUDY, V.90.01
- Fierro, J., Torres-Peimbert, S., & Peimbert, M. 1986. PASP. 98. 1032
- García-Vargas, M. L 1996, *From Stars to Galaxies: the Impact of Stellar Physics on Galaxy Evolution*, eds. C. Leitherer, U. Fritze-von Alvensleben & J. Huchra, ASP Conf. Proc. 98, p. 244
- García-Vargas, M. L., & Díaz, A. I. 1994, ApJS, 91, 553
- García-Vargas, M. L., Bressan, A., & Díaz, A. I. 1995, A&ASS. 112, 13
- García-Vargas, M. L., González-Delgado, R. M., Pérez, E., Alloin, D., Díaz, A., & Terlevich, E. 1997, ApJ, 478, 112
- Garnett, D. R. 1989, ApJ, 345, 282
- Garnett, D. R. 1990, ApJ, 363, 142
- Garnett, D. R., & Shields, G. A. 1987, ApJ, 317, 82
- Garnett, D. R., Dufour, R. J., Peimbert, M., Torres-Peimbert, S., Shields, G. A., Skillman, E. D., Terlevich, E., & Terlevich, R. J. 1995, ApJ, 449, 77
- Garnett, D. R., & Kennicutt, R. C. 1997, in preparation
- González-Delgado, R. M., Leitherer, C., Heckman, T., & Cerviño, M. 1997, ApJ, in press
- Grevesse, N., & Anders, E. 1989, *Cosmic Abundances of Matter*, ed. C. J. Waddington (AIP Conf. Proc. 183)(New York: AIP)
- Henry, R. B. C., & Howard, J. W. 1995, ApJ, 438, 170

- Hodge, P. W., & Kennicutt, R. C. 1983, *An Atlas of H II Regions in 125 Galaxies* (PAPS Document ANJOA88-296-300) (NY: AIP Auxiliary Publication Service)
- Hummer, D. G., & Mihalas, D. M. 1970, MNRAS, 147, 339
- Kelson, D., *et al.* 1996, ApJ, 463, 26
- Kennicutt, R. C. 1983, ApJ, 272, 54
- Kennicutt, R. C. 1984, ApJ, 287, 116
- Kennicutt, R. C. 1991, *Massive Stars in Starbursts*, STScI Symposium Series, eds. C. Leitherer, N. R. Walborn, T. M. Heckman & C. A. Norman (Cambridge University Press), p. 157
- Kennicutt, R. C., & Hodge, P. W. 1986, ApJ, 306, 130
- Kennicutt, R. C., & Chu, Y. 1988, AJ, 95, 720
- Kennicutt, R. C., & Garnett, D. R. 1996, ApJ, 456, 504
- Kahn, F. D., 1974, A&A, 37, 149
- Kudritzki, R.-P., & Hummer, D. G. 1990, ARAA, 28, 303
- Kudritzki, R.-P., Lennon, D. J., Haser, S. M., Puls, J., Pauldrach, A. W. A., Venn, K., & Voels, S. A. 1996, *Science with the Hubble Space Telescope - II*, eds. P. Benvenuti, F. D. Macchetto, & E. J. Schreier (Baltimore: STScI), p. 285
- Kurucz, R. L. 1979, ApJS, 40, 1
- Kurucz, R. L. 1992, *The Stellar Populations of Galaxies*, IAU Symp. 149, ed. B. Barbuy & A. Renzini (Dordrecht: Kluwer), p. 225
- Larson, R. B., & Tinsley, B. M. 1978, ApJ, 219, 46
- Leitherer, C., & Heckman, T. 1995, ApJS, 96, 9L

- Leitherer, C. *et al.* 1996a, PASP, 108, 996
- Maeder, A. 1990, A&AS, 84, 139
- Maeder, A. 1996, *From Stars to Galaxies: the Impact of Stellar Physics on Galaxy Evolution*, eds. C. Leitherer, U. Fritze-von Alvensleben & J. Huchra. ASP Conf. Proc. 98, p. 141
- Maeder, A., & Meynet, G. 1988, A&AS, 76, 411
- Maeder, A., & Conti, P. S. 1994, ARAA, 32, 227
- Mas-Hesse, J. M., & Kunth, D. 1991, A&AS, 88, 399
- Mathis, J. S. 1982, ApJ, 261, 195
- Mathis, J. S. 1985, ApJ, 291, 247
- Mathis, J. S., & Rosa, M. R. 1991, A&A, 245, 625
- McCall, M. L., Rybski, P. M., & Shields, G. A. 1985, ApJS, 57, 1
- McGaugh, S. S. 1991, ApJ, 380, 140
- Melnick, J., Terlevich, R., & Eggleton, P. P. 1985, MNRAS, 216, 255
- Meynet, G. 1995, A&A, 298, 767
- Mihalas, D. 1972, *Non-LTE Model Atmospheres for B and O Stars*, NCAR-TN/STR-76 (Boulder: NCAR)
- Oey, M. S., & Kennicutt, R. C. 1993, ApJ, 411, 137
- Oke, J. B., & Gunn, J. E. 1983, ApJ, 266, 713
- Osterbrock, D. E. 1989, *The Astrophysics of Gaseous Nebulae and Active Galactic Nuclei* (Mill Valley, CA: University Science Books)
- Pagel, B. E. J., Edmunds, M. G., Blackwell, D. E., Chun, M. S., & Smith, G. 1979, MNRAS, 189, 95

- Pagel, B. E. J., Simonson, E. A., Terlevich, R. J., & Edmunds, M. G. 1992, *MNRAS*, 255, 325
- Pellet, A., Astier, N., Viale, A., Courtés, G., Maucherat, A., Monnét, G., & Simien, F. 1978, *A&AS*, 31, 439
- Rubin, R. H., Simpson, J. P., Lord, S. D., Colgan, S. W. J., Erickson, E. F., & Haas, M. R. 1994, *ApJ*, 420, 772
- Salpeter, E. E. 1955, *ApJ*, 121, 161
- Sandage, A., & Tammann, G. A. 1987, *A revised Shapley-Ames Catalog of Bright Galaxies* (2nd ed.; Washington: Carnegie Institution) (RSA)
- Sarazin, C. L. 1976, *ApJ*, 208, 323
- Schaerer, D. 1996, *ApJ*, 467, L17
- Schaerer, D., Meynet, G., Maeder, A., & Schaller, G. 1993a, *A&AS*, 98, 523
- Schaerer, D., Charbonnel, C., Meynet, G., Maeder, A., & Schaller, G. 1993b, *A&AS*, 102, 339
- Schaerer, D., de Koter, A., Schmutz, W., & Maeder, A. 1996a, *A&A*, 310, 837
- Schaerer, D., de Koter, A., Schmutz, W., & Maeder, A. 1996b, *A&A*, 312, 475
- Schaerer, D., & de Koter, A., 1997, *A&A*, in press
- Schaller, G., Schaerer, D., Meynet, G., & Maeder, A. 1992, *A&AS*, 96, 269
- Schechter, P. L., Mateo, M., & Saha, A. 1993, *PASP*, 105, 1342
- Schmutz, W., Leitherer, C., & Gruenwald, R. B. 1992, *PASP*, 104, 1164
- Searle, L. 1971, *ApJ*, 168, 327
- Searle, L., Sargent, W. L. W., & Bagnuolo, W. G. 1973, *ApJ*, 179, 427
- Shields, G. A. 1974, *ApJ*, 193, 335

- Shields, G. A., & Tinsley, B. M. 1976, ApJ, 203, 66
- Shields, G. A., & Searle, L. 1978, ApJ, 222, 821
- Shields, G. A. 1990, ARA&A, 28, 525
- Shields, J. C. 1993, ApJ, 419, 181
- Skillman, E. D. 1989, ApJ, 347, 883
- Skillman, E. D. 1985, ApJ, 290, 449
- Skillman, E. D., & Kennicutt, R. C. 1993, ApJ, 411, 655
- Smith, H. E. 1975, ApJ, 199, 591
- Stasińska, G. 1980, A&A, 84, 320
- Stasińska, G. 1990, A&AS, 83, 501
- Stasińska, G. 1996, *From Stars to Galaxies: the Impact of Stellar Physics on Galaxy Evolution*, eds. C. Leitherer, U. Fritze-von Alvensleben & J. Huchra, ASP Conf. Proc. 98, p. 232
- Stasińska, G., & Leitherer, C. 1996, ApJS, 107, 661
- Stasińska, G., & Schaerer, D. 1997, A&A, in press
- Terlevich, R. J. 1985, *Star Forming Dwarf Galaxies and Related Objects*, eds. D. Kunth, T. X. Thuan & J. T. Thanh Van (Editions Frontières, Paris), p. 395
- Terlevich, R., & Melnick, J. 1981, MNRAS, 195, 839
- Terlevich, E., Díaz, A. I., Terlevich, R., González-Delgado, R. M., Pérez, E., & García-Vargas, M. L. 1996, MNRAS, 279, 1219
- Vacca, W. D. 1994, ApJ, 421, 140
- van den Bergh, S. 1976, AJ, 81, 797

- Viallefond, F. 1985, *Star-forming Dwarf Galaxies and Related Objects*. eds. D. Kunth, T. X. Thuan, & J. T. Thanh Van (Editions Frontières. Paris). p. 207
- Vilchez, J. M., & Pagel, B. E. J. 1988, MNRAS, 231,257
- Vilchez, J. M., Pagel, B. E. J., Díaz, A. I., Terlevich, E., & Edmunds, M. G. 1988. MNRAS, 235, 633
- Zaritsky, D., Kennicutt, R. C., & Huchra, J. P. 1994, ApJ, 420, 87

APPENDIX B

AN *HST* STUDY OF EXTRAGALACTIC OB ASSOCIATIONS

To be submitted for publication in *The Astronomical Journal*.

An HST study of extragalactic OB associations

F. Bresolin

Steward Observatory, University of Arizona, Tucson. AZ 85721

email: fabio@as.arizona.edu

1. Introduction

The investigation of extragalactic OB associations has been subject to several difficulties for a long time. As summarized by Hodge (1986), the lack of observational material with a uniform quality and the appropriate resolution, combined with the subjectivity of the methods adopted by different authors to identify the associations, introduced some confusion in the field, and produced inconsistent results when comparing different works on the same galaxies. While for the Magellanic Clouds and a few other Local Group galaxies the resolution attainable with ground-based telescopes is sufficient for the purpose of studying individually the most massive stars and their grouping properties, with HST it is now possible to extend the investigation of OB associations to a number of more distant galaxies with the required spatial resolution. Moreover, automated algorithms have been introduced to identify OB associations in a more objective and consistent way. After the works of Battinelli (1991) and Wilson (1991) on the SMC and M33, respectively, automated searches of OB associations have been carried out in a few other nearby galaxies (Wilson 1992, Haiman *et al.* 1994, Ivanov 1996). More recently one of these automated methods has been applied to the distribution of Galactic OB stars (Wilson & Bakker 1996); the good match between the groups identified and the known associations is indication of the reliability of the technique.

Bresolin, Kennicutt & Stetson (1996, hereafter BKS; see also Appendix C of this thesis) have begun to extend this line of investigation to more distant galaxies, using HST images of a field in the giant spiral M101. They addressed the question of possible variations of OB association properties, in particular size distribution and massive stellar content, among galaxies. They concluded that

the available data on the six galaxies studied until then with similar automated methods by different authors were consistent with a universal size distribution and average diameter. It is however desirable to study in a consistent manner a larger number of galaxies following the same unbiased procedure. We present here the results of an investigation of seven galaxies observed with HST, and to which an automated search algorithm has been applied. Our main physical motivation is to verify whether the properties of regions of recent or current star formation, as traced by the luminous OB associations, are dependent on the galactic properties, particularly the Hubble type. This study can therefore complement the results of other investigations on star forming regions in galaxies, based for example on nebular diagnostics (Appendix A of this thesis). Information on the massive stars is also obtained from the stellar luminosity function (Section 4) and the star clusters (Section 5).

2. Data analysis

The observations were obtained as part of the HST Distance Scale Key Project, a collective effort to study Cepheid variables in relatively nearby galaxies, in order to constrain the Hubble constant (Kennicutt *et al.* 1995). In the Key Project the stellar photometry of the V (F555W) and I (F814W) WFPC2 images of the target galaxies is performed independently with DAOPHOT/ALLFRAME (Stetson 1994) and DoPHOT (Schechter *et al.* 1993). The present study is based on the ALLFRAME photometry alone (except for NGC 4548, for which the DoPHOT magnitudes are used instead), carried out by several of the team members; the M101 photometry was obtained by the author, as described in BKS. Details about the observations and the photometry can be found in the original Key Project

papers (*e.g.* Ferrarese *et al.* 1996). Most of the seven galaxies in our sample (Table 1) are late-type spirals, only two being of earlier type (Sb). Images of the relative HST fields are shown in Figures 1–7. The distances adopted are those derived from the Key Project work, as referenced in column 4 of Table 1.

The automated search for OB associations was carried out following the procedure described in BKS, to which the reader is referred for details. Briefly, the bright blue star candidates were selected by imposing magnitude ($M_V \leq -4.76$) and color ($(V - I)_0 \leq 0.23$) cutoffs on the photometric data. While for M101 we were able to use $(B - V)$ colors for the selection, the lack of blue data for the remaining galaxies prevented us from adopting the same criteria used by BKS. We then re-analyzed the M101 data using the $(V - I)$ selection criterion. The $(B - V)$ or $(U - B)$ color indexes are more suitable for the selection of blue stars, and U or B HST images of our target galaxies would have been of great help in this study. A friend-of-friends method was applied to the spatial distribution of the bright blue stars, in order to group them into stellar associations. Stars that, as seen in projection on the sky, were found to lie closer to each other than a certain critical distance, to which we will refer to as the search radius, were considered to belong to the same association. The values of the search radius, defined as in our previous M101 study as the length which maximizes the total number of associations containing at least three stars, were found to vary from 35 pc to 84 pc, increasing approximately linearly with the galaxy distance. To account for chance alignments, and to limit our discussion to statistically significant stellar groups, we ran a series of simulations involving random distributions of stars, having the same surface density as the actual blue stars. We estimated the minimum number of stars (N_{\min} , found to vary from 4 to 7) that a clump should contain in order to be considered a *bona fide* association, allowing for at most a 10% contamination from random

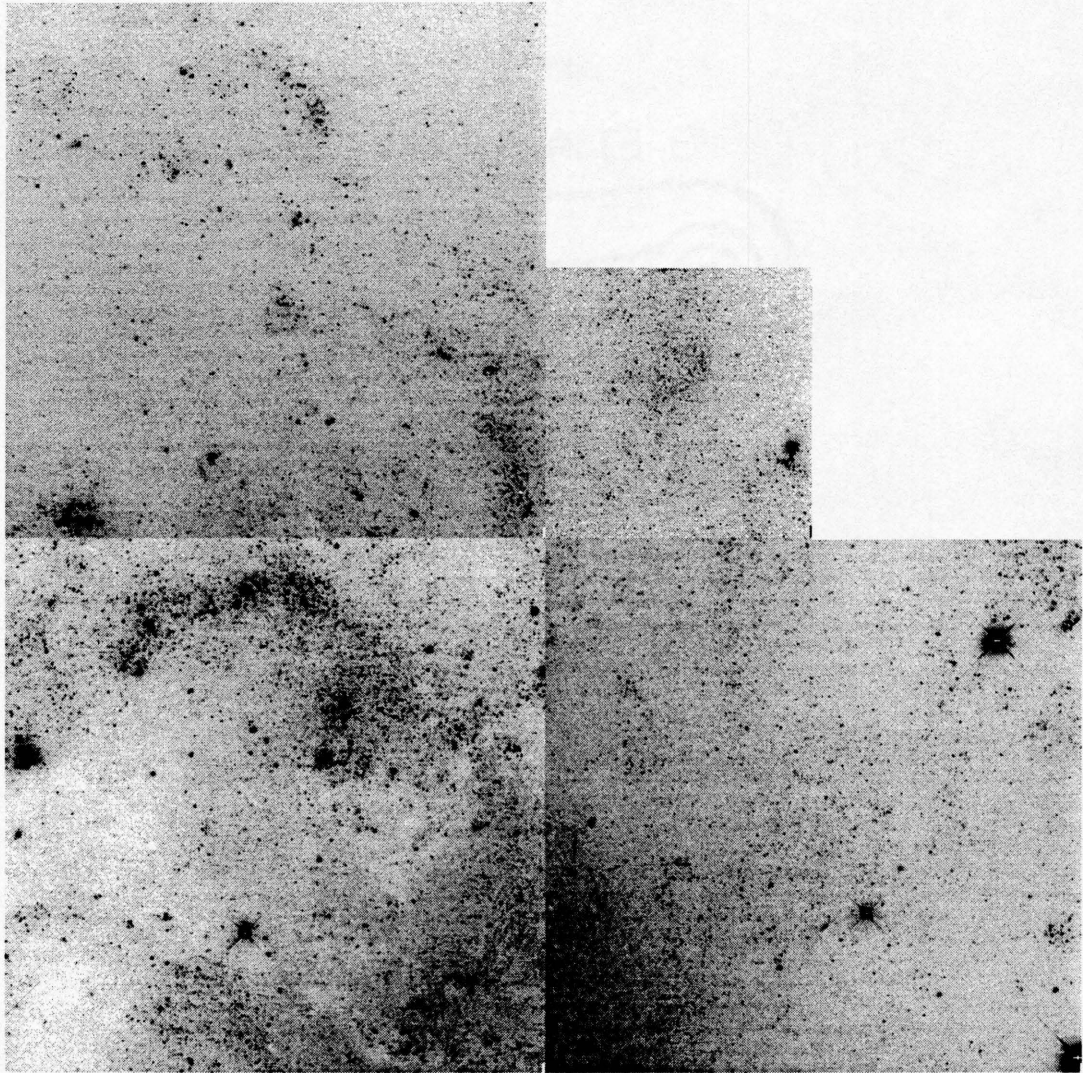


Figure 1 HST image of NGC 925.

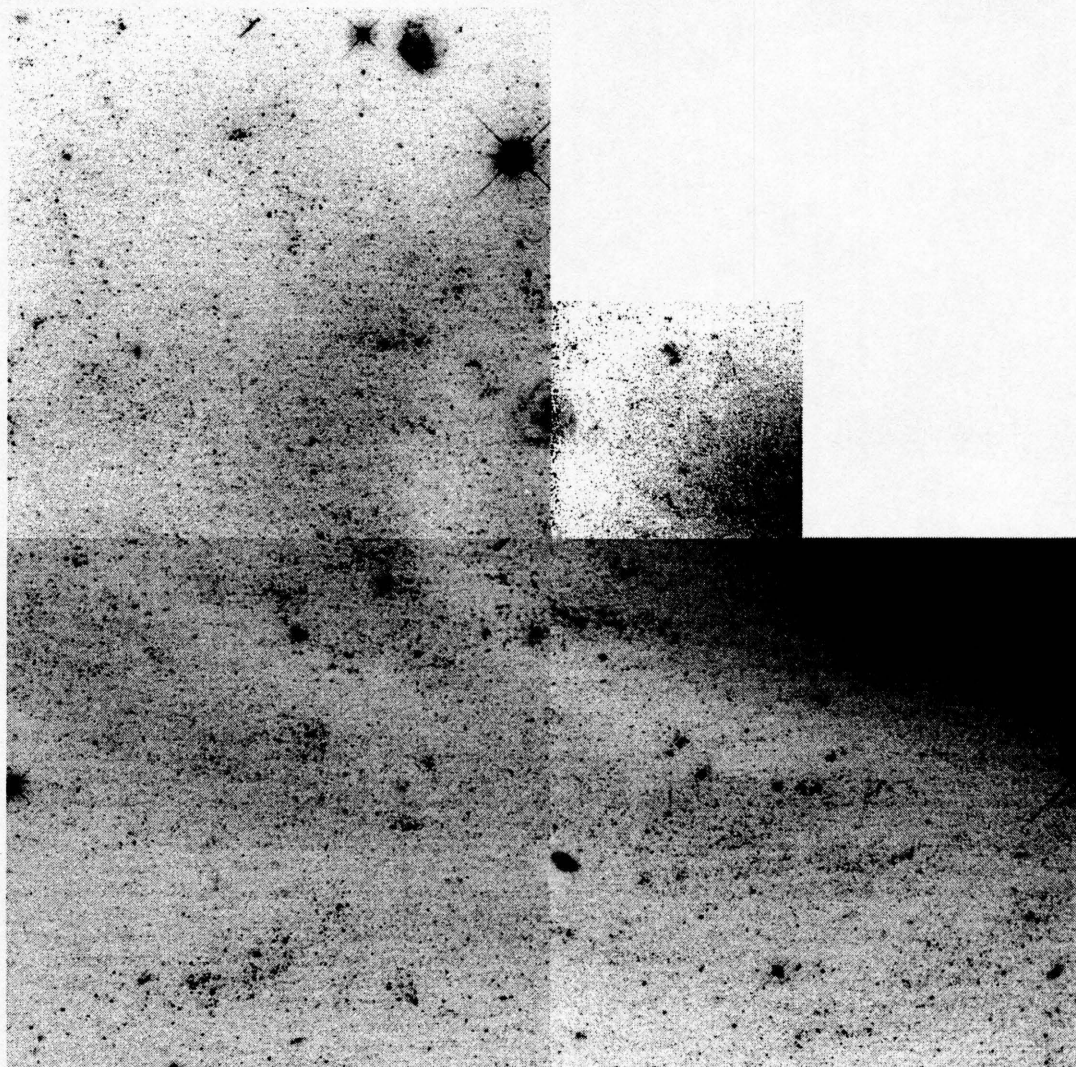


Figure 2 HST image of NGC 2090.

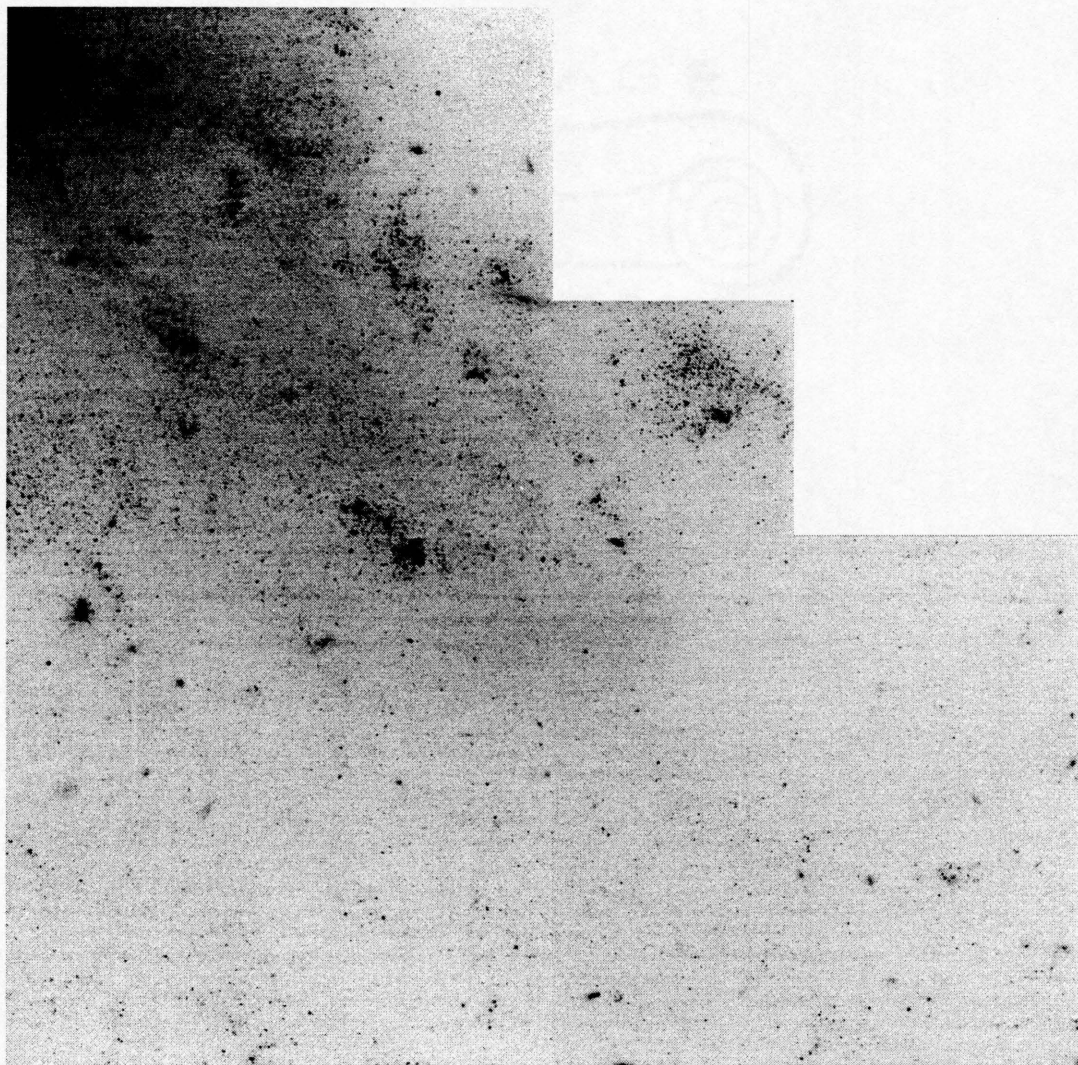


Figure 3 HST image of NGC 2541.

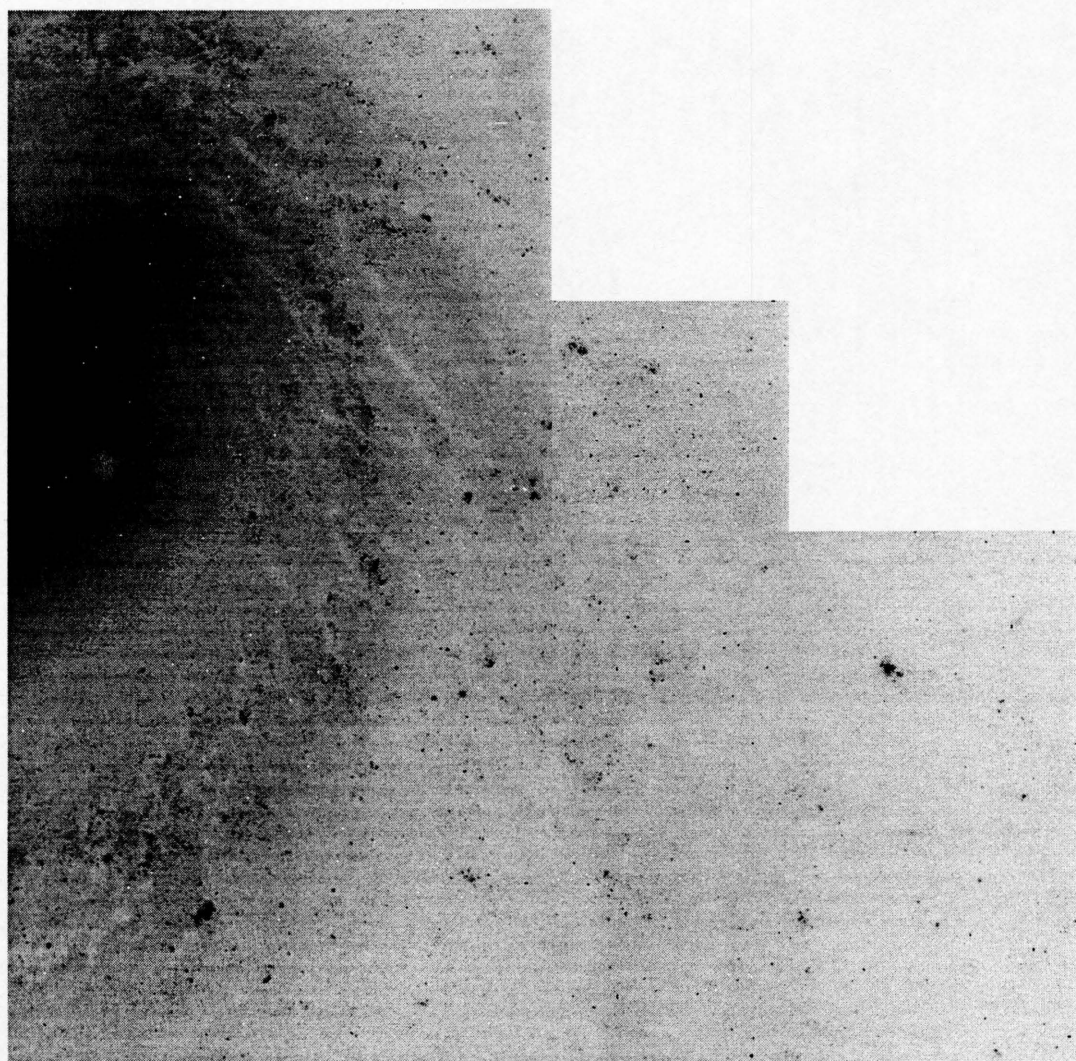


Figure 4 HST image of NGC 3351.

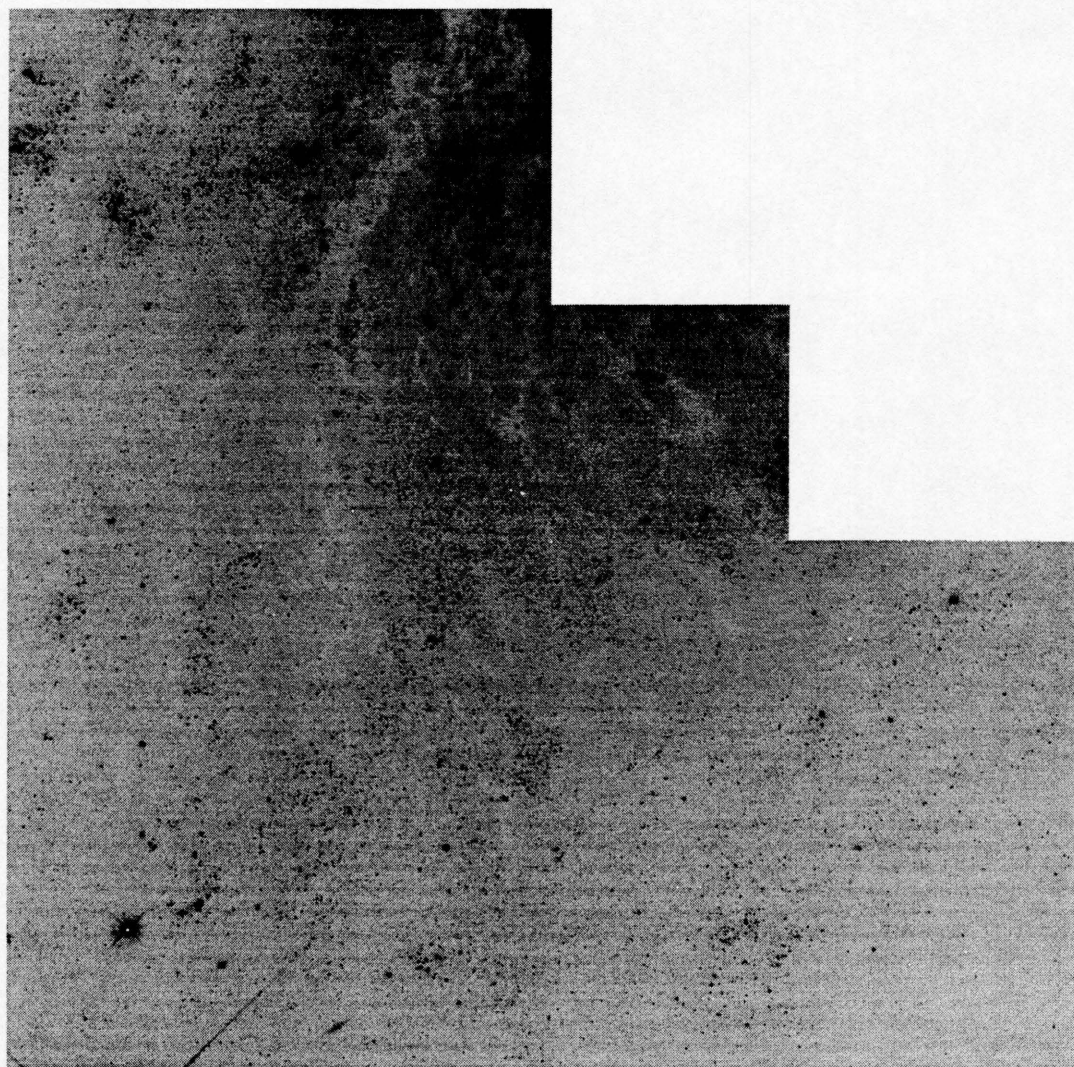


Figure 5 HST image of NGC 3621.

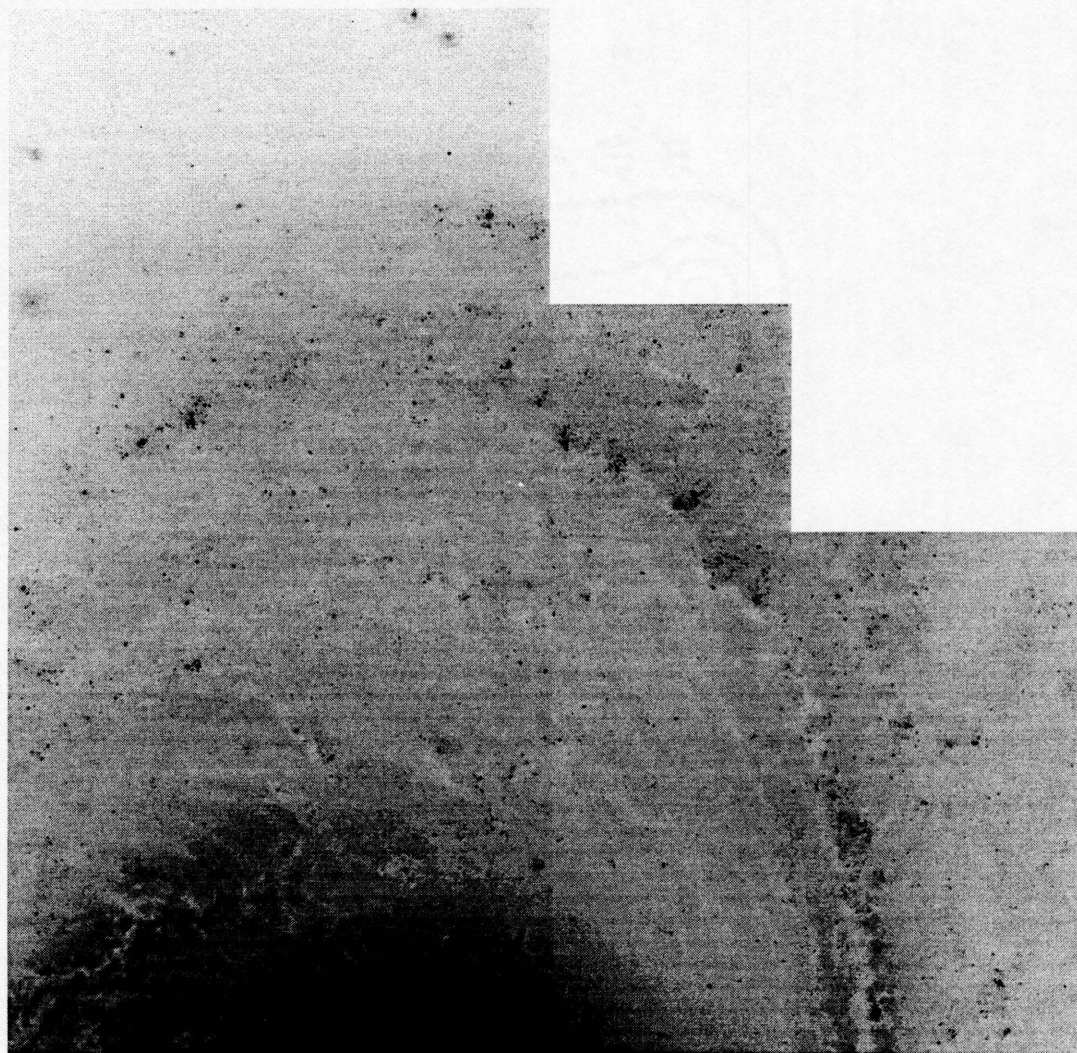


Figure 6 HST image of NGC 4548.

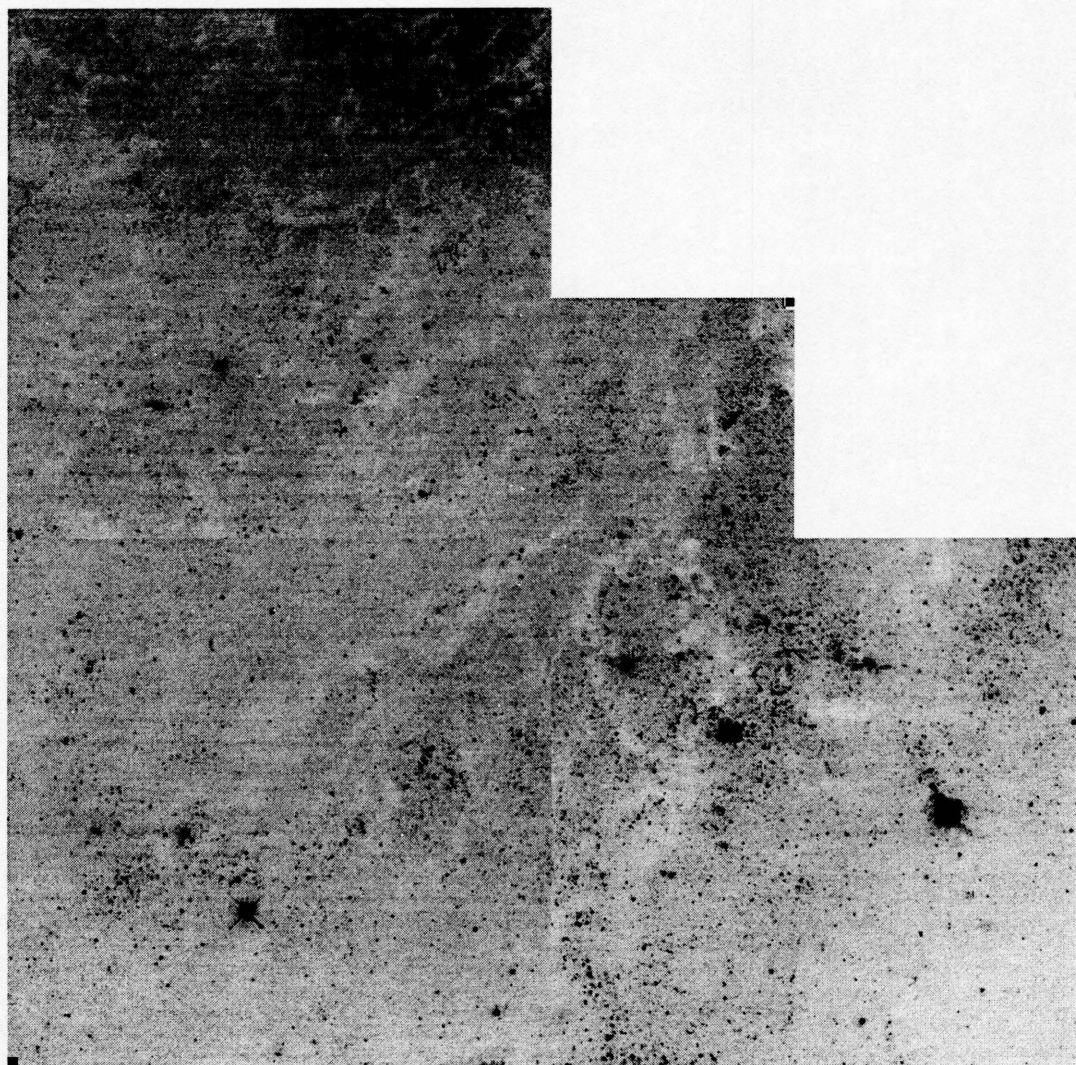


Figure 7 HST image of M101.

groups. We should however keep in mind that this is just a first-order correction, since true OB stars are not distributed at random onto a two-dimensional sheet, but are preferentially found in spiral arms and associations, away from dust lanes, and with a non-zero scale-height perpendicular to the disk.

Maps of the association boundaries resulting from the automated search are shown in Figures 8-14, where we also plot those stars that satisfy the magnitude and color selection criteria defining the blue stars. Figure 15 shows more detailed association maps in selected fields of NGC 3621, NGC 3351, NGC 2541 and NGC 4548, chosen to represent the different distances and Hubble types in our galaxy sample. It can be seen that some of the larger stellar groups contain two or more sub-clumps. The latter can be identified as normal OB associations, which tend to form larger stellar aggregates or complexes, having typical sizes of a few hundred parsecs (Efremov 1995). A similar result was obtained by Wilson & Bakker (1996), who found that $\sim 25\%$ of the groups identified by their automated algorithm in fact contained two or more OB associations. The automatic identification of OB associations within these higher-level structures would require the search algorithm to be run locally, which would result in a smaller search radius (since the density of blue stars is generally higher than in the surrounding areas), and therefore smaller stellar groups. The automated algorithm can in fact be optimized for the search of stellar complexes instead of associations (Battinelli *et al.* 1996). We did not make any attempt to discriminate between these different hierarchical levels, as it would require the application of the automated search to many different zones within each galaxy field. However, when analyzing the size distributions (Section 3) we need to keep in mind that most of the stellar clumps larger than 200 pc should be considered as complexes, rather than single associations.

This last consideration raises the question of the physical significance of the stellar groups identified by the automated algorithm. In the end, this turns into the question of how we define OB associations. The usual definition of an association as a large, gravitationally unbound grouping of O and B stars (Blaauw 1964) is difficult to apply in the case of extragalactic systems where we lack the spectral type and radial velocity information. Their 'looseness' and the existence of different levels of hierarchical structure (Efremov 1995) makes it very difficult to unambiguously define the boundaries of 'real' associations, especially on the basis of visual photometry alone. Galactic associations show substructure in the form of stellar subgroups of different ages, and their typical minimum largest initial dimension is estimated at 40–50 pc (Blaauw 1991). With an average spatial velocity of 4 km/s (100 pc in 25 Myr) the associations can expand to sizes of the order of 100 pc or more before losing their identity as a consequence of their dispersion into the field population. To recognize associations at galactic distances we require a high concentration of young, very bright stars. The friend-of-friends method described above is able to recover these overdensities of bright blue stars rather successfully, as the comparisons with known associations in the Galaxy and in nearby galaxies attest. The typical dimensions (~ 100 pc) found for extragalactic associations agree with those of the galactic OB associations. They also tend to form larger aggregates or complexes, as they do in the Galaxy. It seems thus reasonable that the stellar groups identified by our algorithm are in fact OB associations, in the same sense valid for their galactic counterparts. We must restrict ourselves to these analogies, however, given the observational limits on extragalactic resolved populations.

Table 1. The galaxy sample

Galaxy	Type ^a	D (Mpc)	Reference ^b
NGC 925	SBc(s)II-III	9.3	1
NGC 2090	Sc(s)II	12.1	2
NGC 2541	Sc(s)III	10.2	3
NGC 3351 (M95)	SBb(r)II	10.05	4
NGC 3621	Sc(s)II.8	6.7	5
NGC 4548	SBb(rs)I-II	14.5	6
NGC 5457 (M101)	Sc(s)I	7.4	7

^aFrom Sandage & Tammann 1987

^b1. Silberman *et al.* 1996; 2. Phelps *et al.* 1997; 3. Ferrarese *et al.* 1997b; 4. Graham *et al.* 1997; 5. Rawson *et al.* 1997; 6. Ferrarese *et al.* 1997a; 7. Kelson *et al.* 1997.

Table 2. OB association properties

Galaxy	Search radius (pc)	N _{min}	No. of assoc.	Average diam. (pc)	Median diam. (pc)	Average no. of stars	
						all sizes	D<200 pc
NGC 925	50	5	110	115 ⁺¹⁵ ₋₁₀	88 ⁺⁸ ₋₁₉	18 ⁺³ ₋₄	10 ⁺¹ ₋₂
NGC 2090	84	4	70	104 ⁺¹⁶ ₋₁₈	96 ⁺¹⁴ ₋₁₉	6 ⁺¹ ₋₁	6 ⁺⁰ ₋₂
NGC 2541	48	5	64	116 ⁺¹⁵ ₋₁₁	81 ⁺²⁰ ₋₈	19 ⁺³ ₋₃	10 ⁺² ₋₁
NGC 3351	58	4	73	87 ⁺⁸ ₋₁₅	73 ⁺¹¹ ₋₁₃	8 ⁺¹ ₋₂	7 ⁺¹ ₋₁
NGC 3621	39	5	44	89 ⁺⁶ ₋₁₃	70 ⁺¹⁰ ₋₁₀	14 ⁺² ₋₂	10 ⁺² ₋₂
NGC 4548	84	4	82	125 ⁺²⁵ ₋₃₇	98 ⁺²⁸ ₋₂₅	8 ⁺³ ₋₂	6 ⁺¹ ₋₁
M101	35	7	97	99 ⁺¹⁰ ₋₁₀	80 ⁺⁸ ₋₁₃	20 ⁺³ ₋₃	13 ⁺² ₋₁

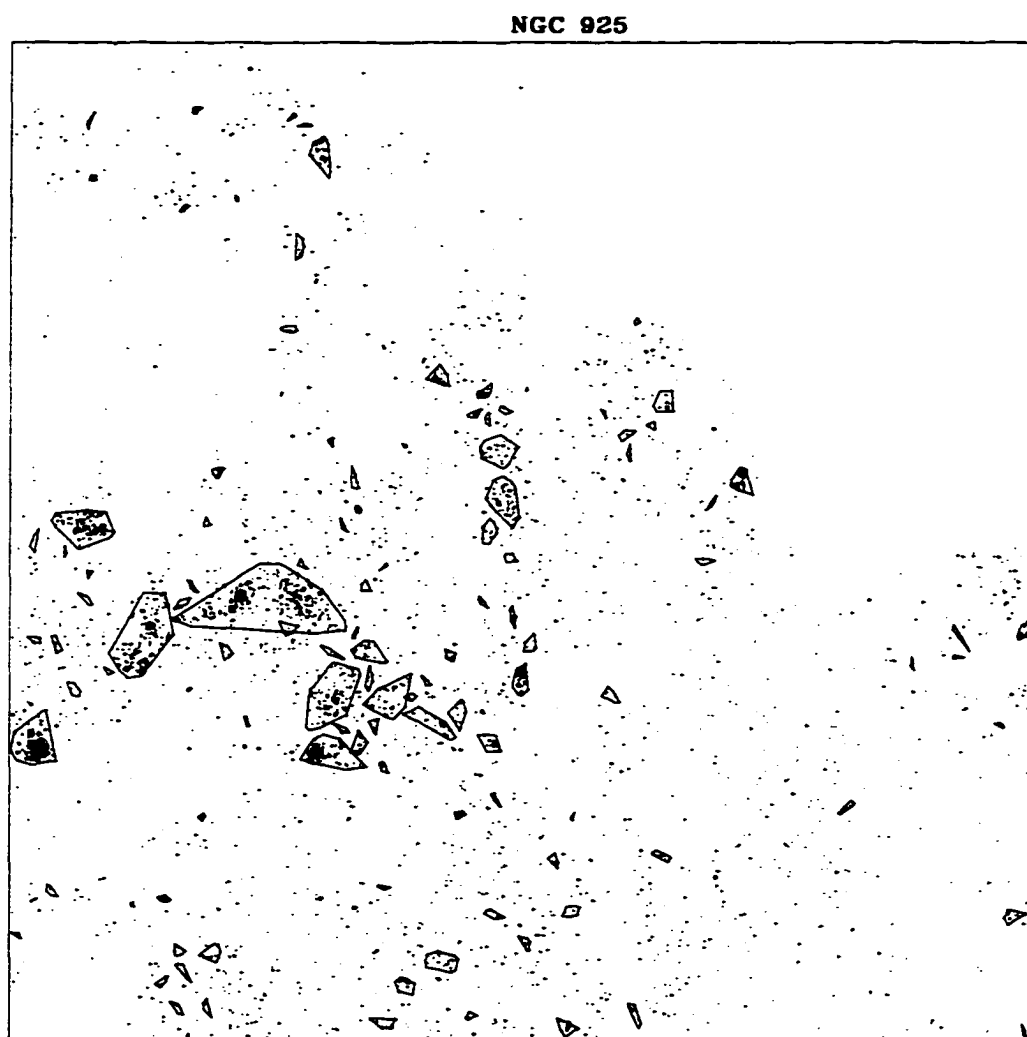


Figure 8 Map of the OB associations in NGC 925. The bright blue stars used for the association search are plotted.

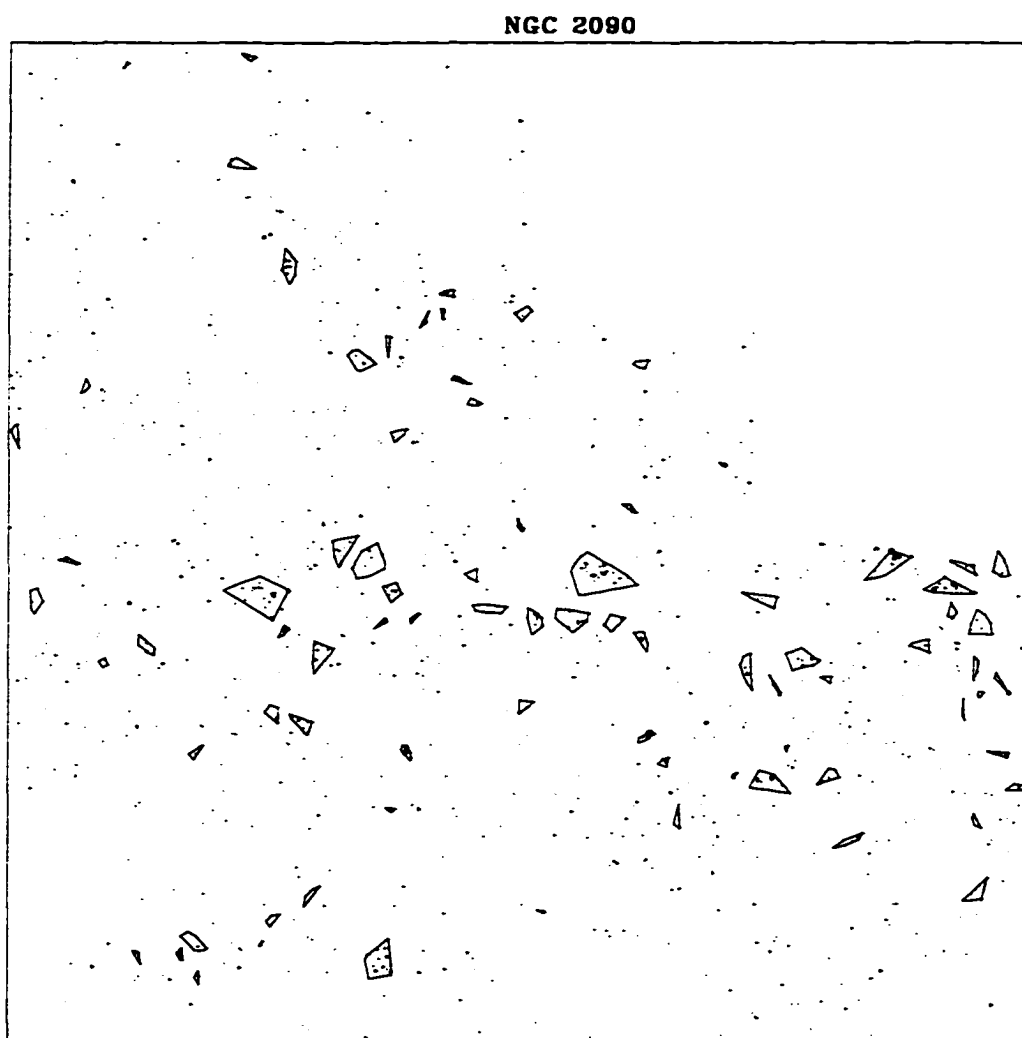


Figure 9 Map of the OB associations in NGC 2090. The bright blue stars used for the association search are plotted.

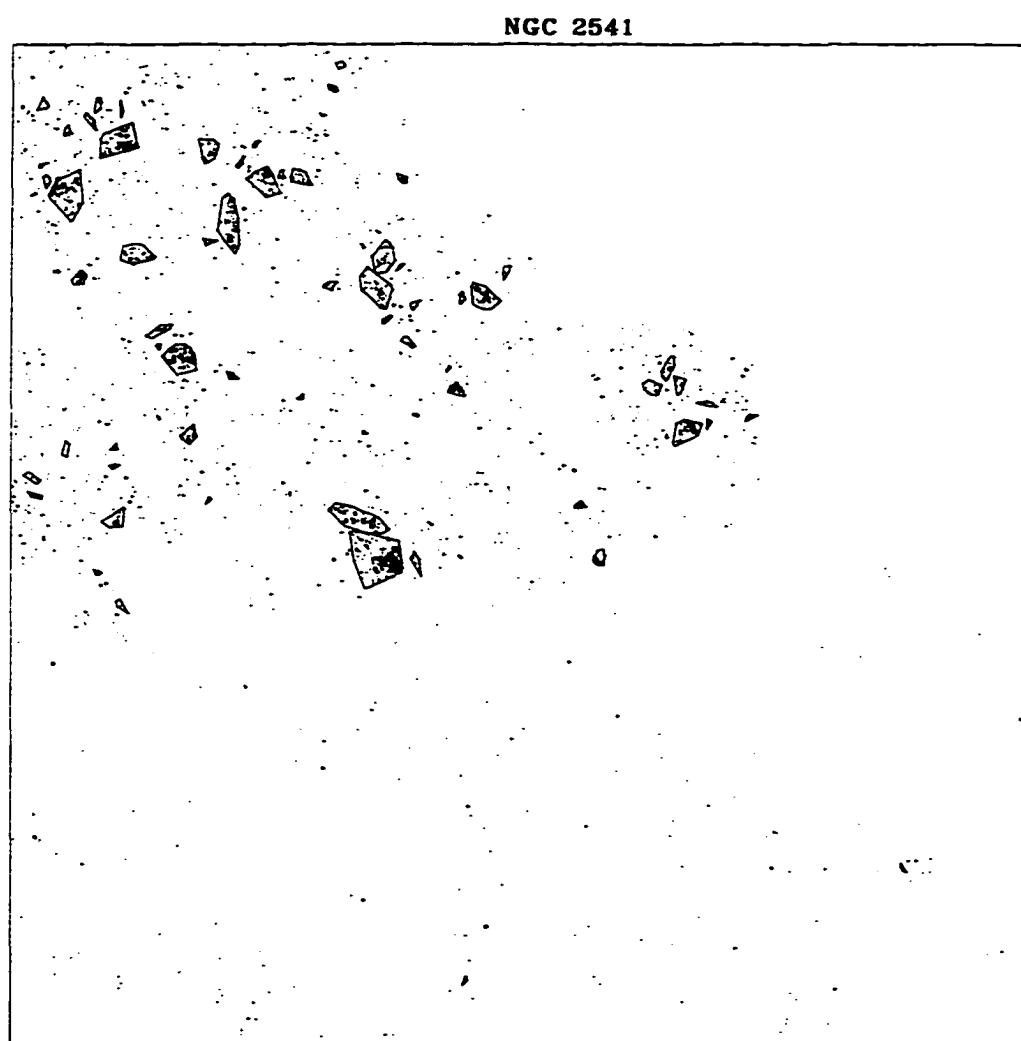


Figure 10 Map of the OB associations in NGC 2541. The bright blue stars used for the association search are plotted.

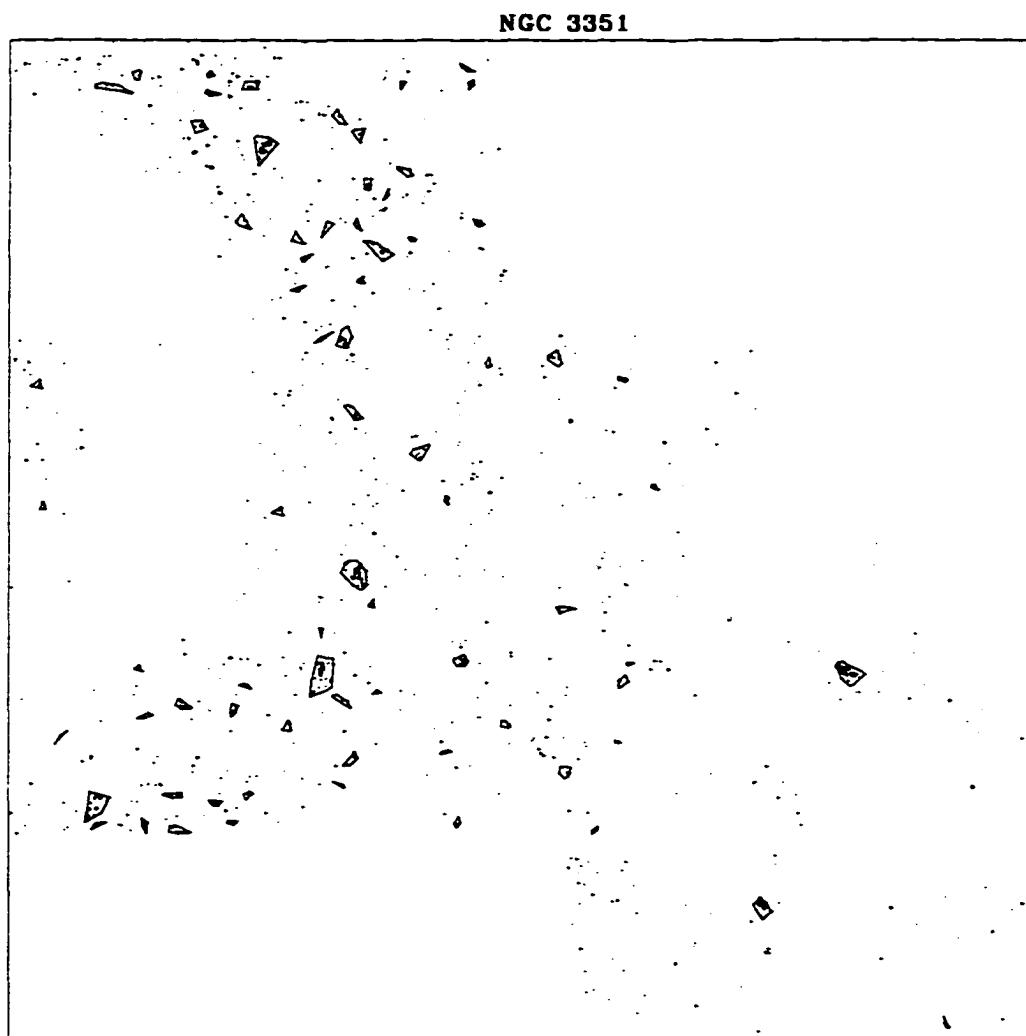


Figure 11 Map of the OB associations in NGC 3351. The bright blue stars used for the association search are plotted.

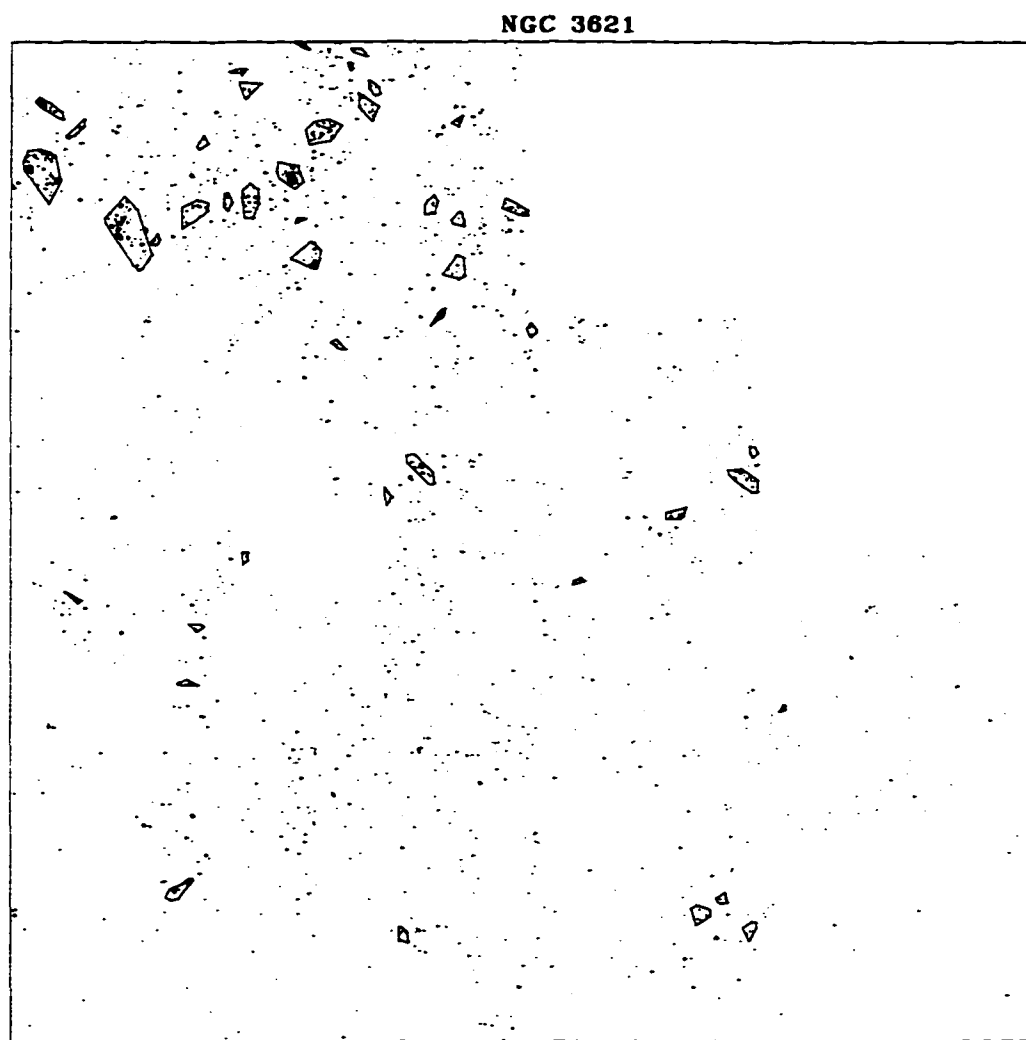


Figure 12 Map of the OB associations in NGC 3621. The bright blue stars used for the association search are plotted.

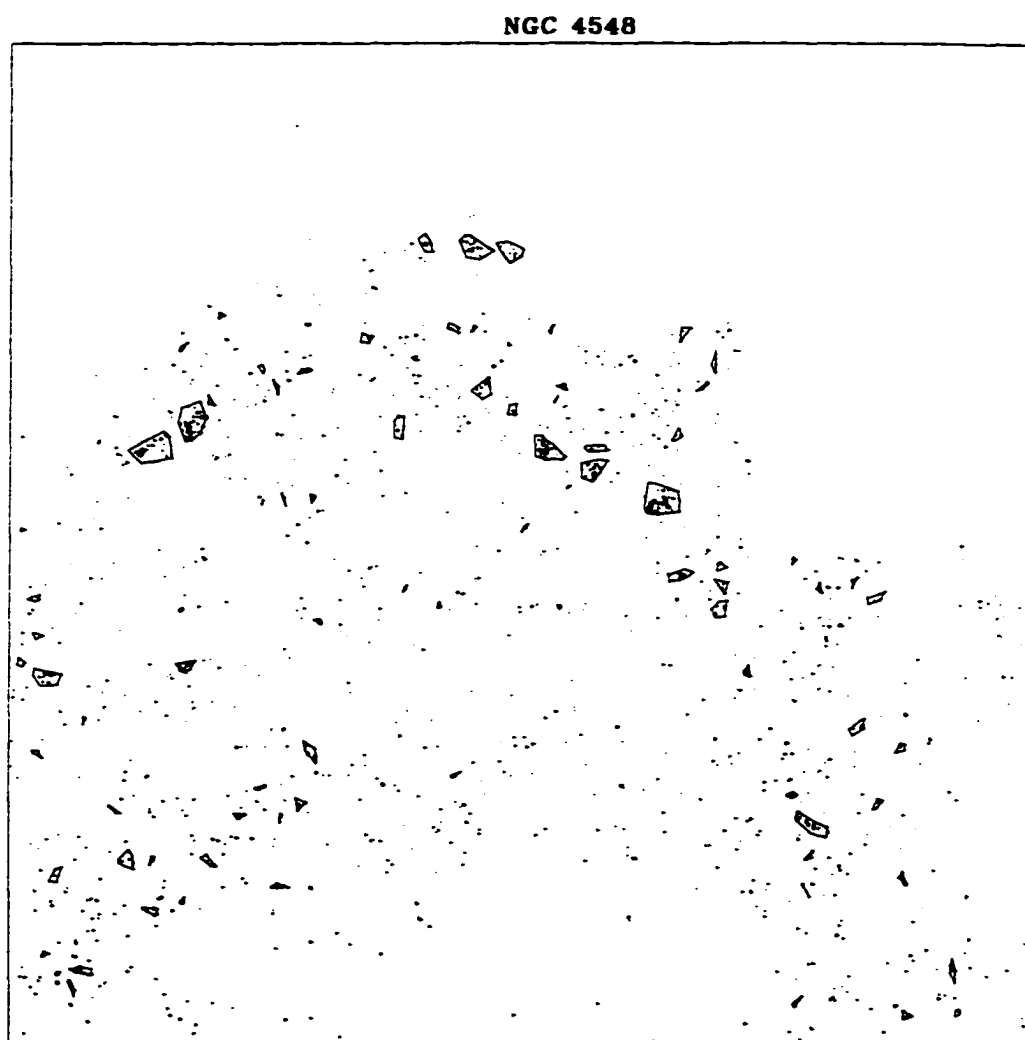


Figure 13 Map of the OB associations in NGC 4548. The bright blue stars used for the association search are plotted.

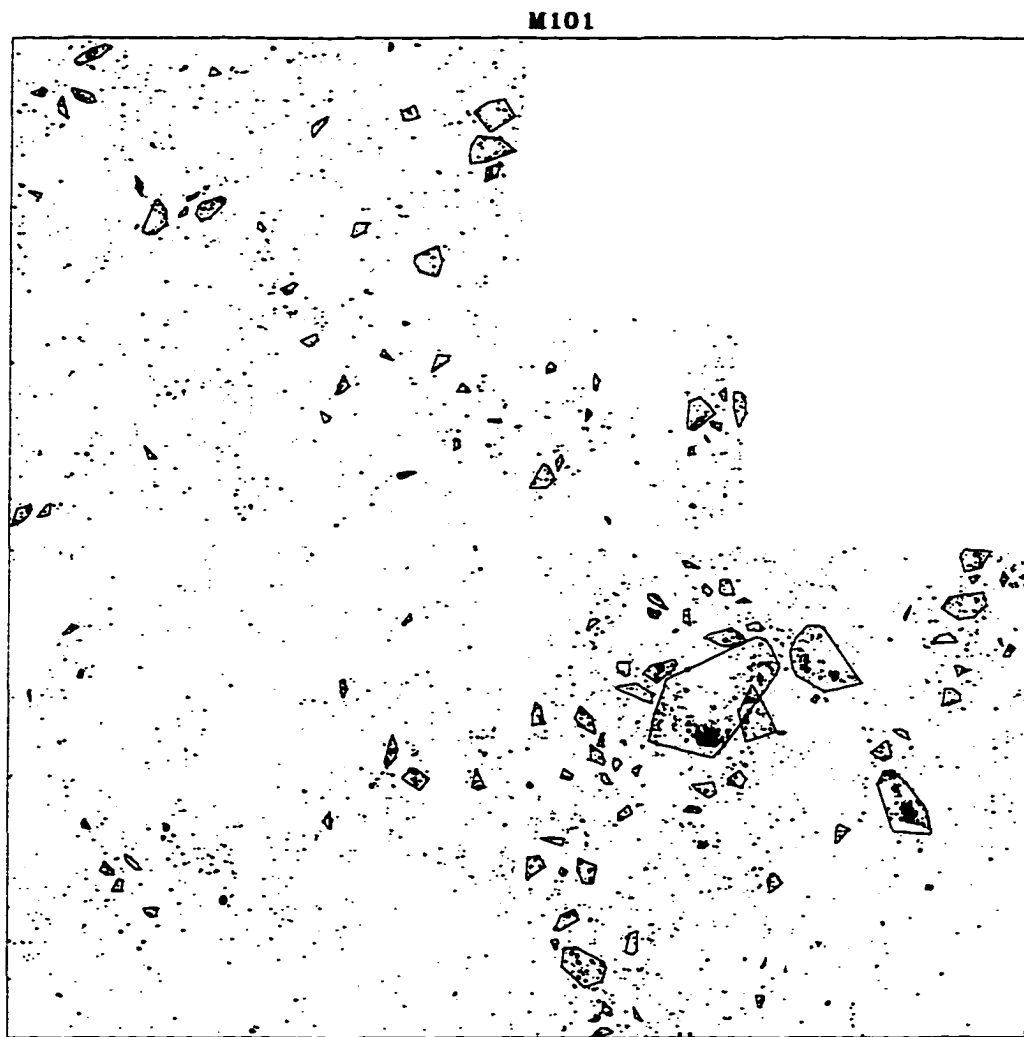


Figure 14 Map of the OB associations in M101. The bright blue stars used for the association search are plotted.

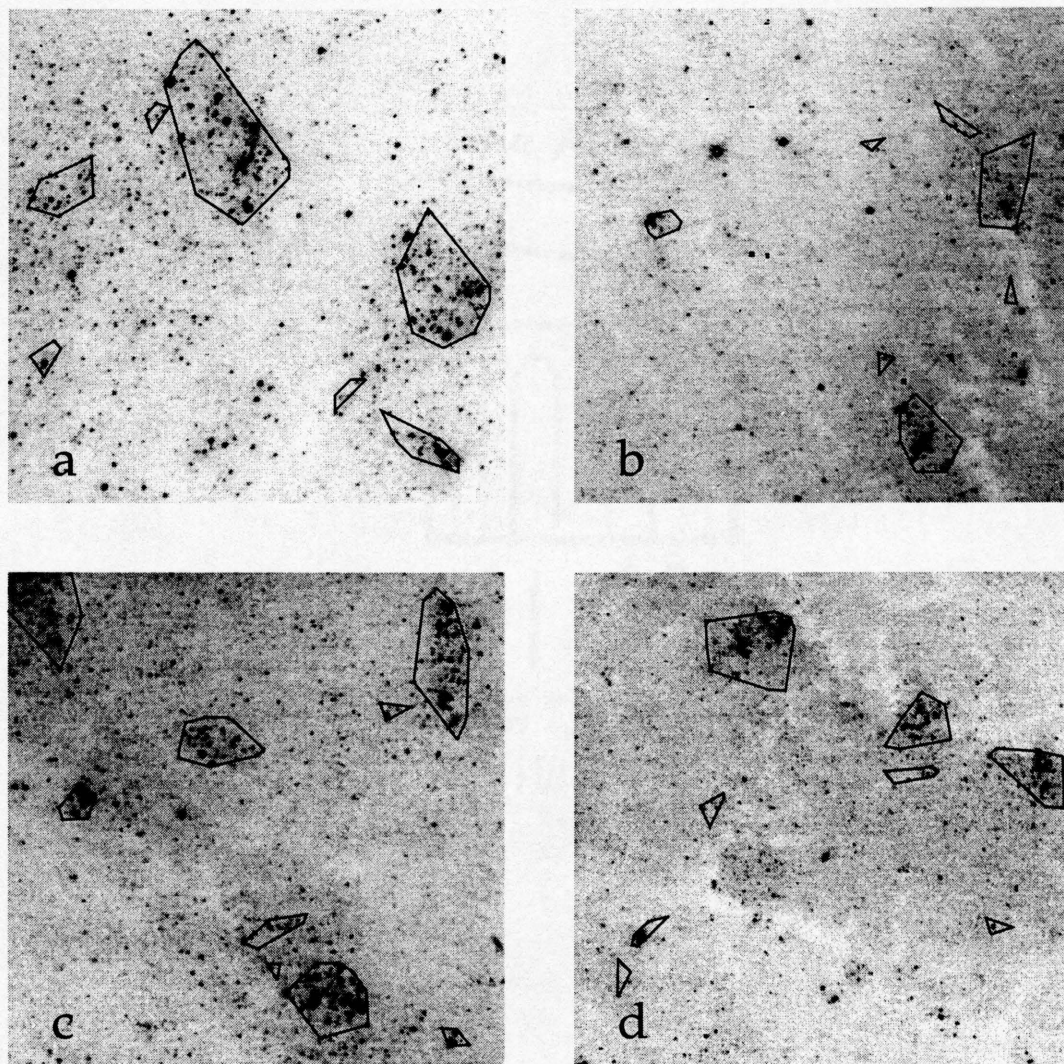


Figure 15 Details of the association maps in selected fields of four galaxies: *a*) NGC 3621; *b*) NGC 3351; *c*) NGC 2541; *d*) NGC 4548.

3. Association properties

The size distribution of the OB associations is shown in Figure 16. It confirms the result of BKS, who, comparing M101 to the Magellanic Clouds, M31, M33 and NGC 6822, found a distribution similar to that of our galaxy sample, peaked between 40 and 80 pc. No indication of a dependence on morphological type is seen. The misidentification of a few aggregates as OB associations is suggested by the tail of the distributions, above ~ 200 pc in diameter. Table 2 summarizes the parameters used for the automated algorithm, namely the search radius and N_{min} , and some of the association properties, namely their total number, the average and median diameter, and the average number of stars. The latter is given both for all associations, regardless of size, and for associations smaller than 200 pc in diameter, to remove the bias introduced by multiple associations. Given the presence of a few large structures (aggregates and complexes), the median diameter better represents the mean size of the OB associations. To show the sensitivity of the final results upon the adopted N_{min} , the quoted uncertainties were obtained by varying its value by ± 1 .

There are two interesting results about the average properties of the OB associations which are worth discussing. First, the mean size is approximately constant across the galaxy sample, the average of the median diameters being 84 ± 10 pc. The average for the six galaxies examined by BKS is 78 ± 16 pc. This finding is not new, having been pointed out by, among others, Efremov *et al.* (1987) and Ivanov (1987), that associations represent the first, smallest step in a hierarchical structure of star forming regions, with typical size equal to 80 pc. More recently Ivanov (1996) gave an average of 84 ± 15 pc, determined from eight galaxies, with photometry collected from the literature and heterogeneous color

and magnitude cutoffs to isolate the blue stars. Our result follows from an unbiased procedure applied consistently to seven different galaxies, all observed under the same conditions. It lends support to the idea of the existence of an elementary scale of star formation in the disks of spiral galaxies, as proposed by Efremov (1995). For comparison with the typical dimensions of related objects, we note that gas structures exist at different scales, similar to those of the star forming regions, from superclouds ($10^7 M_{\odot}$) down to giant molecular clouds (10^3 – $10^6 M_{\odot}$), from which OB associations are formed (Efremov 1995, Elmegreen & Efremov 1996). As regards the gas ionized by the associations, typical sizes for extragalactic H II regions range between 100 and 1000 pc (Kennicutt 1984).

Secondly, the average number of blue stars contained in the associations appears to be a function of Hubble type: between 14 and 20 stars are found in the Sc galaxies (excluding NGC 2090, which has a low density of blue stars, more similar to Sb rather than Sc galaxies), 8 in the two Sb galaxies (NGC 3351 and NGC 4548). This is unlikely to be an effect of differing resolutions, since NGC 3351 is approximately at the same distance of NGC 925 and NGC 2541. However, in the late-type galaxies the automated algorithm detected a higher number of large-scale structures than in early-type galaxies. These bigger clumps contain a large number of stars, therefore biasing the average number of stars contained in associations. Limiting the analysis to associations smaller than 200 pc (last column of Table 2), the difference between early- and late-type galaxies is reduced, but not eliminated. The OB associations in the Sb galaxies contain, on average, about half the blue stars than Sc galaxies. This is an interesting result, since it confirms by direct star counts more indirect suggestions that star forming regions in early-type spirals form less stars than late-type spirals. Bresolin & Kennicutt (1997, see Appendix D of this thesis), for example, argued that a change in the typical number of stars within

the embedded clusters of extragalactic H II regions is the most likely explanation for the variation of the H II region population properties with Hubble type.

The stellar association number density varies by a rather large factor in our sample, showing approximately the same trend found for the average number of stars in the clumps. At the low-density end, NGC 4548 and NGC 2090 have $\sim 0.5 - 0.7$ associations/Kpc² (corrected for galactic inclination), while the remaining Sc galaxies range from ~ 1.3 to almost 4 (in the case of M101) associations/Kpc². These values are however indicative only of the field observed with HST, usually a small fraction of the entire galaxy. We can conclude that, while the number density of OB associations and their number of blue stars show measurable changes among galaxies, the average size of the associations and their size distribution remain approximately constant.

4. The stellar luminosity function

We determined the slope of the V luminosity function (LF), $s = d \log N / dM_V$, for the stars contained within the OB association boundaries by performing a weighted least-squares fit to the data, binned in 0.5 magnitude intervals. Only stars brighter than a magnitude cutoff imposed by the completeness of the photometry and having $(V - I) < (V - I)_{max}$ were used in the fit, to minimize the contamination from evolved stars. Similarly to the selection of the blue stars used in the association search, a color index like $(U - B)$ or $(U - V)$ would have been a better discriminator. $(V - I)_{max}$ was chosen by maximizing the slope of the LF (analogous to the procedure of Freedman 1985, and adopted also by BKS), and requiring that the formal error in the fit be ≤ 0.06 . In this way we avoided the steep values sometimes obtained for very blue color cutoffs, but associated

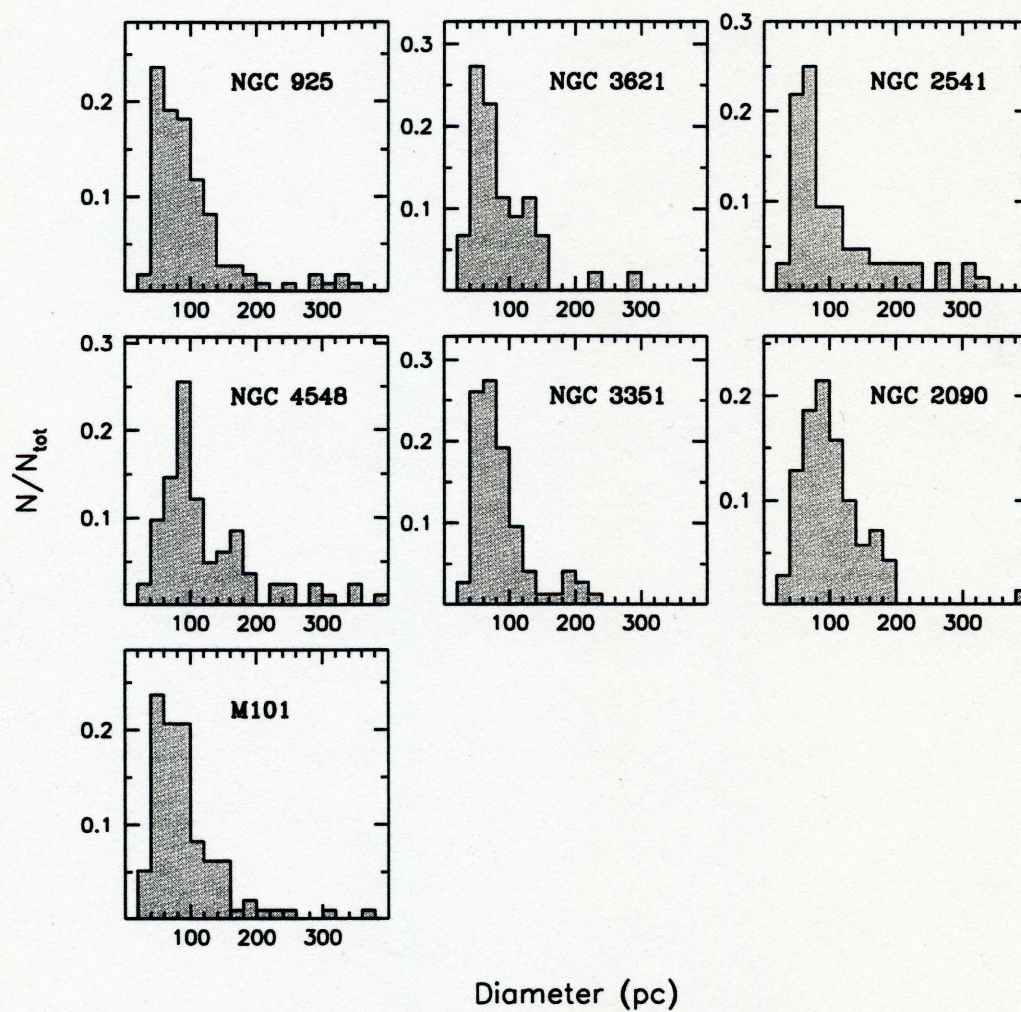


Figure 16 The OB association size distribution. The fraction of the total number of associations is given as a function of diameter.

with large statistical uncertainties (up to 0.2–0.3) due to the small number of stars included in the fit. The results are shown in Figure 17. For each galaxy the slope determined by the linear fit and the corresponding error are indicated. The values of s lie in a restricted range, with an average

$$s = d \log N / dM_V = 0.61 \pm 0.03.$$

For a sample of 10 galaxies Freedman (1985) obtained an average slope of 0.67 ± 0.03 . More recent determinations fall in the 0.58–0.65 range (Hughes *et al.* 1994, Hunter & Thronson 1995). We must stress that the slopes thus derived refer to the brightest stars in galaxies ($M_V < -5$); for somewhat fainter stars in the Milky Way and the Magellanic Clouds the slope becomes considerably flatter (Scalo 1986, Hill *et al.* 1994).

To better compare the LFs among our galaxies, we have scaled them to a common zeropoint, after fitting each individual LF to a line of slope equal to the average, $s = 0.61$. As shown in Figure 18 the data are consistent with a universal slope.

4.1. Consequences for the upper IMF

The stellar luminosity function is rather insensitive to changes in the mass function: Massey (1985) has shown that, over a range of only 2 magnitudes, luminosity functions could not detect differences in the slope of the IMF as big as 1 or 2. The situation improves with a more extended magnitude coverage. The LF is still a useful parameter to measure for distant resolved extragalactic stellar populations, for which stellar spectroscopy is not possible. Variations in the slope of the LF (*e.g.* with metallicity or Hubble type) would point to possible large changes in the upper IMF.

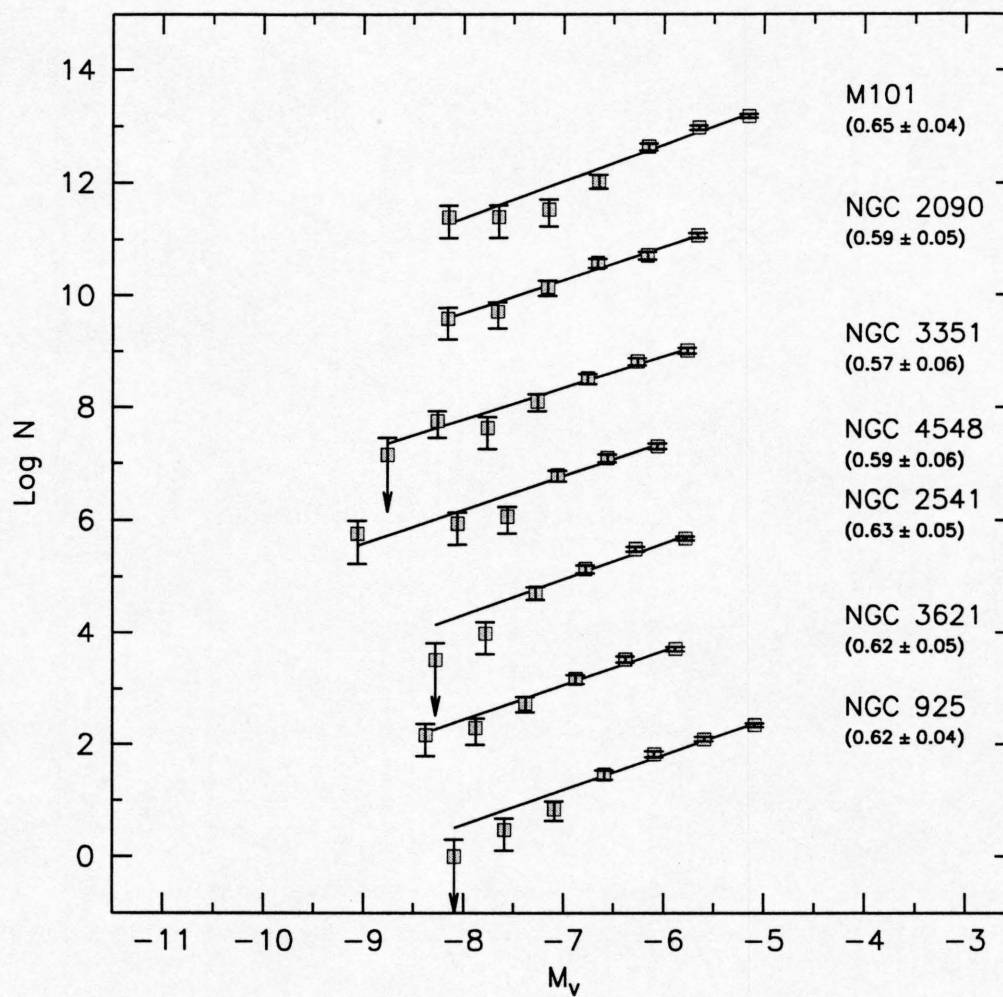


Figure 17 The V luminosity functions for the associations. The slope of the least-square fit to the LF is given in parentheses for each galaxy. The errorbars give \sqrt{N} , where N is the number of stars in each 0.5 magnitude bin.

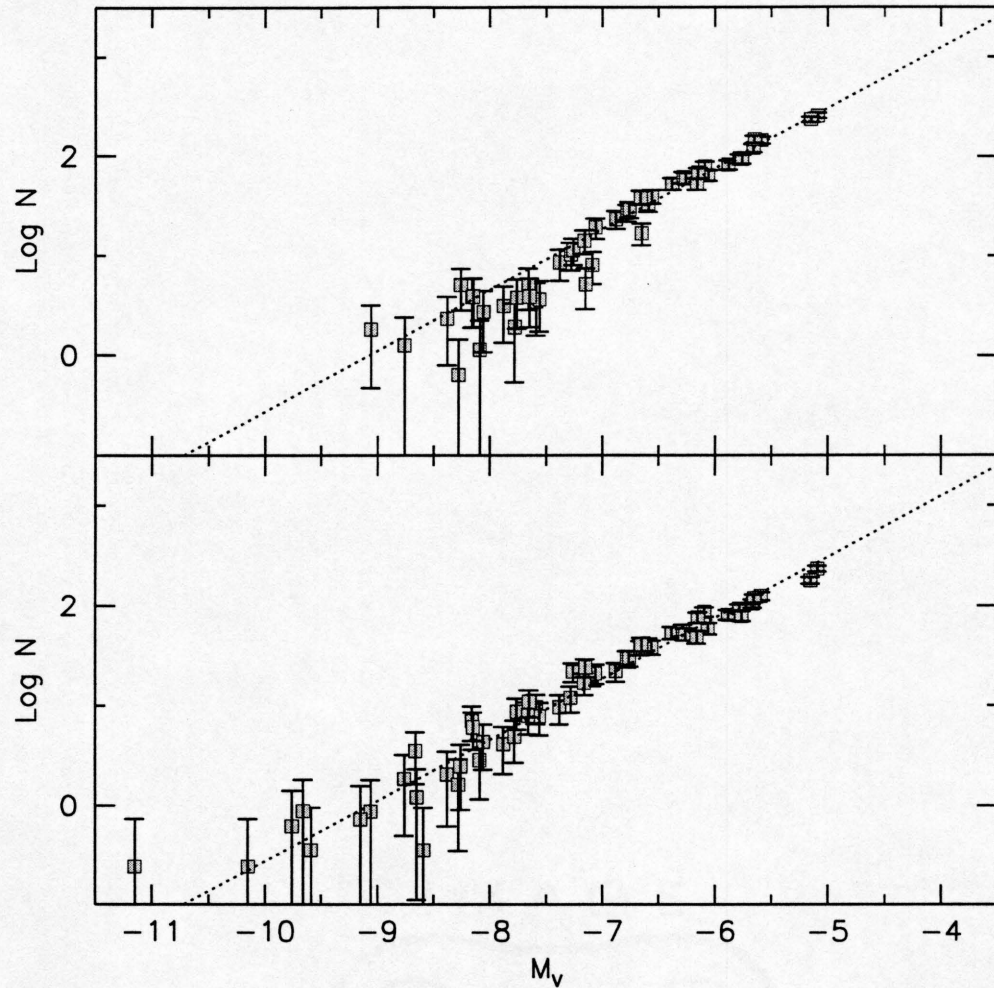


Figure 18 The V luminosity functions scaled to a common zeropoint, after adopting the same slope in the linear fit ($s = 0.61$, the average of the values in Figure 17). (*Top*) The data points are those resulting after imposing the color and magnitude cutoffs used in the determination of the slope of the LF. (*Bottom*) The data points are those resulting after imposing the color and magnitude cutoffs for the blue stars used to define the OB associations.

Following the procedure outlined in Scalo (1986) the range in s for our galaxy sample would correspond to a change in the slope of the IMF of ± 0.5 , probably a lower limit for the actual uncertainty, which might be at least twice as large. Our value for s would correspond to an IMF slope $\alpha \geq 3.0$, steeper than the Salpeter value ($\alpha = 2.35$). However, it's a well-known fact that the IMF cannot be reliably determined from photometry of massive stars alone (Massey *et al.* 1995a), which also leads to calculate artificially steeper slopes (Parker & Garmany 1993). Besides, the slope of the luminosity functions measured in extragalactic populations changes with the magnitude range considered, being steeper ($s \simeq 0.6 - 0.7$) for the brightest stars ($M_V < -5$) than for fainter main sequence stars ($s \simeq 0.3$ for $-4.0 < M_V < -1.0$, Hill *et al.* 1994). Our luminosity function has been determined for stellar populations brighter than $M_V = -5$, which are likely to be affected by evolutionary effects. In fact the stars which are brightest in V are not main-sequence O stars, but rather less massive late-B or early-A supergiant stars ($15-25 M_\odot$, Massey 1997). This complicates considerably any inference on the IMF made from the LF. We must limit the conclusion of this section to the invariance of the upper LF in galaxies, which seems universal. This however provides very little constraint on the variations of the upper IMF. Combining this information with line-emission ratios studies (*e.g.* Appendix A) of the same star forming regions would at most provide a consistency check between the two methods, and no additional constraint on the IMF parameters. The reason is the relative insensitivity of broad-band data to the mass and the spectral type of massive stars: a $100 M_\odot$ O3 main sequence star and a $40 M_\odot$ O6 main sequence star differ only by 0.5 magnitudes in V (Massey 1985). The effects due to the evolution from the main sequence (variations in the visual brightness) and the mixing of stellar populations with different ages make it even more difficult to derive constraints on the IMF parameters from the photometric

data.

5. Star cluster candidates

Our HST images allow us to search the target galaxies for star clusters, albeit with the limitations imposed by having just V and I frames. The discrimination against background galaxies becomes then problematic; in addition, for the more distant galaxies the clusters would remain almost unresolved, 10 pc corresponding to $0''.2$ at a distance of 10 Mpc. We therefore limited our search to galaxies closer than ~ 10 Mpc: NGC 3621, NGC 925, NGC 2541 and NGC 3351; clusters in M101 were studied by BKS.

Cluster candidates were found by visual search of the images. Obvious non-stellar objects ($\text{FWHM} > 2.5$ pixels) with approximately spherical shape (ellipticity smaller than 0.2) were retained, allowing a certain discrimination against galaxies. We cannot be sure, however, that each one of our final cluster candidates is in fact a cluster and not a background galaxy. Given the difficulties involved in this procedure, no attempt at completeness was made, either. We were however interested in the general properties of the cluster system in the galaxies, like the presence of blue globulars. Our search was sufficient for this purpose. The V and I magnitudes were obtained with aperture photometry, using a constant-radius aperture, and applying an aperture correction (typically 0.2–0.3 magnitudes) derived from nearly isolated clusters. Table 3.3 gives the measured V magnitude and $(V - I)$ color. The uncertainty in $(V - I)$ is estimated ~ 0.1 mag, but total magnitudes are more uncertain, because of the difficulty of measuring total fluxes of extended objects in crowded fields.

The color-magnitude diagrams of the cluster candidates are presented in

Figure 19. For comparison the corresponding diagrams for the M33 clusters (Christian & Schommer 1988) and the Milky Way globular clusters (Harris 1996) are shown. Except for a few 'red' globular cluster candidates, the majority of the star clusters in our galaxies have rather blue ($V - I$) colors, comparable to those of most M33 clusters and the 'blue' globulars in the Magellanic Clouds. This property is shared by M101, as shown by BKS. Even though the small number of objects precludes any serious statistical analysis, if the blue objects found are analogous to the populous blue clusters known in a few other galaxies their presence even in an Sb galaxy (NGC 3351) seems to exclude a Hubble type dependence. There still might be a dependence on galaxy morphology in the relative number of blue and red clusters, since the former have preferentially been found in late-type spirals (Kennicutt & Chu 1988). Our data do not allow us to investigate this possibility. Blue data on a larger sample of objects would be desirable to expand our knowledge on the topic.

6. Conclusions

We have presented a study of the OB associations in seven spiral galaxies, identified by objective means. Their properties, including their size distribution and average diameter, and the luminosity function of their brightest stars, do not vary significantly among galaxies, even for changes in Hubble type. These findings support the suggestions about the existence of similarly-sized elementary cells for star formation in galaxies, and the conclusion, obtained by more stringent methods, that the stellar mass function is universal. We have found an indication that the average number of stars in associations depends on morphological type, a direct evidence of the Hubble type dependence of the typical luminosity of star forming

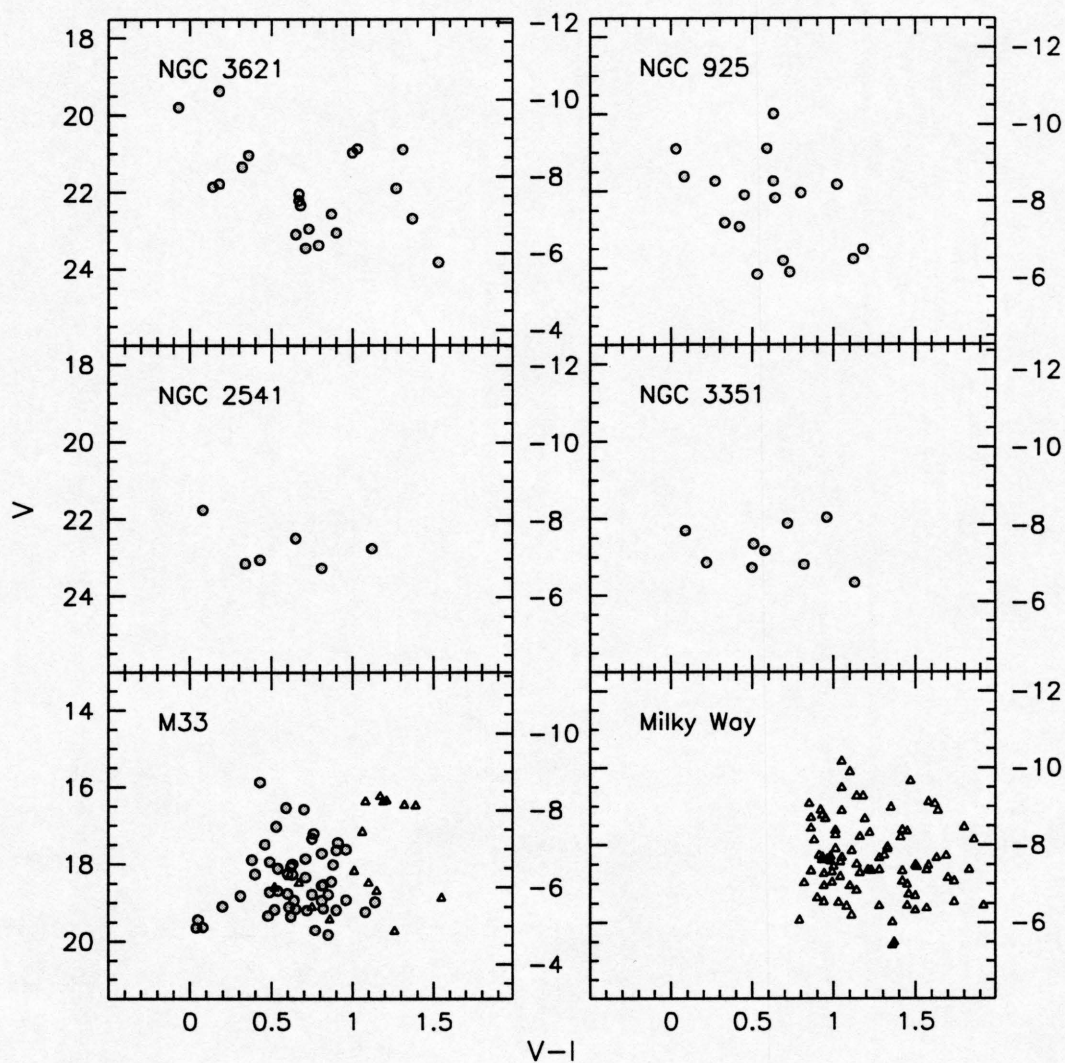


Figure 19 Color-magnitude diagrams of the cluster candidates. The comparison data for M33 (the triangles are the old globular candidates) and the Milky Way globulars are shown. The scale at right in each plot gives the absolute magnitude, M_V .

regions found from H II region studies. Variations in Hubble type or metallicity do not seem to have an influence on the formation of blue, populous star clusters, at least not in the sense of precluding their formation in early-type spirals.

TABLE 3.3. Star cluster candidates

No	RA (2000.0)	DEC (2000.0)	V	$V - I$
NGC 3621				
1	11 ^h 18 ^m 18 ^s .8	-32° 50' 32".8	22.69	1.37
2	11 ^h 18 ^m 18 ^s .8	-32° 50' 42".2	22.33	0.68
3	11 ^h 18 ^m 19 ^s .0	-32° 50' 13".5	20.87	1.03
4	11 ^h 18 ^m 19 ^s .0	-32° 50' 12".7	21.04	0.36
5	11 ^h 18 ^m 18 ^s .9	-32° 50' 24".8	23.38	0.79
6	11 ^h 18 ^m 23 ^s .4	-32° 50' 53".7	21.34	0.32
7	11 ^h 18 ^m 23 ^s .0	-32° 50' 53".3	19.36	0.18
8	11 ^h 18 ^m 24 ^s .1	-32° 50' 54".4	20.97	1.00
9	11 ^h 18 ^m 18 ^s .4	-32° 50' 46".8	22.56	0.87
10	11 ^h 18 ^m 17 ^s .9	-32° 51' 46".9	21.86	0.14
11	11 ^h 18 ^m 18 ^s .0	-32° 51' 38".7	21.90	1.27
12	11 ^h 18 ^m 18 ^s .3	-32° 50' 56".9	20.89	1.31
13	11 ^h 18 ^m 18 ^s .0	-32° 51' 30".9	19.79	-0.07
14	11 ^h 18 ^m 18 ^s .4	-32° 50' 46".4	23.45	0.71
15	11 ^h 18 ^m 18 ^s .4	-32° 50' 46".6	22.95	0.73
16	11 ^h 18 ^m 18 ^s .3	-32° 51' 05".9	23.06	0.90
17	11 ^h 18 ^m 18 ^s .2	-32° 51' 20".9	23.10	0.65
18	11 ^h 18 ^m 18 ^s .4	-32° 50' 48".9	21.78	0.18
19	11 ^h 18 ^m 18 ^s .4	-32° 50' 56".2	23.83	1.53
20	11 ^h 18 ^m 14 ^s .1	-32° 50' 33".2	22.21	0.67
21	11 ^h 18 ^m 18 ^s .4	-32° 50' 38".9	22.04	0.67
NGC 925				
1	2 ^h 27 ^m 06 ^s .2	+33° 35' 10".8	24.10	0.73
2	2 ^h 27 ^m 05 ^s .5	+33° 35' 12".7	22.83	0.33
3	2 ^h 27 ^m 06 ^s .7	+33° 35' 09".3	22.93	0.42
4	2 ^h 27 ^m 05 ^s .7	+33° 35' 12".1	23.80	0.69
5	2 ^h 27 ^m 04 ^s .5	+33° 35' 15".4	24.17	0.53
6	2 ^h 27 ^m 08 ^s .4	+33° 36' 18".8	23.77	1.12
7	2 ^h 27 ^m 08 ^s .3	+33° 36' 12".2	21.74	0.27
8	2 ^h 27 ^m 08 ^s .3	+33° 36' 11".9	22.10	0.45
9	2 ^h 27 ^m 10 ^s .5	+33° 34' 54".0	22.17	0.64

TABLE 3.3. (continued)

No	RA (2000.0)	DEC (2000.0)	<i>V</i>	<i>V</i> − <i>I</i>
10	2 ^h 27 ^m 09 ^s .7	+33° 34′ 56″.4	21.83	1.02
11	2 ^h 27 ^m 06 ^s .8	+33° 35′ 04″.6	19.99	0.63
12	2 ^h 27 ^m 08 ^s .7	+33° 34′ 59″.2	20.89	0.59
13	2 ^h 27 ^m 11 ^s .0	+33° 34′ 52″.9	21.62	0.08
14	2 ^h 27 ^m 10 ^s .0	+33° 34′ 55″.9	20.90	0.03
15	2 ^h 27 ^m 05 ^s .2	+33° 34′ 02″.1	22.04	0.80
16	2 ^h 27 ^m 05 ^s .1	+33° 33′ 58″.5	21.73	0.63
17	2 ^h 27 ^m 06 ^s .2	+33° 34′ 57″.6	23.52	1.18
NGC 2541				
1	8 ^h 14 ^m 40 ^s .7	+49° 02′ 03″.7	22.49	0.65
2	8 ^h 14 ^m 43 ^s .6	+49° 02′ 02″.9	23.26	0.81
3	8 ^h 14 ^m 43 ^s .1	+49° 01′ 55″.6	21.76	0.08
4	8 ^h 14 ^m 45 ^s .6	+49° 02′ 38″.8	23.05	0.43
5	8 ^h 14 ^m 45 ^s .9	+49° 02′ 45″.2	22.75	1.12
6	8 ^h 14 ^m 44 ^s .0	+49° 01′ 39″.9	23.15	0.34
NGC 3351				
1	10 ^h 43 ^m 52 ^s .9	+11° 41′ 37″.4	22.82	0.58
2	10 ^h 43 ^m 52 ^s .7	+11° 41′ 42″.1	23.18	0.82
3	10 ^h 43 ^m 53 ^s .1	+11° 41′ 27″.6	23.66	1.13
4	10 ^h 43 ^m 54 ^s .4	+11° 41′ 29″.5	22.11	0.72
5	10 ^h 43 ^m 57 ^s .3	+11° 41′ 48″.7	22.30	0.09
6	10 ^h 43 ^m 54 ^s .9	+11° 40′ 18″.0	21.96	0.96
7	10 ^h 43 ^m 53 ^s .3	+11° 41′ 09″.2	22.64	0.51
8	10 ^h 43 ^m 49 ^s .0	+11° 41′ 05″.7	23.13	0.22
9	10 ^h 43 ^m 50 ^s .0	+11° 41′ 12″.0	23.26	0.50

REFERENCES

- Battinelli, P. 1991, A&A, 244, 69
- Battinelli, P. Efremov, Y., & Magnier, E. A. 1996. A&A, 314. 51
- Blaauw, A. 1964, ARAA, 2, 213
- Blaauw, A. 1991, *The Physics of Star Formation and Early Stellar Evolution*, eds. C. J. Lada & N. D. Kylafis, p. 125
- Bresolin, F., Kennicutt, R. C., & Stetson, P. B. 1996, AJ, 112. 1009 (BKS)
- Bresolin, F., & Kennicutt, R. C. 1997, AJ, 113, 975
- Christian, C. A., & Schommer, R. A. 1988, AJ, 95, 704
- Efremov, Y. N. 1995, AJ, 110, 2757
- Efremov, Y. N., Ivanov, G. R., & Nikolov, N. S. 1987, Ap&SS, 135. 119
- Elmegreen, B. G., & Efremov, Y. N. 1996, ApJ, 466, 802
- Ferrarese, L., *et al.* 1996, ApJ, 464, 568
- Ferrarese, L., *et al.* 1997a, in preparation
- Ferrarese, L., *et al.* 1997b, in preparation
- Freedman, W. L. 1985, ApJ, 299, 74
- Garmany, C. D., Massey, P., & Parker, J. W. 1994, AJ, 108, 1256
- Graham, J. A., *et al.* 1997, ApJ, 477, 535
- Haiman, Z., *et al.* 1994, A&A, 290, 371
- Harris, W. E. 1996, AJ, 112, 1487
- Hill, R. J., Madore, B. F., & Freedman, W. L. 1994, ApJ, 429, 204
- Hodge, P. W. 1976, ApJ, 205, 728

- Hodge, P. 1986, *Luminous Stars and Associations in Galaxies*, IAU Symposium No. 116, eds. C. W. H. de Loore, A. J. Willis. & P. Laskarides (Reidel, Boston), p. 369
- Hughes, S. M. G., *et al.* 1994, ApJ, 428, 143
- Hunter, D. A., & Thronson, H. A. 1995, ApJ, 452, 238
- Hunter, D. A., Shaya, E. J., Holtzman, J. A., Light, R. M., O'Neill, E. J., & Lynds, R. 1995, ApJ, 448, 179
- Hunter, D. A., Baum, W. A., O'Neil, E. J., & Lynds, R. 1996a, ApJ, 456, 174
- Hunter, D. A., Baum, W. A., O'Neil, E. J., & Lynds, R. 1996b, ApJ, 468, 633
- Hunter, D. A., Light, R. M., Holtzman, J. A., Lynds, R., O'Neil, E. J., & Grillmair, C. J 1997, ApJ, 478, 124
- Ivanov, G. R. 1987, Ap&SS, 136, 113
- Ivanov, G. R. 1996, A&A, 305, 708
- Kelson, D., *et al.* 1996, ApJ, 463, 26
- Kennicutt, R. C., & Hodge, P. W. 1986, ApJ, 306, 130
- Kennicutt, R. C., Freedman, W. L., & Mould, J. R. 1995, AJ, 110, 1476
- Larson, R. B., & Tinsley, B. M. 1978, ApJ, 219, 46
- Massey, P. 1985, PASP, 97, 5
- Massey, P. 1997, *VIII Canary Islands Winter School of Astrophysics: Stellar Astrophysics for the Local Group*, eds. A. Aparicio, A. Herrero & F. Sanchez (Cambridge: CUP), in press
- Massey, P., Strobel, K., Barnes, J. V., & Anderson, E. 1988, ApJ, 328, 315
- Massey, P., Garmany, C. D., Silkey, M., & DeGioia-Eastwood, K. 1989, AJ, 107

- Massey, P., Lang, C. C., DeGioia-Eastwood, K., & Garmany, C. D. 1995a. ApJ. 438, 188
- Massey, P., Johnson, K. E., & DeGioia-Eastwood, K. 1995b, ApJ. 454. 151
- O'Connell, R. W., Gallagher, J. S., & Hunter, D. A. 1994, ApJ. 433, 65
- Parker, J. W., Garmany, C. D., Massey, P., & Walborn, N. R. 1992. AJ. 103. 1205
- Parker, J. W, & Garmany, C. D. 1993, AJ, 106, 1471
- Phelps, R. L., *et al.* 1997, in preparation
- Rawson, D. M., *et al.* 1997, ApJ, in press
- Sandage, A., & Tammann, G. A. 1987, *A revised Shapley-Ames Catalog of Bright Galaxies* (2nd ed.; Washington: Carnegie Institution) (RSA)
- Scalo, J. M. 1986, Fund. Cosm. Phys., 11, 1
- Scalo, J. M. 1990, *Windows on Galaxies*, eds. G. Fabbiano, J. S. Gallagher, & A. Renzini (Kluwer: Dordrecht), p.125
- Schechter, P. L., Mateo, M., & Saha, A. 1993, PASP, 105, 1342
- Silbermann. N. A., *et al.* 1996, ApJ, 470, 1
- Stetson, P.B. 1994, PASP, 106, 250
- van den Bergh, S. 1976, AJ, 81, 797
- Wilson, C. D. 1991, AJ, 101, 1663
- Wilson, C. D. 1992, AJ, 104, 1374
- Wilson, C. D., & Bakker, K. J. 1996, AJ, 112, 1588

APPENDIX C

AN *HST* STUDY OF OB ASSOCIATIONS AND STAR CLUSTERS IN M101

Published in *The Astronomical Journal*, 1996, Vol. 112, p. 1009.

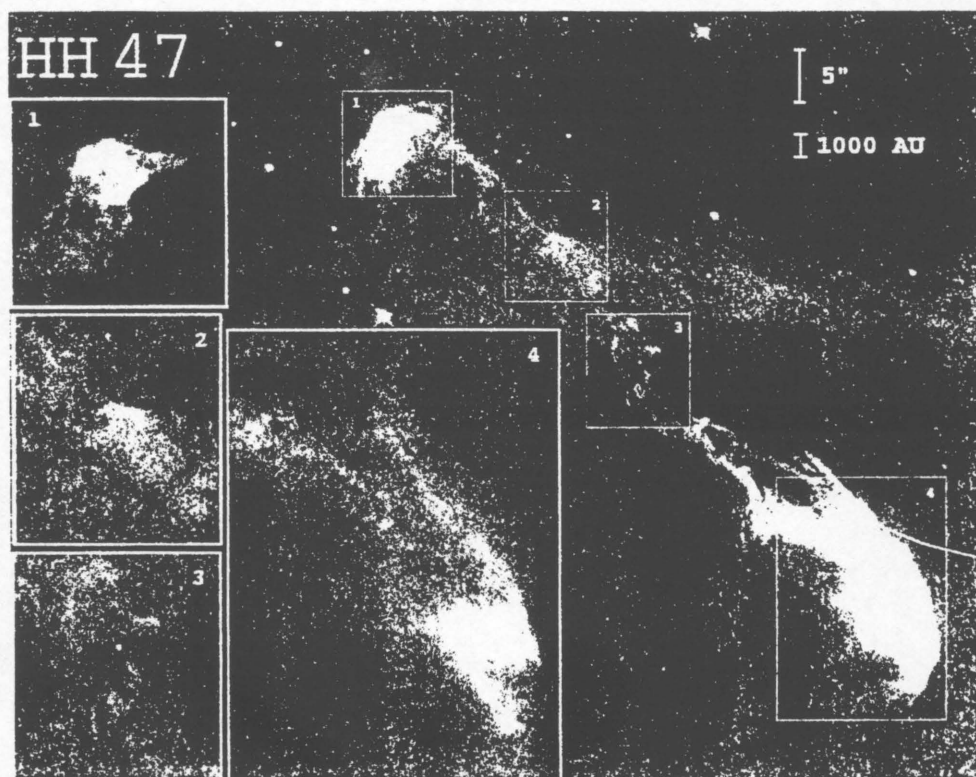
THE ASTRONOMICAL JOURNAL

FOUNDED BY B. A. GOULD
1849

VOLUME 112

September 1996~No. 1689

NUMBER 3



(See Page 1141)

Published for the
AMERICAN ASTRONOMICAL SOCIETY
by the
AMERICAN INSTITUTE OF PHYSICS

**AMERICAN ASTRONOMICAL SOCIETY**

2000 Florida Avenue, N.W. + Suite 400 + Washington, D.C. 20009-1231
202-328-2010 + FAX: 202-234-2560 + aas@aas.org

Dr. Robert W. Milkey
Executive Officer

April 15, 1997

Fabio Bresolin
University of Arizona
Steward Observatory
Cherry Avenue
Tucson, AZ 85721

Dear Mr. Bresolin,

This letter will confirm permission for you to use two articles by Bresolin, et al that appeared in the September 1996 and March 1997 issues of the *Astronomical Journal* as a portion of your dissertation.

Permission extends to microfilming and publication by University Microfilms and the American Astronomical Society is aware that UMI may sell single copies of the dissertation including the copyrighted material for scholarly purposes.

With very best wishes,

Sincerely,

Robert W. Milkey

cc: Paul Hodge

AN *HST* STUDY OF OB ASSOCIATIONS AND STAR CLUSTERS IN M101¹

FABIO BRESOLIN AND ROBERT C. KENNICUTT, JR.

Steward Observatory, University of Arizona, Tucson, Arizona 85721

Electronic mail: fabio@as.arizona.edu, robk@as.arizona.edu

PETER B. STETSON

Dominion Astrophysical Observatory, 5071 West Saanich Road, Victoria, British Columbia V8X 4M6, Canada

Electronic mail: stetson@dao.nrc.ca

Received 1996 March 22

ABSTRACT

The massive stellar content, the OB associations and the star clusters in an *HST* field in M101=NGC 5457 are investigated. A clustering algorithm yields 79 putative associations. Their size distribution is similar to that found in the Magellanic Clouds, M31, and M33, with an average size around 90 pc. The *V* luminosity function for the stars contained within the associations has a slope $d\log N/dV = 0.60 \pm 0.05$, while an average reddening $E(B-V) = 0.21$ mag is measured. The stellar content is further discussed by means of color-magnitude and color-color diagrams. Ages are estimated using theoretical isochrones, and range between 3 and 14 Myr (± 2 Myr). We find a suggestion that the upper mass limit of the IMF for stars in OB associations in M101 may be quite high, contrary to some theoretical expectations that the mass limit should be lower in a high metallicity environment. Forty-one star cluster candidates and two H II region core clusters are identified in the M101 field, and their integrated photometric properties are compared with the cluster system of the Large Magellanic Cloud (LMC) and M33. Most of the M101 clusters probably belong to the class of young, populous star clusters such as are found in the LMC. Red clusters are rare in this field. In the Appendix the objective finding algorithm is applied to the brightest stars in the LMC. © 1996 American Astronomical Society.

1. INTRODUCTION

OB associations provide valuable information on the physical processes that govern star formation in galaxies. Unlike star clusters, which are gravitationally bound systems consisting of presumably coeval stars, OB associations are loose, short-lived entities, and as such they are natural tracers of recent or current star formation (Blaauw 1991). A better understanding of massive stars has resulted from the investigation of these objects in the Galaxy and in the Magellanic Clouds (Garman 1994). The study of the spatial distribution of OB associations can provide an insight into the mode of star formation (stochastic versus density wave triggering), while the size distribution of the associations is directly related to the question of the importance of the associations and star complexes as fundamental building blocks of the structure of spiral galaxies (Efremov & Chernin 1994). On the other hand star clusters hold clues about galactic evolution on longer timescales.

The main advantage of studying OB associations in galaxies other than the Milky Way lies in the possibility of minimizing the difficulties that arise from uncertain distances and high levels of obscuration in the plane of the Galaxy. However we must deal with the long-standing problem of

identifying stellar associations in a consistent way for different galaxies. Hodge (1986) pointed out how the measured association properties depend on several selection effects, among these the quality of the observational material and the identification criteria adopted. To overcome this problem *automated* identification techniques have been recently applied to nearby, resolved galaxies. In this work, which introduces a project aimed at defining some of the properties of OB associations and star clusters in different galactic environments (metallicity, star forming activity, etc.), we present the results obtained for M101 with a similar objective technique, and describe the methodology adopted for investigating associations and clusters in external galaxies. Our goal is to analyze galaxies of different Hubble types and distances (up to 15 Mpc with *HST*), in order to compare their OB associations, their star clusters, and their massive stellar content. This can provide clues on the possible variations of stellar populations and massive star formation among galaxies.

We present the observational material and the data reduction in Sec. 2. Results on the massive stars are discussed in Sec. 3. The identification technique and the size distribution of the OB associations in M101 are discussed in Secs. 4 and 5, respectively. In Sec. 6 we analyze the properties of the stellar content of the associations. In Sec. 7 we draw some tentative conclusions on the stellar IMF in the field studied. The results on star clusters are presented in Sec. 8. In the Appendix we apply the objective algorithm to the Large Ma-

¹Based on observations with the NASA/ESA *Hubble Space Telescope*, obtained at the Space Telescope Science Institute, which is operated by AURA, Inc., under NASA contract NAS 5-26555.

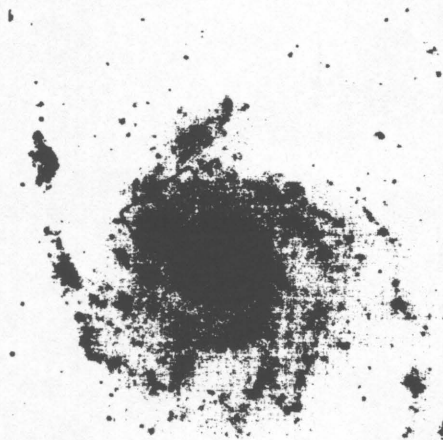


FIG. 2. $H\alpha$ (line + continuum) image of M101 showing the *HST* field studied in this work. North is at the top.

gellanic Cloud (LMC). A distance to M101 of 7.4 Mpc (Kelson *et al.* 1996) is adopted.

2. OBSERVATIONS AND DATA REDUCTION

The *HST* Distance Scale Key Project is observing 18 galaxies to detect Cepheid variables (Kennicutt *et al.* 1995). As a by-product of this effort, a large number of WFPC2 images of spiral galaxies is produced, suitable for the study of their stellar populations. Figure 1 (Plate 39) shows the inner field of M101 = NGC 5457 studied in this work (see also Stetson *et al.* 1996). The apex of the four chips lies at $\alpha = 14^{\text{h}}03^{\text{m}}24^{\text{s}}.0$ and $\delta = 54^{\circ}21'38''$ (2000.0), 1.8 NE of the center of M101, as shown in Fig. 2. The filters used for the observations were F336W (two 1200s exposures), F439W (two exposures, 1000s and 1200s, respectively), F555W (12 1200s exposures) and F814W (one 1000s and four 1200s, exposures). The stellar photometry was carried out with the multiple-frame profile-fitting package ALLFRAME (Stetson 1994). In order to create a master list of stellar objects, a median image of each chip, free of cosmic rays, was generated from all the available single-epoch images. Once the stellar list was made using the PSF-fitting program ALLSTAR, we performed the photometry for each of the single-epoch images with ALLFRAME. The average magnitudes were calibrated and transformed to the *UBVI* system with the equations and zero points of Holtzman *et al.* (1995). For the following analysis only stars that were measured in all four filters were retained, giving a total of 16812 stars.

Table 1 lists the typical photometric errors at various magnitudes. The exposure times for the *B* and *U* frames were not long enough to accurately measure stars fainter than $V \sim 24$. This imposes some limitations on the analysis of the fainter stars, but not on the brighter ones which are of interest here. The incompleteness in the *V* photometry was estimated by reducing copies of the *V* frames of chip 4 (the most

TABLE 1. Median photometric errors.

<i>V</i>	σ_V	σ_I	σ_B	σ_U
20–21	0.031	0.044	0.094	0.115
21–22	0.034	0.048	0.117	0.149
22–23	0.038	0.062	0.125	0.157
23–24	0.048	0.085	0.165	0.202
24–25	0.061	0.122	0.235	0.285
25–26	0.080	0.181	0.361	0.432
26–27	0.107	0.242	0.529	0.618

crowded) to which 1,000 artificial stars were added. Virtually all stars down to $V = 25$ were recovered, 93% at $V = 25.5$, 80% at $V = 26$. However, in our study of the luminosity function (Sec. 6.1), incompleteness is seen to set in at $V \sim 23.5$ and appears to be more severe than stated above at fainter magnitudes. Since only stars recovered in all four filters were included, this can be ascribed to two causes: shorter exposure times in *B* and *U*, and the fact that the artificial stars were added at completely random places within the field, whereas the majority of real stars are — by definition — located in regions of higher-than-average stellar density, and are therefore more subject to crowding and confusion. Approximate completeness limits, without restriction to stars detected in all four filters, are $V \sim 23.5$ in *U* and *B* and $V \sim 25$ in *V* and *I*.

Ground-based images at $H\alpha$ and $H\beta$ of a region partly overlapping with the *HST* field were secured in 1994 March with the Steward Observatory 90-inch telescope on Kitt Peak. These data are used in Sec. 6.2 to independently estimate the reddening in the corresponding OB associations.

3. MASSIVE STARS

Figure 3 shows the color-magnitude diagram (CMD) for $\sim 16,000$ stars recovered in the field studied. The evolutionary tracks, taken from Schaller *et al.* (1992), were converted to the observational plane using the equations of Massey *et al.* (1995a). They were reddened by $E(B - V) = 0.21$, corresponding to the mean extinction measured for the stars. This diagram shows that we are detecting stars typically above $10 M_{\odot}$. The width of the blue plume is ~ 0.5 magnitudes for $V < 24.5$, and increases to one magnitude at the faint end. This is much larger than what is observed in OB associations in the LMC (Massey *et al.* 1989, Hunter *et al.* 1995). The stellar models of Schaller *et al.* (1992) predict a wide main sequence for the H-R diagram of massive stars. However, given the photometric uncertainties (Table 1), the observed scatter is largely explained by photometric errors alone, and perhaps partially by an age spread among non-coeval populations of stars and by differential reddening. Similar conclusions were drawn by Hunter & Thronson (1995) for *HST* data of I Zw 18. Effects of blending are surely present, as many stars are located in crowded regions, so that several of the brightest objects could in fact be groups rather than single stars. To reduce this effect for the brightest objects, we have removed from the CMD all stars brighter than $V = 22$ that do not appear to be isolated stars. The result

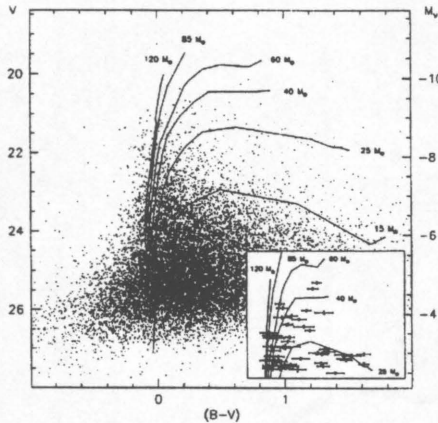


FIG. 3. Color-magnitude diagram of the M101 field with evolutionary tracks from Schaller *et al.* (1992) reddened by 0.21 mag in $(B-V)$. (Inset) The stars brighter than $V=22$ that appear in relatively uncrowded regions are shown with their individual photometric errors.

is shown in the inset of Fig. 3, where the photometric errors for each star are indicated.

4. IDENTIFICATION OF OB ASSOCIATIONS

Recently the question of comparing the clustering properties of massive stars in different galaxies has been attacked by adopting automated algorithms, to remove much of the subjectivity which was intrinsic to previous methods. Wilson (1991) introduced a friends-of-friends algorithm to define groups of bright blue stars in M33. In this method all blue stars lying within a predetermined search radius from another star were included in the same stellar group. The latter was defined as an OB association if it contained at least 10 blue stars. The search radius was determined by the mean surface density of blue stars. A somewhat different method, introduced by Battinelli (1991), determines the search radius that maximizes the number of stellar groups containing a minimum of three stars. The same method has been used by Magnier *et al.* (1993) to identify OB associations in M31.

In this study of M101 we adopted Battinelli's (1991) approach, because of its high level of objectivity and in order to compare association properties of galaxies already studied. The criteria $V < 24.5$ ($M_V < -4.8$) and $(B-V) < 0.4$ (before correcting for reddening) were used to select the blue stars. The search algorithm was applied separately to the four WFPC2 chips because of the gradient in stellar density across the *HST* field. This gave search radii of 2.4 (40 pc), 3.5 (58 pc), 3.9 (64 pc) and 2.2 (36 pc) in chips 1, 2, 3, and 4, respectively. These values are very close (to within ± 0.2 arcsec) to what one obtains using Wilson's (1991) definition of search radius based on the stellar surface density. We must stress that the "associations" defined by the algorithm lie within a two-dimensional projection through a patch of galactic disk or a spiral-arm fragment, and do not necessarily

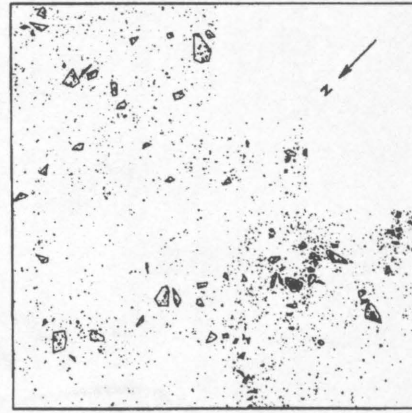


FIG. 4. Outlines of the 79 OB associations which were found by applying the objective clustering algorithm. Stars having $(B-V) < 0.4$ and $V < 25.5$ are plotted.

lie physically close together in three dimensions, share common space motions, or originate in a single coherent star-forming event; thus we cannot be certain that any given one of them is a true OB association as we would define it in our Milky Way Galaxy. Nevertheless, even though we cannot be sure that these asterisms are genuine, physical OB associations, we can at least be confident that they represent objectively defined, localized regions of enhanced surface density in the distribution of young, massive stars.

We can perform a statistical test to ascertain how many of the groups found are likely to be chance coincidences. We applied the algorithm to a set of random distributions of stars, each containing the same number of blue stars as the actual data. The search radius was set equal to the value used for the actual data. The simulations showed that the contamination of false associations was less than 10% when the threshold population was set to seven stars or more. We adopted this criterion, which resulted in a total sample of 79 associations, as shown in Fig. 4. Fifty contain at least 10 blue stars. The average number of blue stars in the associations is 15 (19 for $N_{\text{blue}} \geq 10$). It is likely that the actual number of member stars is larger than these figures, given the possibility of measuring very compact groups of a few stars as a single star. The simulations described do not take into account the fact that young stars are not distributed exactly at random due to the existence of spiral arms and dust lanes.

Our sample is biased against associations that contain very few stars. A major concern is therefore the completeness in the rate of detection of associations. To estimate the incompleteness we made a comparison with the system of associations in the LMC. The area covered by our *HST* field is approximately equal to the area surveyed by Lucke & Hodge (1970) in the LMC, where 122 associations were catalogued. Correcting for inclination effects and scaling to the number of LMC associations, we should have detected ~ 100 associations in the M101 field. We might therefore be

TABLE 2. Properties of OB associations.

ID	RA (14 ^h)	DEC (+54°)	Diameter (pc) ^a	N_{blue}	N_{red}	$E(B-V)$	age (Myr)	ID	RA (14 ^h)	DEC (+54°)	Diameter (pc) ^a	N_{blue}	N_{red}	$E(B-V)$	age (Myr)
1	3 ^m 25 ^s 11	21' 10"	21	11	15	0	14	41	3 ^m 24 ^s 6	21' 24"	83	10	15	0.1	7
2	3 ^m 23 ^s 2	21' 25"	103	12	35	0.3	5	42	3 ^m 25 ^s 2	21' 15"	59	8	13	0	14
3	3 ^m 24 ^s 4	21' 05"	29	6	12	0.3	5	43	3 ^m 25 ^s 6	21' 10"	80	9	15	0.2	6
4	3 ^m 24 ^s 1	21' 02"	61	16	45	0.4	4	44	3 ^m 25 ^s 3	21' 12"	93	10	17	0.2	6
5	3 ^m 24 ^s 2	20' 55"	72	14	26	0.4	6	45	3 ^m 25 ^s 5	21' 08"	94	8	16	0.2	7
6	3 ^m 23 ^s 9	21' 00"	118	11	29	0.3	3	46	3 ^m 24 ^s 4	21' 22"	66	11	16	0	11
7	3 ^m 22 ^s 4	21' 11"	62	6	8	0.2	6	47	3 ^m 25 ^s 7	21' 05"	51	9	9	0.2	4
8	3 ^m 17 ^s 6	21' 00"	119	10	25	0.2	8	48	3 ^m 25 ^s 1	21' 13"	59	10	13	0.3	8
9	3 ^m 17 ^s 9	21' 06"	306	49	125	0.2	5	49	3 ^m 25 ^s 8	21' 04"	38	8	9	0.1	6
10	3 ^m 18 ^s 8	21' 23"	126	12	24	0.3	5	50	3 ^m 25 ^s 6	21' 06"	80	7	15	0.3	7
11	3 ^m 21 ^s 6	21' 45"	96	10	18	0.2	4	51	3 ^m 23 ^s 7	21' 22"	126	23	41	0.3	3
12	3 ^m 16 ^s 6	21' 13"	80	10	16	0.2	5	52	3 ^m 23 ^s 4	21' 26"	46	8	11	0.3	8
13	3 ^m 19 ^s 7	21' 44"	89	11	20	0.2	4	53	3 ^m 23 ^s 5	21' 25"	49	8	10	0.2	4
14	3 ^m 15 ^s 8	21' 24"	108	8	15	0.2	4	54	3 ^m 23 ^s 9	21' 19"	140	19	37	0.3	5
15	3 ^m 17 ^s 8	21' 42"	113	14	26	0.2	6	55	3 ^m 23 ^s 8	21' 18"	91	10	15	0.2	9
16	3 ^m 17 ^s 0	21' 41"	127	12	28	0.3	4	56	3 ^m 23 ^s 7	21' 20"	59	7	10	0.2	5
17	3 ^m 16 ^s 0	21' 45"	129	24	39	0.1	4	57	3 ^m 23 ^s 7	21' 16"	203	105	175	0.2	3
18	3 ^m 15 ^s 7	21' 46"	154	9	15	0.1	6	58	3 ^m 24 ^s 0	21' 14"	89	12	21	0.2	7
19	3 ^m 18 ^s 1	22' 04"	111	10	19	0.2	4	59	3 ^m 24 ^s 1	21' 13"	53	8	10	0	9
20	3 ^m 15 ^s 6	21' 52"	226	21	63	0.2	6	60	3 ^m 24 ^s 2	21' 11"	53	11	12	0.4	4
21	3 ^m 15 ^s 0	21' 51"	43	11	12	0.1	4	61	3 ^m 23 ^s 1	21' 21"	99	23	36	0.2	4
22	3 ^m 13 ^s 1	21' 50"	173	15	30	0.2	6	62	3 ^m 23 ^s 2	21' 16"	76	13	31	0.3	7
23	3 ^m 18 ^s 1	22' 20"	128	8	12	0.1	7	63	3 ^m 23 ^s 3	21' 15"	133	22	50	0.2	6
24	3 ^m 12 ^s 6	21' 46"	121	15	30	0.2	7	64	3 ^m 23 ^s 0	21' 18"	122	22	41	0.3	4
25	3 ^m 13 ^s 1	21' 53"	59	7	8	0.3	4	65	3 ^m 23 ^s 1	21' 17"	77	13	14	0.2	5
26	3 ^m 12 ^s 6	21' 55"	77	7	10	0.1	6	66	3 ^m 23 ^s 2	21' 14"	79	9	12	0.3	7
27	3 ^m 18 ^s 4	22' 33"	143	16	21	0.2	7	67	3 ^m 24 ^s 0	21' 05"	71	12	19	0.3	6
28	3 ^m 21 ^s 4	22' 42"	125	10	23	0.1	6	68	3 ^m 22 ^s 7	21' 16"	230	47	116	0.3	4
29	3 ^m 24 ^s 3	22' 12"	78	9	15	0.2	3	69	3 ^m 22 ^s 6	21' 17"	74	9	11	0.1	7
30	3 ^m 26 ^s 3	22' 00"	105	8	21	0.3	6	70	3 ^m 22 ^s 7	21' 08"	98	11	24	0.2	5
31	3 ^m 25 ^s 7	22' 14"	231	30	65	0.3	4	71	3 ^m 22 ^s 8	21' 09"	88	14	23	0.1	6
32	3 ^m 26 ^s 1	22' 11"	181	22	40	0.2	4	72	3 ^m 22 ^s 8	21' 04"	241	88	221	0.2	3
33	3 ^m 26 ^s 8	22' 04"	102	10	19	0.2	7	73	3 ^m 22 ^s 0	21' 09"	82	10	19	0.3	7
34	3 ^m 25 ^s 9	22' 26"	117	10	18	0.2	6	74	3 ^m 21 ^s 5	21' 13"	61	7	9	0.2	7
35	3 ^m 23 ^s 6	22' 55"	74	9	11	0.2	10	75	3 ^m 21 ^s 6	21' 11"	65	8	12	0	12
36	3 ^m 25 ^s 4	22' 43"	162	17	34	0.2	6	76	3 ^m 21 ^s 4	21' 13"	59	8	10	0.2	7
37	3 ^m 24 ^s 6	22' 55"	232	27	101	0.3	4	77	3 ^m 21 ^s 2	21' 15"	71	15	22	0.3	5
38	3 ^m 28 ^s 3	22' 08"	141	9	20	0.4	4	78	3 ^m 21 ^s 5	21' 12"	67	7	12	0.2	10
39	3 ^m 25 ^s 5	22' 55"	83	7	11	0.2	4	79	3 ^m 21 ^s 1	21' 13"	68	7	8	0.2	9
40	3 ^m 25 ^s 3	21' 16"	68	10	17	0.3	4								

Notes to TABLE 2

^aDiameters are for a distance of 7.4 Mpc

incomplete by 20%, on the assumption that the two galaxies are directly comparable. Appendix A shows however that when the objective algorithm is applied to the LMC, the same number of associations is detected as were found in the works of Lucke & Hodge (1970). A possible cause for incompleteness arises from the difficulty in establishing very small groups of blue stars as real associations. Our search method regards most of the smallest groups as statistically insignificant, but many of them could be very compact associations, for which we are not sensitive enough. This means that we are not detecting "Orion-like" objects in M101. Instead the smallest objects in our sample correspond to Galactic star forming regions with size between that of M8 and the Rosette Nebula (NGC 2244), both in terms of diameter and $H\alpha$ luminosity (Kennicutt 1984). At the high-end we find Galactic counterparts in the Carina and W49 regions, while the most luminous association (# 72) has an $H\alpha$ lumi-

nosity comparable to 30 Doradus in the LMC. On the other hand we think that our search method is conservative, in the sense of disregarding associations of dubious reality, which will be very important when studying galaxies at even larger distances. We are therefore at a necessary trade-off between completeness and reproducibility.

Since we are interested in comparing results for different galaxies in the future, we ran a simple experiment to test how resolution might affect the identification of the associations. New versions of chip 4 images were created, compressed by a factor of 1.5 and 2, to simulate a corresponding increase in distance (the exposure times were assumed increased by a factor of 2.25 and 4.0, respectively). The search radii were reduced by exactly the same factors with respect to the original images. The average size of the clumps did not change significantly in the first case, and increased by 10% in the case corresponding to a doubling of the distance.

TABLE 3. Comparison of OB associations properties.

Galaxy	average diameter (pc)	median diameter (pc)	minimum no. of stars
M101	100	90	7
LMC	80	60	3
SMC	90	70	3
M33	80	60	10
M31	120	100	5
NGC6822	90	90	10

In both cases, most of the original morphology and position of the associations were recovered, while the number of blue stars was reduced by 9% and 19%. These results suggest that we can confidently compare properties of associations in galaxies which differ by at least a factor of 2 in distance.

5. SIZE DISTRIBUTION OF THE OB ASSOCIATIONS

The diameters of the associations found in M101 are given in Table 2, while Fig. 5 compares the size distribution of the M101 associations with other nearby galaxies studied with similar methods. These are the LMC (Appendix), M33 (Wilson 1991; Regan & Wilson 1993), M31 (Haiman *et al.* 1994), the SMC (Battinelli 1991), and NGC 6822 (Wilson 1992). Somewhat different criteria have been used to select the blue stars in these works; our criterion is equivalent to that applied to M33. We note that the size distributions are dependent on the search radius chosen. All galaxies show a similar distribution, and the Kolmogorov-Smirnov test indicates that the data are indeed consistent with a single distribution function. The presence of a peak might at first be attributed to a selection effect, due to the fact that smaller associations are more difficult to detect. However, an absence of associations smaller than 20–30 pc is observed in even well resolved galaxies such as the Magellanic Clouds

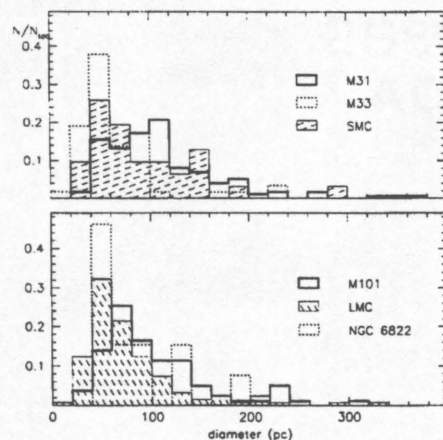


FIG. 5. Comparison of associations size distribution for M101, LMC, SMC, M31, NGC 6822, and M33.

TABLE 4. Slope of the luminosity function.

Color criterion	field + associations	field	associations
$U-V < -0.5$	0.58 ± 0.04	0.58 ± 0.05	0.58 ± 0.06
$U-B < -0.7$	0.62 ± 0.04	0.62 ± 0.05	0.62 ± 0.07
$B-V < +0.4$	0.55 ± 0.04	0.57 ± 0.04	0.53 ± 0.05

(Hodge & Lucke 1970; Hodge 1985), indicating that the observed distributions are indeed peaked. Furthermore in the Galaxy OB associations have a mean size around 140 pc (Garmany & Stencel 1992), much larger than the typical diameters of open clusters (10–35 pc, Janes *et al.* 1988). The peak in the distributions lies around 40–80 pc for M101, LMC, SMC, M33, and NGC 6822, but ~ 110 pc for M31. This hint of a possible Hubble-type dependence deserves further investigation. However, it should be noted that the size distribution that Efremov *et al.* (1987) obtained for the M31 associations shows a behavior more closely resembling that of the remaining galaxies.

We believe the size distribution to be more meaningful than the mean diameter, which is difficult to define and is subject to numerous observational biases (see discussion in Magnier *et al.* 1993). We have however compiled in Table 3 the mean for the galaxies studied, which show similar values of ~ 90 pc. We conclude that the associations in M101, LMC, SMC, M33, NGC 6822, and perhaps M31 have similar size distributions and average sizes. No clear effect of Hubble type or distance (resolution) is observed.

6. PROPERTIES OF THE OB ASSOCIATIONS

6.1 The Stellar Luminosity Function

Many studies of extragalactic stellar populations use the differential luminosity function (dLF) to investigate possible differences in the properties of the most massive stars (Freedman 1985; Blaha & Humphreys 1989). We have determined the LF in V for all stars contained in the 79 associations, as well as for all stars in our frames, regardless of their position, and for field stars only. We followed Freedman (1985) and Berkhuysen & Humphreys (1989) in using different color selection criteria to better isolate the blue stars. It was pointed out by Freedman (1985) that a $U-V$ criterion is to be preferred over $B-V$ because the former is a better discriminator against A supergiant stars. Adopting the usual power-law expression for the LF we then determined the slope $\alpha = d \log N / dV$ for different color cut-offs, as given by a least-square fit and using 0.5 mag interval bins. The color criterion that provides the largest slope is the adopted one. Figure 6 shows the LF in V for stars with $U-V \leq -0.5$. The break in the function for $V > 23.5$ suggests that the data become incomplete at that magnitude, and hence we only include stars with $V < 23.5$ in our fit. Table 4 lists the best fitted power-law slopes for various color criteria, for the entire field population and stars in associations only. The errors listed include statistical uncertainties but not systematic effects due to crowding or incompleteness. There is no important difference among the three color criteria. The slightly smaller value from the $B-V$ selection is hardly significant, and, if real, might be due to the inclusion of some

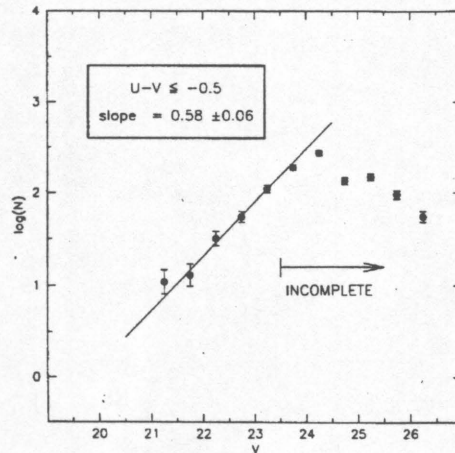


FIG. 6. The differential V luminosity function for the brightest stars in the associations. Only stars having $(U-V) < -0.5$ are included.

later-type stars. It is interesting however that no difference is seen between stars in associations and stars in the field. We conclude that the slope of the V LF in this field is $\sim 0.60 \pm 0.05$.

Freedman (1985) found a value of 0.67 ± 0.03 for the V LF of the brightest stars in nearby galaxies. More recent determinations from *HST* observations are given, among others, by Hughes *et al.* (1994) and Hunter & Thronson (1995). The values found (0.56–0.58 in the case of M81, and between 0.58 and 0.65 for different sets of stars in I Zw 18) are consistent with the slope determined for M101, and confirm that the upper LF does not change significantly. This is perhaps not surprising given the relative insensitivity of the LF slope to changes in the IMF (Massey 1985). However these results appear to rule out any radical variation in IMF slope or stellar mass limit (see Sec. 7).

6.2 Reddening

The substantial extinction in this M101 field is readily inferred from the optical images, which show many dust filaments along the spiral arms, and by the color ($B-V=0$) of the blue plume in the CMD of Fig. 3. Hence it is important to measure the reddening of the OB associations. The extinction law in M101 was found to be similar to the Galactic one ($R_V=3.16$, $R_V=A_V/E(B-V)$) by Rosa & Benvenuti (1994). The foreground extinction in the direction of M101 is virtually zero (de Vaucouleurs *et al.* 1991).

To measure the reddening we used the Johnson Q parameter technique, where $Q=(U-B)-0.72(B-V)$ is a reddening-free quantity. The Q value for stars in associations with $B-V<0.1$ was used to derive, by means of the equations given in Massey *et al.* (1995a), an intrinsic color, $(B-V)_0$, which allowed individual stellar reddenings to be calculated (see Table 5). The mean value for all stars belong-

TABLE 5. Balmer decrement reddening and number of ionizing photons.

Association no.	$E(B-V)$	$\log Q_0$
4	0.82	50.91
11	0.19	49.91
13	0.29	50.33
31	0.29	50.22
36	0.36	49.88
41	0.14	49.25
51	0.19	49.91
52	0.41	49.71
57	0.24	51.17
61	0.47	50.27
67	0.25	50.12
68	0.39	50.94
72	0.29	51.92

ing to the same association was then adopted as the reddening for the entire group. The estimated uncertainty is $E(B-V)=\pm 0.1$. For the stars in our associations the average $\langle E(B-V) \rangle = 0.21$. Wilson (1991) gives an average of 0.3 mag for associations in the inner region of M33 (0.15 in an outer region studied by Regan & Wilson 1993), and values in the range 0.2–0.4 are reported, for example, by Haiman *et al.* (1994).

The ground-based narrow-band imaging was used to measure the extinction for a number of H II regions, some of which match the position of an OB association. The reddening can be measured by the Balmer decrement,

$$\frac{I_{H\alpha}}{I_{H\beta}} = \frac{F_{H\alpha}}{F_{H\beta}} 10^{C(H\beta) \cdot f(\lambda)},$$

where we assume the theoretical value $I_{H\alpha}/I_{H\beta}=2.86$ (case B, $T=10^4$ K, $N_e=100 \text{ cm}^{-3}$, Osterbrock 1989) and the extinction curve $f(\lambda)$ of Seaton (1979). The visual extinction is given as $A_V=2.15 \cdot C(H\beta)$ (Rosa & Benvenuti 1994). The average reddening for 35 H II regions is 0.39 mag, with a large scatter (0.19 mag). Of these, 13 coincide with OB associations (nearly 40 percent of the associations have H II region counterparts, but these are often too faint to be included in the analysis). The comparison with the values from the broad-band photometry is shown in Fig. 7. The Balmer ratio gives, on average, a reddening value ~ 0.1 mag larger than the Q method. This is of the same order as the uncertainties, therefore the difference in the two distributions is to be considered marginally significant. Note also that many of the larger reddening values are found for H II regions that have no OB association counterpart. We could say that the identified OB associations do not lie in the regions with the higher reddening. With such a small sample, though, it is difficult to assert the reality of this effect. In general we expect however that H II regions will be more reddened than the average OB association.

6.3 The Color-Magnitude and Color-Color Diagrams

We show in Fig. 8 the CMD of those stars that lie within the OB associations boundaries. For each association the stars have been dereddened according to the average $E(B-V)$. The CMD morphology is similar to that of Fig. 3, and shows that the selected OB association boundaries contain several evolved stars. The scatter of stars across the diagram can be therefore attributed partly to a spread in age.

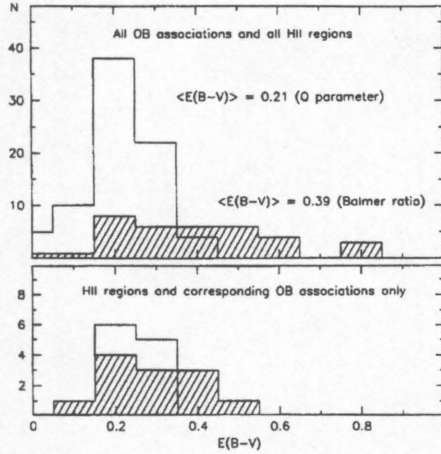


FIG. 7. (a) $E(B-V)$ for all OB associations [measured by the reddening-free parameter $Q = (U-B) - 0.72(B-V)$] and for all the bright H II regions found in the M101 field (measured by the Balmer decrement). (b) $E(B-V)$ for those associations for which both Q and the Balmer decrement were measured.

The age analysis (next section) tends to confirm the presence of stellar groups older than 10 Myr among the selected associations.

The dereddened color-color plot of stars in associations with photometric uncertainties < 0.15 mag is shown in Fig. 9. The sequences for dwarf and supergiant stars have been drawn, adopting the calibrations of Fitzpatrick & Garmany (1990) and FitzGerald (1970). O-B5 stars ($U-V \leq -0.9$)

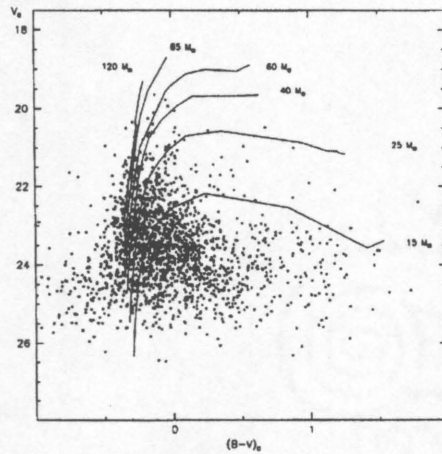


FIG. 8. Color-magnitude diagram for the stars within the OB associations boundaries. For each association the stars have been dereddened according to the average $E(B-V)$ value measured from the Q parameter.

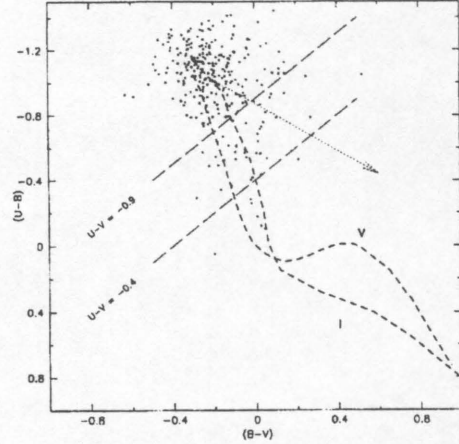


FIG. 9. $(U-B)$ vs $(B-V)$ diagram for those stars in associations having internal photometric errors smaller than 0.15 mag in each band. The reddening correction has been applied as in Fig. 8. The main sequence and supergiants sequence are plotted, together with two lines of constant $U-V$ color (-0.9 , supergiants of spectral type B5, and -0.4 , at the transition between late B and early A supergiants). The arrow represents the reddening vector for a B0 supergiant.

are clumped around the tip of the sequences. A few B5-B9 and A stars are also present at redder colors. According to the calibration of Fitzpatrick & Garmany (1990) stars of luminosity class Ib have $M_V = -5.2$ (-4.3) at $U-V \sim -0.9$ (-0.4) (Ia supergiants are at least one magnitude brighter), corresponding to $V = 24$ (25). At this magnitude both B and U frames are severely incomplete, thus explaining the rapid decline in the number of stars visible below the $U-V = -0.9$ line.

6.4 Estimating the Age

We attempted to estimate the age of the OB associations in M101 by comparing their dereddened CMDs by visual comparison with theoretical isochrones (Schaller *et al.* 1992; Meynet *et al.* 1993). Usually the brightest stars were used in the comparison, since the fainter ones tend to have large photometric errors. The major sources of uncertainty in assigning these ages are the reddening, the small number of stars available in individual associations and photometric errors. The presence of binary stars and unresolved clumps is a further problem. An uncertainty of ± 2 Myr is estimated, based on the fact that typical photometric and reddening errors can produce a variation of a few (~ 2) Myr in the calculated ages.

Figure 10(a) shows an example of this procedure. The isochrones, calculated from 2.5 to 9.5 Myr in steps of 1 Myr, are superposed on the CMD of association # 37. In this case an age of 4 ± 2 Myr was estimated. The evolved stars in the red part of the diagram probably do not belong to the same episode of star formation that created the younger stars. The coexistence of red supergiants and younger OB stars, point-

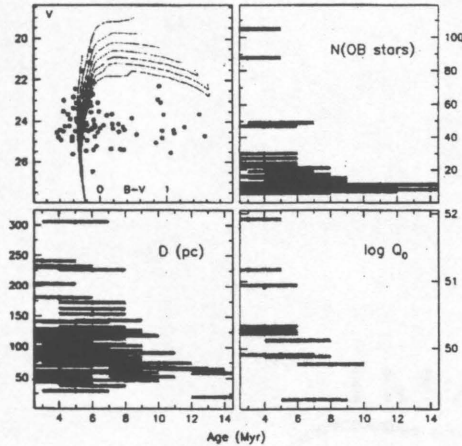


FIG. 10. (a) Example of age determination: theoretical isochrones from the Schaller *et al.* (1992) models from 2.5 to 9.5 Myr in steps of 1 Myr are superposed on the dereddened CMD of association 37. In this case an age of 4 Myr (± 2 Myr) was estimated. (b) Number of blue stars in the associations vs age. (c) Diameter of the associations vs age. (d) Number of ionizing photons (measured from the $H\alpha$ flux) vs age. In these plots the estimated uncertainty of ± 2 Myr is represented by elongated bars.

ing to non-coevality, has been noted in previous studies (Doom *et al.* 1985; Massey *et al.* 1989; Garmany & Stencel 1992). If the observed red stars are indeed members of the associations, it would mean that star formation occurs in episodes separated by several Myr, and that no single age can be assigned. At least qualitatively, though, there is no apparent clumping of the red stars within the associations boundaries. We conclude that they could appear to belong to the associations simply because of projection effects.

We show in the other panels of Fig. 10 the dependence on age of three quantities: the number of blue stars, the size of the associations and the number of ionizing photons Q_0 (calculated from the $H\alpha$ flux) for the H II regions which have been identified also as OB associations. The estimated uncertainty of ± 2 Myr is represented by bars elongated along the time axis. Despite the scatter, this shows how the richest and largest associations are found among the youngest ones. This is probably due to the disruption of the gravitationally unbound associations with time, combined with selection effects, which make it easier to detect stars belonging to young associations. There is also a dependence of Q_0 on age, due to the relation between the number of blue, ionizing stars and age. This plot is consistent with the typical H II region lifetime of 5–6 Myr. Table 2 summarizes the associations properties presented in this section.

7. ON THE UPPER MASS LIMIT OF THE IMF

The use of broad-band photometry to study the IMF of distant populations of stars is subject to several difficulties. First of all is the well-known insensitivity of broad-band

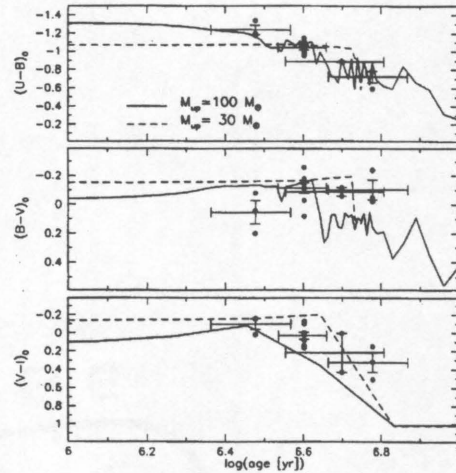


FIG. 11. The integrated and dereddened colors of the richest associations ($N_{\text{blue}} > 15$) compared to Leitherer & Heckman's (1995) population models for an instantaneous burst at solar metallicity. The dots represent the observed colors and the assigned ages. The two lines are for a Salpeter IMF with high-mass limits of 100 and 30 M_{\odot} .

colors to the effective temperature of hot, massive stars (Massey *et al.* 1995a). This makes the task of discriminating stars of different masses practically impossible with photometry alone. Moreover incompleteness in the data hinders the detection of the hottest stars, whose large bolometric corrections make them visually fainter than supergiants of later type. Photometric uncertainties and reddening, together with crowding and blending of unresolved stellar images (particularly in the young clusters within the star-forming regions) complicate matters further. With these caveats in mind, we can look at the CMDs of Figs. 3 and 8. These suggest the presence of stars more massive than 25–30 M_{\odot} , perhaps 60 M_{\odot} or higher. The degeneracy of massive stars in this region of the CMD, though, makes it impossible to say whether very massive stars are unambiguously present or not.

We also attempted to use an evolutionary synthesis model to constrain the upper mass limit of the IMF. Integrated magnitudes and colors for the richest associations (those having more than 15 stars) were measured by adding up all the flux within the association boundaries. The reddening-corrected colors were compared with the models of Leitherer & Heckman (1995) (instantaneous burst, solar metallicity). In Fig. 11 the model predictions for two upper mass limits, 30 and 100 M_{\odot} , of a power-law IMF with Salpeter's slope are superposed on the observed colors and ages. While the comparison for $(U-B)_0$ favors an upper mass limit of 100 M_{\odot} , the other two colors are however more difficult to interpret.

We conclude from these two exercises that there is some evidence for an IMF in M101 with a high cut-off mass (comparable to the $\sim 100 M_{\odot}$ limit found in the Magellanic

Clouds and in the Milky Way by Massey *et al.* 1995b). This field has an oxygen abundance of $\sim 1-2 Z_{\odot}$ (Kennicutt & Garnett 1996) and some authors have suggested previously that the H II regions in this part of M101 have a much lower upper stellar mass limit (e.g., Shields & Tinsley 1976). Our observations suggest that such a strong change in the upper mass limit may not be present, but further observations are needed to make a definitive test. This result also agrees with the study of Rosa & Benvenuti (1994), who found no need to invoke a metallicity effect on the IMF in their study of four giant H II regions in M101.

8. POPULOUS STAR CLUSTERS

The importance of star clusters for the understanding of star formation and evolution has been stressed many times (van den Bergh 1991). The clusters of the Magellanic Clouds in particular have been the subject of intense study, leading to a picture of differing evolutionary histories between the Clouds and the Galaxy. Of great interest is the presence in the Clouds of populous clusters ("blue globulars"), which are absent in the Milky Way. Populous clusters have been observed in a handful of galaxies, and Kennicutt & Chu (1988) suggested a Hubble type dependence, being these clusters preferentially found in late-type (Sc, Irr) galaxies. It is therefore interesting to extend the search for populous clusters to as many galaxies as possible. This could lead to a better understanding of the properties and systematics of star formation in galaxies. Observations with *HST* like those used in the present work are well suited for this search. With typical sizes larger than 10 pc in the LMC (van den Bergh 1991), we expect to be able to identify these objects at least to a distance of 10–12 Mpc on WFPC2 images.

A total of 41 clusters were found by visual search in the WFPC images, with typical FWHM=0.3. Their luminosity was measured with aperture photometry on average images. The estimated uncertainty in the colors is 0.1 magnitudes, based on the variation in the measured fluxes using different apertures and sky annuli. The magnitudes are more uncertain: aperture radii of eight pixels (= 29 pc in the three Wide Field chips) were adopted, but in some cases smaller values had to be used to avoid contamination from nearby objects. The results are summarized in Table 6, while Figs. 12 and 13 show the integrated color-magnitude and color-color diagrams, respectively.

Most clusters are blue ($B - V < 0.5$), and occupy the same region in the ($B - V$) vs V diagram as the LMC blue clusters (Fig. 12). The bluest objects are young nuclei of OB associations, which were included even though they differ from the stable open clusters. The color histogram shows a lack of red clusters relative to the LMC. This color distribution differs even more strongly from the colors of clusters in M33 (Christian & Schommer 1982, 1988) and, especially, in M31 (Hodge *et al.* 1987), where a larger fraction of clusters have ($B - V$) > 0.5.

In Fig. 13(a) the sequence of LMC clusters used for age calibration by Girardi *et al.* (1995) is indicated. Using their age calibration the clusters for which we could measure both $U - B$ and $B - V$ have ages between a few Myr and ~ 500

TABLE 6. Cluster photometry.

ID	RA (14 ^h)	DEC (+54°)	V	U-B	B-V	V-I
1	3 ^m 25 ^s 3	21° 11'	20.51	-0.50	0.21	0.55
2	3 ^m 25 ^s 5	21° 06'	20.93	-0.80	0.26	0.51
3	3 ^m 23 ^s 7	21° 14'	23.26	...	0.58	0.67
4	3 ^m 22 ^s 4	21° 05'	23.71	...	0.24	0.45
5	3 ^m 23 ^s 4	21° 28'	21.59	...	0.38	0.60
6	3 ^m 22 ^s 7	20° 58'	22.48	...	0.30	0.49
7	3 ^m 25 ^s 0	21° 12'	22.29	...	0.31	0.53
8	3 ^m 25 ^s 3	21° 08'	22.51	...	0.06	0.39
9	3 ^m 24 ^s 6	21° 04'	22.07	-0.67	0.29	0.55
10	3 ^m 19 ^s 9	21° 13'	22.31	-0.23	0.10	0.36
11	3 ^m 16 ^s 9	21° 19'	21.88	-0.07	0.33	0.62
12	3 ^m 18 ^s 7	22° 33'	20.86	-0.79	-0.18	0.09
13	3 ^m 21 ^s 9	21° 45'	20.45	-0.89	-0.02	0.34
14	3 ^m 15 ^s 6	22° 13'	21.00	0.34	0.27	0.58
15	3 ^m 14 ^s 1	22° 05'	20.95	-0.27	0.12	0.52
16	3 ^m 17 ^s 7	22° 09'	21.27	0.11	0.25	0.71
17	3 ^m 19 ^s 7	21° 40'	20.04	...	1.01	1.08
18	3 ^m 18 ^s 5	22° 33'	21.65	0.04	0.43	0.59
19	3 ^m 22 ^s 2	22° 49'	21.52	-0.41	0.16	0.60
20	3 ^m 25 ^s 6	22° 41'	21.00	-0.06	0.20	0.37
21	3 ^m 27 ^s 4	22° 15'	21.76	-0.50	0.13	0.68
22	3 ^m 26 ^s 4	21° 58'	21.71	-0.66	0.30	0.99
23	3 ^m 29 ^s 7	22° 24'	20.84	0.09	0.35	0.65
24	3 ^m 29 ^s 3	22° 19'	21.35	...	0.46	0.72
25	3 ^m 28 ^s 4	22° 19'	22.26	...	0.39	0.66
26	3 ^m 22 ^s 2	22° 37'	21.74	...	0.46	0.97
27	3 ^m 24 ^s 1	21° 43'	21.85	-0.93	-0.07	0.48
28	3 ^m 24 ^s 1	21° 57'	22.10	-1.00	0.05	0.29
29	3 ^m 25 ^s 7	22° 09'	21.53	-0.97	-0.02	0.31
30	3 ^m 24 ^s 2	20° 56'	20.50	-0.06	0.22	0.55
31	3 ^m 24 ^s 2	21° 10'	20.46	-0.61	0.29	0.69
32	3 ^m 24 ^s 0	21° 12'	20.56	-0.51	0.38	0.59
33	3 ^m 22 ^s 3	21° 12'	22.34	...	0.99	1.01
34	3 ^m 24 ^s 0	21° 23'	19.58	...	1.14	1.47
35	3 ^m 21 ^s 8	21° 05'	20.76	0.33	0.44	0.70
36	3 ^m 24 ^s 8	21° 11'	21.49	0.17	0.78	1.19
37	3 ^m 24 ^s 6	21° 11'	21.59	0.01	0.27	0.54
38	3 ^m 24 ^s 5	21° 02'	21.48	-0.35	0.38	0.60
39	3 ^m 24 ^s 9	21° 11'	21.91	-0.47	0.42	0.69
40	3 ^m 23 ^s 3	20° 53'	21.46	-0.42	0.29	0.55
41	3 ^m 23 ^s 2	21° 01'	22.03	...	0.51	0.82
42 ¹	3 ^m 22 ^s 8	21° 04'	17.71	-1.10	0.08	0.05
43 ²	3 ^m 23 ^s 7	21° 16'	19.38	-1.05	0.25	-0.09

Notes to TABLE 6

¹H II region core cluster, in association 72.

²H II region core cluster, in association 57.

Myr. No reddening correction has been applied, even though $E(B - V) \approx 0.1$ could probably bring the data to a better fit to the LMC sequence. It seems appropriate to compare the M101 clusters with the cluster system of M33, also an Sc galaxy, studied in detail by Christian & Schommer (1988). Fig. 13(b) compares the ($B - V$) vs ($V - I$) diagram for the two galaxies. The calibration line of Christian & Schommer (1988) is shown. The lack of M101 red clusters, having ($V - I$) > 0.7, is evident. It could be possible that this is an effect of the position in the galaxy where these clusters are found, i.e., close to the nucleus. In the M33 data, however, there is no indication that the red clusters preferentially lie away from the nucleus. The fractional area of M101 surveyed for clusters is too small to draw firm conclusions on the overall cluster population and on its differences relative

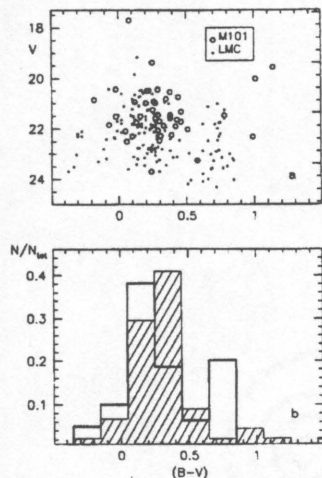


FIG. 12. (a) $(B-V)$ vs V integrated color-magnitude diagram for star clusters in M101 (open circles) and in the LMC (dots, from van den Bergh 1981); (b) color distribution for M101 (hatched) and LMC clusters.

to other galaxies. We however remind the reader that this area roughly equals the extent of the entire LMC. On the basis of our analysis we can only conclude that red clusters ("old globulars" candidates) are rare in the field studied. Many of the remaining clusters are very likely populous clusters of the same kind found in the LMC. The large ratio between the number of blue and red clusters is consistent with previous findings that populous clusters are preferentially found in late-type galaxies.

Two giant H II regions, numbers 972 and 1013 in the catalog of Hodge *et al.* (1990), fall in our *HST* field, corresponding to associations 57 and 72, respectively. Both have a high H α luminosity, with a number of ionizing photons in excess of 10^{51} s^{-1} (Table 5). By comparison, 30 Dor in the LMC has an H α luminosity corresponding to $\sim 10^{52}$ ionizing photons/s. The morphology of the two regions differs somewhat. Region 72 resembles 30 Dor in having a bright, compact core cluster, which is probably responsible for most of the ionizing flux in the nebula. Several fainter clusters or single stars surround the central object. In region 57, on the contrary, we see a normal association of bright stars, similar in structure to the giant H II region NGC 604 in M33. To better quantify the properties of these embedded star clusters, and in order to compare them with similar objects in nearby galaxies, we measured fluxes in different apertures, centered on the brightest object in each of the two H II regions. In region 72, the radius of the core cluster is $\sim 22 \text{ pc}$, with a radius containing one-half the total light $R_{0.5} \approx 7 \text{ pc}$, and a total absolute magnitude $M_V = -12.3$. This object shows some finer structure, namely the presence of 2 distinct clusters, with a peak ratio of about 3:1. Each one has $R_{0.5} \approx 3.6 \text{ pc}$. The brightest component has a luminosity $M_V \approx -12.0$, and a corresponding mean surface brightness $\Sigma_{0.5}$

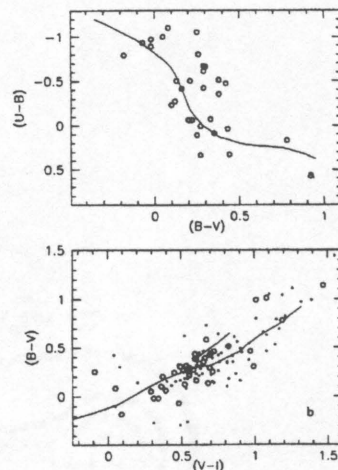


FIG. 13. (a) $(B-V)$ vs $(U-B)$ integrated color-color diagram for the M101 clusters. The sequence of LMC clusters from Girardi *et al.* (1995) is indicated; (b) $(V-I)$ vs $(B-V)$ diagram for clusters in M101 (open circles) and M33 (dots). The theoretical sequence shown is taken from Christian & Schommer (1988).

$= 6.9 \times 10^4 L_{V,\odot} \text{ pc}^{-2}$ inside the radius $R_{0.5}$. This compares with $\Sigma_{0.5} = 1.3 \times 10^5 L_{V,\odot} \text{ pc}^{-2}$, $R_{0.5} = 1.7 \text{ pc}$ and a total absolute magnitude $M_V = -11.1$ for R136 in 30 Dor (Hunter *et al.* 1995). Region 72 is therefore comparable to 30 Dor also quantitatively, even though it is somewhat less compact. We remind the reader that the "super star clusters" found in some galaxies (O'Connell *et al.* 1994) represent more extreme modes of star formation, 10–30 times more luminous than region 72, relative to the same age. In region 57 the main component is not as bright as in region 72, $M_V = -10.7$, while the nearby objects are typically 2 magnitudes fainter, and could be smaller clusters or very bright stars.

9. CONCLUSIONS

We have described an objective algorithm to identify 79 OB associations in an *HST* field of the galaxy M101. The following results were found:

- (1) The size distribution of the associations is comparable to that in the Magellanic Clouds, M33, NGC 6822, and M31, with a typical mean size of 90 pc.
- (2) The stellar luminosity function has a slope $d \log N / dV = 0.60 \pm 0.05$, both in the associations and in the general field.
- (3) H II regions tend to be slightly redder than the average OB association.
- (4) No indication that the upper mass limit of the IMF is lower than in low-metallicity environments is found.
- (5) Most of the star clusters identified in the field belong to the same class of populous clusters found in the LMC. Red clusters are rare.

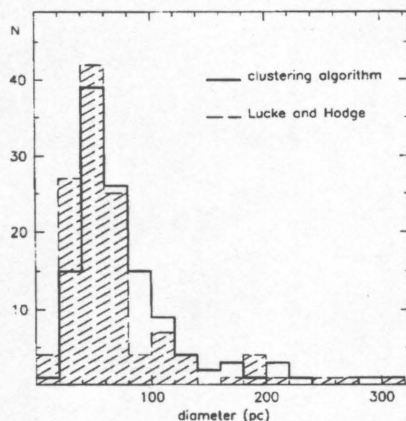


FIG. 14. Histogram of the sizes of the associations in the LMC as determined by the objective algorithm (continuous line) and those found by Lucke and Hodge (dashed line). In the latter case more small agglomerations were found, and less for sizes of 80–100 pc. In general, though, the two distributions are very similar.

We thank the *HST* Distance Scale Key Project team members, Abi Saha in particular, for their support in this work, Paul Hodge for his comments, and Paul Scowen for providing us with unpublished material on H II regions. This work was supported by NASA through grant GO-2227-87A, and by the NSF through grants AST-9019150 and AST-9421145.

APPENDIX: OB ASSOCIATIONS IN THE LMC

As a further application of the objective algorithm described in Sec. 4, data on the LMC were analyzed. Stellar associations in the LMC were catalogued from wide-field photographic plates by Lucke & Hodge (1970) and the characteristics of the 122 associations in the catalog were studied by Hodge & Lucke (1970). We applied the clustering algorithm to the catalog of bright stars of Rousseau *et al.* (1978) (in the updated machine-readable form available through the NASA Astronomical Data Center). It is interesting to compare our numerical association-finding technique with subjective human intelligence when applied to the nearest galaxy, where a resolution of less than a pc ($1'' = 0.24$ pc) is attainable.

Stars were selected with two different criteria, based on spectral type (all cataloged stars with type earlier than B2.5) and on photometric parameters ($V < 13.7$, $B - V < 0.15$, to

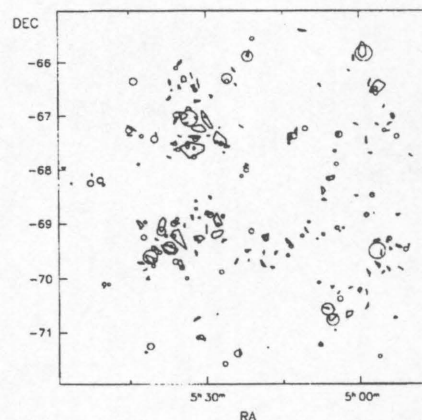


FIG. 15. This map shows the LMC association boundaries determined by the objective algorithm (irregular polygons) together with the associations in the Lucke & Hodge (1970) catalog (circles). Although there are several matching cases, many discrepancies are present. This is likely to be due to the incompleteness of the bright LMC stars catalog in the densest regions and in correspondence of H II regions.

match the criteria adopted for M101 and M33). The two sets of stars gave approximately the same results, so the following discussion concentrates on the photometrically selected one. The search radius determined by the algorithm is 60 pc [the same used by Battinelli (1991) in the SMC]. Out of the 1354 "blue" stars, 725 are distributed in 121 associations. The resulting average size is 78 pc, the same value found by Hodge & Lucke (1970). This includes all agglomerations of stars with at least three stars. A correction, based on the expected contamination by statistical fluctuations, gives 94 pc instead. The distribution of association sizes is shown in Fig. 14 for both Hodge and Lucke's data and this work. They appear remarkably similar, except for a larger number of small associations in Hodge and Lucke. Regarding the case-by-case comparison (Fig. 15), the agreement is far from good. It has been noted (Caplan & Deharveng 1986) that the stars in the Rousseau *et al.* catalog, which is based on an objective prism spectral survey, show no concentration toward H II regions, and we infer that the catalog is under-representing the regions richest in OB stars, which may be the explanation for the poor agreement. For the purpose of making an objective catalog of associations in the LMC a better catalog of the brightest blue stars is needed.

REFERENCES

- Battinelli, P. 1991, *A&A*, 244, 69
 Berkhuijsen, E. M., & Humphreys, R. M. 1989, *A&A*, 214, 68
 Blaauw, A. 1991, in *The Physics of Star Formation and Early Stellar Evolution*, edited by C. J. Lada and N. D. Kylafis (Kluwer, Dordrecht), p. 125
 Blaha, C., & Humphreys, R. M. 1989, *AJ*, 98, 1598
 Caplan, J., & Deharveng, L. 1986, *A&A*, 155, 297
 Christian, C. A., & Schommer, R. A. 1982, *ApJS*, 49, 405
 Christian, C. A., & Schommer, R. A. 1988, *AJ*, 95, 704
 de Vaucouleurs, G., de Vaucouleurs, A., Corwin, H. G., Buta, R. J., Panurel, G., & Fouque, P. 1991, *Third Reference Catalogue of Bright Galaxies* (Springer, New York)
 Doorn, C., De Greeve, J. P., & de Loore, C. 1985, *Apl*, 290, 185

- Efremov, Y. N., & Chernin, A. D. 1994, *Vistas Astron.*, 38, 165
 Efremov, Y. N., Ivanov, G. R., & Nokolov, N. S. 1987, *Ap&SS*, 135, 119
 FitzGerald, M. P. 1970, *A&A*, 4, 234
 Fitzpatrick, E. L., & Garmany, C. D. 1990, *ApJ*, 363, 119
 Freedman, W. 1985, *ApJ*, 299, 74
 Garmany, C. D. 1994, *PASP*, 106, 25
 Garmany, C. D., & Stencel, R. E. 1992, *A&ASS*, 94, 211
 Girardi, L., Chiosi, C., Bertelli, G., & Bressan, A. 1995, *A&A*, 298, 87
 Haiman, Z., *et al.* 1994, *A&A*, 290, 371
 Hodge, P. W., Gurwell, M., Goldader, J. D., & Kennicutt, R. C. 1990, *ApJS*, 73, 661
 Hodge, P. W., Mateo, M., Lee, M. G., & Geisler, D. 1987, *PASP*, 98, 173
 Hodge, P. 1986, *Luminous Stars and Associations in Galaxies IAU Symposium No. 116*, edited by C. W. H. de Loore, A. J. Willis, and P. Laskarides (Reidel, Boston), p. 369
 Hodge, P. W. 1985, *PASP*, 97, 530
 Hodge, P. W., & Lucke, P. B. 1970, *AJ*, 75, 933
 Holtzman, J. A., Burrows, C. J., Casertano, S., Hester, J. J., Trauger, J. T., Watson, A. M., & Worthey, G. 1995, *PASP*, 107, 1065
 Hughes, S. M. G., *et al.* 1994, *ApJ*, 428, 143
 Humphreys, R. M. 1978, *ApJS*, 38, 309
 Hunter, D. A., & Thronson, H. A. 1995, *ApJ*, 452, 238
 Hunter, D. A., Shaya, E. J., Holtzman, J. A., Light, R. M., O'Neil, E. J., & Lynds, R. 1995, *ApJ*, 448, 179
 Jones, K. A., Tilley, C., & Lynga, G. 1988, *AJ*, 95, 771
 Kelson, D., *et al.* 1996, *ApJ* (in press)
 Kennicutt, R. C., & Garnett, D. R. 1996, *ApJ*, 456, 504
 Kennicutt, R. C., Freedman, W. L., & Mould, J. R. 1995, *AJ*, 110, 1476
 Kennicutt, R. C., & Chu, Y.-H. 1988, *AJ*, 95, 720
 Kennicutt, R. C. 1984, *ApJ*, 287, 116
 Leitherer, C., & Heckman, T. 1995, *ApJS*, 96, 9L
 Lucke, P. B., & Hodge, P. W. 1970, *AJ*, 75, 171
 Magnier, E. A., *et al.* 1993, *A&A*, 278, 36
 Massey, P., Johnson, K. E., & DeGioia-Eastwood, K. 1995b, *ApJ*, 454, 151
 Massey, P., Lang, C. C., DeGioia-Eastwood, K., & Garmany, C. D. 1995a, *ApJ*, 438, 188
 Massey, P., Garmany, C. D., Silkey, M., & DeGioia-Eastwood, K. 1989, *AJ*, 97, 107
 Massey, P. 1985, *PASP*, 97, 5
 Meynet, G., Mermillod, J.-C., & Maeder, A. 1993, *A&A*, 98, 477
 O'Connell, R. W., Gallagher, J. S., & Hunter, D. A. 1994, *ApJ*, 433, 65
 Osterbrock, D. E. 1989, *Astrophysics of Gaseous Nebulae and Active Galactic Nuclei* (University Science Books, Mill Valley)
 Regan, M. W., & Wilson, C. D. 1993, *AJ*, 105, 499
 Rosa, M. R., & Benvenuti, P. 1994, *A&A*, 291, 1
 Rousseau, J., Martin, N., Prévot, L., Rebeiro, E., Robin, A., & Brunet, J. P. 1978, *A&AS*, 31, 243
 Schaller, G., Schaerer, D., Meynet, G., & Maeder, A. 1992, *A&AS*, 96, 269
 Seaton, M. J. 1979, *MNRAS*, 187, 73
 Shields, G. A., & Tinsley, B. M. 1976, *ApJ*, 203, 66
 Stetson, P., *et al.* 1996, in preparation
 Stetson, P. 1994, *PASP*, 106, 250
 van den Bergh, S. 1991, *ApJ*, 369, 1
 van den Bergh, S. 1981, *A&A*, 46, 79
 Wilson, C. D. 1992, *AJ*, 104, 1374
 Wilson, C. D. 1991, *AJ*, 101, 1663

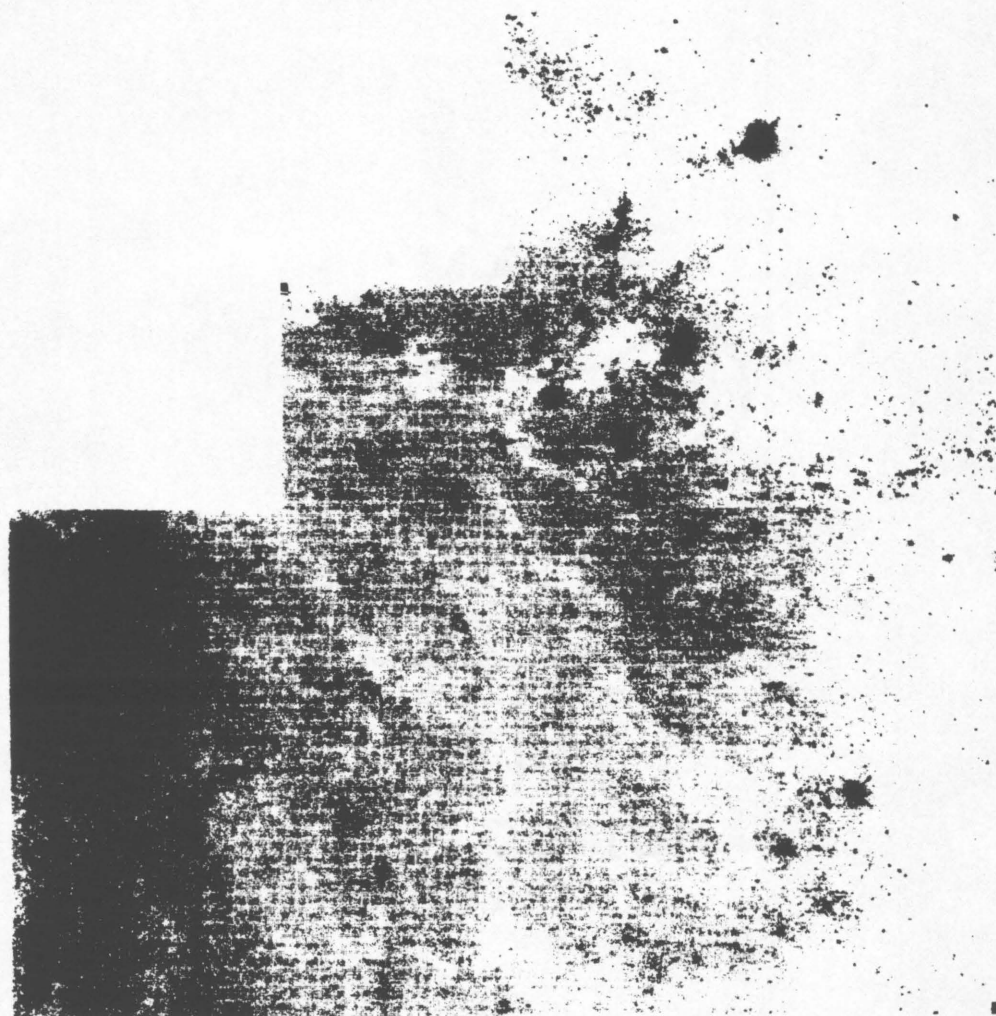


FIG. 1. Mosaic of the four WFPC2 chips. H II regions 1013 and 972 from the catalog of Hodge *et al.* (1990) are the brightest objects in chip 4 (upper right) (courtesy A. Turner).

APPENDIX D

UBVR AND $H\alpha$ PHOTOMETRY OF H II
REGIONS AND OB ASSOCIATIONS IN
GALAXIES: A TEST FOR A VARIABLE
IMF

Published in *The Astronomical Journal*, 1997, Vol. 113, p. 975.

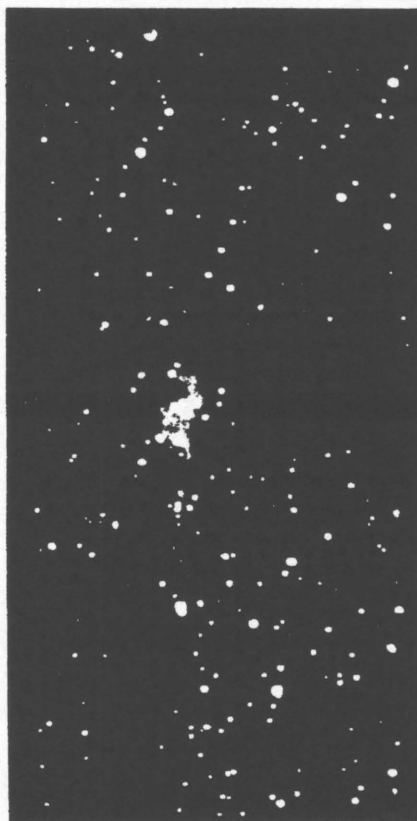
THE ASTRONOMICAL JOURNAL

FOUNDED BY B. A. GOULD
1849

VOLUME 113

March 1997~No. 1695

NUMBER 3



(See Page 1057)

Published for the
AMERICAN ASTRONOMICAL SOCIETY
by the
AMERICAN INSTITUTE OF PHYSICS

UBVR AND H α PHOTOMETRY OF H II REGIONS AND OB ASSOCIATIONS IN GALAXIES:
A TEST FOR A VARIABLE IMF

FABIO BRESOLIN AND ROBERT C. KENNICUTT, JR.

Steward Observatory, University of Arizona, Tucson, Arizona 85721

Electronic mail: fabio@as.arizona.edu, robk@as.arizona.edu

Received 1996 October 17; revised 1996 December 9

ABSTRACT

Photometry in UBVR and H α of H II regions and OB associations in a sample of Sa–Scd galaxies is presented. The distributions of H α equivalent widths for H II regions show no significant dependence on morphological type, and the continuum luminosity functions of the OB associations closely parallel the H α luminosity functions of the H II regions. Both luminosity functions show a strong dependence on Hubble type, in the sense that the characteristic luminosity of the brightest H II regions/OB associations decreases sharply in early-type disks. This implies that the changes in H II region and association properties along the Hubble sequence are most likely due to changes in the clustering properties of massive stars, rather than in the mass function. © 1997 American Astronomical Society. [S0004-6256(97)02303-0]

1. INTRODUCTION

Among the defining characteristics of the Hubble sequence are the rate and history of star formation in galaxies (Searle *et al.* 1973; Larson & Tinsley 1978; Kennicutt 1983). Spatially resolved observations indicate that the strong trend of star formation activity along the Hubble sequence is due to increases in both the luminosity of the individual H II regions and the number of the star forming events per unit area (Kennicutt *et al.* 1989). More than an order of magnitude difference in the luminosity of the brightest H II regions exists between Sa and Sc-Irr galaxies. Although it is commonly assumed that this difference is due to changes in the characteristic number of stars in the star forming regions, this idea remains largely untested, and others possibilities cannot *a priori* be ruled out. In particular lower-luminosity H II regions could be explained if the stellar Initial Mass Function (IMF) is systematically depleted of massive stars in early-type spirals, as first suggested by van den Bergh (1976) and Kormendy (1977). In this paper we investigate this possibility, by analyzing UBVR and H α imaging of H II regions in a sample of spiral galaxies of different Hubble type. The Balmer-line equivalent widths, being sensitive to changes in the upper IMF of the young ionizing clusters, are measured and compared between early-type (Sa–Sb) and late-type (Sbc–Scd) spirals. The broadband luminosity functions of the embedded associations provide an additional check for IMF variations.

Throughout this work a power-law parametrization of the IMF is adopted: $dN/dm \propto m^{-\alpha}$ ($\alpha = 2.35$ for Salpeter slope). The IMF is then characterized by its slope α and its upper and lower cutoff masses M_{up} and M_{low} . The paper is organized as follows: observations and data reduction are presented in Sec. 2; results on the broadband colors, the H α equivalent widths and the continuum luminosity function are given in Sec. 3. We then discuss in Sec. 4 the implications for the IMF.

2. OBSERVATIONS

The observations were obtained with Steward Observatory's 2.3 m telescope in 1995 April and May. A thinned Loral 1200×800 CCD was used, providing a rather limited field of view ($3' \times 2'$), but an excellent response in the blue. Images of each target galaxy were obtained through broadband U, B, V, and R filters, and a narrow-band (FWHM = 70 Å) H α filter. Typical exposure times were 1800 s in U, and 900 s in the remaining filters. Standard stars from the lists of Landolt (1992) and Massey *et al.* (1988) were observed for calibration during each photometric night.

The 10 galaxy sample was chosen to span a wide range in Hubble type (from Sa to Scd), and is described in Table 1. Distances are taken from Tully (1988), except for NGC 3351, NGC 4321, and NGC 5474 (assumed at the M101 distance), for which we have used results from Cepheids (Graham *et al.* 1997; Ferrarese *et al.* 1996; Kelson *et al.* 1997). Most of our objects have distances between 7 and 17 Mpc, since the small field of view forced us to avoid very nearby objects, in order to observe a good fraction of the number of star forming regions in each galaxy. The approximate spatial coverage is indicated in Table 1.

Data reduction proceeded in the standard way for the broadband images. The R-band images were used for continuum subtraction from the H α images, with scaling factors determined from the spectrophotometric standards and from continuum sources in the galaxy frames. The equations of Waller (1990), applied to the measured line and continuum fluxes, were used to determine the H α flux and equivalent width ($=EW(H\alpha)$). A correction for the [N II] contamination from the gaseous emission within the H α filter bandpass was made by assuming [N II]/H α = 0.33, a typical ratio for H II regions in the abundance range considered here. The wavelength shift of the H α emission line due to redshift was accounted for in the calibration. The measured fluxes were finally corrected for foreground Galactic extinction. We did

TABLE 1. The Galaxy sample.

Galaxy	Type	Distance (Mpc)	No. of regions	Fraction covered
NGC 2775	Sa	17.0	6	1.00
NGC 2841	Sb	12.0	23	0.46
NGC 3351 (M95)	SBb	9.8	32	0.31
NGC 3521	Sbc	7.2	31	0.50
NGC 4321 (M100)	Sc	16.1	49	0.31
NGC 4736 (M94)	Sab	4.3	15	0.39
NGC 5194 (M51)	Sbc	7.7	41	0.17
NGC 5248	Sbc	22.7	14	0.39
NGC 5474	Scd	7.4	20	0.39
NGC 6384	Sb	26.6	35	0.21

not correct for nebular continuum emission, which is important during the first few Myr after an initial burst of star formation, particularly in the R band. After ~ 3 Myr the relative contribution can however be neglected ($< 10\%$, Mas-Hesse & Kunth 1991).

A total of 266 H II regions which showed both continuum and line emission were interactively selected from the images. We note that several objects were bright in the continuum only, probably corresponding to OB associations or star complexes which are too old to have a detectable H α emission. For a few other regions it was difficult to define a common center for the continuum and H α objects, and it was decided to exclude them from our analysis. The radius for the aperture photometry (typically 2–3 arcsec) and the position for sky+background subtraction were then chosen for each region. For the faintest regions this is rather critical, since small variations in sky+background measurements determine rather large changes in the total flux, which therefore is affected by a large uncertainty. The fluxes within the circular apertures were measured with the PHOTOMETRY routine in DAOPHOT (Stetson 1987), and an aperture correction was then applied to account for flux not included within the aperture. This correction was measured from stars in the field and from calibration stars as a function of seeing, and in principle applies to point sources only. It was nevertheless decided to apply the correction (typically 0.1 magnitudes) also to the H II regions, even though in many cases they are spatially resolved. Because of uncertainties introduced by the selection of the aperture radii and the sky+background level, by the effect of merging and crowding, and by the amount of flux falling outside of the apertures, it is difficult to quantify the error in the total fluxes. Colors and EW(H α) were found somewhat less sensitive to these problems. Measurements with different radii and sky+background values indicate that the typical uncertainties are $\sim 15\%$ in $(U-B)$ and $(B-V)$, 5% in $(V-R)$, and 15%–20% in EW(H α). The uncertainty in the H α flux is of the order of 15%.

A comparison of H α fluxes for regions in common with Kennicutt (1988) shows good agreement ($\sim 10\%$ scatter, and no zero point offset), except for NGC 3351 and NGC 5474 (0.2 dex fainter and 0.3 dex brighter, respectively). In both these cases however we have indication of possible non-photometric conditions when our observations were made. For the rest of the data the sky was photometric. No $UBVR$ H II region photometry from the literature was avail-

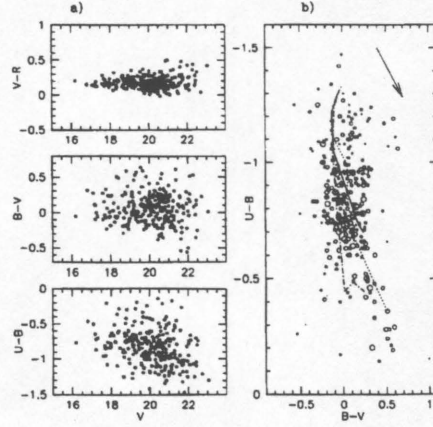


FIG. 1. (a) Distribution of the broadband colors as a function of V magnitude. (b) $(B-V)$ vs $(U-B)$ diagram. Symbol size scales with brightness. Model predictions (age < 10 Myr) by Leitherer & Heckman (1995) are indicated: Salpeter IMF with $\alpha = 2.35$, $Z = Z_{\odot}$ (continuous line); $\alpha = 3.3$, $Z = Z_{\odot}$ (dotted line); $\alpha = 2.35$, $Z = 2Z_{\odot}$ (dashed line); $\alpha = 2.35$, $Z = 0.1Z_{\odot}$ (dot-dashed line). The reddening vector corresponding to $A_V = 1$ mag is indicated at the upper right.

able for comparison; in particular we have no object in common with the only other work of this kind known to us (Mayya 1994).

3. RESULTS

3.1 General Results

The broadband colors of the measured H II regions are shown as a function of V magnitude in Fig. 1(a). Part of the color spread is due to observational uncertainties, but some of it must be related to reddening and metallicity effects. This is suggested by the distribution in the $(B-V)$ vs $(U-B)$ diagram [Fig. 1(b)]. We also show the model predictions by Leitherer & Heckman (1995) for an instantaneous burst, for different choices of metallicity and IMF (age < 10 Myr). We remind the reader that in these models the contribution of the nebular continuum emission is taken into account. Even though the observed colors are consistent with those predicted for young star forming regions, it is clear that it is impossible from the broadband data alone to disentangle the effects of reddening, metallicity, age and IMF, an already well-known result (e.g., Larson & Tinsley 1978).

Some of the observed H II region properties are displayed in Fig. 2. The data points have been indicated separately for regions in early-type spirals (Sa through Sb; open circles) and late-type spirals (Sbc and later; solid circles). In Fig. 2(a) model predictions are coded as in Fig. 1(b). This plot shows a trend of decreasing EW(H α) with increasing $(U-B)$, which reflects the evolution of the embedded stellar population. A correlation between H α luminosity and EW [Fig. 2(b)] is also expected from evolutionary considerations: as the most luminous stars evolve, decreasing the total output of

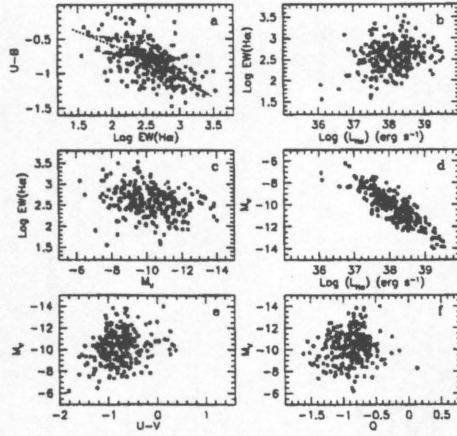


FIG. 2. Correlations between H II region observed properties for early-type spirals (open circles) and late-type spirals (solid circles). In (a) the same models as in Fig. 1 are shown.

ionizing radiation, the red continuum is enhanced by the evolved supergiants. This leads to a net decrease in both $EW(H\alpha)$ and $L(H\alpha)$. Such an effect is not seen in the correlation with M_V [Fig. 2(c)], because the continuum energy output remains approximately constant during the first 10^7 years from the initial burst of star formation. In Fig. 2(f) the reddening-free quantity $Q = (U-B) - 0.72(B-V)$ is plotted, as an estimate of the amount of extinction. The most important result from Fig. 2 is that the star forming region properties in early-type spirals are virtually the same as in late-type spirals, except for their luminosity. No H II region brighter than $L(H\alpha) = 10^{39} \text{ erg s}^{-1}$ ($M_V \approx -12.5$) is found among the Sa's and Sb's, while in the Sc's the brightest objects reach $L(H\alpha) = 10^{39.5} \text{ erg s}^{-1}$ ($M_V \approx -14$). Our coverage of the disks of these galaxies is generally incomplete, but this result is consistent with the finding of Kennicutt (1988), Kennicutt *et al.* (1989), and Caldwell *et al.* (1991) that Sa and early Sb spirals have no H II region brighter than $L(H\alpha) = 10^{39} \text{ erg s}^{-1}$, while in late-type spirals and irregulars the most luminous H II regions are brighter than $L(H\alpha) = 10^{40} \text{ erg s}^{-1}$. However, our data suggest no other obvious difference, in particular the $EW(H\alpha)$ values and colors are comparable between the two sets. This will be discussed further in the next section.

3.2 Equivalent Widths Distribution vs Hubble Type

The Balmer emission-lines equivalent widths are a measure of the relative proportion of ionizing photons (produced mostly by massive stars, $M > 10 M_\odot$) and continuum photons emitted by the whole cluster embedded in the H II region (plus a contribution from the gas, which is significant, $> 30\%$, in the R-band continuum for ages $< 3 \text{ Myr}$). As such they are sensitive, in principle, to variations in the upper IMF. An analysis of the distribution of the equivalent widths might therefore tell us if IMF changes are required to explain

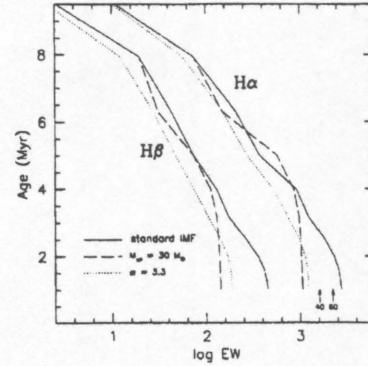


FIG. 3. Evolution of the H α and H β equivalent widths as predicted by theoretical models at solar metallicity (from Leitherer & Heckman 1995). The solid and dashed lines refer to a Salpeter IMF with upper mass limit of 100 and 30 solar masses, respectively. The arrows labeled 40 and 60 show the 1 Myr value of $EW(H\alpha)$ for $M_{up}=40$ and $M_{up}=60$ solar masses, respectively (C. Leitherer, private communication).

the differing H II region properties along the Hubble sequence. There is nevertheless a complication, due to the difficulty in separating IMF and age effects. As the most massive stars evolve and vanish, the EWs for an embedded cluster become degenerate with IMF after 3–4 Myr from the initial burst of star formation, as indicated by evolutionary population synthesis models (Leitherer & Heckman 1995; Mas-Hesse & Kunth 1991). In order to test for an IMF change we must therefore consider regions as young as 2–3 Myr, when different IMFs produce equivalent widths differing by as much as 0.3–0.4 dex (see Fig. 3). Since subtle variations are clearly difficult to detect, only largely different IMFs ($M_{up}=100 M_\odot$ and $30 M_\odot$, $\alpha=2.35$ and 3.3) will be considered in the remainder of the paper. We will refer to the “standard” IMF as the one characterized by $M_{up}=100 M_\odot$ and $\alpha=2.35$. It is important to notice that our $EW(H\alpha)$ s are calculated from continuum and line emission measured across great part of the extension of the nebulae, and not from sampling a small fraction of the H II regions, as is often the case in spectroscopic observations. This condition is important if we want to draw conclusions on variations in the IMF parameters (Copetti *et al.* 1985; Rosa & Benvenuti 1994), since “local” measurements could be not representative of the whole nebulae and their ionizing clusters.

Figure 4 compares the $EW(H\alpha)$ distributions for the H II regions in our galaxy sample, subdivided into Sa, Sb, and Sc types. No obvious trend with morphological type is seen. The $EW(H\alpha)$ and $EW(H\beta)$ distributions from the data of Kennicutt *et al.* (1997), consisting of spectra of more than one hundred H II regions in 21 spiral galaxies, also show no clear dependence on the parent galaxy Hubble type. The upper limit of the $EW(H\alpha)$ distribution lies around $\log EW(H\alpha)=3.4$ – 3.6 , independent of Hubble type. We note from Fig. 3 that for young (age $< 2 \text{ Myr}$) star forming regions $\log EW(H\alpha)=3.4$ for the standard IMF and $\log EW(H\alpha)=3.0$ for either $M_{up}=30 M_\odot$ or $\alpha=3.3$ in the

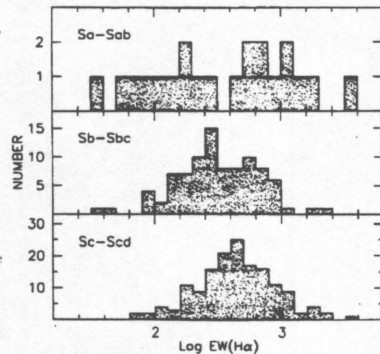


FIG. 4. Histogram of the measured $EW(H\alpha)$ as a function of Hubble type.

Leitherer & Heckman (1995) models at solar metallicity.

These results immediately allow us to exclude radically different IMFs between Sa, Sb, and Sc spirals, and suggest that a standard IMF is consistent with the observations. We cannot exclude modest changes in the upper IMFs, for example a systematic change in M_{up} from $100 M_{\odot}$ to $\sim 60 M_{\odot}$ over this range of galaxy types. However our data rule out (at the $\sim 2\sigma$ level) more extreme variations, for example the low mass cutoffs ($M_{up} < 30 M_{\odot}$) proposed in some luminous infrared starbursts (e.g., Rieke *et al.* 1993), or the even lower cutoffs in early-type spirals suggested by van den Bergh (1976) and Kormendy (1977).

3.3 Broadband Luminosity Functions

The sample of H II regions described so far is not complete. As mentioned before, only objects in common between the $H\alpha$ and continuum images have been measured. Typically this restricts the analysis to young, bright objects. In order to have more complete information on the star clusters, we measured the luminosity of H II regions and continuum knots (OB associations and star complexes), without restricting to detection in both $H\alpha$ and continuum, in four of the galaxies, NGC 2775, NGC 2841, M51, and M100, which span most of the range of Hubble types in our sample. The results of this comparison are shown in Fig. 5, where it can be seen that those continuum knots which have an $H\alpha$ counterpart (solid dots) are generally the bluest (youngest).

Luminosity functions (LFs) are presented in Fig. 6. The continuous line refers to H II regions, the dashed line to continuum knots. The turnover at low luminosities is due to incompleteness. A word of caution: for a given galaxy the fluxes for most knots and H II regions were measured with the same aperture size and annulus for sky+background subtraction. This reduces the accuracy of the photometry, especially in the continuum bands and for late-type spirals, where background variations due to dust lanes, spiral arms, crowding, etc., are more important than in $H\alpha$ and for early-type spirals.

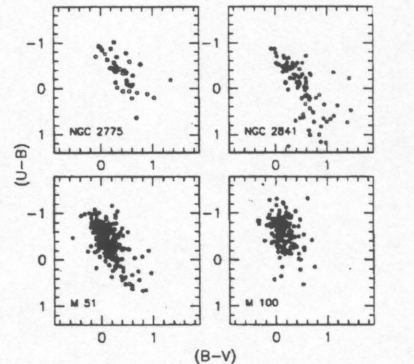


FIG. 5. $(B-V)$ vs $(U-B)$ diagram for the continuum knots ($V < 21$) measured in a restricted sample of galaxies. Solid dots correspond to objects having an $H\alpha$ counterpart.

Of the four galaxies in Fig. 6, NGC 2775 is the only one for which we have complete coverage; for the other three the area surveyed is a fraction of the total extension of the galaxies, therefore the numbers should be scaled upward to get total numbers. In the case of NGC 2775 the slope $a = d \log N/d \log L(H\alpha) = -2.8$, consistent with the average value $a = -2.6$ found by Caldwell *et al.* (1991) for the H II region LFs of seven Sa galaxies (indicated by the dotted line). The brightest $H\alpha$ and continuum luminosities are also comparable. The dotted line in the plots for the remaining galaxies has a slope of -2 , a typical value found for Sbc-Sc galaxies by Kennicutt *et al.* (1989). For M100 the actual slope seems somewhat flatter, while in M51 a break in the LF can be traced at $\log L(H\alpha) \approx 38.6$, or $M_V \approx -12$.

The continuum LF matches the H II LF remarkably well, considering the uncertainties of the adopted measurement process, as mentioned above. It is particularly interesting that both the slope of the bright, linear part and the maximum luminosity vary with Hubble type. This result allows to extend to the continuum LF what Kennicutt *et al.* (1989) found for the H II region LF, namely that the maximum luminosity of the star forming regions varies by more than an order of magnitude from early-type to late-type spirals and irregular galaxies. The slope of the LF, which can be represented by a power-law function $N(L) \propto L^a$, where $a = -2 \pm 0.5$, flattens out towards Sc-Irr galaxies, such that the distribution is dominated by large, bright objects in late-type spirals ($a > -2$), whereas in early-type spirals relatively more low-luminosity objects are present ($a < -2$). According to Fig. 6 the slope of the continuum LF therefore can be roughly expressed as $b = d \log N/d M_V = 0.4a$. It is worth noting that the continuum slope for late-type spirals and irregulars is comparable to the slope of the *stellar* LF in nearby galaxies ($b \approx 0.65$, e.g., Freedman 1985).

4. DISCUSSION

It is generally assumed that the $H\alpha$ luminosity of star forming regions scales with the mass of the ionizing clusters,

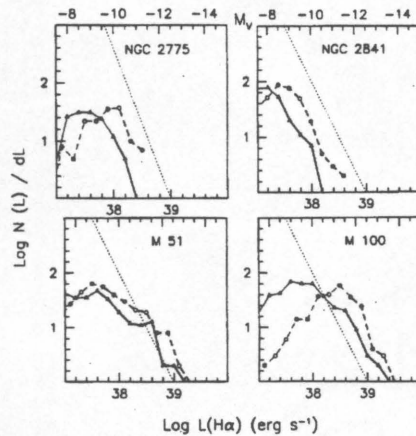


FIG. 6. Luminosity functions for H II regions (continuous line) and continuum knots (dashed line) in a subsample of four galaxies. The approximate range of completeness is indicated by thicker lines. The dotted line is shown for comparison and has a slope of -2.6 in the case of NGC 2775, and -2 for the remaining galaxies.

and it is this assumption that underlies the use of the H α luminosity as a quantitative measure of the star formation rate. Since the continuum luminosity of a starburst is dominated (after 1–2 Myr) by the stellar flux of the embedded clusters, the results just presented allow us to establish that the H II region LF variations seen across the Hubble sequence reflect analogous changes in the luminosity and mass functions of the ionizing clusters.

Similarities in the H α and continuum LFs have been noted before, e.g., for the star clusters of the LMC Elson & Fall (1985) found a slope of the B LF $a = -1.5$, consistent with $a = -1.75$ for the H II regions (Kennicutt *et al.* 1989). Caldwell *et al.* (1991) studied the continuum knots in a sample of Sa spirals, obtaining a similar result. The Galactic molecular cloud masses are also distributed in a similar fashion, with $a = -1.6$ (Williams & McKee 1997). Moreover our results on the continuum LF are in agreement with the study of Wray & de Vaucouleurs (1980), who found a strong galaxy type dependence in the luminosities of the brightest superassociations in spirals and irregulars. Therefore the idea that the bright star clusters are associated with H II complexes, for spirals of all types, receives further support from our data. As a consequence, the observed variations in the H α properties of the star forming regions along the Hubble sequence are likely due to a differing mass spectrum of the regions themselves.

However other scenarios could in principle explain the observed trend. Extinction differences between early- and late-type spirals seem to be ruled out by the investigations of Oey & Kennicutt (1993) and Zaritsky *et al.* (1994). The main other explanation follows from the suggestion made by van den Bergh (1976) and Kormendy (1977) that the stellar IMF is depleted of massive stars in Sa and Sb galaxies, an idea

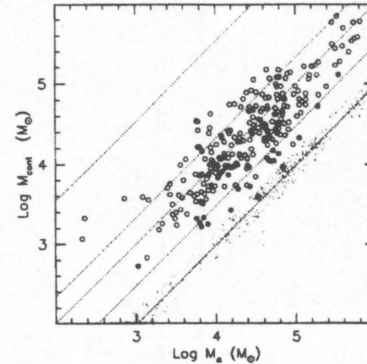


FIG. 7. Isochrones for 2, 4, 6, 8, and 10 Myr (from lower right to upper left) calculated as explained in the text are shown for comparison with the observed points, transformed into mass values using theoretical models. Solid dots indicate H II regions for which $EW(H\alpha) > 3.2$, darker open symbols have been used for $EW(H\alpha)$ between 3.0 and 3.2. The shaded area represents the uncertainty in the position of the isochrones assuming a 20% flux error.

originated at the time since many blue knots, but no H II regions, could be observed in these galaxies. The subsequent detection of H II regions even in S0/Sa galaxies (Caldwell *et al.* 1994) has weakened the importance of this argument (stars more massive than 10–15 M_{\odot} must be present in order to ionize the gas), but less dramatic changes in the upper IMF could still be possible. In Sec. 3.2. we have shown evidence for comparable H II region equivalent width distributions in spirals of different Hubble type. We can strengthen our assertion that indeed early- and late-type spirals produce H II regions with similar IMF, if we can show that the high-EW objects are young enough to be sensitive to IMF variations, since older objects will have similar EWs even for largely different IMFs.

In order to estimate the ages of the H II regions we make the simplifying assumption that star formation in a giant H II region occurs in a single, isolated burst. In reality distinct non-coeval star clusters are observed to coexist in nearby superassociations (e.g., 30 Dor). At much larger distances, as for our H II region sample, these clusters will remain unresolved. Nevertheless our simplification will allow us to define a “mean” age, weighted by the age and size of each separate cluster. Our approach relies on the fact that in principle for radiation-bounded regions the estimates of the ionizing cluster mass, M_{α} and M_{cont} , derived by adding the contribution from all stellar masses to the ionizing flux and to the continuum luminosity, respectively, must coincide. We then used the Leitherer & Heckman (1995) models with standard IMF and solar metallicity to approximate the age of an H II region by the time at which $M_{\alpha} = M_{\text{cont}}$.

In Fig. 7 we show the results, after correcting the data for an average visual extinction of one magnitude. Points along a selected isochrone (dotted line) will satisfy the condition $M_{\alpha} = M_{\text{cont}}$. The scales along the axes, giving the total mass

of the clusters (in stars in the 1–100 M_{\odot} mass range), arbitrarily refer to the 6 Myr isochrone, while the shaded area gives the uncertainty in the position of the isochrones considering a 20 percent error in the measured fluxes. Figure 7 shows that the high-EW regions, represented by the solid dots, are, as expected, the youngest in our sample, with ages ≤ 4 Myr. Our values are consistent with other determinations of H II region ages (e.g., Copetti *et al.* 1985), which give values between 1 and 3 Myr for the youngest H II regions in spirals. Changing M_{up} from 100 to 30 M_{\odot} is expected to produce as much as a 0.4 dex lowering in the EWs in this age interval. Not only this is not observed in our galaxy sample, as explained in Sec. 3.2, but also the maximum EWs are consistent with the theoretical values for the standard IMF.

A limitation of our data and technique is that values of the

upper mass limit differing by as much as 40 M_{\odot} (between 100 and 60 M_{\odot}) are indistinguishable, as shown in Fig. 3. We can however conclude that even though it is not possible to rule out variations of this order of magnitude, they alone cannot explain the large changes in H II region properties along the Hubble sequence. Differences in the number of stars per star forming region and in the number of regions per unit area are more likely to be responsible for the systematic trend with morphological type.

We thank C. Leitherer for providing us with unpublished evolutionary models. Comments from an anonymous referee helped to improve the manuscript. This work was supported by grant AST-9421145 from the National Science Foundation.

REFERENCES

- Caldwell, N., Kennicutt, R., Phillips, A. C., & Schommer, R. A. 1991, *ApJ*, 370, 526
 Caldwell, N., Kennicutt, R., & Schommer, R. A. 1994, *AJ*, 108, 1186
 Copetti, M. V. F., Pastoriza, M. G., & Dottori, H. A. 1985, *A&A*, 152, 427
 Elson, R. A. W., & Fall, M. 1985, *PASP*, 97, 692
 Ferrarese, L., *et al.* 1996, *ApJ*, 464, 568
 Freedman, W. L. 1985, *ApJ*, 299, 74
 Graham, J. A., *et al.* 1997, *ApJ* (in press)
 Kelson, D., *et al.* 1997, *ApJ* (in press)
 Kennicutt, R. C. 1983, *ApJ*, 272, 54
 Kennicutt, R. C. 1988, *ApJ*, 334, 144
 Kennicutt, R. C., Edgar, B. K., & Hodge, P. W. 1989, *ApJ*, 337, 761
 Kennicutt, R. C., Bresolin, F., & Garnett, D. 1997, in preparation
 Kormendy, J. 1977, in *The Evolution of Galaxies and Stellar Populations*, edited by B. M. Tinsley and R. B. Larson (Yale University Obs., New Haven), p. 131
 Landolt, A. U. 1992, *AJ*, 104, 340
 Larson, R. B., & Tinsley, B. M. 1978, *ApJ*, 219, 46
 Leitherer, C., & Heckman, T. 1995, *ApJS*, 96, 9L
 Mas-Hesse, J. M., & Kunth, D. 1991, *A&AS*, 88, 399
 Massey, P., Strobel, K., Barnes, J. V., & Anderson, E. 1988, *ApJ*, 328, 315
 Mayya, Y. D. 1994, *AJ*, 108, 1276
 Oey, M. S., & Kennicutt, R. C. 1993, *ApJ*, 411, 137
 Rieke, G. H., Loken, K., Rieke, M. J., & Tambllyn, P. 1993, *ApJ*, 412, 99
 Rosa, M. R., & Benvenuti, P. 1994, *A&A*, 291, 1
 Searle, L., Sargent, W. L. W., & Baguolo, W. G. 1973, *ApJ*, 179, 427
 Stetson, P. B. 1987, *PASP*, 99, 191
 Tully, R. B. 1988, *Nearby Galaxy Catalog* (Cambridge University Press, Cambridge)
 van den Bergh, S. 1976, *AJ*, 81, 797
 Waller, W. H. 1990, Ph.D. thesis, University of Massachusetts
 Williams, J. P., & McKee, C. F. 1997, *ApJ* (in press)
 Wray, J. D., & de Vaucouleurs, G. 1980, *AJ*, 85, 1
 Zaritsky, D., Kennicutt, R. C., & Huchra, J. P. 1994, *ApJ*, 420, 87

REFERENCES

- Bresolin, F., Kennicutt, R. C., & Stetson, P. B. 1996, AJ, 112, 1009 (BKS)
- Campbell, A. 1988, ApJ, 335, 644
- Cassinelli, J. P., Cohen, D. H., MacFarlane, J. J., Drew, J. E., Lynas-Gray, A. E.,
Hoare, M. G., Vallergera, J. V., Welsh, B. Y., Vedder, P. W., Hubeny, I., &
Lanz, T. 1995, ApJ, 438, 932
- Cassinelli, J. P., Cohen, D. H., MacFarlane, J. J., Drew, J. E., Lynas-Gray, A. E.,
Hubeny, I., Vallergera, J. V., Welsh, B. Y., & Hoare, M. G. 1996, ApJ, 460,
949
- Cerviño, M., & Mas-Hesse, J. M. 1994, A&A, 284, 749
- Conti, P. S., Leitherer, C., & Vacca, W. D. 1996, ApJ, 461, L87
- Contini, T., Davoust, E., & Considère, S. 1995, A&A, 303, 440
- Doyon, R., Puxley, P. J., & Joseph, R. D. 1992, ApJ, 397, 117
- Ferland, G. J. 1996, HAZY: A Brief Introduction to CLOUDY, V.90.01
- García-Vargas, M. L. 1996, *From Stars to Galaxies: the Impact of Stellar Physics
on Galaxy Evolution*, eds. C. Leitherer, U. Fritze-von Alvensleben & J.
Huchra, ASP Conf. Proc. 98, p. 244
- García-Vargas, M. L., & Díaz, A. I. 1994, ApJS, 91, 553
- García-Vargas, M. L., Bressan, A., & Díaz, A. I. 1995, A&ASS, 112, 13
- García-Vargas, M. L., González-Delgado, R. M., Pérez, E., Alloin, D., Díaz, A., &
Terlevich, E. 1997, ApJ, 478, 112
- Garmany, C. D., Massey, P., & Parker, J. W. 1994, AJ, 108, 1256

- González-Delgado, R. M., Leitherer, C., Heckman, T., & Cerviño, M. 1997, ApJ, in press
- Hodge, P. 1986, *Luminous Stars and Associations in Galaxies*, IAU Symposium No. 116, eds. C. W. H. de Loore, A. J. Willis, & P. Laskarides (Reidel, Boston), p. 369
- Hunter, D. A., & Thronson, H. A. 1995, ApJ, 452, 238
- Hunter, D. A., Shaya, E. J., Holtzman, J. A., Light, R. M., O'Neill, E. J., & Lynds, R. 1995, ApJ, 448, 179
- Hunter, D. A., Baum, W. A., O'Neil, E. J., & Lynds, R. 1996a, ApJ, 456, 174
- Hunter, D. A., Baum, W. A., O'Neil, E. J., & Lynds, R. 1996b, ApJ, 468, 633
- Hunter, D. A., Light, R. M., Holtzman, J. A., Lynds, R., O'Neil, E. J., & Grillmair, C. J 1997, ApJ, 478, 124
- Kennicutt, R. C. 1983, ApJ, 272, 54
- Kennicutt, R. C. 1991, *Massive Stars in Starbursts*, STScI Symposium Series, eds. C. Leitherer, N. R. Walborn, T. M. Heckman & C. A. Norman (Cambridge University Press), p. 157
- Kennicutt, R. C., & Hodge, P. W. 1986, ApJ, 306, 130
- Kennicutt, R. L., Roettiger, K. A., Keel, W. C., van der Hulst, J. M., & Hummel, E. 1987, AJ, 93, 1011
- Kurucz, R. L. 1992, *The Stellar Populations of Galaxies*, IAU Symp. 149, ed. B. Barbuy & A. Renzini (Dordrecht: Kluwer), p. 225
- Larson, R. B., & Tinsley, B. M. 1978, ApJ, 219, 46
- Leitherer, C 1997, *VIII Canary Islands Winter School of Astrophysics: Stellar Astrophysics for the Local Group*, eds. A. Aparicio, A. Herrero & F. Sanchez

(Cambridge: CUP), in press

Leitherer, C., & Lamers, H. J. G. L. M. 1991, 373. 89

Leitherer, C., & Heckman, T. 1995, ApJS, 96, 9L

Leitherer, C., Robert, C., & Heckman, T. M. 1995, ApJS, 99, 173

Leitherer, C. *et al.* 1996a, PASP, 108, 996

Leitherer, C., Vacca, W. D., Conti, P. S., Filippenko, A. V., Robert, C., & Sargent,
W. L. W. 1996b, ApJ, 465, 717

Maeder, A. 1990, A&AS, 84, 139

Maeder, A. 1996, *From Stars to Galaxies: the Impact of Stellar Physics on Galaxy
Evolution*, eds. C. Leitherer, U. Fritze-von Alvensleben & J. Huchra, ASP
Conf. Proc. 98, p. 141

Maeder, A., & Conti, P. S. 1994, ARAA, 32, 227

Massey, P. Garmany, C. D., Silkey, M., & DeGioia-Eastwood, K. 1989, AJ, 107

Massey, P., Lang, C. C., DeGioia-Eastwood, K., & Garmany, C. D. 1995a, ApJ,
438, 188

Massey, P., Johnson, K. E., & DeGioia-Eastwood, K. 1995b, ApJ, 454, 151

Mas-Hesse, J. M., & Kunth, D. 1991, A&AS, 88, 399

McGaugh, S. S. 1991, ApJ, 380, 140

Melnick, J., Terlevich, R., & Eggleton, P. P. 1985, MNRAS, 216, 255

Meurer, G. R., Heckman, T. M., Leitherer, C., Kinney, A., Robert, C., & Garnett,
D. R. 1995, AJ, 110, 2665

Meynet, G. 1995, A&A, 298, 767

O'Connell, R. W., Gallagher, J. S., & Hunter, D. A. 1994, ApJ, 433, 65

- Oey, M. S., & Kennicutt, R. C. 1997, MNRAS, submitted
- Olofsson, K. 1989, A&AS, 80, 317
- Pagel, B. E. J. 1990, *Evolution in Astrophysics*, ed. E. J. Rolfe (Paris: ESA). ESA SP-310, p. 159
- Parker, J. W, & Garmany, C. D. 1993, AJ, 106, 1471
- Rieke, G. H., Lebofsky, M. J., Thompson, R. I., Low, F. J., & Tokunaga. A. T. 1980, ApJ, 238, 24
- Rieke, G. H., Loken, K., Rieke, M. J., & Tamblyn, P. 1993, ApJ, 412, 99
- Robert, C., Leitherer, C, & Heckman, T. M. 1993, ApJ, 418, 749
- Salpeter, E. E. 1955, ApJ, 121, 161
- Scalo, J. M. 1986, Fund. Cosm. Phys., 11, 1
- Scalo, J. M. 1990, *Windows on Galaxies*, eds. G. Fabbiano, J. S. Gallagher, & A. Renzini (Kluwer: Dordrecht), p.125
- Schaerer, D. 1996, ApJ, 467, L17
- Searle, L. 1971, ApJ, 168, 327
- Searle, L., Sargent, W. L. W., & Bagnuolo, W. G. 1973, ApJ, 179, 427
- Sekiguchi, K., & Anderson, K. S. 1987, AJ, 94, 644
- Shields, G. A. 1974, ApJ, 193, 335
- Shields, G. A., & Tinsley, B. M. 1976, ApJ, 203, 66
- Shields, G. A., & Searle, L. 1978, ApJ, 222, 821
- Shields, G. A. 1990, ARA&A, 28, 525
- Shields, J. C. 1993, ApJ, 419, 181

- Stasińska, G. 1996, *From Stars to Galaxies: the Impact of Stellar Physics on Galaxy Evolution*, eds. C. Leitherer, U. Fritze-von Alvensleben & J. Huchra. ASP Conf. Proc. 98, p. 232
- Stasińska, G., & Leitherer, C. 1996, ApJS, 107, 661
- Terlevich, R., & Melnick, J. 1981, MNRAS, 195, 839
- Vacca, W. D., Robert, C., Leitherer, C., & Conti, P. S. 1995, ApJ, 444, 647
- van den Bergh, S. 1976, AJ, 81, 797
- Viallefond, F. 1985, *Star-forming Dwarf Galaxies and Related Objects*, eds. D. Kunth, T. X. Thuan, & J. T. Thanh Van (Editions Frontières, Paris), p. 207
- Vílchez, J. M., & Pagel, B. E. J. 1988, MNRAS, 231, 257
- Walborn, N. R. 1991, *Massive Stars in Starbursts*, eds. C. Leitherer, N. Walborn, T. Heckman & C. Norman (Cambridge: CUP), p. 145
- Wilson, C. D. 1992, AJ, 104, 1374